Vol (1) №(1) March 2017

LIBYAN JOURNAL
FOR ENGINEERING RESEARCH

A Refereed Scientific Journal issued semi-annually by Faculty of Engineering - Benghazi University

ISSN226-335

All correspondences should be addressed to:

Editor in Chief of Libyan Journal for Engineering Research.

Faculty of Engineering, Benghazi University, Libya.

Email: LyJER@uob.edu.ly

ULR: www. *lyjer.uob.edu.ly*

Volume (1) № (1) March 2017

LIBYAN JOURNAL
FOR ENGINEERING RESEARCH

A Refereed Scientific Journal issued semi-annually by Faculty of Engineering **ISSN226-335**

Aims of the Journal

This journal aims to provide a reliable source of information on current research and development in the fields of basic and applied sciences, on the national and international levels, as well as exchange of ideas and information for experts in these fields. Moreover, it will provide an opportunity for researchers to publish their works.

Editorial Board Looks forewords to develop the journal and to promote it to be at the level of international scientific journals, and expand their reach circle to allow the largest possible number of interested to follow it by publishing all its issues through the internet web site.

Call for Papers

The Editorial Committee invites teaching staff members, postgraduate students, engineers, researchers and all those concerned with basic and applied sciences, and technology fields to submit their research work to be published in the journal. The journal publishes scientific papers (basic and applied research, review papers) technical reports, technical notes and book reviews in the mentioned fields.

Terms of Publication in the Journal

1. The papers and reports should be an original work and not considered for publication elsewhere. Papers published in conferences may be considered for publication in the journal after they go through the evaluation process and if they do not conflict with the copyright of the conference proceedings.
2. All papers and reports are subject to evaluation and may not be published unless all the required corrections are met and the author's guide for publication is followed.
3. The accepted papers could be written in Arabic (with English abstract), or in English (with Arabic abstract).
4. After acceptance of the paper or report for publication in the journal, it should not be considered for publication in another journal and the author should sign a copyright agreement with the editorial board of the journal.
5. Authors should include the full title of the paper, the author's full name, Author's affiliation and address, e-mail address.
6. Papers not written according to the stated instructions will not be considered for refereeing.

LIBYAN JOURNAL
FOR ENGINEERING RESEARCH
A Refereed Scientific Journal issued semi-annually by Faculty of Engineering

Volume (1) № (1) March 2017

ISSN226-335

Typing Instruction

In spite that an electronic paper template is available, Authors are kindly requested to abide by the following instructions:

1. Manuscripts should not exceed 10 (A4) pages including figures and tables, produced using Microsoft word, with Times New Roman font 9.5pt single space typewritten. The page setup left and right margins of 13.5 mm and top margin of 25.4 mm and bottom margin of 21.8 mm.
2. The original and two copies should be submitted, and on a CD disc. The file on the disc should exactly correspond to the hard copies.
3. Authors have to the following format:
   a. ***Title page***, headed by a concise but informative full title font size 15pt**bold**, name(s) font size 12pt, and address of the place where the work was carried out font size of 8pt.
   b. ***Abstract***, containing brief but informative details of the contents and conclusions of the paper and should not exceed 200words, size 8.5.
   c. ***Introduction,*** stating the reasons for carrying out the work, size of 9.5pt.
   d. ***Materials and Methods***, containing sufficient experimental details so that methods can be reproduced by researchers (in experimental papers), size 9.5pt.
   e. ***Results*** should be described as concise as possible, size of 9.5pt.
   f. ***Discussion*** should not recapitulate results in detail or contain new information but should emphasize the relevance and significance of the findings reported, size of 9.5pt.
   g. ***Conclusion***, size of 9.5pt.
   h. ***Acknowledgement***, size of 9.5pt.
   i. ***References*** should be cited in the text a number in square brackets **[ ]**. All references should be included at the end of the manuscript successively with size of 8pt. Correct references are the responsibility of the author.

Notes

1. the Journal has the right to publish these researches and makes use of them in scientific fields without referring to their owners, provided always referring to the owners of these studies/research according to generally accepted rules.
2. Manuscripts submitted for publication does not respond to their owners, whether published or not, the applicant is not entitled to claim them.
3. Editors of the journal reserve the right to make editorial changes in any manuscript accepted for publication for the sake of style or clarity. Authors will be consulted only if the changes are substantial.
4. Author/s must pay all the expenses incurred in the review process if s/he decides to withdraw his/her research paper whilst it is undergoing review.

Volume (1) № (1) March 2017

LIBYAN JOURNAL
FOR ENGINEERING RESEARCH

A Refereed Scientific Journal issued semi-annually by Faculty of Engineering ***ISSN226-335***

Volume (1) № (1) March 2017

LIBYAN JOURNAL
FOR ENGINEERING RESEARCH
A Refereed Scientific Journal issued semi-annually by Faculty of Engineering ***ISSN226-335***

Contents

English Part

Research Papers

Volume (1) № (1) March 2017

LIBYAN JOURNAL
FOR ENGINEERING RESEARCH
A Refereed Scientific Journal issued semi-annually by Faculty of Engineering ***ISSN226-335***

ISSN 2522-6967

Using Least Square for Develop a New Formation Resistivity Factor Correlation and Relationship between the Salinity and the Corrosion

Neima Mazeb and Nassr AlFadil

Petroleum Engineering Dept., Benghazi University, Benghazi, Libya
Corresponding author. Tel.: +218-91-813-8563; e-mail: nassr.mussa@uob.edu.ly & fatima_n1967 @yahoo.com

ABSTRACT

Formation resistivity factor (Fr),introduced by Archie , is an important parameter for electric log interpretation .It is defined as the resistivity of rock fully saturated with brine (Ro) divided by the resistivity of brine (Rw). This factor is function of porosity, resistivity, tortuosity and cementation factor, which are consequently affected also by particle size and degree of compaction .Formation resistivity factor is usually determined experimentally or by using empirical approach. During the present paper, we try to develop a new formation resistivity factor (Fr) correlation based on statistical methods, Least square, by taking into account different parameter such as brine salinity, particle size and degree of compaction. In addition, this study aims to determine the relationship between salinity and corrosion.

Keywords: *Formation Resistivity factor, Porosity, Tortuosity, Particle size, compaction, Salinity, Corrosion*

1. Introduction

Sedimentary formations are capable of transmitting an electric current only by means of the interstitial and adsorbed water they contain. They would be non-conductive if they were entirely dry.

The interstitial or connate water containing dissolved salts constitutes an electrolyte capable of conducting current, as these salts dissociate into positively charged cations, such as Na^+ and Ca^{++} , and negatively charged anions, such as Cl^- and SO_4^{--} .

These ions move under the influence of an electrical field and carry an electrical current through the solution. The greater the salt concentration, the greater the conductivity of the connate water. The electrical resistivity (reciprocal of conductivity) of a fluid-saturated rock is its ability to impede the flow of electric current through that rock. Dry rocks exhibit infinite resistivity. The resistivity of reservoir rocks is a function of salinity of formation water, effective porosity, and quantity of hydrocarbons trapped in the pore space [1]. Relationships among these quantities indicate that the resistivity decreases with increasing porosity and increases with increasing petroleum content. Resistivity measurements are also dependent upon pore geometry, formation stress, and composition of rock, interstitial fluids, and temperature. Resistivity is, therefore, a valuable tool for evaluating the producibility of a formation. A rock that contains oil and/or gas will have a higher resistivity than the same rock completely saturated with formation water and the greater the connate water saturation, the lower the formation resistivity.

Archie defined the formation resistivity factor Fr as [2]:

$$Fr = Ro/Rw \qquad (1.1)$$

Where Ro is the resistivity of a formation that is fully saturated with water, Rw is the resistivity of the water .Ro will be greater than Rw and Fr will always be greater than unity.

Figure (1.1) shows the qualitative effect of brine resistivity (assuming all other factors, such as porosity, cementation, and amount of shale remain constant) on (Fr) for limestone and clean sand, and shaly (dirty) sand. The formation factor is essentially constant for clean sand and limestone. For dirty or shaly sand, (Fr) decreases as brine resistivity, Rw, increases; and although Ro increases, it does not increase proportionately because the clay in the water acts as a conductor.

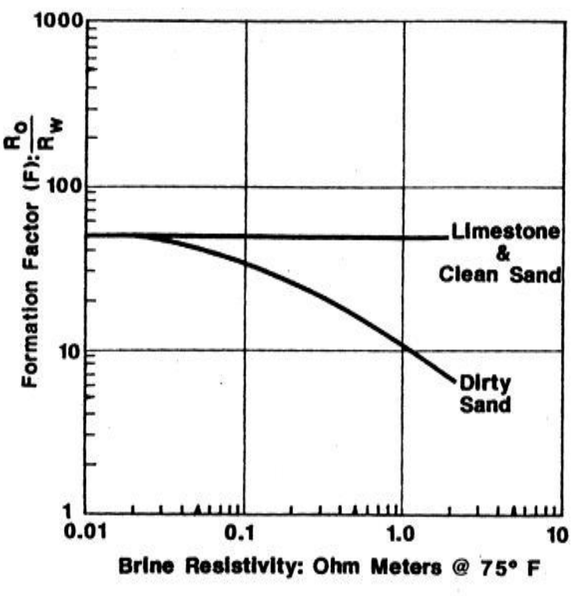

Figure 1.1: General relationship between formation factor Fr and brine resistivity Rw factor (Courtesy of Core Laboratories). [2]

This effect is dependent upon the type, amount, and manner of distribution of the clay in the rock Equation (1.1) is an important relation in well-log interpretation for locating potential zones of hydrocarbons. Several methods for determining the reservoir water resistivity have been developed, including: chemical analysis of produced water sample, direct measurement in resistivity cell, water catalogs, spontaneous potential (SP) curve, resistivity-porosity logs, and various empirical methods.

2.0 Literature Review

The value of Fr is one of the most important parameters in water saturation calculations. The presence of Fr or equivalent parameters in all different formulas of water saturation calculation such as Archie, Indonesia, Popoun, etc… indicate the important role of this parameter in original oil in place estimation of a field.

2.1. Theoretical Formula for F_r

The formation resistivity factor,

$$Fr = a\, Ø^{-m} \tag{2.1}$$

has theoretical derivation in some of the early literature and textbooks on well log analysis and core analysis. Most all published derivations start with the fundamental definition of formation resistivity factor.

$$Fr = Ro / Rw \tag{2.2}$$

Where R_o is the resistivity of the porous media 100% saturated with a conductive fluid and R_w is the resistivity of the conductive fluid.

Each derivation requires a simplified model of the porous media using geometric shapes of pores, pore throats, and bulk volume that are easily described in terms of length and cross-sectional area for the conduction of ions through the model.

A general derivation similar to Amyx et al [3]is shown here. The definition of resistivity (R) of many materials is

$$R = rA/L \tag{2.3}$$

where, r = resistance of the material.
A = the cross-sectional area perpendicular to ionic flow.
L = Length of the ionic flow path.

Using a cube of salt water, the resistance of the cube could be defined as:

$$r_w = (R_w L)/A \tag{2.4}$$

where L and A describe the dimensions of the cube of water. A cube of porous media of the same dimension of the cube of water would have a lesser volume available for water. The matrix is assumed to be an insulator as such the portion of the cube. That can conduct ionic flow is only the pore space.

Therefore, an apparent cross-sectional area (Aa) and apparent flow path (La) are used. The resistance of the cube is

$$r_2 = R_w L_a / A_a \tag{2.5}$$

By definition the resistivity of the cube of core saturated with water is

$$R_o = r_2\, A/L \tag{2.6}$$

Substituting the last two equations yields:

$$R_o = R_w L_a\, A/A_a L \tag{2.7}$$

Using this definition of R_o in the F_r equation result in:

$$F_r = \frac{L_a/L}{A_a/LA} \tag{2.8}$$

which is the ratio of the apparent flow path to the length of the cube compared to the ratio of the apparent cross-sectional area to the cross-sectional area of the cube. The ratio of the lengths is proportional to tortuosity and is given the symbol a, the tortuosity factor. The apparent cross-sectional area is assumed to be equal to the product of the actual area and the porosity of the porous media (ØA). Using this definition yields

$$\boldsymbol{F_r = \frac{a}{Ø}} \tag{2.9}$$

Porosity has no power as such m can be seen as one. Several attempts have been made to obtain a universal formula relating porosity, formation resistivity, and cementation factor. If an electric current is passed through a block of non-conducting porous rock saturated with a conducting fluid, only a portion of the pore space participates in the flow of electric current. Consequently, total porosity Ø can be divided into two components such that [4]:

$$\Phi = \Phi_{ch} + \Phi_{tr} \tag{2.10}$$

Where Øch and Øtr are, the flowing porosity associated with the channels and the porosity associated with the regions of stagnation (traps) in a porous rock, respectively. It seems that, Øch is corresponding to the ' effective porosity ' used by Chilingarian and Øtr is corresponding to the irreducible fluid saturation [5].Figures (2.1)and (2.2) show that the electrical current can flow only through the channel indicated by C, while no current can flow through the trap indicated by T. In Figure 2.1, the traps are of the dead-end type. The trap in figure 2.2 is called an open or symmetry trap. A universal relationship between Fr and $Ø_f$ may be written as [6]:

$$F_r = 1 + f_G\left[\frac{1}{Ø_{ch}} - 1\right] \tag{2,11}$$

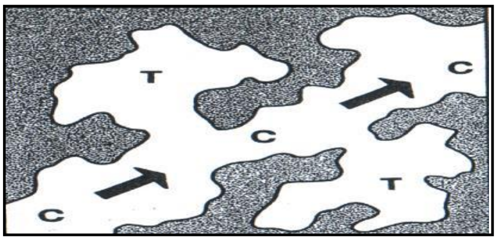

Figure 2.1: Portion of porous rock showing dead end trap [4]

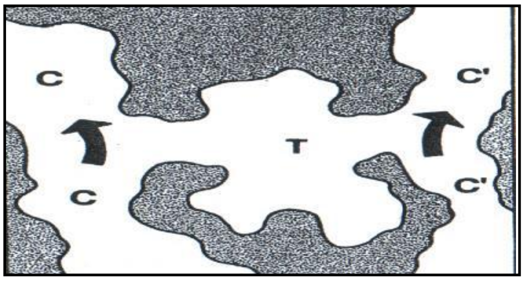

Figure 2.2: Portion of porous rock showing an open or symmetry trap [4]

$$Ø_{ch} = Ø^{m} \quad (2.12)$$

Where f_G is defined as the interior geometry parameter of the porous rock, and m ≥ 1. Combining Equations 2.11 and 2.12 gives:

$$F_r = 1 + f_G\left[\frac{1}{Ø^m} - 1\right] \quad (2,13)$$

This is the Rosales relationship between formation resistivity, porosity, and cementation factor. If f_G = 1, Equation 2.13 gives Archie's formula. Equation 2.13 can be expressed as:

$$F_r = \frac{f_G}{Ø^m} + (1 - f_G) \quad (2,14)$$

The value of f_G for most porous rocks is close to unity. Hence, fG/Øm>>(1-f_G) and Equation 2.14 can be approximated by :

$$F_r = \frac{f_G}{Ø^m} \quad (2,15)$$

This expression is the Humble formula where $\mathbf{f_G}$ = a. Thus, Archie's formula and Humble's formula are special cases of Rosales general formula. Rosales showed experimentally that, for sandstones, Equation 2.15 can be written as follows [6]:

$$F_r = 1 + 1.03\left[\frac{1}{Ø^{1.73}} - 1\right] \quad (2,16)$$

This expression was compared graphically with the Humble formula, Equation 2.17, and Timur et al. formula [7]:

$$R_{wc} = \frac{E}{I_{wc}}\frac{ØA(L/L_a)}{L} \quad (2,17)$$

$$F_r = \frac{1.13}{Ø^{1.73}} \quad (2,18)$$

Figure 2.3 is a log-log plot of Humble Equation (line A), 2.11 (line B), and 2.18 (line C). The three formulas give approximate results within the region of practical interest, i.e., 10 ≤ Ø ≤ 40. As Ø approaches unity, however, Equation (2.11) gives a curved line that satisfies the condition Fr =1 when Ø =1, whereas Humbler's formula and Timur's et al. formula (Equation 2.18) are straight lines for all values of Ø, which does not satisfy that condition.

The tortuosity is:

$$\tau = ØF_r \quad (2.19)$$

Substituting Equation 2.13 into Equation 2.19 yields a general expression for calculating tortuosity:

$$\tau = Ø\left[1 + f_G\left(\frac{1}{Ø^m} - 1\right)\right] \quad (2.20)$$

Inasmuch as the value of f_G is approximately equal to unity for most porous rocks, Equation 2.20 can be written as follows:

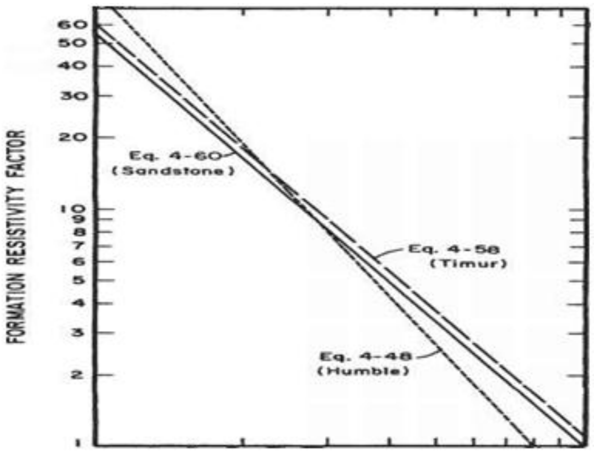

Figure 2.3: Graphical comparisons of Humble Equation (A), Rosales Equation (B), and Timur Equation (C) [4].

Table 3.1: Natural core samples (sandstone) (Attia 2005) [12]

Core #	Compaction pressure(psi)	Porosity (fraction)	Fr at 0.3% NaCl	Fr at 1% NaCl	Fr at 5% NaCl
1	3000	0.30	3.15	5.80	5.64
2	4000	0.29	3.91	5.96	7.11
3	5000	0.29	3.62	6.09	7.52
4	3000	0.28	2.66	6.85	6.78
5	4000	0.27	3.65	7.58	9.79
6	5000	0.25	3.57	7.75	10.20
7	3000	0.24	4.12	9.76	11.13
8	4000	0.24	4.57	9.38	13.75
9	5000	0.22	3.87	10.13	15.18
10	3000	0.21	6.42	13.19	14.08
11	4000	0.20	7.56	13.47	21.14
12	5000	0.19	6.51	13.06	18.55

$$\tau = \frac{1}{Ø^{m-1}} \quad (2.21)$$

Combining Equations 2.10, 2.12, and 2.21 gives:

$$\tau = 1 + \frac{Ø_{tr}}{Ø_{ch}} \quad (2.22)$$

This expression indicates the physical significance of tortuosity in terms of stagnant and flowing porosities. Equation 2.22 is approximation valid only for consolidated porous rocks. For unconsolidated sands, the general expression (Equation 2.20) should be used, where f_G= 1.49 and m =1.09.

2.2 Formation Resistivity Factor, Fr and Porosity

As clean sedimentary rocks conduct electricity by virtue of the salinity of water contained in their pores, it is natural that the porosity is an important factor in controlling the flow of electric current.

As a first approximation, one would expect that the current conductance would be no more than that represented by the fractional porosity, e.g., a formation with 20% connate water saturation and 80% oil saturation would be expected to transmit no more than 20% of the current that would be transmitted if the entire bulk volume conducted to the same degree as the water [8].

Table (3-2) clean sandstone 0.3%NaCl

Fr	Ø	Log Fr = Yi	Log Ø = Xi
5.7971	0.3038	0.7632	-0.5174
5.9613	0.2926	0.7753	-0.5337
6.0851	0.2922	0.7843	-0.5343
6.8483	0.2792	0.8355	-0.5540
7.5760	0.2654	0.8794	-0.5761
7.7475	0.2525	0.8892	-0.5977
9.7597	0.2410	0.9894	-0.6179
9.3788	0.2387	0.9721	-0.6221
10.1348	0.2217	1.0058	-0.6542
13.1945	0.2085	1.1203	-0.6808
13.4740	0.2015	1.1295	-0.6957
13.0598	0.1870	1.1159	-0.7281
		? 11.2599	? -7.312

$$F_r = (1/Ø) \quad (2\text{-}23)$$

- Shlumberege [9], well surving corporations stated that the relation between (Fr) and porosity is reported as:

$$F_r = (0.81/Ø_2) \quad (2\text{-}24)$$

- Zaafran et al, found that the formation resistivity factor may well correlated to the porosity and introduce this equation based on the better sandstone samples.

$$F_r = (1.48/Ø_{1.66}) \quad (2\text{-}25)$$

- Perez Rosales, et al. [11], Reported a new formulation for formation resistivity factor of fracture porous media .

They tried to fit an Archie type equation to the investigated data. They showed that it is impossible to get a good match . They established a new model based on the physical consideration and according to that they obtained the following formula:

$$F_r = (1/1-(1-Ø)_{0.78}) \quad (2\text{-}26)$$

3.0 For Natural Core Sample

To predict a correlation represents the relation between the formation resistivity factor and each of rock porosity and cementation factor , we used the laboratory measurements of the formation resistivity factor and the porosity for 12 natural core samples .The measurements were taken from a previous study and are shown in Table (3.1) [12].

By measuring the electric resistivity of the fully saturated samples with (Ro) and water resistivity (Rw), the formation resistivity factor (Fr) using the known formula Fr=Ro/Rw for each core was determined.

Resistivity factor and core porosity was obtained.

Table (3-3) clean sandstone, Fr at 1% NaCl.

Fr at 0.3% NaCl	Ø	Fr=Yi	Log Ø = Xi
3.1526	0.3038	0.4986	-0.5174
3.9148	0.2926	0.5927	-0.5337
3.6180	0.2922	0.5584	-0.5343
2.6633	0.2792	0.4254	-0.5540
3.6520	0.2654	0.5625	-0.5761
3.5735	0.2525	0.5530	-0.5977
4.1154	0.2510	0.6144	-0.6179
4.5727	0.2387	0.6601	-0.6221
3.8690	0.2217	0.5875	-0.6542
6.4150	0.2085	0.8071	-0.6808
7.5588	0.2015	0.8784	-0.6957
6.5118	0.1870	0.8137	-0.7281
		? 7.55187	? -7.312

Table (3-4): clean sandstone, Fr at 5% NaCl

Fr	Ø	Log Fr = Yi	Log Ø = Xi
05.6410	0.3038	0.7513	-0.5174
07.1090	0.2926	0.8518	-0.5337
07.5190	0.2922	0.8761	-0.5343
06.7760	0.2792	0.8309	-0.5540
09.7878	0.2654	0.9906	-0.5761
10.1968	0.2525	1.0084	-0.5977
11.1310	0.2410	1.0465	-0.6179
13.7517	0.2387	1.1383	-0.6221
15.1780	0.2217	1.1812	-0.6542
14.0810	0.2085	1.1486	-0.6808
21.1420	0.2015	1.3251	-0.6957
18.5500	0.1870	1.2683	-0.7281
		? 12.4171	? -7.312

Tables (3-2) to table (3-4) Show the calculations of using the least square method. The best correlation obtained for these different values of water salinities were obtained as follows:

1. Fr at 0.3% NaCl

   $$Fr = (a / Ø_m) = (1/Ø_{1.057}) \text{ least square} \quad (3\text{-}1)$$

2. Fr at 1% NaCl

   $$Fr = (a/Ø_{m}) = (1/Ø_{1.427}) \text{ least square} \quad (3\text{-}2)$$

3. Fr at 5% NaCl

   $$Fr = (a/Ø_m) = (1/Ø_{1.698}) \text{ least square} \quad (3\text{-}3)$$

A general correlation is obtained by using each of least square method determine an average value for the cementation factor m= 1.427 and constant a=1 the general correlation is given as:

$$Fr = (a/Ø_m) = (1/Ø_{1.427}) \text{ general equation} \quad (3\text{-}4)$$

ISSN 2522-6967

Validity of the obtained resistivity factor correlations:

To check the validity of the obtained correlations and possibility of its applications. We used the new correlations obtained for the natural core samples equation (3-1) through equation (3-4) and compared it with the other different correlation in literature. Table (3-5) shows this comparison for a core samples have different values of porosity (Ø) and cementation factor (m). The difference between the data obtained by equation (3-4) and the other correlations is due to neglecting the effect of water salinity and confined pressures.

Table (3-5) comparison of equation Humble equation. Perez equation. Zaafran equation Shlumberege equation and present study.

Porosity (Ø)	Fr Eq.(3-4)	Fr Eq.(Humble)	Fr Eq.(Perez)	Fr Eq.(Zaafran)	Fr (Shlumberege)
0.10	26.73	87.58	12.67	67.65	81
0.15	14.98	36.63	8.399	34.51	36
0.20	9.94	19.73	6.26	21.41	20.25
0.25	7.23	12.21	4.97	14.78	12.96
0.30	5.57	8.25	4.12	10.92	9
0.35	4.47	5.92	3.50	8.45	6.61

4.0 Conclusions

Based on the results obtained from this study, we can conclude the followings:

1. The formation resistivity factor which is the ratio of the electrical resistivity of porous medium fully saturated with water to the water resistivity is very important factor in electric log interpretation.
2. Using some of the natural core samples specifications measurements; porosity water salinity and formation resistivity factor a new correlation for the formation resistivity factor was obtained as Fr =Ø-1.427 .
3. To check the validity of the obtained correlations and its applications. A comparison between the results of using these corrections and those obtained by the different correlations present in literature. This comparison showed a reasonable agreement between them.
4. The formation resistivity factor increases by increasing the confined pressure (compaction pressure). This is as mentioned before, due to the decrease of the electric current path by increasing the confined pressure that cause an increase in the resistivity of formation and respectively increase the formation resistivity factor. It is clear that the water salinity affect the rate of increasing of resistivity factor.

The formation resistivity factor increases with relatively high rate at high degree of salinity.

References

[1] Pirson, S.J. Handbook of well log analysis. Prentice-Hall, 1963, 326pp.

[2] Archie, G.E.” The electrical resistivity log as an aid in determining some reservoir characteristics, ”Trans., AIME, VOL.146, 1942.

[3] Amyx, J.W., Bass, Jr., D. M., and Whiting, R.L.,: petroleum reservoir engineering, McGraw-Hill, New York 1960.

[4] Rosales “C.P.” on the relationship between formation resistivity factor and porosity.” Soc. Petrol. Engr. J. Aug.1982.

[5] Chilingarian, G.V. “Relationship between porosity, permeability and grain size distribution of sands and sandstones.” in: L.M.J.U. van straitens (Ed), Deltaic and Shallow Marin Deposits, I. Elsevier Sci. Pub., Amsterdam’1964, pp, 71-75.

[6] Rosales, C. P., ”generalization of the Maxwell equation formation resistivity factors .” Soc. petrol.engr.J.petr.tech., July 1976.

[7] Timur, A., Hemkins, W.B.and Worthington , A.E.” porosity and pressure dependence of formation resistivity factor for sandstones . “Proc. Canadian well logging soc., 4th formation Eval. Symp. Calgary, May 9-10, 1972.

[8] Calhoun, J.C., Jr. Fundamentals of reservoir engineering,fourthed. University of Oklahoma press, Norman, 1960,426 pp.

[9] Shlumberger, Inc. Log interpretation-principles Schlumerger Educational Services, Houston, 1972.

[10] Zaafran, Z.M., Ph.D. Thesis, Leeds University England. 1975.

[11] Perez-Rosales, C., Cruz Hernandez ,J., IsIas-Juarez, R., and Mercade –Diaz, A:"New formulation for formation resistivity of fracture porous media , "SPE 58991 presented at the 2000 Int. Pet. Conf. and Exhib. In Mexico, Villahermosa, 1-3 feb.2000.

[12] Attia M. Attia 2005. £ Effects of petrophsical rock properties on tortuosity factor “. Paper PETROL 1289 Journal of petroleum science and engineering, volume 48, Lssues 3-4, ages 185-198.

ISSN 2522-6967

Meta-Model Based Scaling Laws of a Two-Winding Transformer

Ahmed Tahir

Electrical and Electronics Engineering Department, University of Benghazi, P. O. Box: 9476 Benghazi, Libya
Tel.: +218-94-459-3897; e-mail ahmed.taher@uob.edu.ly

ABSTRACT

Recently, there has been growing interest in system-based global optimization techniques for the design of small systems such as micro-grids. To reduce the search space of the global optimization technique, a meta-model based scaling law was introduced. In this paper, a scaling technique was derived in which a transformer mass and power loss were expressed in terms of rated power, specified current density, and frequency. Curve-fitting techniques were used to derive a meta-model for the scaled mass and power loss. To achieve more generality, the meta-model was also defined as a function of frequency.

Keywords: Scaling laws, Meta-model, integrated energy resources, micro grids.

1. Introduction

Meta-model based algorithms are used to capture the performance of a component in a multiple component system such as a transformer in a micro-grid system [1]-[3]. To achieve that, the concept of scaling laws is introduced. By deriving the meta-model for each component, system-based optimization can be conducted to obtain efficient and compact systems with the possibility of varying frequency over ratings.

Global optimization techniques such as genetic algorithms may be utilized to derive the meta-model on the basis of the trade-off between competing performance equations [4]-[8]. This trade-off may be between mass and power loss or between volume and cost. To set the stage, a scaled analytical model of the two winding transformer is first derived in terms of general quantities such as current density, frequency, and rated power. Such quantities do not depend on the transformer size or ratings and thus the meta-model will be general to a wide range of transformer ratings.

To achieve an optimum design of a multi-component system, the coupling between the components of the system should be taken into account. Therefore, it is not accurate to optimize each component separately since the performance of one component affects the performance of another component in the system [1]. For instance, the temperature of a transformer has an affect on the performance of a cascaded converter. In other words, an optimum design of an individual device may not be necessarily the optimum design if the device is a component of a multi-component system.

In another perspective, when all components are considered as a single optimization problem this will lead to a large number of parameters and thus large number of degrees of freedoms. This may preclude the optimization based design of the system to converge to the desired solution. By introducing component's meta-model based scaling laws this issue may be resolved.

The objective of the work presented in this paper is to explore the possibility of developing meta-model based scaling laws for a power transformer. Such scaling laws enable one to approximate key performance metrics, i.e. loss and mass, based upon device power ratings without requiring one to perform a component optimization. Often, large degree of freedom component-level optimization cannot be performed when system-level optimization is considered.

This paper is organized as follow. In Section 2, a model is derived for the two-winding transformer. The scaling laws are then defined in Section 3. The scaled design process is considered in Section 4. In Section 5, the meta-model which represent the transformer optimum designs as function of rated power, frequency, and current density is obtained. Finally, Section 6, concludes the work of this paper.

2. Two-Winding Transformer Model

To explore scaling laws, a simplified two winding, core type transformer shown in Fig. 1. The α-winding (lighter orange) is wound on the left leg and the β-winding (darker orange) is wound on the right leg. For simplicity, the two windings are assumed to have the same dimensions and the clearances between the windings and the core are neglected; therefore,

$$w_\alpha = w_\beta = \frac{w_{ci}}{2} \tag{1}$$

and

$$h_\alpha = h_\beta = \frac{h_{ci}}{2} \tag{2}$$

where w_α, w_β, and w_{ci} are the widths of α-winding, β-winding, and core interior window respectively and h_α, h_β, and h_{ci} are the heights of α-winding, β-winding, and core interior window respectively.

Prior to considering scaling, it is useful to define and describe several key parameters of the transformer. The rms current density for winding j is expressed as

$$J_j = \frac{N_j I_j}{A_j k_{pf}} \tag{3}$$

where N_j and I_j are winding x number of turns and rms current respectively, k_{pf} is the winding packing factor, and A_j is the area of winding j. The winding area is represented by

$$A_j = w_j h_j \tag{4}$$

ISSN 2522-6967

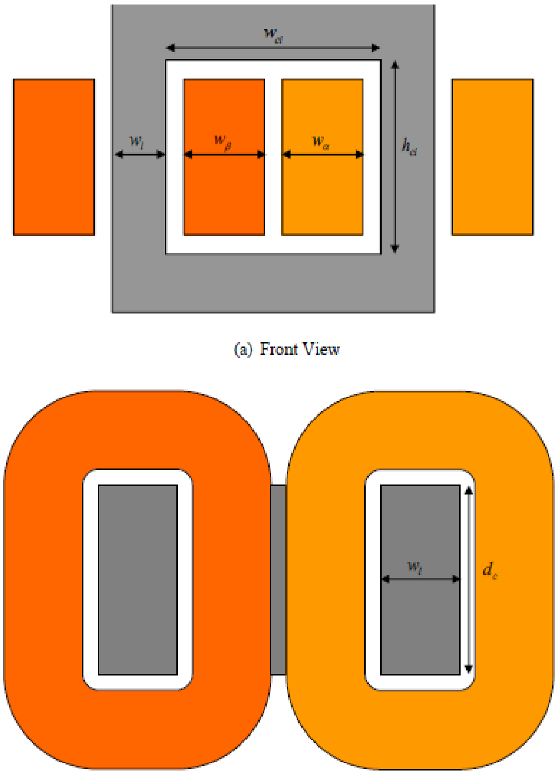

(a) Front View

(b) Top View

Fig. 1: Two Winding Core Type Transformer Cross-Section

In the work herein, the α-winding and β-winding rms current densities are assumed to be equal

$$J_\alpha = J_\beta = J \tag{5}$$

The mass is another quantity of interest and it is given by

$$M = 2d_c w_l \left(w_{ci} + h_{ci} + 2w_l \right) \rho_c + \sum_{j=\alpha,\beta} k_{pf} U_j \rho_{jc} \tag{6}$$

where ρ_c and ρ_{jc} are the mass density of core material and j-winding conductor respectively and U_j is the volume of winding x which is calculated by

$$U_j = h_j w_j \left(2\left(d_c + w_l \right) + \pi w_j \right) \tag{7}$$

Typically, it is convenient to utilize a T-equivalent circuit when analyzing transformers. The T-equivalent circuit shown in Fig. 2 is considered herein. Within the circuit, the referred (primed) α-winding rms voltage, rms current and resistance are expressed as

$$V_\alpha^{'} = \frac{N_\beta}{N_\alpha} V_\alpha \tag{8}$$

$$I_\alpha^{'} = \frac{N_\alpha}{N_\beta} I_\alpha \tag{9}$$

$$r_\alpha^{'} = \left(\frac{N_\beta}{N_\alpha} \right)^2 r_\alpha \tag{10}$$

As shown, the leakage flux is neglected in the model considered for scaling. The flux path inside the core is assumed to be the average path. The peak flux density is expressed

$$B_{pk} = \frac{\sqrt{2} N_\beta I_m P}{A_c} \tag{11}$$

where I_m is the rms magnetizing current, A_c is the core cross-sectional area, and P is the core permeance which is calculated using the relationship

$$P = \frac{\mu A_c}{l_p} \tag{12}$$

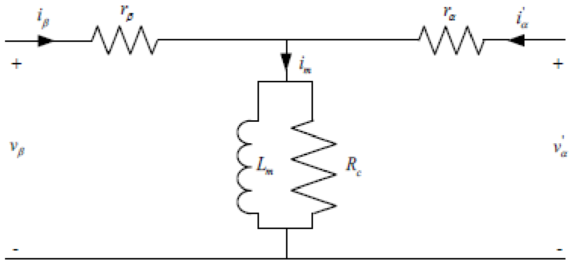

Fig. 2: Transformer T-equivalent Circuit

In (12), μ is the core material permeability and l_p is the flux path average length inside the core which is expressed as

$$l_p = 2\left(w_{ci} + h_{ci} + 2w_l \right) \tag{13}$$

Neglecting the core loss resistance and the voltage drop on the resistance of the β-winding, r_β; the rms magnetizing current can be approximated

$$I_m = \frac{V_\beta}{\omega_e L_m} \tag{14}$$

where V_β is the rms value of the β-winding terminal voltage, ω_e is the angular frequency of the sinusoidal primary voltage, and L_m is the magnetizing inductance which is defined as

$$L_m = N_\beta^2 P \tag{15}$$

Using (3), (12)-(15) and (11) and simplifying one can approximate the peak flux density using:

$$B_{pk} = \frac{\sqrt{2} P_r}{J_\beta A_c A_\beta \omega_e k_{pf}} \tag{16}$$

where P_r is the transformer rated power.

Typically, the magnetizing current is required to be much less than the rated current. This can be achieved by enforcing this constraint

$$I_m < \frac{P_r}{V_\beta} k_m \tag{17}$$

where k_m is a constant which is much less than 1. Substituting equations (3), (14), and (15) into (17) and simplifying yields

$$J_\beta^2 > \frac{P_r}{\omega_e k_m A_\beta^2 k_{pf}^2 P} \tag{18}$$

ISSN 2522-6967

It is very interesting to consider (17) and (18). Although the magnetizing current is equal to the sum of the α-winding and the β-winding currents as in Fig. 2, its upper limit can be enforced by setting a lower limit on the β-winding current density.

3. Scaling Laws

The objective of this section is to set the stage for the normalization process by defining the normalization base. The goal is to scale all quantities tied to ratings (i.e. dimensions) and not those that are rating independent (i.e. flux density and field intensity).

One can note from the previous section that many of the key constraints can be expressed in terms of current density. This makes the current density a good candidate to be a parameter in the scaling laws (in addition to power and frequency). Another advantage of selecting the current density as a parameter is that it is a general quantity. In other words, a particular value of the current density may correspond to a wide range of transformer sizes, power ratings, and voltage levels.

3.1. Geometrical Quantities

To establish the meta-model, the linear dimensions are scaled as [1]

$$\hat{x} = x / D \tag{19}$$

In (19), the notation '^' denotes the scaled quantity and D is the normalization base. The area and volume are scaled accordingly using [1]

$$\hat{a} = a / D^2 \tag{20}$$

$$\hat{U} = U / D^3 \tag{21}$$

Substituting (19) and (21) into (6), normalized mass is expressed as

$$\hat{M} = 2\hat{l}_c \hat{w}_l \left(\hat{w}_{ci} + \hat{h}_{ci} + 2\hat{w}_l \right) \rho_c + \sum_{j=\alpha,\beta} k_{pf} \hat{U}_j \rho_{jc} \tag{22}$$

where

$$\hat{M} = M / D^3 \tag{23}$$

3.2. Electrical Quantities

It is desired not to scale the flux density when deriving the meta-model. Considering (11), (12), (19), and (20), to keep B_m unscaled the current must be scaled as [1]

$$\hat{i} = i / D \tag{24}$$

From (3), (20), and (24), the current density is expressed

$$\hat{J} = JD \tag{25}$$

The flux linkage associated with winding j is expressed as

$$\lambda_j = N_j \int_{S_j} B \cdot ds \tag{26}$$

where B is the flux density and S_j is the surface.

Since the flux density is not scaled [1], then from (20), the scaled flux linkage can be expressed as

$$\hat{\lambda} = \lambda / D^2 \tag{27}$$

The j-winding instantaneous voltage is calculated using

$$v_j = \frac{l_j N_j}{\sigma a_j} i_j + \frac{d\lambda_j}{dt} \tag{28}$$

where l_j and a_j are the winding j wire length and area respectively, i_j is winding j instantaneous current and σ is the winding conductor material conductivity.

If time is scaled as [1]

$$\hat{t} = t / D^2 \tag{29}$$

then from (1), (2), (5), (10), (11) and (12), the voltage can be expressed in terms of scaled quantities as [1]

$$v_j = \frac{\hat{l}_j N_j}{\sigma \hat{a}_j} \hat{i}_j + \frac{d\hat{\lambda}_j}{d\hat{t}} \tag{30}$$

From which one can observe that voltage is not scaled.

The frequency is the reciprocal of time and therefore, from (29) the frequency is scaled as

$$\hat{f} = fD^2 \tag{31}$$

Since the relationship between the angular frequency and the frequency is

$$\omega = 2\pi f \tag{32}$$

then

$$\hat{\omega} = \omega D^2 \tag{33}$$

From (16), (19), (25), and (33), the flux density is expressed in terms of the scaled quantities as

$$B_{pk} = \frac{\sqrt{2}\hat{P}_r}{\hat{J}_\beta \hat{A}_c \hat{A}_\beta \hat{\omega}_e k_{pf}} \tag{34}$$

where the scaled rated power is defined as [1]

$$\hat{S}_r = S_r / D \tag{35}$$

From (12), (19), and (20) the scaled permeance is

$$\hat{P} = \frac{\mu \hat{A}_c}{\hat{l}_p} \tag{36}$$

where

$$\hat{P} = P / D \tag{37}$$

The constraint on current density (18) can be expressed in terms of scaled quantities

$$\hat{J}_\beta^2 > \frac{\hat{P}_r}{\hat{\omega}_e k_m \hat{A}_\beta^2 k_{pf}^2 \hat{P}} \tag{38}$$

3.3. Voltage Regulation

Due to the winding resistances and leakage inductances, the secondary voltage of a transformer varies with load condition. It is desired in practice to keep this variation within a specified margin which depends on the type of the load and its sensitivity to voltage variations. During normal operation of a transformer, the largest variation in the secondary voltage occurs when the load condition changes from no-load to full-load. Thus, the voltage regulation is defined as the absolute difference between the secondary voltage at full-load and the one at no-load relative to the voltage at no-load:

ISSN 2522-6967

$$\chi = \left| \frac{V'_{\alpha,fl} - V'_{\alpha,nl}}{V'_{\alpha,nl}} \right| \quad (39)$$

To simplify analysis, the leakage inductances are neglected in the initial scaling derivations as shown by the transformer electric equivalent circuit in Fig. 2. The leakage inductances will be accounted for in the future research. In addition, the voltage drop on the primary resistance is neglected at no-load since the magnetizing impedance is relatively large compared to the primary resistance. The magnetizing current is neglected at full-load since it is much smaller than the rated load current as enforced by (17). Therefore, the transformer voltage regulation can be approximated as

$$\chi = \left(r_\beta + r'_\alpha\right)\frac{I'_\alpha}{V_\beta} \quad (40)$$

Using (3), (9), (10), and (40) the voltage regulation can be expressed as

$$\chi = \frac{J_\alpha J_\beta k_{pf}}{\sigma P_r}\left(\frac{A_\alpha}{A_\beta}U_\beta + \frac{A_\beta}{A_\alpha}U_\beta\right) \quad (41)$$

Although voltage is not scaled, the voltage regulation can be expressed in terms of scaled quantifies

$$\chi = \frac{\hat{J}_\alpha \hat{J}_\beta k_{pf}}{\sigma \hat{P}_r}\left(\frac{\hat{A}_\alpha}{\hat{A}_\beta}U_\beta + \frac{\hat{A}_\beta}{\hat{A}_\alpha}\hat{U}_\beta\right) \quad (42)$$

3.4. Loss

Transformer power loss is comprised of transformer winding electrical resistance loss and core loss. The resistive power lost in winding j is calculated using

$$P_{loss\_j} = I_j^2 N_j^2 \frac{U_j}{k_{pf} A_j^2 \sigma} \quad (43)$$

From (3) and (43), the resistive power lost due to winding j may be formulated in terms of the rms current density as

$$P_{loss\_j} = \frac{U_j k_{pf} J_j^2}{\sigma} \quad (44)$$

It is noted that the resistive power loss in both windings are equal since the current density and the winding dimensions are assumed to be the same for both windings. Thus, the total resistive loss is twice that in (44). Expressed in terms of scaled quantities using, (21), (25), and (35) to (44) yields

$$\hat{P}_{loss\_j} = \frac{\hat{U}_j k_{pf} \hat{J}_j^2}{\sigma} \quad (45)$$

Core loss includes hysteresis loss and eddy current loss. To demonstrate the hysteresis loss, Fig. 3 is first considered. At each cycle, the flux density follows the lower path when it is increasing and it follows the upper path when it is decreasing. Therefore, the trajectory of the flux density forms a loop and the area of this loop represents energy lost in the core in form of heat. This lost energy is referred to as hysteresis loss. Typically, the flux density waveform is not a pure sinusoidal function due to the effect of saturation. In the analysis herein, the flux density waveform is assumed to be sinusoidal by neglecting the saturation effect. Thus the hysteresis loss is estimated using

$$P_h = k_h B_{\max}^{\beta_h} f^{\alpha_h} U_c \quad (46)$$

where k_h, α_h, and β_h are the hysteresis loss constants.

The eddy current loss is also approximated using MSE [8]

$$P_e = k_e B_{\max}^2 f^2 U_c \quad (47)$$

where k_e is the eddy current loss constant.

The total core loss is the sum of the hysteresis and eddy current loss; thus,

$$P_{cl} = P_h + P_e \quad (48)$$

To enable scaling of the hysteresis loss in (46), the constant α_h must be an integer. Typically α_h is very close to 1 and thus it is herein approximated to be 1. The hysteresis loss is thus modeled

$$P_h = k_h B_{\max}^{\beta_h} f U_c \quad (49)$$

Applying (21), (31), and (35) to (49) yields a scaled loss

$$\hat{P}_h = k_h B_{\max}^{\beta_h} \hat{f}\hat{U}_c \quad (50)$$

To obtain the scaled eddy current loss, (21), (31), and (35) are substituted into (47) which yields

$$\hat{P}_e = \left(k_e B_{\max}^2 \hat{f}\hat{U}_c\right) f \quad (51)$$

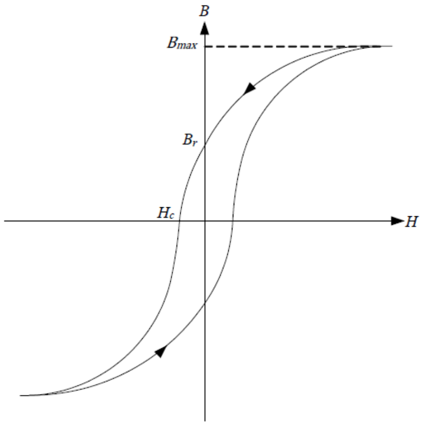

Fig. 3: Magnetizing Curve for a Soft Magnetic Material.

The scaled eddy current loss is a function of the nominal frequency which is undesired in the scaling process. This problem can be addressed by not scaling the frequency or by considering only the hysteresis loss to represent the total core loss. The latest resolution is acceptable in the low frequency range where the hysteresis loss is the dominant core loss. Therefore, if only low frequencies are of interest then only the hysteresis loss is used to represent the total core loss.

3.5. Nominal Design Performance

Before starting the scaled design process, it is useful to explain how one can apply the equations derived thus far to a specific design. If the voltage of winding *j* and transformer rated power are defined, then the winding *j* rated current is calculated using

$$I_j = \frac{P_r}{V_j} \quad (52)$$

If the winding *j* current density is defined and the winding dimensions are known, then the number of turns for the corresponding winding is calculated using (3). After calculating the current density, the transformer performance equations can be evaluated.

3.6. Normalization Base Selection

The selection of the normalization base is a very crucial step. Since transformers are typically defined in terms of the rated power, the base of normalization is selected to be the rated power; thus,

$$D = P_r \tag{53}$$

4. Scaled Design Process

Using the scaled model defined by equations (19)-(51), transformer design is considered to establish Pareto-optimal fronts from which a meta-model can be proposed.

The first step in the design process is to define the design vector as

$$\hat{\boldsymbol{\theta}} = \begin{bmatrix} \hat{J} & \hat{h}_{ci} & r_{ci} & r_l & r_c \end{bmatrix}^T \tag{54}$$

where the ratios r_{ci}, r_l, and r_c are defined as

$$r_{ci} = \frac{\hat{w}_{ci}}{\hat{h}_{ci}} \tag{55}$$

$$r_l = \frac{\hat{w}_l}{\hat{h}_{ci}} \tag{56}$$

$$r_c = \frac{\hat{l}_{ci}}{\hat{h}_{ci}} \tag{57}$$

The second step is to implement the design constraints. The less-than and greater-than functions are used to represent the scaled design constraints. [7]

The first constraint is the constraint on the current density

$$c_1 = \text{gte}\left(\hat{J}, \hat{J}_{mnr}\right) \tag{58}$$

where the minimum required current density $\hat{J}_{mnr}$ is

$$\hat{J}_{mnr} > \sqrt{\frac{\hat{P}_r}{\hat{\omega}_e k_m \hat{A}_\beta^2 k_{pf}^2 \hat{P}}} \tag{59}$$

The second constraint is imposed on the voltage regulation as

$$c_2 = \text{lte}\left(\chi, \chi_{mxa}\right) \tag{60}$$

In the analysis used to develop the scaled model, the magnetic material is assumed to be linear. Therefore, a constraint is imposed on the flux density as

$$c_3 = \text{lte}\left(B_{pk}, B_{mxa}\right) \tag{61}$$

A final constraint is imposed on the total power loss $\hat{P}_l$ as follows

$$c_4 = \text{lte}\left(\hat{P}_l, \hat{P}_{l,mxa}\right) \tag{62}$$

The fitness function used for the performance evaluations is defined as:

$$f(\theta) = \begin{cases} \begin{bmatrix} \frac{1}{\hat{M}} & \frac{1}{\hat{P}_l} \end{bmatrix}^T & c = 1 \\ (c-1)\begin{bmatrix} 1 & 1 \end{bmatrix}^T & c < 1 \end{cases} \tag{63}$$

where c is defined as

$$c = \frac{1}{n_c}\sum_{i=1}^{n_c} c_i \tag{64}$$

and n_c is the number of constraints.

The fitness function is calculated using the Pseudo-code as illustrated in Fig. 4.

```
Step 1- define ω̂, k_pf, the material parameters, χ_mxa, and B_mxa
Step 2-determine the parameters of the design vector in (54)
evaluate transformer dimensions
 evaluate χ using (42) and B_pk using (34)
calculate Ĵ_mnr using the RHS of (38).
3-evaluate c1, c2, c3, and c4 using (58) and (60)-(62).
evaluate c using (64)
4-calculate M̂ using (22)
calculate P̂_loss_j using (45)
calculate P̂_h using (50)
evaluate the total loss P̂_l = 2P̂_loss_j + P̂_h
use (63) to evaluate the fitness function
return to step 2
end
```

Fig. 4: Multi-Objective Optimization Pseudo-Code.

To define the search space of the multi-objective optimization process, the range of the scaled parameters is defined as follows: $10^5 \le \hat{J} \le 10^{20}$ AW/m^2, $10^{-12} \le \hat{h}_{ci} \le 0.1$ m/W, $0.1 \le r_{ci} \le 10$, $10^{-2} \le r_l \le 10$, and $0.1 \le r_c \le 10$, where r_{ci}, r_l, r_c, and are unit-less. The packing factor k_{pf} is selected to be 0.6, the maximum allowed ratio between the magnetizing and the rated current k_m is chosen to be 0.05, the maximum voltage regulation χ_{mxa} is set to 0.05, the upper limit on the flux density B_{mxa} is 1.4 T, the winding conductor is selected to be copper which has a conductivity σ of 5.959*10^7 S/m and a mass density of 8890 Kg/m^3, and the steel material is chosen to be linear with relative permeability μ_r that is equal to 5000, mass density of 7402 Kg/m^3, and the hysteresis loss constants are chosen to be 64.064 J/m^3 for k_h and 1.7991 for β_h. After defining the design parameters, specifications, and constraints, a multi-objective optimization is conducted with a population size of 2000 and for 2000 generations.

5. Multi-Objective Optimization Results

The normalized loss versus normalized mass when the normalized frequency is 3.75*10^{10} HzW^2 is shown in Fig. 5. This value corresponds to a nominal frequency of 60 Hz at rated power of 25 kW. As shown by Fig. 5, the relationship between normalized loss and normalized mass is composed of two linear regions in the log-log scale. Typically, transformers tend to operate around the knee of the magnetization curve. Since the steel material in the work herein is assumed to be linear, the operating point of the transformer will tend to be against the upper flux density limit. Therefore, the region where the designs are against the upper flux density limit (plotted in red) is selected to obtain the meta-model based scaling law.

ISSN 2522-6967

In order to construct meta-model based scaling laws that relate normalized mass and normalized loss to normalized frequency and normalized current density, the multi-objective optimization is conducted at several values of the normalized frequency. Then the values of $\hat{J}$ at each frequency is evaluated and used to obtain plots of the normalized mass versus normalized current density and normalized loss versus normalized current density at each normalized frequencies. These are depicted in Fig. 6 and Fig. 7 respectively.

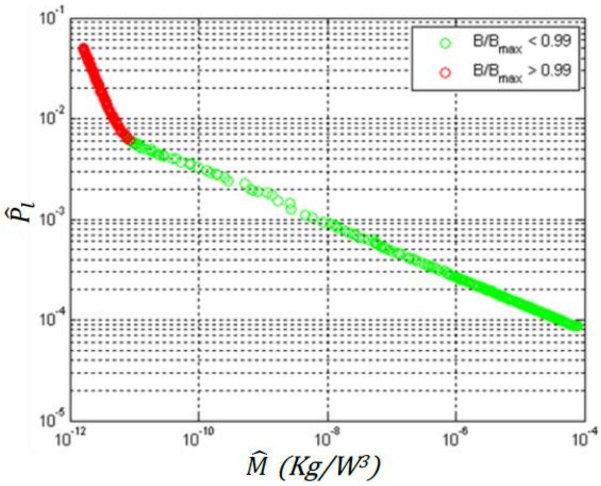

Fig. 5: Normalized Pareto-Optimal Front

By using curve-fitting techniques, a meta-model based scaling law can be constructed from the results shown in Fig. 6 and Fig. 7. The goal is to express the normalized mass and loss as functions of normalized frequency and current density. Relationships of the form

$$\hat{M} = C_M \hat{f}^{\,nfM} \hat{J}^{\,nJM} \tag{65}$$

$$\hat{P}_l = C_l \left(\hat{J}\hat{f}^{\,nfl1} + b_{Jl} \right)^{nJl} \hat{f}^{\,nfl2} \tag{66}$$

are considered herein.

The parameters of the meta-model expressed by (65) and (66) are calculated using curve fitting techniques and listed in Table. 1 The resulting curves are plotted with the original data in Fig. 6 and Fig. 7. Comparing values, one can see that the meta-model obtained by the curve fitting techniques represents the normalized mass and loss for different values of normalized frequency and current density very well.

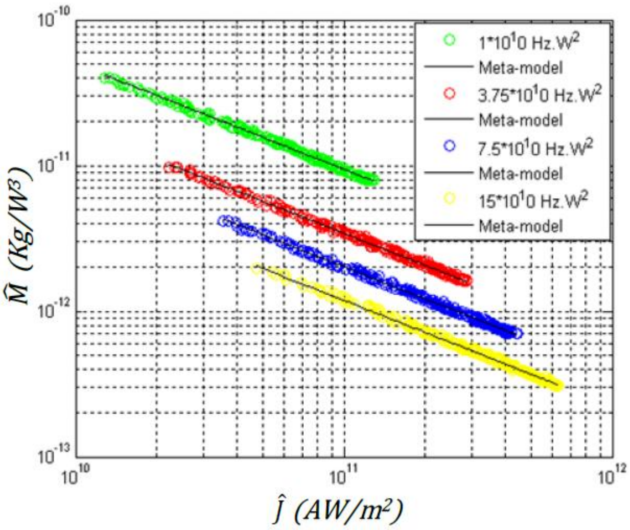

Fig. 6: Normalized Mass versus Normalized Current Density.

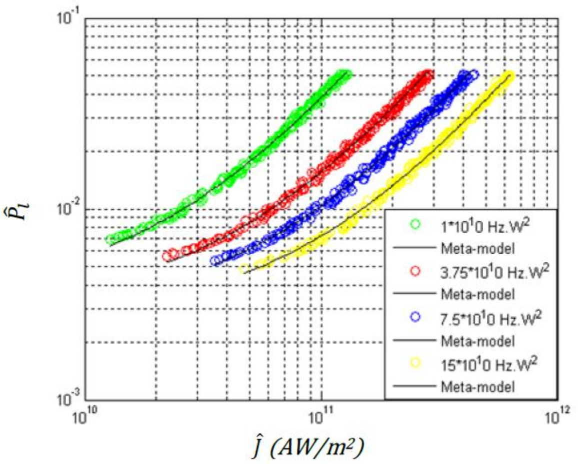

Fig. 7: Normalized Loss versus Normalized Current Density

Table 1. Meta-Model Parameters.

Parameter	Value	Parameter	Value
C_M	$4.0298*10^{4}$	b_{Jl}	$1.9054*10^{5}$
n_{fM}	-0.7656	n_{Jl}	1.5276
n_{JM}	-0.7251	n_{fl1}	-0.5142
C_l	$3.5328*10^{-10}$	n_{fl2}	-0.1069

In practice, it is most useful to express the meta-model in terms of the physical quantities. This can be achieved by applying (25), (33), (35), and (52) to (65) and (66) which yields

$$M = C_M P_r^3 \left(f P_r^2 \right)^{nfM} \left(J P_r \right)^{nJM} \tag{67}$$

$$P_l = C_l P_r \left(J P_r \left(f P_r^2 \right)^{nfl1} + b_{Jl} \right)^{nJl} \left(f P_r^2 \right)^{nfl2} \tag{68}$$

ISSN 2522-6967

Equations (67) and (68) can be used to generate the pareto-optimal front for transformers whith specified power rating, (low) operating frequency, and current density. Thus, for any transformer with a defined operating voltage, rated power, and frequency, pareto-optimal front for that transformer can be obtained by sweeping the range of the current density values.

6. Conclusion

In the work herein, meta-model that capture the optimum designs of wide range of two-winding transformer ratings and frequencies is derived using scaling laws. First, the transformer performance equations are derived in terms of general quantities such as rated power, frequency, and current density. Then scaling laws are applied to the transformer model. Using genetic algorithms, a pareto-optimal front which represent the trade-off between scaled mass and loss is obtained. Using curve fitting techniques, a meta-model which relate the transformer mass and loss to its general parameters is derived.

References

[1] Sudhoff, S.D.; *Shane*, G.M.; Suryanarayana, H. "Magnetic-Equivalent-Circuit-Based Scaling Laws for Low-Frequency Magnetic Devices" *Energy Conversion, IEEE Transactions on,* On page(s): 746 - 755 Volume: 28, Issue: 3, Sept. 2013.

[2] Francisc C. Schwarz, J. Ben Klaasens, Frans B. Gerritse and B. Heijden, "Optimal *Design* of a Class of High Frequency Power Inductors," *IEEE Trans. Magn*, vol. mag-16, no. 5, pp. 752-754, September 1980.

[3] R. A. M. Browne, S. W. H. De Haan, J. B. Klaassens, J. D. Lodder and D. J. *Verheul*, " Computer-Aided Design of Toroidal Air-Core Inductors for High Energy Levels," *IEEE Trans. Ind. Electron.*, vol. 35, no. 2, pp. 329-337, May 1988.

[4] Steurer, M.; Bosworth, M.; Soto, D.; Sudhoff, S.D.; Pekarek, S.D.; Swanson, R.; Herbst, J.; Pish, S.; Gattozzi, A.; Wardell, D.; Flynn, M.; Fikse, T. "Analysis of experimental rapid power transfer and fault performance in DC naval power systems", *Electric Ship Technologies Symposium (ESTS), 2015 IEEE,* On page(s): 433 - 440

[5] S. Chakraborty and M. G. Simoes, "Advanced active filtering in a single phase high frequency AC microgrid," in IEEE 36th Power Electronic Specialists Conference, 2005.

[6] Jain, P.; Pahlevaninezhad, M.; Pan, S.; Drobnik, J. "A Review of High-Frequency Power Distribution Systems: For Space, Telecommunication, and Computer Applications", *Power Electronics, IEEE Transactions on,* On page(s): 3852 - 3863 Volume:

[7] S.D. Sudhoff, Power Magnetic Devices: *A Multi-Objective Design Approach*, IEEE Press/Wiley, Jan. 2013.

[8] A. A. Taher, S. D. Sudhoff, S. D. Pekarek, "Calculation of a Tape-Wound *Transformer* Leakage Inductance Using MEC Model" *Energy Conversion, IEEE Transactions on,* On page(s): Volume: Issue: Feb 2015

ISSN 2522-6967

Analysis of the Influence of EDM Parameters on Material Removal Rate and Electrode Wear Ratio of Al-Cu

Hussam El-Din F. El-Sheikh[a]*and Tarek S. El-Gnemi[b]

[a]Associate Professor, School of Engineering, Libyan Academy, Tripoli – Libya.
[b]M.Sc., National Bureau for Research and development, Mechanical Technology Branch.
*E-mail: hussam.elsheikh2@mail.dcu.ie

ABSTRACT

الهدف من هدا العمل هو إيجاد الظروف المثلى لمتغيرات التشغيل بالتفريغ الكهربي (EDM)،وقد استخدمت سبيكة من الألومونيوم والنحاس كمعدن تشغيل بينما أداة التشغيل كانت من النحاس النقي. استخدمت طريقة (Taguchi) لتصميم عدد من التجارب، والتي أنجزت على آلة (ROBOFORM 2-LC)،ولتحليل تأثير كل متغير على خصائص التشغيل وللتنبؤ بالخيار الأمثل لكل المتغيرات مثل قطبية الشغلة، مدة تفريغ الشحنة، كثافة التيار, كفاءة الأداء. كذلك تم تحليل التباين (ANOVA) باستخدام اختبار (F) للتحقق من أي متغيرات التشغيل المؤثرة على خصائص الأداء وإيجاد النسبة المئوية لكل هذه المتغيرات على معدل إزالة المعدن (MRR)،ونسبة تآكل الآلكترود (EWR). توصل هذا العمل إلى أن كثافة التيار تؤثر بشكل ملحوظ على معدل إزالة المعدن (MRR)، بينما مدة تفريغ الشحنة تؤثر بشكل رئيسي على نسبة تآكل الآلكترود(EWR).

الكلمات المفتاحية: *التشغيل بالتفريغ الكهربائي،طريقة Taguchi،متغيرات التشغيل المثلى، معدل إزالة المعدن (MRR)، نسبة تآكل الآلكترود (EWR).*

The objective of this work is to determine the optimal setting of the process parameters on the electro-discharge machining (EDM), The Aluminium copper cast alloy were used as a work piece and pure copper were used as the electrode. The experiments were done on an FORM 2-LC machine by using Taguchi methodology. The Taguchi method is used to formulate the experimental layout and analyze the effect of each parameter on the machining characteristics, and to predict the optimal choice for each EDM parameter such as polarity, Pulse-on time, discharge currant, and duty factor. Analysis of variance (ANOVA) used F-test to investigate which process parameters significantly affect the performance characteristics and the percent contribution of these parameters on material removal rate (MRR) and electrode ware ratio (EWR). In general, it is found that the discharge currant significantly affects the MRR, while the Pulse-on time mainly affects the EWR.

Key words*: Electrical discharge machining (EDM), Taguchi method, Material Removal Rate (MRR), Electrode Wear Ratio (EWR).*

1. Introduction

Electrical Discharge Machining (EDM) is defined as the non-traditional process of material removal of electrically conductive materials to produce the part with intricate shapes and profiles. This process is done by applying high-frequency pulsed, AC, or DC current to the workpiece through an electrode or wire, which melts and vaporizes the workpiece material. Positioned very precisely near the workpiece, the electrode never touches the workpiece but discharges its potential current through an insulating dielectric fluid (distill water or oil) across a very small spark gap. The spark is reported to be in the range of 8000 to 12000°C, and it vaporizes and melts the workpiece material. This process is used when the workpiece material is too hard, or the shape or location of the detail cannot easily be conventionally machined. This makes many formerly difficult projects more practical and many times it can be the only feasible way to machine a part or material [1].

The electrical discharge machining (EDM) has become an important nontraditional machining process because it can machine the complex shapes, i.e. machining materials like die for manufacturing plastic, which cannot be machined by conventional machining processes [3]. Electrical discharge machining (EDM) is a widely accepted non-traditional material removal process used to manufacture components with intricate shapes and profiles. in the modern world today's, many kind of materials have been invented, so the best parameters need to be find in order to get the best result for machining the materials such as al alloys.

In the machining processes by using electrical discharge machining (EDM), it is involved some parameters setting and there is no fixed setting for all the materials. In traditional practical, the machining condition relying heavily on the operator's experiences or conservative technological data provided by the EDM equipment manufacturers, which is lead to the inconsistent machining performance [3].

A strategy that is done to get the optimal cutting of EDM process planning start from roughing to finishing operations. This process including the number of machining process that is done and its corresponding machining parameters setting for each operation that has been proposed. This method can produce better performance than that achieve by a well skilled operator. A good surface finish, maximum material removal rate and minimum electrode ware ratio can be achieved in less machining time.

To get the perfect result of the machining process by using the EDM it is needed to find the correct parameter setting. Until now, there is no perfect parameter setting for any type of materials. So, it is important to find the best parameter setting before start the machining process in order to achieve the maximum result in its material removal rate (MRR), electrode ware ratio (EWR) and surface roughness (Ra).

In this work, Aluminum Copper cast alloys (Al-Cu) 201.0, which is commonly used for space and aircraft application as well as high performance automotive that require materials with high corrosion resistance and strength [2], has been used as the workpiece material.

The main objective in this work is to optimize the maximum material removal rat, minimum electrode ware ratio and minimum surface roughness.

Also in this work the best combination of certain input parameters to obtain optimum performances will be determined. These parameters are selected because it is significantly can affect the machining performances. Therefore these factors are the controllable factors. The first factor is intensity (I) it represents the maximum value of the discharge current intensity. The intensity values used in the EDM machine programming are power levels of the generator, these corresponding with values of the peak intensity. The second factor is ON time which is defined as the sparks occur time generated during a pulse which to perform the machining process. The third factor is OFF time and defined as the interval time between spark in a single pulse. The fourth factor is polarity of the workpiece. The collection of data is based on these selected factors. This set of data can be used to perform the best result in

ISSN 2522-6967

machining Al-Cu cast alloys 201.0 by using EDM machine. All the data will be used to produce one best setting to obtain the maximum material removal rate (MRR), minimum electrode ware ratio (EWR) and minimum surface roughness (Ra).

2. Literature Review

Various experimental and theoretical conducted on the EDM which is considered as a non-traditional machining process. Jensen et al (1993) and Leu et al (1998) have shown comparisons between non-traditional electroformed electrodes and traditional machined electrodes. Jensen et al have shown a general comparison between electroformed electrodes and machined electrodes but do not give much detail into performance of the electrodes. Research by Leu et al shown a more details comparison of the different electrodes in terms of MRR, EWR and Ra [5,6].

N.F. Petrofes and A.M, (1995) A significant difference in the optimal machining parameters when the machining surface is drastically reduced. According to the experimental results greater the electrode [7]. J.C. Rebelo, A. Dias Morao, D. Kremer and J.L. Lebrun, (1999) Optimization of the complicated multiple performance characteristics can be greatly simplified. The optimal setting of the parameters are determined through experiments planned, conducted and analyzed using the Taguchi method. It is found that EWR reduces substantially, within the region of experimentation, if the parameters are set at their lowest values, while the parameters set at their highest values increase the MRR drastically [8]. Guu Y.H. (2001) proposed the surface morphology, surface roughness and micro-crack of AISI D2 tool steel machined by the electrical discharge machining (EDM) process were analyzed by means of the atomic force microscopy (AFM) technique [9]. C.J. Luis, I. Puertas and G. Villa, (2003) The Taguchi methodology was used to study that influence. The result of the verification test for workpiece surface roughness was a strong confirmation [10]. Guu Y.H. et al, (2003) proposed the electrical discharge machining (EDM) of AISI D2 tool steel was investigated. The surface characteristics and machining damage caused by EDM were studied in terms of machining parameters. Based on the experimental data, an empirical model of the tool steel was also proposed. Surface roughness was determined with a surface profilometer [11]. Kansal, H.K, et al., (2005) study has been made to optimize the process parameters of powder mixed electrical discharge machining (PMEDM). Response surface methodology has been used to plan and analyze the experiments [12]. Pecas, P, et al. (2008) presents on EDM technology with powder mixed dielectric and to compare its performance to the conventional EDM when dealing with the generation of high quality surfaces [13]. S.Prabhu, et al (2008) analyzed the surface characteristics of tool steel material using multiwall carbon nano tube to improve the surface finish of material to nano level [14]. Ozlem Salman, et al (2008) proposed roughness values obtained from the experiments that have been modeled by using the genetic expression programming (GEP) method and a mathematical relationship has been suggested between the GEP model and surface roughness and parameters affecting it. Moreover, EDM has been used by applying copper, copper–tungsten (W– Cu) and graphite electrodes to the same material with experimental parameters designed in accordance with the Taguchi method [15].

From the review, it was concluded that much research was still needed to understand the EDM process fully and there is an evolution on the production of copper tools for EDM that lead to saving costs and manufacturing time, and this copper was the tool material chosen for the research.

There is a consensus that in the initial stage of the discharge and transitory stage of the EDM process the tool wear rate is high. So, the influence of the input parameters on the output parameters needed to be investigated in order to evaluate if they were the sole cause of the EWR optimization. Thus, the investigation in the work reported here was therefore directed to develop techniques for improving the EDM performance of copper tools.

3. Experimental Set-Up and Procedure

Series of experiments was conducted on FORM 2-LC electrical discharge machine to examine the effects of input machining parameters such as for instance intensity (I), pulse on time (t_i), duty factor (ή), and electrode polarity. In the tests the machining characteristics, i.e. the output variables, namely the optimum selection of manufacturing condition is important in manufacturing process as surface quality (Ra), metal removal rate (MRR), and electrode wear ratio (EWR) were measured using different techniques and equipment.

3.1 Workpiece Material

The workpiece material used in this study was Al-Cu cast alloys 2010. Table 1 lists the chemical composition (wt.%) of the material, while Table 2 lists the mechanical properties of the Al-Cu cast alloys 2010 [37].

Table 1: Chemical composition of the Al-Cu cast Alloys 2010.

Elements	Al	Cu	Fe	Mg	Mn	Si	Ti	Zn
Wt. %	91.83	5.22	0.28	0.55	0.43	0.83	0.02	0.05

Table 2: Mechanical properties of the Al-Cu cast Alloys 2010.

Property	**Value in metric unit**		**Value in US unit**	
Density	2.80 x10³	kg/m³	175	lb/ft³
Modulus of elasticity	71	GPa	10300	ksi
Thermal expansion (20 ºC)	34.7×10^{-6}	ºC⁻¹	$19.3*10^{-6}$	in/(in* ºF)
Specific heat capacity	963	J/(kg*K)	0.230	BTU/(lb*ºF)
Thermal conductivity	121	W/(m*K)	841	BTU*in/(hr*ft²*ºF)
Electric resistivity	5.4×10^{-8}	Ohm*m	$5.4*10^{-6}$	Ohm*cm
Heat of fusion	$3.89*10^{5}$	J/kg	167	BTU/lb
Liquidus temperature	649	ºC	1200	ºF
Solidus temperature	571	ºC	1060	ºF
Tensile strength (T6)	485	MPa	70300	psi
Yield strength (T6)	435	MPa	63100	psi
Elongation (T6)	7	%	7	%
Shear strength (T6)	290	MPa	42100	psi
Hardness (T6)	135	HB	135	HB
Solution temperature	516	C°	960	ºF
Aging temperature	154	C°	310	ºF
Aging time	12-20	hrs.	12-20	hrs.

3.2 Electrode Material

The electrode materials investigated in this research was copper with the characteristic shown in Table 3.

Table 3: Electrode material properties [25].

Material	Copper
Composition	99% copper
Density (g/cm)	8.904
Material point (C°)	1083
Electrical resistivity (μΩcm)	9
Hardness	H_B 100

3.3 Dielectric Fluid

The dielectric fluid used in this study was Kerosene.The quality, viscosity and composition of the dielectric are important parameters

ISSN 2522-6967

for guaranteeing optimum spark erosion conditions. Charmilles Technologies uses FLUXELF 2. The dielectric must be changed once per year [18].

3.4 Instruments and Equipment Required

3.4.1 Balance Sensitive

The Balance sensitive used in this study was Balance Electronic Model EUROPE 500. Maximum load is 510 g and its precision is 3 digits.

3.4.2 Spectrometers

Spectrometers model (J.Y 132F) to test the chemical composition for the specimens (Al-Cu) 2010 was used.

3.4.3 Surface Roughness Measurement

Roughness measurement was done using a portable stylus type profilometer, Talysurf (Taylor Hobson, Surtronic 3+). The profilometer was set to a cut-off length of 0.8 mm, filter 2CR, and traverse speed 1mm/s and 4 mm evaluation length roughness measurements, in the transverse direction, on the workpieces were repeated four times and average off the measurements was recorded. The measured profile was digitized and processed through the dedicated advanced surface finish analysis software, Talyprofile, for evaluation of the roughness parameters.

3.5 Experimental Preparation

The raw materials were machined as using conventional methods such as turning and grinding. The electrode were made to a size of 20 mm diameter and length 100 mm as shown Figure 1

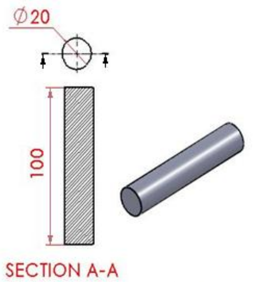

Diameter	Dimensions	Quantity
D	20 $\pm^{0.02}$mm	56

Fig. 1: Electrode design.

The specimens were made to a size of diameter 20 mm and length 20 mm as shown Figure 2. After that numbering all the workpieces and put it in the container box.

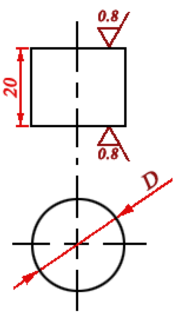

Diameter	Dimensions	Quantity
D	20 $\pm^{0.02}$mm	56

Fig. 2: Workpiece design.

3.6 Experiments Steps

The method adopted in the Kerosene experiments was as follows:

The electrode and specimen were cleaned and dried before every test, then weighed before and after every run. The electrode was tightened into the spindle chuck and passed through the jig. The machining parameters were preset on the control panel generator. Once it had been verified that the ventilation was working, the machine and timer were switched on in the same action. After the specified time had elapsed, the cycle was ended by switching off the machine.

The electrode and specimen were released, and then cleaned with dry compressed air and tissue paper. The electrode and specimen were weighed after machining and the values noted as shown in the Appendix - Table 18. The emergency switch on the machine and the mains supply were both switched off and the machine was cleaned as per scheduling. During the test, the Kerosene level was maintained so that it covered the specimen to a height of (30 – 40) mm, to prevent the spark igniting the Kerosene and the fumes becoming dissolved in it.

3.7 Measurements

The electrodes and specimens were dried by tissue paper and dry compressed air after each experiment and before weighing. Then MRR and EWR were calculated by weighing the specimen and electrode on the digital single pan balance with an accuracy of ± 0.001g and by recording the test time with a stop clock.

4. Experimental Design

Design of experiments (DOE) is used to study the effect of multiple variable simultaneously, which is a powerful statistical technique introduced by R. A. Fisher in England in 1920's [*]. Reacting to Fisher's methods in the design of experiments, Taguchi interpreted Fisher's methods as being adapted for seeking to improve the mean out come of a process. The method could be used not only to improve quality, but also to quantify the improvements made in terms of saving money. The experimental design and analyze of the results can be done with less effort and expenses by using the Taguchi method. Since the method enormously reduces the number of experiments. A well planned set of experiments, in which all parameters of interest are varied over a specified range, is a much better approach to obtain systematic data. Mathematically speaking, such a complete set of experiments ought to give desired results. In many cases, particularly those in which some optimization is required, the method does not point to the BEST settings of parameters [42,43].

4.1 Taguchi Method

Dr. Taguchi of Nippon Telephones and Telegraph Company, Japan has developed a method based on "ORTHOGONAL ARRAY" experiments which gives much reduced "variance" for the experiment with "optimum settings "of control parameters. Thus the marriage of Design of Experiments with optimization of control parameters to obtain BEST results is achieved in the Taguchi Method. "Orthogonal Arrays" (OA) provide a set of well balanced (minimum) experiments and Dr. Taguchi's Signal-to-Noise ratios (S/N), which are log functions of desired output, serve as objective functions for optimization, help in data analysis and prediction of optimum results [44,45].

4.2 The Steps in Taguchi Methodology

Taguchi Method is a process/product optimization method that is based on 8-steps of planning, Table 4, conducting and evaluating results of matrix experiments to determine the best levels of control factors. The primary goal is to keep the variance in the output very low even in the presence of noise inputs. Thus, the processes products are made ROBUST against all variations [43,44].

The Taguchi method can optimize performance characteristics through the settings of process parameters and reduce the sensitivity of the system performance to sources of variation. As a result, the Taguchi method has become a powerful tool in the design of experiment methods, the applications of DOE for EDM to optimizing process parameters to achieve low electrode wear and high machining rate.

ISSN 2522-6967

Table 4: Steps for conducting experimental design [42].

Step	Details
1-	Identify the main function, side effects, and failure mode
2-	Identify the noise factors, testing conditions, and quality characteristics
3-	Identify the objective function to be optimized
4-	Identify the control factors and their levels
5-	Select the orthogonal array matrix experiment
6-	Conduct the matrix experiment
7-	Analyze the data; predict the optimum levels and performance
8-	Perform the verification experiment and plan the future action

As a research, the DOE method has been used to study the performance of the EDM process using Kerosene for Al-Cu cast Alloys 2010 under different control parameters. EDM is a very complicated process. It is very difficult to monitor its working conditions effectively; there is a lack of adequate knowledge on the discharge mechanism. The statistical analysis in this experimental work consists of Taguchi approach that is applied to find the optimal combinations and the optimal parameter design; computer simulations are performed to show the control performances of operating parameters [45, 46].

4.3 Improving EDM Performance Based on the Taguchi Method

The definition of performance characteristics such as lower-the-better, higher-the-better, and nominal-the-better contains a certain degree of uncertainty and vagueness. Therefore, optimization of the performance characteristics with Taguchi method has been considered in this research.

Experimental design methods are too complex and not easy to use. Also, a large number of experiments have to be carried out as the number of the process parameters increases. To solve this important task, the Taguchi method uses a special design of orthogonal array to study the entire parameter space with only a small number of experiments. The experimental results are then transformed into a signal-to noise (S/N) ratio. The S/N ratio can be used to measure the deviation of the performance characteristics from the desired values. Usually, there are three categories of performance characteristics in the analysis of the S/N ratio. The lower-the-better, the higher-the-better, and the nominal-the-better. Regardless of the category of the performance characteristic, a larger S/N ratio corresponds to better performance characteristic. Therefore, the optimal level of the process parameters is the level with the highest S/N ratio. Finally experiment is conducted to verify the optimal process parameters obtained from the parameter design.

Basically, the Taguchi method is designed to handle the optimization of a single performance characteristic [44,46].

4.4 Experimental Design Methods

Design of experiments is a powerful analysis tool for modeling and analyzing the influence of process variables over some specific variable. Taguchi method requires the knowledge about the domain that is examined, since the main function, side effects and failure modes have to be identified. A wrong decision in this step makes all other steps useless. The aim of experimentation is to find the significant machining parameters for the material removal rate (MRR) and electrode wear ratio (EWR) and surface roughness (Ra) and verify the optimal machining parameters. Taguchi methodology were applied to optimize the machining parameters for current intensity I, plus on time ti, duty factor ή, and Workpiece polarity when machining Al-Cu cast Alloys 2010 with copper electrode, three electrodes were used in experiments. Control factors and their levels, to reduce the number of experiments, only the most important factors should be considered. Two or three factor levels can be chosen. In the latter case, the levels should be evenly distributed. The factor levels should be placed very carefully, since the Taguchi method defines the significant and optimal parameters only within the levels.

4.5 Design Factors and Technological Response Variables Analyzed

Electrical discharge machining (EDM) has been used effectively in the machining of hard, high-strength, and temperature-resistant materials. Material is removed by means of rapid and repetitive spark discharges across the gap between the tool and the workpiece. In electrical discharge machining, it is important to select machining parameters for achieving optimal machining performance. Usually, the desired machining parameters are determined based on experience. However, this does not ensure that the selected machining parameters result in optimal or near optimal machining performance for that particular electrical discharge machine and environment. To solve this task in the present research, the Taguchi method is used as an efficient approach to determine the optimal machining parameters in the electrical discharge machining process. Solid copper electrodes with outer diameter of 20 mm were used. The schematic diagram of the experimental set-up is shown in Figure 3. The workpiece and electrode were separated by a moving dielectric fluid (Kerosene). In the experiments, kerosene was used as the dielectrics for comparison. Machining experiments for determining the optimal machining parameters were carried out by setting:

(A) Polarity (-,+) of the workpiece,

(B)A pulse-on time in the range of (800, 1600, 2400) μsec,

(C)A discharge current in the range of (9, 12.5, 23) A, and

(D)A duty factor in the range of (0.5, 0.8, 0.95).

The Four initial parameters and three levels, which were related to the EDM working conditions, as in Table 5, which presents the relationship between the design factors and their corresponding selected variation levels: workpiece polarity, pulse-on time, discharge current and duty factor.

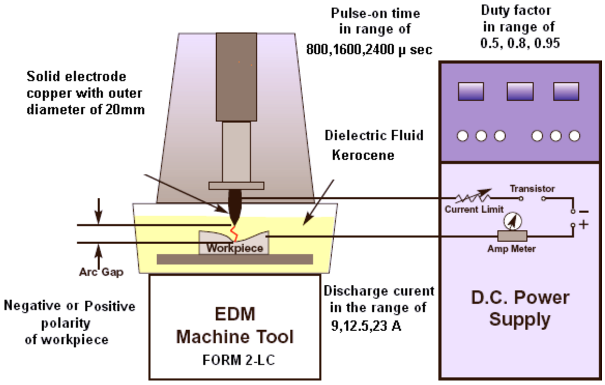

Fig.3: Schematic diagram of the EDM experimental arrangement.

Table 5: Machining parameters and their levels

Symbol	Control factor	Level			Observed values
		1	2	3	
		Minimum	Intermediate	Maximum	
A	Workpiece polarity	Negative	Positive	-	1. MRR 2. EWR 3. Ra
B	Pulse on time, μsec.	800	1200	2400	
C	Discharge current, A	9	12.5	23	
D	Duty factor	0.5	0.8	0.95	

ISSN 2522-6967

4.6 Calculation of the Optimal Control Parameters

The use of the Taguchi approach to determine the machining control parameters with optimal machining performance in the EDM process is illustrated in Figure 4 [46].

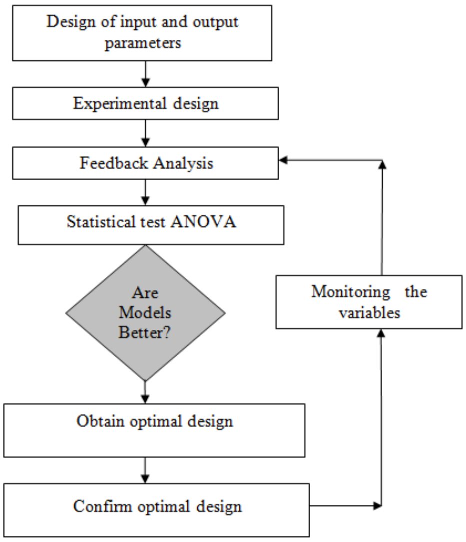

Fig. 4: Procedure of the experiments

4.7.1 Orthogonal Array (OA) Experiment

The experimental procedure using the Taguchi approach can be explained as follows:

(a) The number of factors and interactions to be considered in the experiment and the number of levels of the factors were found.

(b) The appropriate orthogonal array was selected (OA) to:-

- The required degree of freedom Design Of Experiments (DOF) from the factors and interactions was determined, the degrees of freedom of a factor are one less than the number of levels of the factor. The DOF of a particular orthogonal array is obtained by the sum of the individual DOF for each column in the array [47,48].
- The appropriate orthogonal array is the one whose DOF is equal to or more than the required DOF of the factors. The smallest array satisfying this requirement is normally chosen for efficiency.

(c) With the appropriate orthogonal array chosen, and the linear graph that fits the relationships of the factors of interest was choose. The factors can then be assigned to the columns of the orthogonal array according to the linear graph.

(d) The experiments and analyses the results was conducted. And a confirmation experiment was run finally by using the results obtained.

Hence, the selection of the appropriate OA, assigning factors to columns and the total degrees of freedom need to be computed, describing each trial condition and deciding the order and repetitions of trial conditions. The total number of DOF needs to be determined to select an appropriate orthogonal array for the experiments. The DOF are defined as the number of comparisons that need to be made to determine which level is better, and specifically how much better it is. A two-level parameter has one degree of freedom. The present analysis does not include the interaction between process parameters, so there are two DOF due to three process variables. The selection of the OA is subject to the condition that the DOF for the orthogonal array should be greater than or at least equal to those for the process parameters. In the present study, the interaction between the machining parameters is neglected. Therefore, there are 11 DOF arising from one two-level machining parameter and three three-level machining parameters in the EDM process. Once the DOF are known, the next step is selecting an appropriate OA to fit the specific task. The DOF for the OA should be greater than or at least equal to those for the process parameters. In this study, a L18 OA was chosen because it has 11 degrees of freedom, more than the 7 degrees of freedom in the machining parameters. This array has 4 columns and 18 rows. Each machining parameter is assigned to a column and 18 machining parameter combinations are required. Therefore, only 18 experiments are needed to study the entire machining parameter space using the L18 OA. The experimental combinations of the machining parameters using this array are shown in Table 6[47, 48].

Table 6: Design of experimental layout using an L18 orthogonal array.

No.	Workpiece Polarity (A)	Pulse-on Time (B)	Discharge Current (C)	Duty Factor (D)
1	1	1	1	1
2	1	1	2	2
3	1	1	3	3
4	1	2	1	1
5	1	2	2	2
6	1	2	3	3
7	1	3	1	2
8	1	3	2	3
9	1	3	3	1
10	2	1	1	3
11	2	1	2	1
12	2	1	3	2
13	2	2	1	2
14	2	2	2	3
15	2	2	3	1
16	2	3	1	3
17	2	3	2	1
18	2	3	3	2

4.7 Signal-To-Noise Ratio

Optimization of the observed values was determined by comparing the S/N ratio, which was also based on the Taguchi method. The higher observed values such as MRR are called "**the higher the better**" (HB), while the lower observed values such as EWR and Ra are "**the lower the better**" (LB). Calculating the deviation of the performance characteristic from the desired value, the S/N ratio η_{ij} for the i^{th} performance characteristic in the j^{th} experiment can be expressed as:

$$\eta_{ij} = 10 \log L_{ij} \cdots\cdots\cdots\cdots \qquad (1)$$

As mentioned earlier, there are three categories of quality characteristics, i.e. the-lower-the-better, the-higher-the-better, and the-nominal-the-better. The loss function of the higher-the-better performance characteristic can be expressed as:

$$\text{HB:} \quad L_{ij} = \frac{1}{n}\sum_{k=1}^{n}\frac{1}{y_{ijk}^2} \quad \cdots\cdots\cdots\cdots (2)$$

On the other hand, the-lower-the-better quality characteristics for the loss function L_{ij} of the lower-the-better performance characteristic can be expressed as:

$$\text{LB:} \quad L_{ij} = \frac{1}{n}\sum_{k=1}^{n} y_{ijk}^2 \quad \cdots\cdots\cdots\cdots (3)$$

Where L_{ij} is the loss function of the i^{th} performance characteristic in the j^{th} experiment, n the number of tests, and y_{ijk} is the experimental value of the i^{th} performance characteristic in the j^{th} experiment at the kth test [43,44,45].

4.8 Statistical Test – Analysis Prediction Confidence

Once the optimal level of the process parameters has been selected, the final step is to predict and verify the improvement of

ISSN 2522-6967

the performance characteristics using the optimal level of the process parameters. The estimated S/N ratio $\acute{\eta}$ using the optimal level of the process parameters can be calculated as:

$$\acute{\eta} = \eta_m + \sum_{i=1}^{q} (\eta_i - \eta_m) \quad \cdots\cdots\cdots\cdots (4)$$

Where η_m is the total mean of the MRR, EWR, Ra, η_i the mean of the MRR, EWR and Ra at the optimal level, and q is the number of the process parameters that significantly affect the performance characteristics. The estimated MRR, EWR and Ra using the optimal machining parameters can then be obtained. Tables8-12show the results of the confirmation experiment using the optimal machining parameters.

4.9 Analysis Of Variance (ANOVA)

The purpose of the ANOVA and the F test(standard analysis) is to investigate which process parameters significantly affect the performance characteristics. This is accomplished by separating the total variability of the performance indexes, which is measured by the sum of the squared deviations from the total mean of the MRR, EWR and Ra, into contributions by each of the process parameter and the error. First, the total sum of the squared deviations SST from the total mean of the MRR, EWR, Ra can be calculated as[48,49]:

4.9.1 Total Variation

$$SST = SSA + SSW \quad \cdots\cdots\cdots\cdots (5)$$

SST=Total Sum of Squares (Total variation).

SSA=Sum of Squares among Groups (Among-group variation).

SSW=Sum of Squares within Groups (Within-group variation).

Total Variation = the aggregate dispersion of the individual data values across the various factor levels (*SST*).

Among-Group Variation = Dispersion between the factor sample means (SSA).

Within-Group Variation = Dispersion that exists among the data values within a particular factor level (*SSW*).

$$SST = \sum_{j=1}^{c} \sum_{i=1}^{nj} (X_{ij} - \bar{\bar{X}})^2 \quad \cdots\cdots\cdots\cdots (6)$$

Where:

SST = Total sum of squares.

c = number of groups (levels or treatments).

n_j = number of observations in group *j*.

X_{ij} = i^{th} observation from group *j*.

$\bar{\bar{X}}$ = grand mean (mean of all data values).

$$Mean\ Square\ Total = \frac{SST}{Degrees\ of\ Freedom}$$

$$MST = \frac{SST}{n-1} \quad \cdots\cdots\cdots\cdots \quad (7)$$

$$SSA = \sum_{j=1}^{c} n_j (\bar{X}_j - \bar{\bar{X}})^2 \quad \cdots\cdots\cdots\cdots (8)$$

Where:

SSA = Sum of squares among groups.

c = number of groups or populations.

n_j = sample size from group *j*.

$\bar{X}_j$ = sample mean from group *j*.

$\bar{\bar{X}}$ = grand mean (mean of all data values).

$$Mean\ Square\ Among = \frac{SSA}{Degrees\ of\ Freedom}$$

$$MST = \frac{SSA}{c-1} \quad \cdots\cdots\cdots\cdots \quad (9)$$

$$SSW = \sum_{j=1}^{c} \sum_{i=1}^{nj} (X_{ij} - \bar{X}_j)^2 \quad \cdots\cdots\cdots\cdots (10)$$

Where:

SSW = Sum of squares within groups.

c = number of groups.

n_j = sample size from group *j*.

$\bar{X}_j$ = sample mean from group *j*.

X_{ij} = i^{th} observation in group *j*.

$$Mean\ Square\ Within = \frac{SSW}{Degrees\ of\ Freedom}$$

$$MSW = \frac{SSW}{n-c} \quad \cdots\cdots\cdots\cdots (11)$$

4.9.2 Test Statistic

In this study, the analysis of variance (ANOVA) and *F*-test were performed to see statistically significant process parameters and the percent contribution of these parameters on MRR, EWR and Ra. Larger *F* value indicates that the variation of the process parameters makes a big change on the performance characteristics.

$$F = \frac{MSA}{MSW} \quad \cdots\cdots\cdots\cdots (12)$$

MSA= mean squares among variances.

MSW=mean squares within variances.

The percentage contribution by each of the process parameter in the total sum of the squared deviations *SST* can be used to evaluate the importance of the process-parameter change on the performance characteristics. In addition, the *F*-test can also be used to determine which process parameters have a significant effect on the performance characteristic. Usually, the change of the process parameter has a significant effect on the performance characteristic when the *F* value is large.

5. Results and Discussions

The optimization of EDM performance requires the maximum material removal rate (MRR), minimum electrode wear ratio (EWR) and good surface finish (Ra) are attained.

The mean effects plots of the S/N ratios for the output measures are obtained using Minitab 15 software. Plots with the steeper slope along with longer lines shows that the factor has significant impact on the output parameter.

5.1 EDM Performance Evaluation

As mentioned earlier, there are four input parameters whose affect EDM performance. Some of these are likely to have a much more significant effect on the output process parameters than others and the first set of experiments was designed using the Taguchi method to determine which parameters could likely improve the EDM performance.

An Ll8 orthogonal array was chosen because the aim of the study was optimization; according to Taguchi this is done using two and three-level parameters. The values for the input process parameters from A to D were allocated using the EDM cut values.

ISSN 2522-6967

The levels of each setting used and results obtained are shown in Appendix - Table 17.

The MRR and EWR results were obtained from the measured values of change in weight. Detailed results are given in Appendix -Table 18. The Ra values were obtained from directly measured data as shown in Appendix -Table 18.

5.2 Analysis of Material Removal Rate (MRR)

The average values of S/N ratios for MRR at different levels are plotted in Figure 5 keeping the objective as "larger is better". In order to study the significance of the parameters in effecting the quality characteristic of interest i.e. Table 7 shows initial machining condition. The comparison of the S/N ratios between the initial machining parameters and the optimal machining parameters is also shown in Table 8. It is shown clearly that the MRR and S/N ratios are greatly improved through this study.

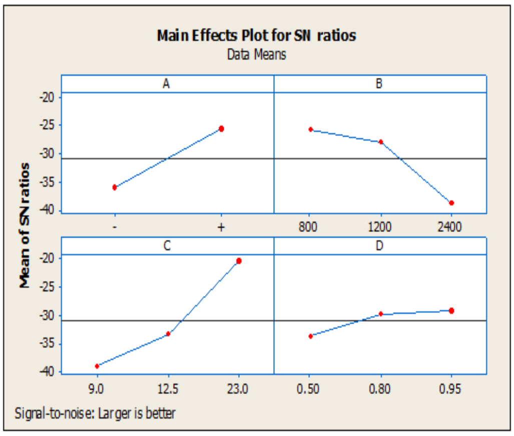

Fig. 5: Mean effect plot for S/N ratios for material removal rate, (MRR).

It is clear from Figure 5 that MRR is maximum at the 2nd level of parameter A, 1st level of parameter B, 3rd level of parameter C and 3rd level of parameter D. The S/N ratio analysis suggests the same levels of the parameters (A2, B1, C3and D3) as the best levels for maximum MRR.

Table 7: Initial machining condition based on result of EWR.

Factors	Level	Level Description	MRR g/min	S/N Ratio
A	2	+	0.2494	-12.0620
B	1	800		
C	3	23		
D	3	0.95		

Table 8: Optimum machining condition: MRR Predicted values.

Factors	Level	Level Description	MRR g/min	S/N Ratio
A	2	+	0.3871	-8.2435
B	1	800		
C	3	23		
D	3	0.95		

5.3 Analysis of Electrode Ware Ratio (EWR)

The average values of S/N ratios for EWR at different levels are plotted in Figure 6 keeping the objective as "minimum is better". In order to study the significance of the parameters in effecting the quality characteristic of interest i.e. Table 9 shows initial machining condition. The comparison of the S/N ratios between the initial machining parameters and the optimal machining parameters is also shown in Table 10. It is shown clearly that the EWR and S/N ratios are greatly improved through this study.

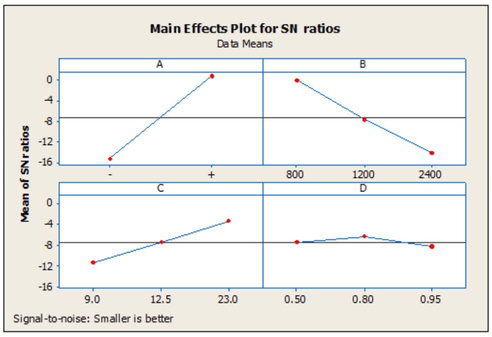

Fig. 6: Mean effect plot for S/N ratios for electrode ware ratio (EWR).

It is clear from Figure 6 that EWR is minimum at the 2nd level of parameter A, 1st level of parameter B, 3rd level of parameter C and 2nd level of parameter D. The S/N ratio analysis suggests the same levels of the parameters (A2, B1, C3and D2) as the best levels for maximum EWR.

Table 9: Initial machining condition based on result of EWR.

Factors	Level	Level Description	EWR%	S/N Ratio
A	2	+	0.204	13.8073
B	1	800		
C	3	23		
D	2	0.8		

Table 10: Optimum machining condition: EWR Predicted values.

Factors	Level	Level Description	EWR%	S/N Ratio
A	2	+	0.1866	14.5817
B	1	800		
C	3	23		
D	2	0.95		

5.4 Analysis of Surface Roughness (Ra)

The average values of S/N ratios for Ra at different levels are plotted in Figure 7 keeping the objective as "smaller is better". In order to study the significance of the parameters in affecting the quality characteristic of interest i.e. Table 11 shown initial machining condition. The comparison of the S/N ratios between the initial machining parameters and the optimal machining parameters is also shown in Table 12. It is shown clearly that the Ra and S/N ratios are greatly improved through this study.

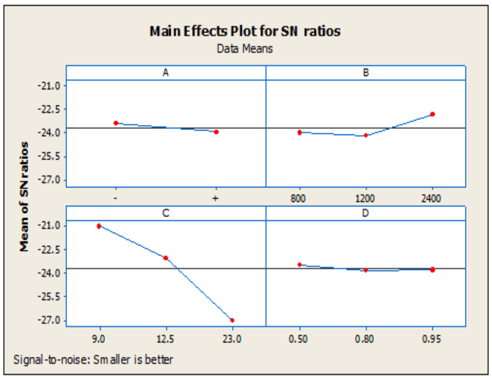

Fig. 7*:* Mean effect plot for S/N ratios for Surface Roughness (Ra).

It is clear from Figure 7 that Ra is minimum at the 1st level of parameter A, 3rd level of parameter B, 1st level of parameter C and 1st level of parameter D. The S/N ratio analysis suggests the same levels of the parameters (A1, B3, C1and D1) as the best levels for maximum Ra.

Table 11: Initial machining condition based on result of Ra.

Factors	Level	Level Description	Ra (µm)	S/N Ratio
A	1	-	9	-19.0848
B	3	2400		
C	1	9		
D	1	0.5		

ISSN 2522-6967

Table 12: Optimum machining condition: Ra Predicted values.

Factors	Level	Level Description	Ra (µm)	S/N Ratio
A	1	-	8.33	-18.4129
B	3	2400		
C	1	9		
D	1	0.5		

5.5 Data analysis

In this study, all the analysis based on the Taguchi method is done by Taguchi DOE software (Minitab15) to determine the main effects of the process parameters, to perform the analysis of variance (ANOVA) and to establish the optimum conditions. The main effects analysis is used to study the trend of the effects of each of the factors, as shown in Figures 5-7. The machining performance (ANOVA-significant factor) for each experiment of the L18 can be calculated by taking the observed values of the MRR as an example from Table 17. Table 13 lists the ANOVA and F test results for MRR. $F_{0.05;\ n1,n2}$ is quoted from "Statistical Tables" [50]. If the calculated F_z values exceed $F_{0.05;\ n1,n2}$ (Table 13), then the contribution of the input parameters, such as discharge currant, is defined as significant. Thus, the significant parameters can be categorized into two levels which are significant and sub significant. All of them are based on the fact that the F_z values are much larger than $F_{0.05;\ n1,n2}$ and denoted as ** and *, respectively. For instance, to evaluate the MRR, the significant parameter is discharge currant. The remaining parameters only slightly contribute to the evaluation of the MRR. Similar calculations are also applied in evaluating the EWR and Ra. Tables 14, 15 and 16 summarized the correlated results, indicating the significant parameters in evaluating the EWR and Ra, respectively, and Figures 8-10 graphically, has been explicate the percent of control Parameters on MRR, EWR and Ra.

Table 13: Analysis of Variance for MRR.

Parameter	DOF	Sum of Square	Mean Square	F	$F_{0.05;n1,n2}$	Contribution (%)
A	1	0.014959	0.014959	14.08*	4.96	20.35
B	2	0.007678	0.003839	3.61	4.10	10.44
C	2	0.034716	0.017358	16.34**	4.10	47.24
D	2	0.005509	0.002754	2.59	4.10	7.49
Error	10	0.010625	0.001062			14.45
Total	17	0.073487				100

Table 14: Analysis of Variance for EWR.

Parameter	DOF	Sum of Square	Mean Square	F	$F_{0.05;n1,n2}$	Contribution (%)
A	1	44.579	44.579	5.59*	4.96	19.08
B	2	77.972	38.986	4.89**	4.10	33.38
C	2	29.324	14.662	1.84	4.10	12.55
D	2	1.948	0.974	0.12	4.10	0.83
Error	10	79.727	7.973			34.13
Total	17	233.55				100

Table 15: Analysis of Variance for Ra.

Parameter	DOF	Sum of Square	Mean Square	F	$F_{0.05;n1,n2}$	Contribution (%)
A	1	5.227	5.227	1.86	4.96	1.12
B	2	16.041	8.021	2.86	4.10	3.45
C	2	412.374	206.187	73.48**	4.10	88.87
D	2	2.271	1.136	0.40	4.10	0.48
Error	10	28.062	2.806			6.01
Total	17	463.976				100

Table 16: Summarization of significant parameters on the machinability of EDM.

Parameter	MRR	EWR	Ra
A	*	*	
B		**	
C	**		**
D			

**Significant parameter;*Sub significant parameter.

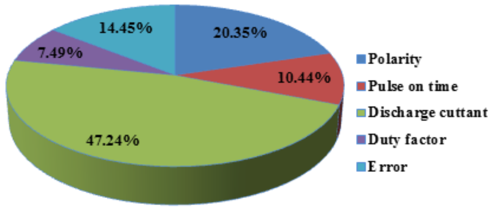

Figure 8: percent of control Parameters on MRR.

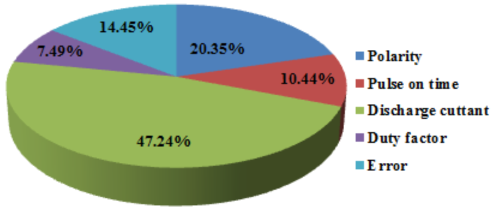

Figure 9: percent of control Parameters on EWR.

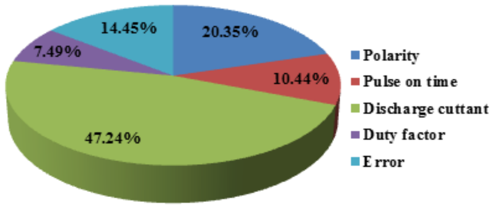

Figure 10: Percent of control Parameters on Ra.

6. Conclusion

From the experiments concerned with electrical discharge in kerosene as a dielectric, it was found that:

(1) Taguchi method indicate optimal experimental from all experiments, the experimental results for the (MRR) number twelve is the best through the higher signal to noise ratio which calculate (-12.0620), and there machining parameters was [Workpiece polarity(+), Discharge current (23 A), Pulse-on time (800 µs) and Duty factor (0.95)]. And the experimental results for the (EWR) number twelve is the best through the higher signal to noise ratio which calculate (13.8073), and there machining parameters was [Workpiece polarity(+), Discharge current (23 A), Pulse-on time (800 µs) and Duty factor (0.8)].

(2) By using Taguchi Analysis Predicted values:

- Improve the MRR from 0.2494 g/min to 0.3871 g/min by increase 55.2% improve the EWR from 0.204% to 0.1866% decreases by 8.5%
- Improve signal to noise ratio (S/N) MRR from -12.0620 to -8.2435 by increase 31% and signal to noise (S/N) EWR from 13.8073to 14.5817 by increase 5.6%

(3) Analysis of variance (ANOVA) investigate the process parameters significantly affect the performance characteristics. The most effective parameters the discharge

currant of EDM mainly affects the MRR. The Pulse-on time largely affects the EWR.

(4) The electrode wear ratio is close to zero at any pulse duration or discharge current because the energy absorbed by the anode is greater than that absorbed by the cathode.

(5) Due the experiments it was found that the surface roughness is quit rough, and to improving the quality of this surface roughness is possible by using rough and finishing machining stages.

REFERENCES

[1] Guitrau, E. P., "The EDM handbook," 1997 by E.P. Guitrau.

[2] William F. S., "Structure and properties of Engineering Alloys" second Edition, 1993 by McGraw-Hill, printed in the United States of America.

[3] Hassan El-Hofy, "Advanced Machining Processes (Nontraditional and hybrid machining processes)," 2005 by The McGraw-Hill Companies, Inc.

[4] *- Nibu Mathew, Dinesh Kumar, Naveen Beri, Anil Kumar, "Study of Material Removal Rate of Different Tool Materials During Edm of H11 Steel at Reverse Polarity", International Journal of Advanced Engineering Technology, Vol. V/Issue II/April-June,2014/25-30

[5] Jensen, K.L. and R. Hovtun. Making electrodes for EDM with rapid prototyping. 2nd European conference of rapid prototyping. 1993

[6] Leu, M.C.,B, Yang, and W. Yao, feasibility study of EDM tooling using metalized stereo lithography models. Technical paper – Society of manufacturing engineers. MR,1998

[7] N.F. Petrofes and A.M. Gadalla, Processing aspects of shaping advanced materials by electrical discharge machining, Adv Mater Manuf Process (1995), pp. 127–153.

[8] J.C. Rebelo, A. Dias Morao, D. Kremer and J.L. Lebrun, Influence of EDM pulse energy on the surface integrity of martensitic steel. J. Mater. Process. Technol. 84 (1999), pp. 90–96

[9] Guu, Y.H.(2001) 'AFM surface imaging of AISI D2 tool steel machined by the EDM process', Applied Surface Science, Vol242, pp 245–250.

[10] C.J. Luis, I. Puertas and G. Villa, Material removal rate and electrode wear study on the EDM of silicon carbide, J Mater Proc Tech 164–165 (2003), pp. 889–896

[11] Guu Y.H. et al, (2003) 'Effect of electrical discharge machining on surface characteristics and machining damage of AISI D2 tool steel', Materials Science and Engineering, Vol 358, pp37-43.

[12] Kansal, H.K, et al., (2005) 'Parametric optimization of powder mixed electrical discharge machining by response surface methodology', Journal of Materials Processing Technology, vol169, pp427–436.

[13] Pecas, P, et al. (2008) 'Electrical discharge machining using simple and powder-mixed dielectric: The effect of the electrode area in the surface roughness and topography', journal of materials processing technology, vol200, pp250–258.

[14] Prabhu.S, et al (2008) 'Nano surface generation in grinding process using carbon nano tube with lubricant mixture', International journal of nanotechnology and application, Vol 2, No 2-3, Pp 149-160.

[15] Ozlem Salman., et al (2008) 'Evolutionary programming method for modeling the EDM parameters for roughnesses, journal of materials processing technology, v200, Pp 347–355.

[16] Tomas J. D., et al "Tool and Manufacturing Engineering Handbook," volume 1, machining, 1983, printed USA.

[17] Victor E. R., et al "Machine Tool Technology,"1984 / McGraw-Hill companies.

[18] www.charmilles.com. (Charmilles Technologies SA .Co)

[19] www.wisegeek.com. (Department of Industrial and Management systems engineering Center for non-traditional manufacturing research University of Nebraska-Lincoln 940 North 17th Lincoln, NE, USA 68588) "Evolution of the EDM process."

[20] Steve F. K., et al "Technology of Machine Tools" Fifth edition, 1979 Glencoe McGraw - Hill.

[21] krar S. F., et al "Machine Tool Operations," 1983, by the Glencoc Division of Macmillan, by McGraw-Hill, Inc.

[22] Nekrashevichand I. G., et al "Present State of The Theoretical Concepts Of The Electric Erosion Of Metals," Electro spark Machining of Metals, volume 3, authorized translation from the Russian (page 17-22).

[23] Chen. S. L., et al "Studies on electric-discharge machining of non-contact seal face grooves," Journal of Materials Processing Technology, 2003 Elsevier B.V. All rights reserved.

[24] Khanra A. K., et al "Electrical Discharge Machining Studies On Reactive Sintered Feal," Vol. 29, No. 3, June 2006, Pp. 277-280. Indian Academy of Sciences.

[25] Lee. S. H., et al "Study of the effect of machining parameters on the machining characteristics in electrical discharge machining of tungsten carbide," Journal of Materials Processing Technology 115 (2001) 344-358, 2001 Published by Elsevier Science B.V., www.elsevier.com.

[26] Puertas. I., et al "A study on the machining parameters optimization of electrical discharge machining," Journal of Materials Processing Technology, 2003 Elsevier Science B.V. All rights reserved www.elsevier.com.

[27] www.me.gatech.edu/jonathan.colton/me4210/chimie.swf. chimie, (Georgia Institute of.

[28] Mohan. B., et al "Effect of SiC and rotation of electrode on electric discharge machining of Al-SiC composite," Journal of Matenals Processing Technology, 2002 Elsevier Science By, All rights reserved, www.elsevier.com.

[29] www.manufacturingcenter.com "Tooling & Production" EDM electrodes a matter of choosing wisely, 2006 by Nelson Publishing, Inc.

[30] Sharma. P.C., "A Textbook of Production Technology" (manufacturing processes), Six Edition 2006, printed in India.

[31] Lin. J. L., et al "Optimization of the electrical discharge machining process based on the Taguchi method with fuzzy logics," Journal of Materials Processing Technology, Vol 102, 2000, pages 48-55.

[32] www.claymore.engineer.gvsu.edu. (Ball State University/2000 W. University Ave./Muncie, 2007 "Engineer on a Disk," 1993-2001, Hugh Jack, pages (369-386).

[33] Dal Koshal., "Manufacturing Engineer's Reference Book," Butterworth-Heinemann 1993 / Printed and bound in Great Britain by Bath Press Ltd, Avon.

[34] Tariq. S. J., et al "Experimental Investigations In to The Performance of Water as Dielectric in EDM," Journal Mechanical Tool Design., Vol. 24 pp 31-43, 1984 /printed in Great Britain.

[35] Jeswani. M. L., "Electrical Discharge Machining In Distilled Water," Wear, 72(1981) pp 81-88, Elsevier Sequoia S.A., Printed in The Netherlands.

[36] www.moldmakingtechnology.com/articles/060201.htm1.(MoldMaking Technology Online is a trademark of Gardner Publications, Inc, 2007. Steve Slate., "Keys to Controlling Electrode Wear," Mold making Technology.

[37] Antoine. D "characterization of electrical discharge machining plasmas", Centre de Recherche en Physique des Plasmas/section de physique, Lausanne, April 2006.

[38] Marafona. J., et al "A new method of optimizing material removal rate using EDM with copper–tungsten electrodes Manufacturing Engineering and Operations Management", University of Nottingham, University Park.

[39] Department of industrial and manufacturing Engineering and technology, Bradley University. Peoria, Illinois, USA. And college of power and Environmental Engineering, wuhan university of technology, wuhan, Hubei, PR china.

[40] Donatas Tijunelis., et al "Manufacturing High Technology Handbook," 1987 By Marcel Decker, Printed in the United States of America.

[41] www.unl.edu/nmrc/Diesinking/surfaceint/surface.com.(Department of Industrial and Management systems engineering/Center for non-traditional manufacturing research /University of Nebraska-Lincoln/940 North 17th /Lincoln, NE, USA 68588, 2003 University of Nebraska-Lincoln) "Surface Integrity."

[42] William Y. fowlkes. Et al "Engineering Methods for Robust Production Design" using taguchi Methods in Technology and Product Development, 1995 by Addison-Wesley Publishing Company.

[43] www.statsoft.com/textbook/stexdes.htm#mixturea, "Experimental Design," (Industrial DOE) / Statistical is a trademark of Stat Soft, pp 20-34, Inc., 1984-2003.

[44] Antony. J., et al "Applications of Taguchi approach to statistical design of experiments," www.emeraldinsight.com/researchregister, International Journal of Productivity and Performance Management Vol. 53 No. 5, 2004.

ISSN 2522-6967

[45] Antony. J., et al "Teaching the Taguchi method to industrial engineers," Volume 50 Number 4 2001 pp, 141-149, www.caledonian.ac.uk.com/ University of Warwick, Coventry, UK.

[46] Klaus. H., et al "Design and Analysis of Experiments," Volume 2 Advanced Experimental Design, 2005 by John Wiley & Sons, Inc, Printed in the United States of America.

[47] Lin. J. L., et al "The use of the orthogonal array with grey relational analysis to optimize the electrical discharge machining process With multiple performance characteristics," International Journal of Machine Tools and Manufacture Volume 42, Issue 2, 2002, Pages 237-244.

[48] Jeya. M. C., "Statistical Quality Control," 2001 by CRC Press LLC/ Printed in the United States of America.

[49] Ozkan Kucuk., "Application of Taguchi method in the optimization of dissolution of ulexite in NH4C1 solutions," Korean J. Chem. Eng., 23(1), 21-27, 2006.

[50] J. Murdoch and J.A. Barnes, "Statistical Tables", Macmillan, London, 1986.

Table 17: Orthogonal array L18 with the levels result and its *S/N* ratio.

No.	Workpiece Polarity (A)	Pulse-on Time (B)	Discharge current (C)	Duty Factor (D)	MRR		EWR		Ra	
					Observed Value of MRR [g/min]	S/N Ratio [dB] Decibel	Observed Value of EWR [%]	S/N Ratio [dB] Decibel	Ra [µm]	S/N Ratio [dB] Decibel
1	-	800	9	0.5	0.0085	-41.4116	4.891	-13.7879	10.8	20.6684-
2	-	800	12.5	0.8	0.0259	-31.7340	5.007	13.9915-	14.1	22.9843-
3	-	800	23	0.95	0.0956	-20.3908	5.096	-14.1445	24.4	27.7477-
4	-	1200	9	0.5	0.0072	-42.8533	5.456	-14.7374	11.1	20.9064-
5	-	1200	12.5	0.8	0.0206	-33.7226	4.824	-13.6681	13.7	22.7344-
6	-	1200	23	0.95	0.0802	-21.9165	5.804	-15.2745	23.1	27.2722-
7	-	2400	9	0.8	0.0022	-53.1515	10.920	-20.7644	10.3	20.0206-
8	-	2400	12.5	0.95	0.0045	-46.9357	4.992	-13.9654	13.2	22.4114-
9	-	2400	23	0.5	0.0231	-32.7277	7.539	-17.5462	19.1	25.6206-
10	+	800	9	0.95	0.0691	-23.2104	0.207	13.6805	12.9	22.2117-
11	+	800	12.5	0.5	0.0521	25.6632-	0.210	13.5556	16	24.0824-
12	+	800	23	0.8	0.2494	-12.0620	0.204	13.8073	20.7	26.3184-
13	+	1200	9	0.8	0.0287	-30.8423	3.387	-10.5963	14	- 22.9225
14	+	1200	12.5	0.95	0.0985	-20.1312	0.815	1.7768	15.9	24.0279-
15	+	1200	23	0.5	0.1215	-18.3084	0.515	5.7638	24	27.6042-
16	+	2400	9	0.95	0.0080	-41.9382	12.624	-22.0239	9	-19.0848
17	+	2400	12.5	0.5	0.0084	-41.5144	7.801	-17.8430	12.5	21.9382-
18	+	2400	23	0.8	0.1510	16.4206-	0.439	7.1507	24.5	-27.7833

WRW: Workpiece Removal weight [grams].
EWW: Electrode Wear Weight [grams].
MRR: Material Removal Rate [mm^3/hr].
EWR: Electrode Wear Ratio.

ISSN 2522-6967

Table 18: Sample for experimental result for the MRR and EWR.

No. of Experiment	Control Factors	Workpiece Weight Before Expr. [g]	Workpiece Weight after Expr [g]	WRW [g]	Average WRW [g]	Electrode Weight Before [g]	Electrode Weight After [g]	EWW [g]	Average EWW [g]	Average MRR [g/min]	Average EWR
	1 A	17.8983	17.6380	0.2603		105.2960	105.2846	0.0114			
1	1 B	17.9120	17.6526	0.2594	0.2576	103.5217	103.5079	0.0138	0.0126	0.0085	4.891
	1 C	17.6424	17.3892	0.2532		112.4561	112.4433	0.0128			
	2 A	18.0245	17.2196	0.8049		0.0392	103.4811	103.5203			
2	2 B	17.8978	17.1322	0.7656	0.7789	0.0462	108.7075	108.7537	0.039	0.0259	5.007
	2 C	17.9545	17.1881	0.7664		0.0316	113.0141	113.0457			
	3 A	2.8642	15.0453	17.9095		0.1317	109.0891	109.2208			
3	3 B	2.8876	14.7823	17.6699	2.8687	0.1647	111.0183	111.1830	0.1426	0.0956	4.970
	3 C	2.8545	15.0036	17.8581		0.1314	113.2570	113.3884			
	4 A	0.2452	17.7859	18.0311		0.0127	105.2719	105.2846			
4	4 B	0.2029	17.6065	17.8094	0.2181	0.012	103.4959	103.5079	0.0119	0.0072	5.456
	4 C	0.2062	17.6579	17.8641		0.011	112.4323	112.4433			
	5 A	0.6305	17.1737	17.8042		0.030	103.4511	103.4811			
5	5 B	0.6232	17.0079	17.6311	0.6198	0.0296	108.6779	108.7075	0.0299	0.0206	4.824
	5 C	0.6059	17.1593	17.7652		0.0302	112.9839	113.0141			
	6 A	2.3651	15.4056	17.7707		0.1367	108.9524	109.0891			
6	6 B	2.4424	15.0223	17.4647	2.4086	0.141	110.8773	111.0183	0.1398	0.0802	5.804
	6 C	2.4184	15.4688	17.8872		0.1418	113.1152	113.2570			
	7 A	0.1884	17.7908	17.9792		0.0238	105.2481	105.2719			
7	7 B	02010	17.4235	17.6245	0.2271	0.0252	103.4707	103.4959	0.0248	0.0022	10.920
	7 C	0.2920	17.3061	17.5981		0.0254	112.4069	112.4323			
	8 A	0.1429	17.7872	17.9301		0.0081	103.4430	103.4511			
8	8 B	0.1249	17.6066	17.7315	0.1362	0.0063	108.6716	108.6779	0.0068	0.0045	4.992
	8 C	0.1409	17.7901	17.9310		0.0061	112.9778	112.9839			
	9 A	0.7054	17.2237	17.9291		0.0528	108.8996	108.9524			
9	9 B	0.6917	16.6068	17.2985	0.6937	0.0519	110.8254	110.8773	0.0523	0.0231	7.539
	9 C	0.6842	16.9778	17.6620		0.0524	113.0628	113.1152			
	10A	17.9193	1.9948	15.9245	2.0759	0.0046	105.2479	105.2525	0.0043		
10	10B	17.6340	2.0358	15.5982		0.0036	103.4704	103.4740		0.0691	0.207
	10C	17.6983	2.1971	15.5012		0.0048	112.4021	112.4069			
	11A	17.6467	1.6298	16.0169		0.0033	103.4430	103.4463			
11	11B	17.7120	1.581	16.1310	1.5657	0.003	108.6716	108.6746	0.0033	0.0521	0.210
	11C	17.7390	1.4864	16.2526		0.0036	112.9778	112.9814			
	12A	17.9648	6.8431	11.1217		0.0193	108.8803	108.8996			
12	12B	17.5426	7.2188	10.3238	7.4833	0.0051	110.8203	110.8254	0.0153	0.2494	0.204
	12C	17.9932	8.3882	9.6050		0.0217	113.0411	113.0628			
	13A	17.8793	0.6326	17.2467		0.0471	105.2008	105.2479			
13	13B	17.4994	1.134	16.3654	0.8619	0.0165	103.4539	103.4704	0.0292	0.02873	3.387
	13C	17.8983	0.8192	17.0791		0.024	112.3781	112.4021			
	14A	17.6939	2.6127	15.0812		0.022	103.4210	103.4430			
14	14B	17.8751	3.2886	14.5865	2.9552	0.0257	108.6459	108.6716	0.0241	0.0985	0.815
	14C	17.6116	2.9643	14.6473		0.0246	112.9532	112.9778			
	15A	17.6567	3.8984	13.7583		0.0116	108.8687	108.8803			
15	15B	17.8402	3.2587	14.5815	3.6459	0.0369	110.7834	110.8203	0.0188	0.1215	0.515
	15C	17.6975	3.7807	13.9168		0.0079	113.0332	113.0411			
	16A	0.2421	17.3214	17.5635		0.0258	105.1750	105.2008			
16	16B	0.2378	17.7847	18.0225	0.2408	0.0154	103.4385	103.4539	0.0304	0.0080	12.624
	16C	0.2425	17.6594	17.9019		0.0501	112.3280	112.3781			
	17A	0.2427	17.5062	17.7489		0.0138	103.4072	103.4210			
17	17B	0.2684	17.7280	17.9964	0.2538	0.0287	108.6172	108.6459	0.0198	0.0084	7.801
	17C	0.2505	17.4230	17.6735		0.0171	112.9361	112.9532			
	18A	6.4884	11.1526	17.6410		0.0170	108.8517	108.8687			
18	18B	2.3512	15.6313	17.9825	4.5319	0.0206	110.7628	110.7834	0.0199	0.1510	0.439
	18C	4.7561	13.1435	17.8996		0.0222	113.0110	113.0332			

Libyan Journal for Engineering Research (LyJER) Volume (1) № (1) March 2017
ISSN 2522-6967

Investigations into the Integration of Low-Cost GPS/INS Sensors

Mustafa Amami

Department of Civil Engineering, Benghazi University, Benghazi, Libya
Tel.: +218-94-523-9326; e-mail: mam8476@yahoo.com

ABSTRACT

Global Positioning System (GPS) provides a method for directly obtaining instantaneous position and velocity estimates using satellites based passive range measurements. GPS is a whole day, all weather, passive, satellite-positioning system. Inertial Navigation System (INS) is a navigation aid system that uses a computer, Inertial Measurement Unite (IMU) that include motion sensors and rotation sensors to continuously calculate the position, orientation, and velocity relative to a known starting point. The integration of GPS/INS can help to overcome the limitations of the two systems providing integrated system better than either on a stand-alone basis. The integration of low-cost INS with dual frequency GPS has been widely studied and the same for the integration of tactical grid INS with low-cost GPS. However, during the last a few years, a number of low-cost GPS\low-cost INS integrated system have been introduced and become more and more common. For such integration level to be used in engineering applications, reliable investigations into the advantages and limitations are still needed and more efforts are required, which will be the focus of this paper.

The methodology followed in this paper for evaluating the integration of low-cost GPS/INS sensors depends on evaluating the two sensors individually and comparing the results with those of the integrated system. The results show that low-cost single frequency GPS receivers are able to provide a comparable accuracy level in both static and kinematic carrier phase differential GPS(DGPS). As for low-cost Micro-Electro-Mechanical System (MEMS) based IMU, the accelerometers have provided instability comparing to gyros. The performance of gyros can be improved based on modelling the linear behaviour of the gyro drift. Tests show that such integration level degrades the precision of the gyro measurements and may not add any improvements to the quality of the individual GPS positioning.

Keywords: Low-cost GPS, Low-cost INS, IMU, Code positioning, Single frequency DGPS, GPS/INS integration. .

1. Introduction

Global Positioning System (GPS) provides a method for directly obtaining instantaneous position and velocity estimates using satellites based passive range measurements. GPS is a whole day, all-weather, passive, satellite positioning system. It provides high accuracy, instantaneous position, and time information across the world. GPS satellites transmit two L-band frequencies, namely: L1 (1575.42MHz) and L2 (1227.6MHz) with carrier wavelengths of approximately 19cm and 24cm, respectively. Two codes are modulated onto the carriers, namely: the Coarse/Acquisition (C/A) code and the Precise (P) code. The first is modulated onto the L1 carrier only with a wavelength of nearly 300m, whereas the second has a wavelength of 30m and modulated onto both L-band frequencies. In addition to these two codes, the system transmits a navigation message including the satellite ephemeris, satellite clock coefficients, satellite health data and ionospheric modeling factors. Almanac is also transmitted to help the receiver in finding out the satellites reducing the searching time. GPS has a number of ground-based control stations for monitoring the satellites, determining the satellite orbits, and uploading the navigation messages [1].

The GPS pseudo-range between receiver and satellite is obtained by matching the satellite code with the internal code generated by the receiver and scaling the time difference by the speed of light. Pseudo-range GPS C/A code observables can provide absolute stand-alone positioning with 3D accuracy of a few meters. Stand-alone GPS C/A code positioning needs at least four satellites to solve the four unknowns of each epoch (the 3D coordinates of the position and the receiver clock time). The limited accuracy of this positioning technique is attributable to different error sources, including: satellite errors (clock and orbit), propagation errors (ionosphere, troposphere, and multipath), and receiver errors (clock, measurements noise, and phase center variation). Stand-alone GPS C/A code positioning can be used for a wide range of engineering applications not requiring high accuracy, such as car navigation, approximate positioning, Unmanned Aerial Vehicle (UAV), mapping for GIS applications, agriculture, disaster relief, emergency services, and tours [2].

The carrier phase observation is formed by stripping the code from the received signal. Carrier phase observation can be measured to the level of 0.01 cycles giving millimeters accuracy. Just the fractional phase with the accumulated integer number of wavelengths can be measured by the receiver as the connection between the satellite and receiver is available. As for the initial total number of integer wavelengths, it is unknown which makes the absolute standalone one epoch based positioning impossible for carrier observations. This initial unknown number is known as the integer ambiguity. Differencing GPS (DGPS) observations can be used for solving this problem providing precise relative positioning. Relative positioning aims at determining the coordinates of an unknown point with respect to a known point or determining the vector between the two points and this requires simultaneous observations at the two points. With DGPS, some of GPS errors are reduced or removed based on the high correlation between these errors over short baselines. Differencing observations can be formed using code or carrier phase taking one of the following forms: single, double and triple differences. Single differences can be formed between two receivers, two satellites, or two epochs. Double differences are formed between any two single differences, whereas triple differences are between the three forms of single differences, including two receivers, two satellites, and two epochs [3].

Carrier phase DGPS can be formed using single frequency (L1) or dual frequency (L1&L2). The dual frequency GPS receivers are high-cost comparing to the single frequency receivers as they can deal with ionospheric error providing accuracy of millimeters level. Such rate of positioning quality can be used in precise applications, such as cadastral surveying, geodetic control, and strictures deformation. Low-cost GPS receivers (single frequency) can also provide carrier phase DGPS positioning based on L1 frequency; but the accuracy level tends

ISSN 2522-6967

to be degraded with increasing the baseline length as the ionospheric error becomes significant. Single frequency GPS receivers have become more and more desirable due to their low cost and used in a wide range of engineering applications, such as mapping, geo-referencing, GIS data collection, aerial and close range photogrammetry, and transportation [4]. Figure (1) shows

examples of low-cost single frequency GPS receivers.

Fig. 1: u-blox GPS receiver.

Inertial Navigation System (INS) is a navigation aid system that uses a computer, motion sensors and rotation sensors to continuously calculate the position, orientation, and velocity relative to a known starting point. The basic idea behind INS is to integrate acceleration and rotation measurements into relative speed of movement and direction of a moving object without the need for external references. Modern IMUs consist of three orthogonally mounted gyroscopes and accelerometers, measuring angular velocity and linear acceleration, respectively. Three magnetometers tend to be added to this system for bounding the significant drift of low-cost gyroscope with time [5].

The accuracy of INS depends mainly on: the initial state accuracy, inertial sensor quality, such as accelerometers and gyros, and calculation accuracy including corrections. Also, the accuracy tends to be a function of the cost which increases hand by hand with increasing the stability and reliability of inertial sensors. INS is a self-contained navigation passive, worldwide, easy to operate and independent system and it can be used in all weather and attitude. However, INS should be provided with initial position and rotations for achieving absolute orientation. When it has been initialized, no more help is needed for navigation. INS has become a necessary request in a great deal of application, such as the aircraft navigation, submarines and ships, tactical and strategic missiles and spacecraft. Current developments in the Micro Electro Mechanical System (MEMS) construction of devices lead to manufacturing undersized and light IMUs opening the doors for such system to be used in more applications, such as human and animal motion capture. Examples of low-cost MEMS based INS are shown in Figure (2).

INS suffers from different type of errors, some of them can be bounded, such as those of acceleration, velocity and initial tilt, and others hard to be bounded including azimuth misalign, leveling gyro drift and azimuth gyro drift. Small errors in the acceleration and angular velocity measurement are cumulated with time to be great errors in position where each position is calculated from the previous calculated position. Therefore, the position must be regularly updated from another navigation system depending on the quality of the sensors used and the accuracy required from the system [5,6].

INS, based on MEMS technology, has become commonly used due to the significant low-cost, tiny size and not including any spinning wheels. As a result, noise, inertial forces and mechanical failures can be avoided. MEMS based gyros have many advantages over conventional gyros, such as power independent memory, very low power consumption, not including bearings, lubricants or fluid, very short start up time,

and very rugged and reliable. On the other hand, they are very sensitive to temperature changes, analogue output requires sampling, high gyro drift rates (20 to 30 degrees/hour), and not accurate enough for higher performance applications [4].

Fig. 2: Microstrain IMU.

The integration between GPS and INS can help to overcome the limitations of the two systems providing integrated system better than either on a stand-alone basis. For example, INS position error drifts with time, whereas GPS solution is time independent. Also, INS outputs are relatively high frequency, whereas GPS solution is low frequency. INS is totally self-contained and autonomous operation, while GPS is dependent on the availability of satellites. Attitude capability is limited in the case of GPS comparing to INS which can provide accurate and high rate attitude data. The need of initialization is another limitation of INS where it just provides relative positioning and rotations. This is not the case with GPS, which can self-initialize in flight. In the integrated system, INS aids GPS to reduce susceptibility to jamming, sensitivity to vehicle manoeuvres, velocity errors and satellite acquisition and reacquisition times. On the other hand, GPS helps INS to reduce propagation of errors with time and to provide initial positioning and rotating. This integration can be carried out in one of three main integration levels, namely: uncoupled, loosely coupled, and tightly coupled [7].

Uncoupled integration is the simplest level of integration as the INS indicated position and velocity are reset at regular intervals of time using the position and velocity estimated by GPS. This method engages minimum changes to both systems and it does not help to enhance the performance and avoid jamming. Also, when GPS is hidden, the quality of positioning solution decreases rapidly [4,6]. The loosely coupled integration is the typical integration of stand-alone INS and GPS. In this integration level, the GPS is run autonomously and, at the same time, INS and GPS integrated solution is enabled. The estimated position and velocity, provided by INS and GPS are compared and the differences are inputted to the estimation filter. The advantage of this approach comes from its redundancy where two navigation solutions are provided: that of stand-alone GPS and the other of GPS/INS integration. This integration approach can be used with any INS and GPS receiver if the necessary number of GPS satellites is available. Also, loosely integration has high flexibility and modularity as well as less computation and complexity due to the independent operation. When GPS is hidden or less than the necessary number of satellites are available, the INS stand-alone solution based on Kalman filter is used to fill in the gap which will drift in time depending on the

ISSN 2522-6967

stability of the accelerometers and gyros used [6,7]. The tightly coupled integration is another GPS/INS integration method, in which no separated GPS navigation solution is given. In this method, a single integration filter is used to combine the raw GPS measurements and those constructed from INS prediction. The filter straight accepts their differences to get the INS error estimates. This integration gives a more accurate solution than the previous methods. This can be attributed to the fact that the GPS observables used in the combination process of the tightly coupled integration are not in the same correlation level of the position and velocity solutions used in the loosely coupled approach [4].

In this paper, the integration of low-cost single frequency GPS with low-cost MEMS based INS will be evaluated in order to investigate whether this integration can help to overcome the limitations of the two systems and provide integrated system better than either on a stand-alone basis. This level of integration has become more and more common and a number of integrated systems have been introduced during the last a few years. Figure (3) show an example of low-cost GPS/INS integrated sensors.

Fig. 3: Xsens low-cost GPS/INS system.

The integration of low-cost INS with dual frequency GPS has been widely studied and the same for the integration of tactical grid INS with low-cost GPS. See [8] & [9]. However, reliable investigations into the integration of the two low-cost level sensors are still needed and more efforts in this area are required, which will be the focus of this paper.

2. Methodology

The methodology followed in this paper for evaluating the integration of low-cost GPS/INS sensors depends on evaluating the two sensors individually, and comparing the results with those of the integrated system Firstly, the low-cost single frequency GPS receiver will be tested individually in different GPS environments with different positioning techniques to investigate the accuracy level can be obtained from such sensor. Secondly, low-cost MEMS based INS will also be tested individually to investigate the gyros drifting rates and the accelerometers performance. After that, the integration of these two low-cost sensors will be evaluated comparing to the stand-alone performance of each sensor. The data used in this paper has been collected as a part of the author's PhD, studied at Nottingham University, UK, 2014, and funded by Benghazi University, Libya.

3. Evaluating Low-Cost Single Frequency GPS Receivers

u-blox GPS receivers are considered to be from the most common low-cost L1 frequency (C/A Code) GPS receivers which are used in a great range of navigation and positioning applications. These receivers can provide an estimated accuracy of 2.5 and 5 m in plan and height, respectively. According to the manufacturer, this small and light receiver, with size of 25.4 mm x 25.4 mm x 3 mm and weight of just 3 grams, has several advantages, such as excellent navigation accuracy even at low signal level, powerful multipath detection and removal, fast time to first fix, high acquisition and tracking sensitivity, ultra-low power consumption and industrial operating temperature range between -40 and 85°C. This is in addition to its ability to be supported by DGPS networks, such as WAAS and EGNOS providing comparable accuracy level. u-blox GPS receiver performs the whole GPS signal processing in one receiver with Patch antenna providing uncomplicated and effortless integration with short time, low-cost and minimum design risks [10,11].

Two common low-cost u-blox GPS receivers (u-blox 4 & u-blox 6) have been chosen in this paper to be tested and evaluated in different GPS environments with different positioning techniques. The two receivers have been connected with dual frequency GPS receiver (Leica GS10) to the same vertical dipole antenna by antenna splitter. Using the same antenna and applying the tests at the same time help the receivers to be evaluated under the same GPS conditions, such as satellite geometry and multipath environment. Leica Geo Office 8.3 software has been used to process the raw data of each receiver as static carrier phase DGPS. This software needs the u-blox files to be converted to RINEX format using, for example, Teqc software. The coordinates achieved from each receiver have been compared to the 'true' coordinates achieved via dual frequency GPS receiver with several hours of static carrier phase DGPS. Different periods of static carrier phase DGPS have been tested to investigate the effect of fixing time on the positioning quality. Figure (4) shows the 3D positioning accuracy as a function of fixing time.

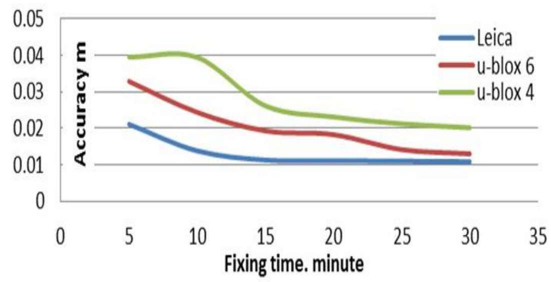

Fig. 4: Static carrier phase DGPS positioning accuracy as a function of fixing time.

It is clear from the figure that the accuracy, in general, is a function of fixing time where the more observations, the better outputs. This can be attributable to the fact that increasing the number of observations for measuring the same variables tends to close the final results to the absolute mean value which is achieved using infinity number of observations. This absolute mean value is equal to the true value when cancelling out the systematic errors. From the figure, the positioning quality provided by the two single frequency GPS receivers is less than that of dual frequency receiver. This can be referred to the following reasons:

1. Dual frequency receivers have the ability to mitigate the effect of ionosphere delay through a linear combination of code or carrier measurements which is named Ionosphere-free.

ISSN 2522-6967

2. Dual frequency receivers has the ability to mitigate the effect of multipath using powerful and complex technique called narrow correlation, whereas the low-cost GPS receivers used in this test are provided with simple mitigation filters and depend mainly on the recommended Patch antenna to eliminate the effect of the signals reflected from low angles.
3. Using dual frequency receiver as a base station allows for better differential processing where the measurements of the two receivers are more precise due to the ionosphere and multipath mitigation techniques.

Table 1: u-blox 6 Vs. u-blox 4: K DGPS & A/C Code.

Positioning technique	u-blox 6(RMSE)			u-blox 4 (RMSE)		
	E m	N m	H m	E m	N m	H m
K DGPS	0.043	0.049	0.084	0.047	0.058	0.109
A/C Code	1.087	1.163	1.972	1.191	1.312	2.400

Also, it can be seen from the figure that the accuracy of the Leica receiver has taken the shortest fixing period to be nearly constant. This is a clear indication about the precision degree of the dual frequency observations comparing to L1 based receivers. With precise measurements and neglected systematic errors, small number of observations can provide results close to the absolute mean value and increasing the number of such precise observations makes the outputs more reliable and the change in the accuracy level tends to unnoticeable.

u-blox 6 has given the second best results close to those of Leica. This is because with carrier phase DGPS, even using single or dual frequency receivers, some GPS errors are eliminated, such as satellite orbit and clocks, and others are mitigated, such as ionosphere and troposphere delays. These last depend on the baseline and the difference in height between the base station and the rover which have been within 20 m and a few mm, respectively in this test. However, the dual frequency receiver is still better due to the reasons mentioned above.

The differences between receivers have been in centimeters level with short fixing time and getting smaller with longer period. This might be because the observations of single frequency receiver are, theoretically, less precise than those of dual frequency due to the ability of the last to mitigate the effect of ionosphere delay significantly and reduce the effect of multipath using narrow correlation technique. As a result, with small number of observations, the differences between the two receivers can be clear. However, with increasing the number of observations, the accuracy of the less precise measurements increases significantly compared to that of precise measurements which might improve slightly. The other theoretical reason behind the less accurate results of the low-cost receivers is the receiver noise which is often significant in such receivers [12]. This GPS source error cannot be reduced or cancelled out with DGPS rounding about one centimeter. However, the receiver noise of the low-cost GPS receivers used in this project has been evaluated, as will be shown later, and found as small as can be neglected.

It is also clear from the figure that u-blox 6 has been better than u-blox 4 to some extent. According to the manufacturer, u-blox 6 receiver has been developed for better positioning but these developments have not been mentioned in the manual. The only clear reason behind these differences in the results might be the number of channels of each receiver, where u-blox 6 is provided with 50 channels comparing to 16 channels for the other receiver. In addition to reducing power consumption, increasing the number of channels helps to speed up satellite acquisition, increase the sensitive for GPS signals and reduce the probability of losing a 3D fix even in urban and dense areas. All of these advantages can help to provide better positioning accuracy [4].

For more investigations, the same data have been processed as kinematic carrier phase DGPS to evaluate the accuracy of each receiver with mobile solution. The position of each epoch has been compared to the antenna position and the Roth Mean Squares Error (RMSE) has been calculated. Moreover, code measurements of the two low-cost receivers have been evaluated to assess the quality of stand-alone code positioning which is one of the main navigation options adopted in low-cost integration systems. Table (1) illustrates the results.

It can be seen from the table that u-blox 6 receiver is better than u-blox 4 in both kinematic carrier phase DGPS and A/C code positioning, which can be attributed to the above mentioned reasons. It is clear from the table that, in general, the plan quality is better than the altitude quality which can be referred to the satellite geometry. Theoretically, the best overall quality can be achieved with 4 satellites distributed with 90 degrees in azimuth and at 40 to 50 elevation angle. Increasing this last helps to achieve better plan quality and leads the vertical quality to be reduced and vice versa [1].

On the other hand, using low elevation satellites tends to be avoided affecting the attitude quality. This is because GPS signal path of the low elevation satellite passes through more atmosphere than the vertical satellite. This is important where the positioning calculation in GPS is based on the assumption that GPS signal travels in a vacuum. Therefore, signals of low elevation satellites have more delay and consequently give less precise results. Also, passing the signal through the atmosphere for longer distances tends to make it noisier and not clean affecting the goodness of data [1, 2, 4]. Satellite geometry can also be the reason behind being the quality in E direction, generally, better than N direction as seen from the table. In GPS, the number of satellites in E-W direction is more than that of N-S direction due to the inclination angle of the satellite orbits. GPS satellite orbits have 55 inclination angles which mean the satellites fluctuate in the area between +55 degree and -55 degree from the Equator [4].

This means that in areas located above this degree, the majority of satellites are locate overhead and on E, W and S directions and a few satellites can be detected in the north with low elevation angles due to the height of the satellite above the Earth. Figure (5) shows the ground track of the satellite with an inclination angle of 45°, Figure (6) shows an example of the satellite distribution over Nottingham University and Figure (7) illustrates how the satellites appear in the North.

ISSN 2522-6967

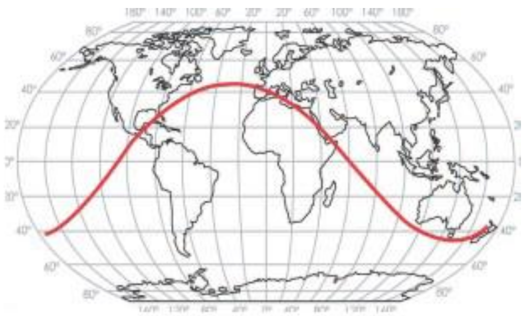

Fig. 5: Satellite ground track

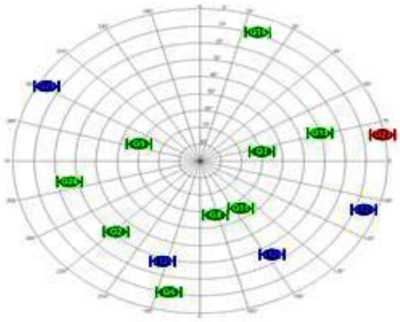

Fig. 6: GPS satellite distribution.

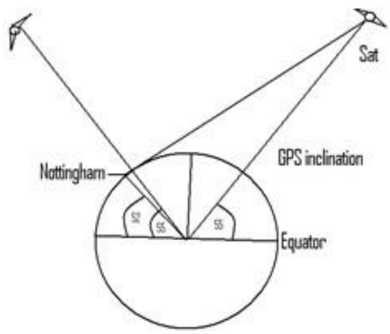

Fig. 7: Satellites in North direction.

Another test has been applied to investigate the possibility of using such low-cost GPS receivers as a base and rover for single frequency DGPS. This can help to reduce the cost significantly where the user just needs one known point within a few Kilometers from the working area and then low-cost static and kinematic carrier phase DGPS can be applied. Two u-blox 6 GPS receivers have been fixed on known points and the raw data has been collected for different periods and static and kinematic DGPS have been applied using GravNav software. Leica dual frequency receiver has also been used as a base station in this test to investigate the effect of using different types of receivers as a base station. Figure (8) and table (2) illustrate the results.

Table 2: Using Leica and u-blox 6 as a base station for kinematic carrier phase DGPS (RMSE).

u-blox receiver.			Leica receiver		
E m	N m	H m	E m	N m	H m
0.037	0.048	0.091	0.042	0.045	0.078

The results show that an accurate single frequency DGPS can be applied using such low-cost single frequency GPS receivers as a rover and a base station, both in static and kinematic positioning. It should be mentioned that when using single frequency receiver as a rover, just L1 measurements are used from the base station file for applying carrier phase DGPS even if dual frequency receiver is used. This logically means there should be no differences in the results between utilizing different receivers as a base station. However, the results illustrate some differences which might be attributed to the differences in the two raw data files where GPS observations tend to be filtered in the receiver before recorded and these filters are different between receivers based on the required quality and applications.

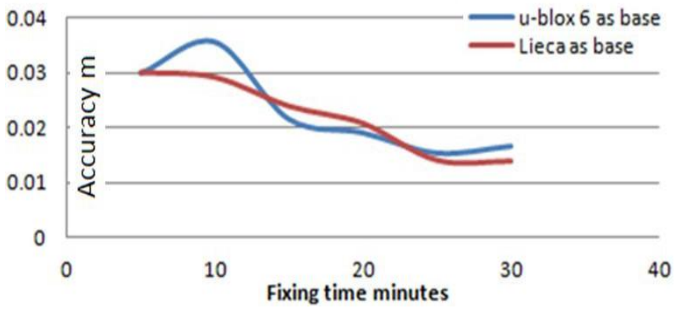

Fig. 8: Static carrier phase DGPS with low-cost GPS receivers as a rover and a base station.

As mentioned above, the receiver noise is one of the GPS error sources not mitigated or cancelled out with the carrier phase DGPS and can be doubled. To investigate the level of these low-cost receiver noise, all errors, except receiver noise, should be cancelled out. To do that, zero baseline test has been applied using GPS simulator. This guarantees that all GPS source errors are cancelled out with static DGPS, except the receiver noise. Zero baseline test using GPS simulator overcomes the outdoor zero baseline tests in terms of cancelling out the antenna noise effect. Two u-blox 6 GPS receivers have been tested for 12 hour to be tested with all possible satellite constellations. Zero baseline test has been carried out between the two receivers, each one as a rover and a base station and the outputs have been comparing to the true position chosen in the simulator. The results show that the noise levels of the two receivers are within 1 to 2 millimeters as illustrates in table 3.

Table 3: u-blox 6 GPS receiver noise level (RMSE) mm.

Receiver	Test 1	Test 2	Test 3
No.1	1.584	1.335	1.530
No. 2	1.437	1.646	1.438

According to [2], in the case of the low cost receiver, the carrier phase observation is expected to be slightly degraded compared to that recorded using a higher grade receiver, perhaps with an increased noise level due to lower grade components. Increasing system noise on the dynamic range of the carrier tracking loop can affect a carrier phase pseudo-range observable giving a greater number of cycle slips due to signal loss and could result in greater noise levels due to the need to increase tracking loop bandwidth.

In conclusion, in this section, low-cost single frequency GPS receivers have been tested to assess their performance as an initial step to be tested with the integration system. The receivers have been tested in different GPS environments with different positioning techniques. Tests show that low-cost GPS receivers, such as those tested, are able to provide a comparable positioning accuracy level in both static and kinematic DGPS solutions. The results show the ability of such sensors to provide accuracy of 1

ISSN 2522-6967

cm with static carrier phase DGPS and a mobile solution with 5 and 10 cm accuracy in plan and height, respectively. Furthermore, the tests show also the high possibility of these receivers to be used as a rover and a base station to carry out low-cost static and kinematic DGPS. In terms of A/C code positioning, 3D accuracy of a few meters can be obtained, deceasing significantly in multipath GPS environments.

4. Evaluating Low-Cost Inertial Navigation System (INS)

The Microstrain 3DM-GX3-25 Inertial Measurement Unit (IMU) used in this paper is inexpensive vibrating structure gyroscopes manufactured with MEMS technology. This sensor, according to the manufacture, can provide attitude heading range of 360 degree about all 3 axes with static accuracy of 0.5 degree and dynamic accuracy of 2 degrees. Also, the sensor with its amazing size and weight can be used in operating temperature between -40o and 70o with a gyro drift rate of 0.25 degree/second. In this section, the sensor will be tested to evaluate the rotations quality and to investigate the possibility of improving the outputs by studying, modeling and correcting the gyro angular drifts.

The sensor has been connected to a data logger and tested several times as stationary for about an hour. Figure (9) illustrates an example of the drifts of Pitch angle, from different tests as a function of time.

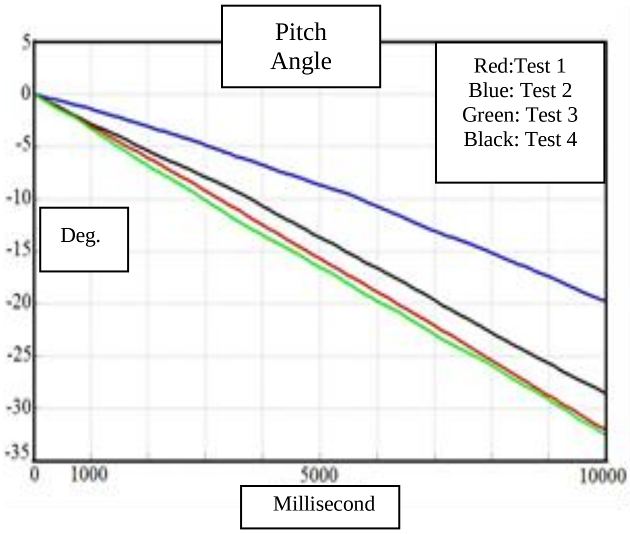

Fig. 9: Low-cost gyro drifts (Pitch angle).

The results show that the Euler angles drift with time, in average, by 0.29 deg./sec, which is close to that mentioned by the manufacturer. This drift rate is good compared with other low-cost IMUs, such as Inertial-Cube3 and Honeywell 3000, which have been tested beside this sensor giving drift rate of nearly 1 deg./sec when stopping the help of magnetometers. It can be seen also that the general trend of drifts, in all tests, increases quasi-linear but with different slops which is useful for modeling and correcting the drifts. Gyros and accelerometers data collected during these tests have also been processed to calculate the relative positioning accuracy level can be provided by the sensor. The results have reflected instability in the performance of accelerometers and considerable random changes in the position although the sensor is stationary.

Based on the linearity of the general tendency of drifting, a simple linear filter has been designed to provide more precise rotations. The idea of the filter is based on determining the average drift rate of each angle using the best fit line and least squares and using this rate as a correction for the following rotations. When the sensor is stationary, the change in Euler angles should be zero. The average drift rate for each angle has been calculated based on the observations of the first 10s and used to correct the rest of data. Results show amazing improvements in the gyro drifts where the errors are reduced to be less than 0.05 deg./sec.

Figure (10) illustrates the drift rate before and after applying the linear filter and Figure (11) shows the results of several tests carried out to investigate the ability of this filter for bounding the gyro drifts.

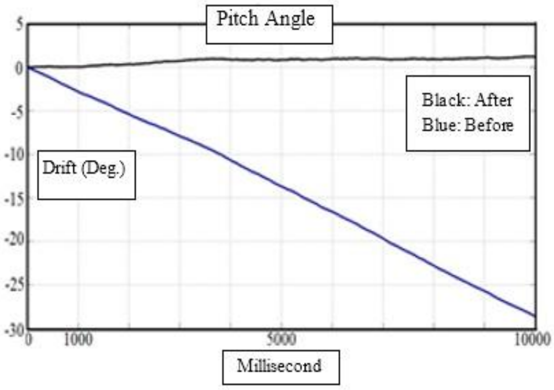

Fig. 10: Gyro drifts before and after applying the linear correction on Pitch angle.

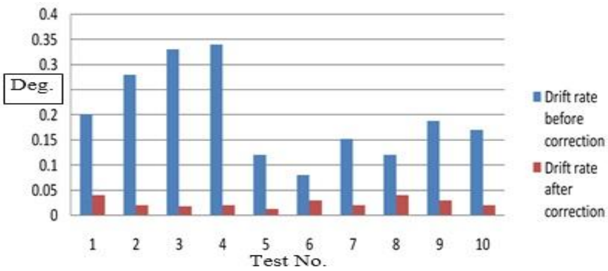

Fig. 11: Drift rate in Pitch before and after filtering

In conclusion, Microstrain 3DM-GX3-25 IMU used in this project has been evaluated in terms of rotation quality, drift rate, and modeling and correcting gyro drifts. Tests show that the sensor can provide drift rate of about 0.29 deg./sec and the angular drift of this sensor is quasi-linear. Instability in the performance of accelerometers has been recorded during the tests providing considerable errors even in stationary case. Simple linear filter has been designed and used to correct the angular drifts reducing the drift rate to round about 0.05 deg./sec.

5. Evaluating The Integration Of Low-Cost GPS/INS Sensors

In this section, the integration between the two low-cost GPS and INS sensors, tested above, is evaluated. NovAtel GPS/INS system, u-blox 6 GPS receiver, Microstrain 3DM-GX3-25 IMU,

ISSN 2522-6967

and data logger have been fixed in the GPS/INS testing van of Nottingham University. NovAtel system is used as a reference where it includes dual frequency GPS receiver and high precise tactical IMU. In addition to comparing the low-cost navigation solution to that of NovAtel, the individual performance of the low-cost GPS receiver as well as IMU will be compared with the low-cost navigation solution to evaluate whether such integration is useful for the two sensors. Kinematic data for about an hour has been collected in different GPS environments such as open sky, between buildings and under dense trees. Also, the GPS antenna has been switched off in some areas for testing the sensors when GPS signals are completely hidden.

The data of NovAtel system have been loaded to GrafNav software to be integrated tightly with the row data of the Nottingham Geospatial Institute base station. This is because tightly coupled (TC) does not need full GPS solution to achieve a full navigation solution and it can provide more precise results than the other integration levels with precise IMU. The same base station data has been used with the low-cost GPS and INS data which have been integrated loosely (LC) and tightly (TC) and compared to NovAtel results. Figure (12) shows examples of the results of low-cost GPS/INS integration compared to NovAtel system.

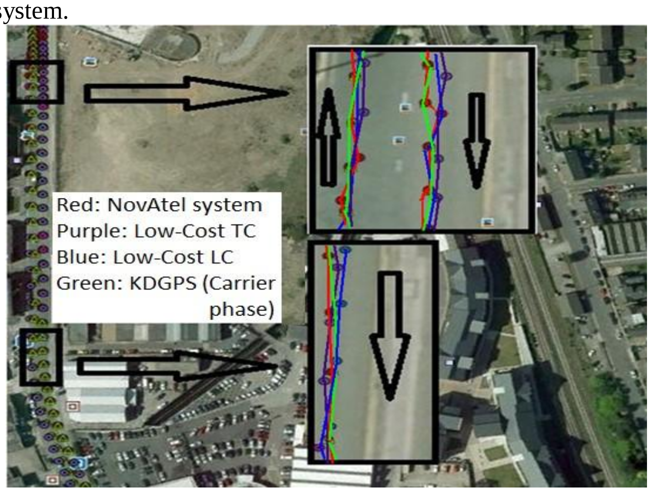

Fig. 12: GPS/INS integration in Open sky.

As seen from Figure (12), in open sky where a significant number of satellites is available, the low-cost GPS/INS integration has provided excellent positioning results close to that of NovAtel using both TC and LC integration levels (RMSE of 3.281 cm and 3.301 cm, respectively). This is because when GPS is available and healthy, the navigation solution in the case of low-cost loosely coupled GPS/INS integration depends completely on GPS carrier phase and partially on code measurements for determining the receiver position and uses the INS measurements to fast the signal reacquisition. In the case of tightly coupled integration, the measurements of GPS and INS are solved together based on the inputted weights to determine the receiver position. Therefore, with enough number of satellites and small INS weights, as in the case of the low-cost IMU used in the test, the effect of the IMU measurements on the tightly coupled navigation solution will be insignificant. Also, the quality of the achieved results can be referred to using 10Hz GPS data rate. This helps to reduce the updating periods of the IMU and consequently better results can be adopted from the navigation solution which takes the IMU data rate.

When the number of satellites decreased due to the dense tress as shown in Figure (13), the loosely coupled navigation solution has degraded comparing to that of tightly solution. This is because when GPS measurements are not adequate for getting 3D solution, loosely coupled solution depends on the IMU measurements smoothed by Kalman filter to fill in the gaps which are degraded rapidly due to the instability of accelerometers and gyros. However, the tightly coupled solution uses the available GPS measurements (even if they are not enough for providing a full GPS solution) with the IMU observations which keep the solution better.

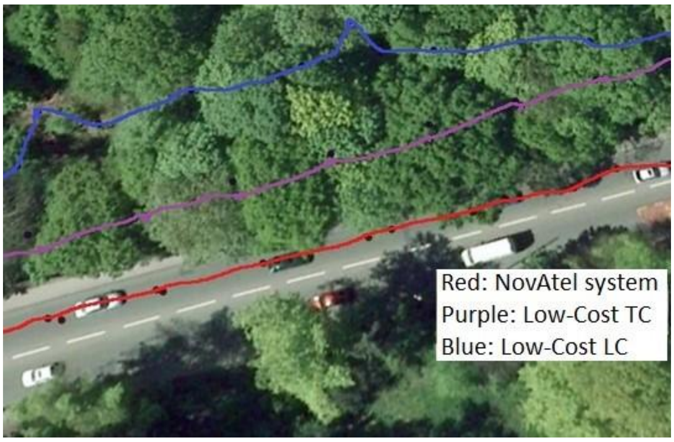

Fig. 13: GPS/INS integration with limited satellites.

When GPS is hidden under very dense tress or when switching the antenna off, the low-cost loosely and tightly solutions are degraded significantly comparing to NovAtel system as shown in Figure (14). This is expectable because of the high and fast drifting rates of the low-cost gyros and accelerometers. These drifts grow even in stationary case reaching several degrees and meters per seconds for the gyros and accelerometers, respectively. In the dynamic case, the drifts tend to be considerable, especially in the case of accelerometers where any vibration in the platform is translated as change in the position.

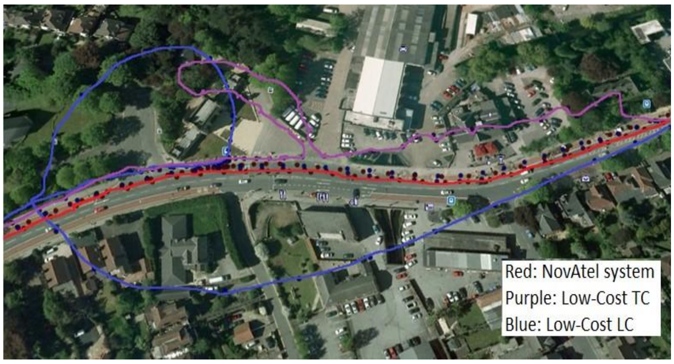

Fig. 14: GPS/INS integration when GPS is hidden.

Moreover, it can be noted that although the two solutions depend mainly on the INS measurements when GPS is hidden, the behavior of the two navigation solutions are completely different. This is because the prediction and smoothing steps in Kalman filter depend completely on the inputted and used measurements which are different in the two cases as GPS and IMU measurements are used together in

ISSN 2522-6967

TC solution. Also, it can be seen that the navigation solution, when GPS is hidden, depends on the trajectory direction, as seen in Figures (15&16). In the straight path, the solution has been acceptable for a good period before start drifting. However, in the case of curvy path, the solution starts drifting directly and significantly. This is because the prediction step in Kalman filter is affected considerably by the behavior of the latest updated measurements and tends to follow the same manners. The higher rotating and horizontal vibrating levels in the case of curvy paths can also affect the quality of the IMU measurements comparing to straight path.

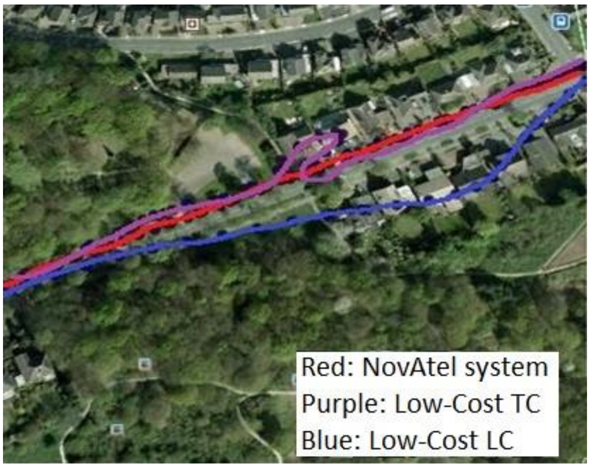

Fig. 15: GPS off (Straight path).

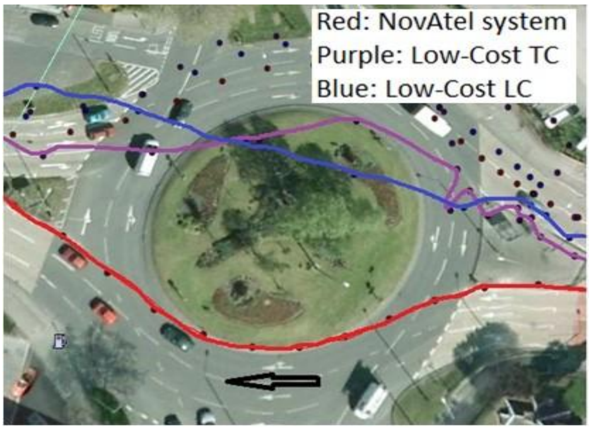

Fig. 16: GPS off (Curvy path).

In curvy paths, the horizontal vibration and suddenly changing in the velocity are translated as changing in the sensor's positions. The gyro drift can also play a role in these errors where the vibrations are considered as angular velocities. These last are integrated and translated as changing in the sensor's directions. The gyro drifts can be seen as limited in terms of value but they have a significant effect on the navigation solution where rotations are used hand by hand with accelerations to determine the relative positioning of the IMU.

When comparing the performance of the low-cost GPS receiver individually with the low-cost navigation solutions, it has been noted that, in open sky as in Figure (12), the individual carrier phase DGPS is very similar to the two navigation solutions of NovAtel and low-cost GPS/INS. This is because in loosely coupled integration, the navigation solution depends completely on GPS measurements to provide a 3D solution and the IMU measurements are just used to help the GPS for faster reacquisition. In the case of tightly coupled, the effects of IMU measurements in the solution is reduced due to the low weights given to the IMU measurements. As for the small differences between the individual GPS and the two navigation solutions, this can be attributed to the synchronizing between the time of individual GPS readings and the time of navigation solution obtained from GrafNav software. This is of course in addition to the differences in the performance of the single and dual frequency GPS receivers.

In GPS/INS integration, GPS is used to correct the change in position provided by the INS. These relative positioning changes depend on the measurements of accelerometers and gyros. Therefore, when correcting the change in the position, values of both acceleration and rotation are corrected. The rotations provided by the gyros, as mentioned above, can be modeled and corrected to be more precise. The rotations achieved from the low-cost navigation solution and those of NovAtel solution have been compared to the rotations determined directly from the sensor and the results are illustrated in Figure (17).

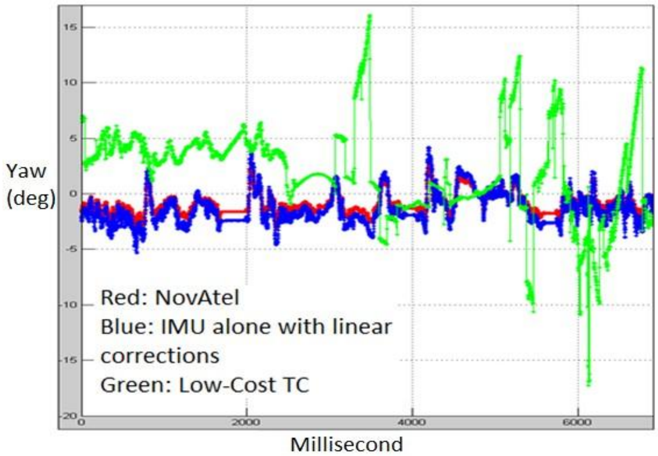

Fig. 17: Yaw angle: Individual IMU and GPS/INS

From the figure, it is clear that the rotations achieved individually from the sensor and those of NovAtel are close to each other and this is not the case with the low-cost navigation solution. This can be attributed to the effect of the ionosphere delay on the GPS measurements where in the case of single frequency GPS receivers, this effect is only mitigated using the base station corrections. This means that the precision of single frequency GPS measurements are less precise than those of dual frequency GPS positioning which use ionosphere-free method. The precision degree of GPS measurements plays a considerable role in the quality of the INS outputs where they are used as a main source for correcting the measurements of the accelerometers and gyros.

In the case of low-cost accelerometers such as those used in this test, even less precise GPS measurements are useful where the quality of the accelerometer measurements is much less precise than single frequency GPS and even A/C code positioning. However, the performance of the IMU in terms of rotations is good as shown in the previous section, especially when modeling and correcting the drifts. Therefore, when using less precise GPS measurements to bound the gyro drifts, no improvement can be seen. The other expected reason behind achieving less precise GPS measurements with the low-cost GPS receiver is the multipath effect where NovAtel GPS receiver has

ISSN 2522-6967

the ability to mitigate such effect using narrow correlation technique.

In conclusion, in this test, the integration of low-cost single frequency GPS with low-cost MEMS based INS has been evaluated in order to investigate whether this level of integration can help to overcome the limitations of the two systems and provide integrated system better than either on a stand-alone basis. Tests show that the main aim behind the integration of GPS/INS is difficult to be obtained in the case of integrating low-cost GPS/INS sensors. Tests show that such integration degrades the precision of the gyro measurements and may not add any improvements to the quality of the individual GPS positioning.

6. Conclusion

In this paper, the integration of low-cost L1-band based GPS receiver with low-cost MEMS based INS has been evaluated in order to investigate the advantages of such integration level over the individual performance of the two sensors. For reliable assessing, the low-cost single frequency GPS receiver and MEMS based INS used in this study have been tested individually to investigate the accuracy level can be obtained from such sensors; then, the integration of these two low-cost sensors has been evaluated comparing to the stand-alone performance of each sensor. The results show that low-cost single frequency GPS receivers are able to provide a comparable positioning accuracy level in both static and kinematic carrier phase DGPS solutions. The results show the capability of such sensors to provide accuracy of nearly 1 cm with static carrier phase DGPS and a mobile solution with 5 and 10 cm accuracy in plan and height, respectively. The tests show also the high possibility of these receivers to be used as a rover and a base station to carry out low-cost static and kinematic DGPS. In terms of A/C code positioning, 3D accuracy of a few meters can be obtained, deceasing significantly in multipath GPS environments.

As for the low-cost MEMS based INS (Microstrain 3DM-GX3-25 IMU), the sensor has been evaluated in terms of rotation quality, drift rate, and modeling and correcting gyro drifts. Tests show that the sensor can provide drift rate of about 0.29 deg./sec and the angular drift of this sensor is quasi-linear. Instability in the performance of accelerometers has been recorded during the tests providing considerable errors even in stationary case. Simple linear filter has been designed and used to correct the angular drifts reducing the drift rate to round about 0.05 deg./sec.

The integration of low-cost single frequency GPS with low-cost MEMS based INS has been evaluated in order to investigate whether this level of integration can help to overcome the limitations of the two systems and provide integrated system better than either on a stand-alone basis. Tests show that the main aim behind the integration of GPS/INS may not be possible to be obtained in the case of integrating low-cost GPS/INS sensors. Tests show that such integration degrades the precision of the gyro measurements and may not add any improvements to the quality of the individual GPS positioning.

References

[1] El-Rabbany, A., 2002. Introduction to GPS: The global positioning system. Artech House.

[2] Hoffman, B., Wellenhof, H. L. and Collins, J., 2001. GPS theory and practice. Springer.

[3] Hofmann-Wellenhof, B., Lichtenegger, H. and Wasle, E., 2007. GNSS global navigation satellite systems: GPS, GLONASS, Galileo, and More. Springer Science & Business Media.

[4] Amami, M., 2015. Low Cost Vision Based Personal Mobile Mapping System. Doctoral dissertation, Nottingham university, UK.

[5] Titterton, D and Weston, J., 2004. Strapdown inertial navigation technology, 2nd ed. London : Institution of Engineering and Technology.

[6] Grewal, M. S., Andrews, A. P. and Bartone, C. G., 2013. Global navigation satellite systems, inertial navigation, and integration. John Wiley & Sons.

[7] Groves, P. D., 2013. Principles of GNSS, inertial, and multi-sensor integrated navigation systems. Artech House.

[8] Brown, A., 1998. High accuracy targeting using a GPS-aided inertial measurement unit. Proceedings of the 54th Annual Meeting. The Institute of Navigation (ION), Denver, CO.

[9] Cina, A., De Agostino, M. and Piras, M., 2009. A full-state low-cost GNSS/INS system for mobile mapping applications. Proceedings of the 6th Symposium on Mobile Mapping Technologies, Presidente Prudente (BRA).

[10] Takasu, T. and Yasuda, A., 2009. Development of the low-cost RTK-GPS receiver with an open source program package RTKLIB. In International Symposium on GPS/GNSS, International Convention Centre, Jeju, Korea. November.

[11] Xiangyu, J., Sentang, W., Xiang, L., Yang, D. and Jiqiang, T., 2010. Research and design on physical multi-UAV system for verification of autonomous formation and cooperative guidance. International Conference of Electrical and Control Engineering (ICECE), IEEE, pp. 1570-1576. June.

[12] Blake, S., 2007. Heave compensation using time-differenced carrier observations from low-cost GPS receivers. Doctoral dissertation, University of Nottingham, UK.

ISSN 2522-6967

Tuning of Velocity PID-Fuzzy Power System Stabilizer by Particle Swarm Optimization

T. Hussein Elmenfy[a]*and Samah Abdelsalam[b]

[a]Electrical and Electronics Engineering Dept, University of Benghazi, Benghazi , Libya
[b] Higher Institute for Technical and Science, Regdalleen, Libya
*Auther e-mail: Tawfiq.elmenfy@uob.edu.ly

ABSTRACT

Power system stabilizer (PSS) is used to damping power system oscillation. It will act as supplementary feedback through the generator excitation system, which produce a component of electrical torque in phase with speed variation. Fuzzy controllers are nonlinear. It is more difficult to set the fuzzy controller gains compared to conventional PID controller. This research proposed velocity (PID-FPSS) its gains are tuned by particle swarm optimization technique (PSO). The objective is to damp local-area oscillation that occur following power system small or large disturbances. The effectiveness of the proposed technique is illustrated by applying the velocity PID-FPSS to a single-machine infinite bus power system that is typically used in the literature to test the performance of power system stabilizers. The simulation has been conducted in MATLAB, SIMULINK (R2013a) package . A comparison between the proposed PID-FPSS and a well-designed robust power system stabilizer (RPSS) confirms the superiority of the proposed technique.

Keywords: single machine infinite-bus system, velocity pid controller, fuzzy logic system, and swarm optimization technique.

1. Introduction

Power system stabilizers are used for many years as supplementary feedback control signal in automatic voltage regulator (AVR) to add damping of the electromechanical oscillations. It will act through the generator excitation system, which produces a component of electrical torque in phase with speed variations to the speed deviation [1, 2].

The parameters of conventional PSS (CPSS) [3] are derived from mathematical model of the plant and designed at one operating condition. This confirm that CPSS is not a suitable for a wide range of operating conditions. In CPSS the parameters are evaluated at particular loading conditions.

The design requirements are considered in [4] introduced both time domain and frequency domain specifications which are initially specified before designing the PSS controller, the optimization based linear control design technique is used to determine the optimal controller parameters. [5] proposed fuzzy expert system, the generator speed deviation and acceleration are chosen as input signals to fuzzy logic power system stabilizer and the desired output is integral square time square error and simulation results shows the superior of proposed technique over CPSS.

Fuzzy logic based PSS for stability enhancement of a two-area four-machine system are designed in [6]. In order to accomplish the stability enhancement, speed deviation ($\Delta\omega$) and active power deviation (ΔP) of the rotor synchronous generator were taken as the inputs to the fuzzy logic controller. These variables take significant effects on damping the generator shaft mechanical oscillations. The stability signals were computed using fuzzy membership function depending on the variables. The design of a proportional, derivative and integral (PID) based power system stabilizer (PSS) introduced in [7], that design carried out using a new Meta heuristic harmony search algorithm (HSA) to optimize the parameters. The design of PID controller is considered with an objective function based on eigenvalue shifting to guarantee the stability of nonlinear plant for a wide range of conditions using HSA. The use of the cost function to minimize the summation of the absolute value is used to design Conventional PSS in [8], and the absolute value is composed of the difference between the square of required compensation phase in excitation system and the square of phase provided by CPSS which should be minimum.

In this paper, a velocity PID-Fuzzy Power System Stabilizer and its gains are tuned by Particle Swarm Optimization is presented. This stabilizer uses the speed deviation, the derivative of the speed deviation and the output electrical -power as inputs to the fuzzy controller (obtained online and assumed to be measured from the output of the plant). This controller is used to provide the necessary damping to the plant.

2. Velocity PID Controller

On form of the controller widely used in the industrial process, control is called a three terms of Proportional-Integral-Derivative (PID) controller [9]. The PID controller are the most commonly used in industrial process (plant) control. The PID controller has the following formula.

$$u(t) = c_{0+}K_p\left[e(t) + \frac{1}{T_i}\int_0^t e(t)dt + T_d\frac{d}{dt}e(t)\right] \qquad (1)$$

Where:

$u(t)$:Control action

K_p: Proportional gain

T_i: Integration time

T_d: Derivative time

c_0: Controller bias

$e(t) = y_{sp} - y_s$= set point- process measurement.

The disadvantages of the controller in eq.(1) are the derivative of the error is subject to the derivative kick and the integral part not compatible to the digital computer. Also set point (y_{sp}) can change instantly in a step change- this cause $e(t)$ to have a step change whenever set point is changed.

The sudden step change in $e(t)$ cause the derivative of $e(t)$ to be infinite- this cause the derivative part to be huge whenever the set point is changed (derivative kick).

To eliminate the derivative kick, the derivative part should be calculated based on the measurement (y_s) rather than the error e(t) as in eq.(2).

$$u(t) = c_0 + K_p \left[e(t) + \frac{1}{T_i} \int_0^t e(t)dt + T_d \frac{d}{dt} y_s(t) \right] \quad (2)$$

As mentioned before, the integral part not compatible with digital computers.

Since, $e(t) = y_{sp} - y_s$ (3)

Then,

$$\frac{d}{dt} e(t) = \frac{d}{dt} y_{sp} - \frac{d}{dt} y_s \quad (4)$$

Under normal operating conditions, when set point is not changing:

$$\frac{d}{dt} e(t) = -\frac{d}{dt} y_s \quad (5)$$

The integral part can be replaced with summation and the derivative part replaced by finite difference.

Then eq.(2) can be rewrite at time (t) as:

$$U(t) = c_0 + K_p \left[e(t) + \frac{\Delta t}{T_i} \sum_{i=1}^{n} e(\Delta t) - T_d \left(\frac{y_s(t) - y_s(t - \Delta t)}{\Delta t} \right) \right] \quad (6)$$

In eq.(6) summation can cause overflow errors on digital computers and (Δt) is sampling time and must be small compared to process response time.

Velocity PID controller form development as:

- Evaluate position form at (t) to get u(t).
- Evaluate position form at $(t - \Delta t)$to get $u(t - \Delta t)$.
- Subtract to get $\Delta u(t) = u(t) - u(t - \Delta t)$

$$u(t - \Delta t) = c_0 + K_p \left[e(t - \Delta t) + \frac{\Delta t}{T_i} \sum_{i=1}^{n} e(\Delta t) - T_d \left(\frac{y_s(t - \Delta t) - y_s(t - 2\Delta t)}{\Delta t} \right) \right] \quad (7)$$

Subtract Eq.(6) from Eq. (7) to get velocity form:

$$\Delta u(t) = K_p \left[e(t) - e(t - \Delta t) + \frac{\Delta t}{T_i} e(t) - T_d \left(\frac{y_s(t) - 2y_s(t - \Delta t) + y_s(t - 2\Delta t)}{\Delta t} \right) \right] \quad (8)$$

The gains to be tuned in velocity PID controller by PSO are $K_p,\ T_i$ *and* T_d.

3. Overview of Particle Swarm Optimization

Particle swarm optimization (PSO) is a population based algorithm and it is collection of particles move in steps of regions and its developed by Dr. Eberhart and Dr. Kennedy in 1995, inspired by social behavior of bird flocking or fish schooling [10].

The features of the PSO are as follows

- The method is based on searching on groups or swarm such as fish schooling and bird flocking.
- PSO is easy to implement as algorithm which is written in a very few lines of code and there are few parameters to adjust.
- PSO learned from the scenario and its used to solve the optimization problems

PSO is a method used for optimization of continuous nonlinear functions. According to the research results for the bird flocking, birds find the foods by flocking not by each individual. Each particle keeps track of its coordinates in the space, which are associated with the best solution. This value is called pbest. Another best value that is tracked by the global version of the particle swarm optimizer is the overall best value, and its location obtained so far by any particle in the group, is called gbest.

The PSO concept is, at each time step, changing the velocity of each particle toward its pbest and gbest location.

The modified velocity of each agent can be calculated using the current velocity and the distance from pbest and gbest as shown below

$$v_i^{k+1} = w_i v_i^k + c_1 rand \times (pbest - s_i^k) + c_2 rand \times (gbest - s_i^k) \quad (9)$$

Where,

v_i^k : Current velocity of particle i at iteration k,

v_i^{k+1} : Modified velocity of particle i,

$rand$: random number between 0 and 1,

s_i^k : current position of particle i at iteration k,

pbest : pbest of particle i,

gbest : gbest of particle i,

w_i : Weight function for velocity of agent i,

c_i : Weight coefficient.

Using the above equation, a certain velocity that gradually gets close to pbest and gbest can be calculated. The current position (searching point in the solution space) can be modified by the following equation.

$$s_i^{k+1} = s_i^k + v_i^{k+1} \quad (10)$$

Figure (1) shows the concepts of modification of a searching point by PSO.

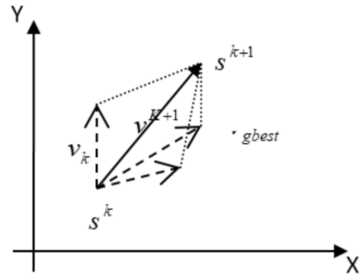

Fig. (1): Concept of modification of a searching point.

ISSN 2522-6967

s^k : current searching point,

s^{k+1} : modified searching point,

v^k : current velocity,

v^{k+1} : modified velocity,

v_{pbest} : velocity based on pbest,

v_{gbest} : velocity based on gbest.

Figure (2) shows a searching concept with agent in a solution space.

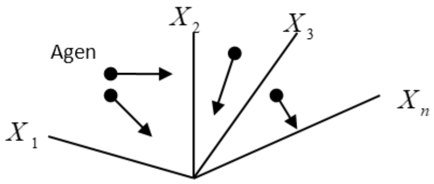

Fig. (2): Searching concept with agent in a solution space by PSO.

The algorithm of PSO

The proposed algorithm of PSO for searching the optimal PID-FPSS gains as follow

1. Initialize the swarm with random positions and velocities.
2. Calculate the fitness function of each particle by:

   $$\frac{1}{2} sum\left(y_{sp} - y_s\right)^2 t \qquad (11)$$

   In this paper (y_{sp}) is actual speed set point and (y_s) is actual speed measurement.
3. Determine the $pbest$ and the $gbest$ positions.
4. Update the velocity of particle using Eq. (9).
5. Update the position of particle using Eq. (10).
6. If the evaluation value of each particle is better than the previous $pbest$, the value is set to $gbest$. If the best $pbest$ is better than $gbest$, the value is set to $gbest$.
7. If the iteration number reaches the maximum iteration number, then go to step 8. Otherwise, go to step 2.

Plot est , $gbest$ and compute the Eq. (11) for the control candidates with optimal values of PID-FPSS gains.

4. Design of Velocity PID-FPSS

The control problem is to design velocity PID controller in eq. (8) as fuzzy logic controller. Velocity PID controller can be converted into a fuzzy controller in a nonlinear manner to enhance robustness.

Consider fuzzy PID controller with three inputs as ($\Delta\omega, \Delta\dot{\omega}$ &ΔP_e) and out put (Δu).

Where:

$\Delta\omega$: Speed deviation (actual speed deviation – actual speed measurement).

$\Delta\dot{\omega}$: Derivative of speed deviation.

ΔP_e: Electrical power deviation.

Δu: Control action

The proposed PID-FPSS is designed as follow [11]:

1. Identification of inputs and output variables as ($\Delta\omega, \Delta\dot{\omega}$, ΔP_e& Δu).
2. Select the membership functions for the inputs and outputs as in Fig. (3).
3. Construction the fuzzy control rules as in table (1).
4. Selection of the compositional rule of inference.
5. Defuzzification method, transformation of fuzzy control set into fuzzy control action.

The center of area method is used for defuzzification. Gaussian membership function to represent the inputs/ output linguistic variables. For each inputs/ output variables, three labels are defined as shown in Fig. (3).

Table 1. Fuzzy rule base of PID-FPSS.

$\Delta\dot{\omega}$ \ $\Delta\omega$	*N*	*Z*	*P*
N	*N*	*N*	*Z*
Z	*N*	*Z*	*P*
P	*Z*	*P*	*P*

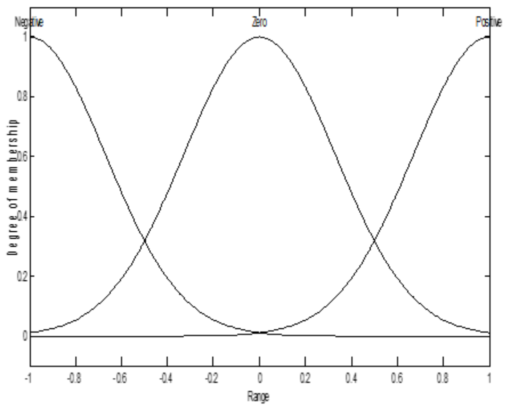

Fig. (3): Fuzzy variable, X_i, three-membership function.

N, Z and P stand for negative, zero and positive. The value X_{max} and X_{min} represent maximum and minimum variation of the input and output signals. The values are selected based on simulation information. A decision table is constructed consisting of 9 rules. An example of the i^{th} rule is:

If Δ ω is N and Δ *P* is P then U is Z

A symmetrical fuzzy rule set is used to describe the PID-FPSS behavior as shown in Table 1.

The procedure to design a FLC can be found in [1].

The PID-FPSS parameters are getting by particle swarm optimization (PSO) are:

$$K_p = 7 \quad ; T_i = 0.32 \quad ; T_d = 0.12$$

5. Implementation to Single Machine Infinite-Bus Model

Figure (4) shows the system under study. It comprises a single machine connected to an infinite bus through a tie line. The machine is equipped with a static exciter. The system is represented by the block diagram proposed by deMello and Concordia [12]. The generator is represented by third-order nonlinear model and the static exciter is represented by a first-order model. The nonlinear equations of the machine are given in [13].

6. Simulation Results

The PSS that is used for comparison is a simple robust power system stabilizer (RPSS) is designed in [13] that can

ISSN 2522-6967

properly function over a wide range of operating conditions and extend the machine load ability. The lead compensator design is achieved by drawing the root loci for a finite number of extreme characteristics polynomials. Such polynomials are obtained, using the kharitonov theorem [13], to reflect wide loading conditions on characteristics equation coefficient.

For a comparison purpose, the system is configured to switch between two control techniques. In order to show the response of PID-FPSS and RPSS as shown in Fig. (4).

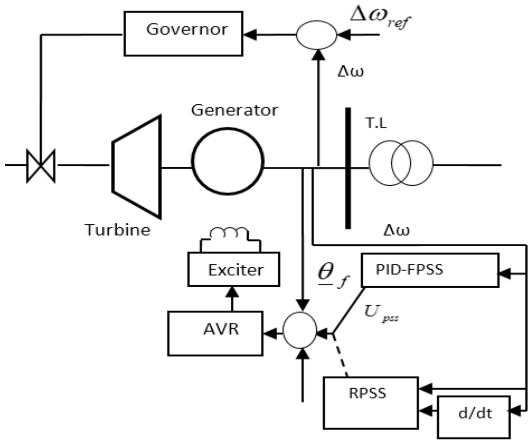

Fig. (3): Fuzzy variable, X_i, three-membership function

To investigate the power system performance. The system responses to a three-phase fault at t = 0 sec. and cleared after 100ms, will show the response of the system for two operating conditions.

The performance of each control law was measured by the performance index as in eq. (11)

The selected loading conditions are as follows:

a) ***Operating Condition 1***: Electrical Power ($P_e = 0.8\,pu$).

b) ***Operating Condition 2***: Electrical Power ($P_e = 0.3\,pu$)

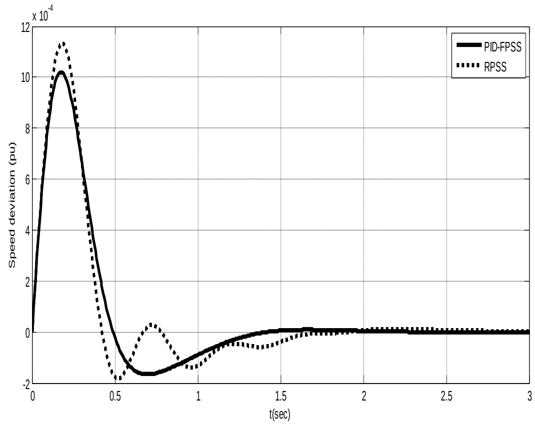

Fig. (5): Speed deviation response at ($P_e = 0.8\,pu$).

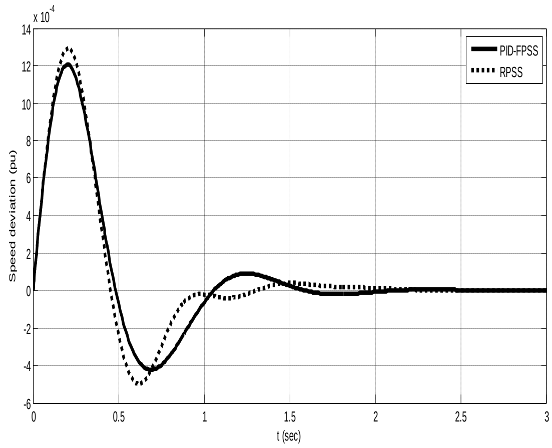

Fig. (6): speed deviation response at ($P_e = 0.3\,pu$).

TABLE 2. The performance index of ($\Delta\omega$), at operating condition 1**.**

Controller	Speed Deviation
PID-Fuzzy PSS	225
Robust PSS	256

TABLE 3. The performance index of ($\Delta\omega$), at operating condition 2.

Controller	Speed Deviation
PID-Fuzzy PSS	450
Robust PSS	501

7. Conclusion

PID-FPSS technique was designed based velocity PID controller and its gains are tuned by particle swarm optimization technique.

Fuzzy Power system stabilizer was developed based on linguistic rules of fuzzy basis function. The performance of the proposed stabilizer was investigated and compared with the robust PSS was designed in [13]. Through the dynamic simulations of a single machine infinite bus power system, the simulations form Fig. (5), Fig. (6), Table (2) and Table (3) have shown that a significant improvement can be achieved with PID-FPSS for a two different operating points.

References

[1] W. Watson and Manchur, "Experience with supplementary damping signals for generator excitation systems" IEEE Trans. on power apparatus and systems, vol PAS–1973, PP. 193-203.

[2] F. P. deMello, L. N. Hannett and M. Undrill “Practical approaches to supplementary stabilizing from accelerating power" IEEE Trans. On power apparatus and systems, vol PAS-1978, PP. 1515-1522.

[3] H. Joe Chow, E. G. Boukarim and A. Murdoch “Power system stabilizer as undergraduate control design project" IEEE Trans. On power apparatus and systems, vol PAS-2004, PP. 144-151.

[4] G. Y. Rajaa Vikhram, S. Latha " Design of power system stabilizer for power system damping improvement with multiple design requirements" international journal of soft computing and Engineering (IJSCE) ISSN: 2231-23077, vol. 2, 2012.

[5] M. Megala, Rajan, C. Cristober Asir “Design of fuzzy logic power system stabilizer in multi-machine power system"

ISSN 2522-6967

proceedings of the international conference on frontiers of intelligent computing: theory and application 2013.

[6] P. Kripakaran, M. Vigneshan, S. Asvnth, B. Sivachandiran " performance of power system stabilizer using fuzzy logic controller" journal of electrical and electronic engineering (JOSR-JEEE) , vol. 9. 2014, pp. 42-49.

[7] D. K. Sambariya, R. Prasad " Design of robust PID power system stabilizer for multimachine power system using HS algorithm" American Journal of Electrical and Electronic Engineeringvol. 3, No. 3, 2015, pp 75-82.

[11] John H. “Fuzzy control and identification" published by John Wiley & Sons, 2010.

[12] F. P. Demello, C. Concordia " Concepts of Synchronous Machine Stability as Affected Excitation Control" IEEE

[8] X. Li, Z. Wang, Junhua Xu, and B. Chen "Power system stabilizer parameters designing based on genetic simulated annealing algorithm" JOCET 2016 vol.4, No.3, 2016, pp 178-182.

[9] Haider A. and Sulochana W. "Intelligent PID Controller Tuning for Higher Order Process System" International Journal of u- and e- Service, Science and Technology Vol.8, No. 6, 2015, pp.323-330.

[10] T. Hussein and A. Shamekh “Performance Assessment of Fuzzy Logic Power System Stabilizer on North Benghazi Power Plant" Hindawi Publishing Corporationn Conference Papers in Engineering , 2013.

Transactions on Power Apparatus and Systems, vol. pas-88, no. , pp 316-328. 1969.

[13] H. M. Soliman, A. L. Elshafei, A. A. Shaltout and M. F. Morsi " Robust Power System Stabilizer" IEE Proceeding on Electrical Power Aplication, vol 14, pp 285-291.

ISSN 2522-6967

Energy and Exergy Analysis for Unit13E1 of Benghazi Combined Cycle Power Plant

Idris Elfeituri* and Hamza El Gehani

University of Benghazi, Benghazi, Libya
⁎Corresponding author. Tel.: +218944710641; e-mail: idrisffff@yahoo.com

ABSTRACT

Presented in this paper, an exhaustive energy-exergy analysis of a 476 MW combined cycle power plant located in Benghazi-Libya, as an example to illustrate the utility and importance of exergy analysis compared with energy analysis. The proposed power plant cycle was simplified into sub-systems and modelled. These models of mass, energy and exergy balance equations were applied to each sub-system and farther validated by the manufacturer's data at design operating condition. The results indicate that, the power plant has an overall energy and exergy efficiencies of 55.0% and 52.0% respectively. The total exergy destruction rate is found to be 444.2 MW (48.3 % of fuel input exergy). Significant exergy destruction rate is found to occur in the combustion chamber which contributes a major share of 340.7 MW (37.06%), followed by heat recovery steam generator with 35.7MW (4. %). Moreover, the results of the exergy analysis are compared with those of energy analysis. The comparison is quite of interest. The exergy analysis is much more enlightening, because the dissipations and efficiencies measured with availability are true one, where as those measured with energy are erroneous and misleading. The benefit of this study has enabled us to identify sites where loss of useful energy (exergy) takes place in a power plant and its performance can be evaluated. The results presented here are of real practical value in many ways, they can be valuable for the academic research interest.

Keywords: *Combined Cycle Power Plant, Modelling, Energy, Exergy Analysis.*

1. Introduction

The availability of production electricity is essential to the economic strength of a nation. Electricity demand has therefore gained remarkable attention over the last few decades due to the higher standard of living and increasing number of consumers etc. Among the existing technologies, combined power plants dominate nowadays the electricity generation worldwide due to their high thermal efficiencies and power. In Libya, some of these plants are being installed [1]. Power plants where gas turbines are combined with steam cycles are particularly interesting for their higher overall efficiency (50 -60%) than either of the cycles executed individually [3, 4, 5].

The combination of the two kinds of cycles is possible due to the high exhaust heat temperature of gas turbines. The electricity generating companies are striving to improve the efficiency and performance of their power plants. To achieve this, the locations and causes of useful energy destruction and losses in the power plant components have to be investigated and found. Exergy analysis has increasingly attracted the interest of many researchers to achieve the above goal. The purpose of exergy analysis is generally to identify the location, the source and the magnitude of true thermodynamic inefficiencies in power plants. Moreover, the results provided by exergy analysis can be used as a guide for reducing the thermodynamic inefficiencies of power plants and improving their performance [6, 7, 8].

Exergy analysis has been widely used by many researchers in evaluation, optimization and improvement of thermal power plants. Many researchers, such as Ameri *et al.* [2], kotas [9], Moran [10], Rahim [11] Ersayin*et al* [12] have carried out exergy analysis on combined cycles power plant. According to their results, most of exergy is lost during the combustion process. Balli et al [13] carried out the exergy analysis of a gas turbine cogeneration power plant the results showed that 68% of the overall exergy destructed is occurring in the combustion chamber. The exergy concept has also play an important role in making an energy policy as elaborated by Rosen and Dancer [14]. According to them exergy does not only address the impact of energy resource use on the environment but prove to be a suitable technique for promoting the goal of improved energy conversion.

The exergy analysis is not so popular among industrial fraternity (friends) in Libya and it needs much more attention and application so that the irreversibility can be minimized and thus the systems can be operated at much higher efficiency and less emissions. There have been no enough studies on the exergy evaluation of power plants in Libya and it needs mulch more attention and application so that the useful energy destruction and losses can be minimized to the plants can be operated at higher efficiency.

The present work is one such effort to explain the application of energy-exergy analysis of a 476 MW combined cycle power plant located in Benghazi-Libya. The thermodynamic model and performance evaluation for the power plant by energy-exergy analysis using the design data at full load are presented.

2. Energy and Exergy Analysis

Energy analysis is based on the first law of thermodynamics, which is related to the conservation of energy. While exergy analysis is based on the second law of thermodynamics which state: the conservation of mass and degradation of the quality of energy along with the entropy generation in the analysis of energy systems [6]. The exergy analysis calculates the system performance based on exergy, which defined as the maximum possible reversible work obtainable in bringing the state of the system to equilibrium with the environment [6,7]. The loss of useful energy in power plants cannot be justified by the energy analysis, as it does not differentiate between the quality and quantity of energy [14]. Energy analysis presents only quantities results while exergy analysis presents qualitative results about actual energy consumption [6, 8, 9]. On the other hand, exergy analysis, based on the exergy analysis recognizes magnitudes and locations of the useful energy losses during any thermodynamic process. The primary objectives of exergy analysis are to analyze the energy system components separately and to identify and quantify the sites having the maximum energy and exergy losses.

ISSN 2522-6967

3. Power Plant Process Description

The Benghazi-North combined cycle power plant was selected for the present work. The power plant was installed and commissioned by ABB in 1995, the design and arrangement of the plan was done in view later combined cycle conversion (1999) [1]. The plant consists of two gas turbines (GTs) units type 13E, 167 MW each, and one steam turbine (ST) unit with 142 MW. The detailed process flow-sheet of the plant is shown in Fig. 1. The gas turbine (Siemens, AG Germany) is shown as a topping plant cycle, whereas the steam turbines (HP and LP) forms the low temperature cycle. Each of GT-unit consists of compressor, combustion chamber and gas turbine. The ST-unit consists of condenser, Deaerator, feed-water heater, high-pressure drum, low and high pressure economizers, high pressure evaporator and super-heater. The connecting link between the two cycles is the heat recovery steam generator (HRSG).

The principle of the combined cycle considered in this study is that, air enters into compressor at state point ‘1’ and compressed at state ‘2’ and transferred to combustion chamber (CC) where combustion of fuel (natural gas injected at state point ‘5’) takes place and producing high-temperature flue gases (1142.0 °C). These high pressure-temperature gases are expanded in a GT unit from state point ‘3’ to state point ‘4’ and doing useful shaft work to drive an electrical generator for producing electricity. The exhaust gases (530.0°C) from the GT have still some energy which recovered in HRSG. In the steam cycle there are two levels of steam pressures on each evaporator. The superheated steam (515 °C, 80 bar) HP-E enters into HP-ST at state point ‘17’ for farther expansion. The superheated steam (288 °C, 5.5 bar) from LP-E before entering the LP-ST mixes with the exit steam coming from HP-ST turbine at state point ‘20’. The exit steam from LP-ST at state point ‘30’ is condensed into a condenser up to a pressure of 0.06 bar. The condensate steam is then directed to the FWH and DA. The BFWP circulates the feed-water to HRSG through the low pressure economizer and evaporator then the flow is divided into three streams to continue the cycle. The operational data at design condition was collected from the Ministry of electricity and the power plant manufacturer. This data includes the state of all streams and the power output at design condition. The design parameters of the power plant are presented in Table 1.

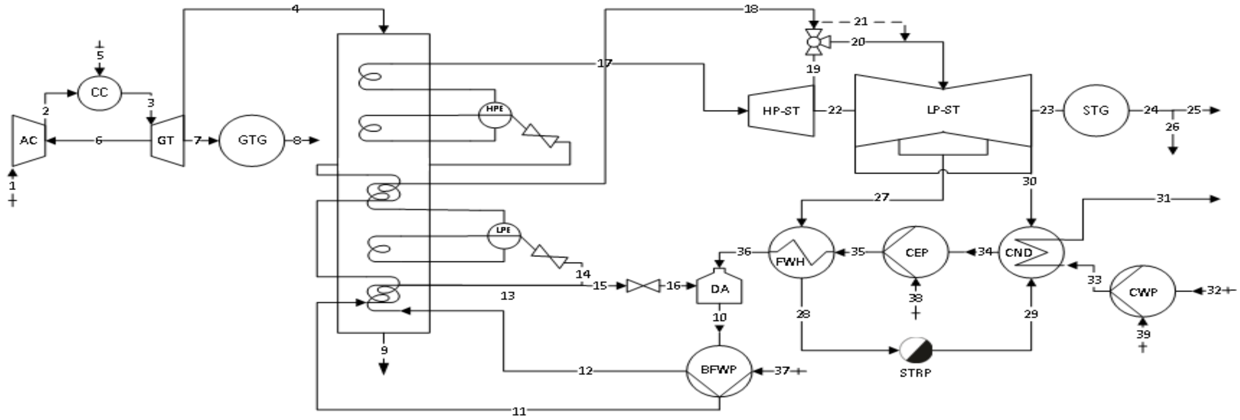

Fig.1: Schematic diagram of the selected combined cycle power plant.

Table 1: Design data and parameters of the plant [1].

Parameters	Values
Ambient condition	25 °C/1.013 bar
Compressor inlet temperature	25 °C
Compressor inlet pressure	1.013bar
Compressor pressure ratio	12.5 [-]
Compressor air mass flow rate	2x450 kg/s
Compressor efficiency	89.0 %
Air gas constant	0.288 kJ/kg.K
Air “kappa”	1.38
Specific heat capacity air	1.06 kJ/kg.K
Combustion efficiency	98%
Combustor pressure drop	0.5 bar
LHV (NG) of fuel	44.5 MJ/kg
Turbine inlet temperature	1142.0 °C
Turbine exit pressure	1.023 bar
Gas turbine efficiency	90.3%
Temperature of gases at HRSG outlet	125.8 °C
Exhaust gas constant	0.288 kJ/kg.K
Exhaust “kappa”	1.38
Continue Table 1;	
Specific heat capacity for gas	1.134 kJ/kg.K
HP steam turbine inlet temperature	515.0 °C
Steam turbine efficiency	82.3 %
Deaerator pressure	1.19 bar
Condenser pressure	0.063 bar
Cooling water inlet temperature	27 °C
Cooling water outlet temperature	34.3 °C
Generator efficiency	98. %

4. Thermodynamic Model and Analysis

The present study introduces a comparative energy and exergy analysis for Benghazi-North combined power plant based on the design condition with the following assumptions:

1. Full load, design operating condition of the power plant is considered.
2. Air and combustion products are treated as ideal gas.
3. The kinetic and potential energies of fluid streams are neglected.
4. Natural gas is supplied to the system as fuel.
5. Only the chemical exergy of the fuel is considered.
6. 2xHRSG and 2xGT are treated as one control volume each.

With regard of the Figure 1, each component in the power plant was considered as a control volume and analyzed separately. Three balance equations were written for each component including mass, energy and exergy. The basic balance equations are [10];

For mass balance: $\sum \dot{m}_{in} - \sum \dot{m}_{out} = 0.0$ (1)

ISSN 2522-6967

for energy balance:

$$\sum \dot{m}_{in} h_{in} - \sum \dot{m}_{out} h_{out} + \sum Q_{in} - \sum Q_{out} + \sum P_{in} - \sum P_{out} = 0.0 \quad (2)$$

and for exergy balance:

$$\sum EX_{in} - \sum EX_{out} + \sum P_{in} - \sum P_{out} - EXD = 0.0 \quad (3)$$

4.1. Energy Analysis

4.1.1. Air compressor (AC)

Knowing the air inlet pressure and temperature, outlet pressure and compressor efficiency, the final outlet temperature of the compressor is calculated as:

$$T_2 = T_1 \times \left(1 + \left(\frac{1}{\eta_C}\right) \times \left(r_C^{\frac{\gamma_C - 1}{\gamma_C}} - 1\right)\right) \quad (4)$$

The required power for the compressor is equal to

$$P_6 = \dot{m} \times Cpa \times (T_2 - T_1) \quad (5)$$

4.1.2. Combustion Chamber (CC)

From the energy balance in the combustion chamber, the fuel mass flow rate (m_5) can be calculated from the equation

$$\dot{m}_5 = \frac{\dot{m}_2 (C_{pg} \times T_3 - C_{pa} \times T_2)}{\eta_{cc} LHV - C_{pg} \times T_3} \quad (6)$$

Thus, the mass flow rate of the combustion products is given by

$$\dot{m}_3 = \dot{m}_2 + \dot{m}_5 \quad (7)$$

Where is fuel mass flow rate (kg/s), is air mass flow rate (kg/s), LHV is low heating value (kJ/kg), T_3 turbine inlet temperature, Cp_a and Cp_g are the specific heats of air and gas product respectively.

4.1.3. Gas Turbine (GT)

The exhaust gases temperature from the gas can be expressed as:

$$T_4 = T_3 \times \left[1 - \eta_T \times \left(1 - (r_T)^{\left(\frac{\gamma_T - 1}{\gamma_T}\right)}\right)\right] \quad (8)$$

The total output mechanical power of the gas turbine is expressed as:

$$P_T = \dot{m}_3 C_{pg} (T_3 - T_4) \quad (9)$$

Hence the net mechanical power (P_7) output from the gas turbine is

$$P_7 = P_T - P_6 \quad (10)$$

The gross electrical power (P_8) output from gas turbine is

$$P_8 = P_7 \times \eta_G \quad (11)$$

4.1.4. Heat Recovery Steam Generator (HRSG)

Gas side

$$\dot{m}_4 - \dot{m}_9 = 0.0 \quad (12)$$

Steam side

$$\dot{m}_{11} - \dot{m}_{17} = 0.0 \quad (13)$$

$$\dot{m}_{12} - \dot{m}_{13} = 0.0 \quad (14)$$

$$\dot{m}_{14} - \dot{m}_{18} = 0.0 \quad (15)$$

The overall energy balance equation of the steam and flue gases is:

$$\dot{m}_{11} h_{11} + \dot{m}_{12} h_{12} - \dot{m}_{13} h_{13} + \dot{m}_{14} h_{14} - \dot{m}_{17} h_{17} - \dot{m}_{18} h_{18} + \dot{m}_4 h_4 - \dot{m}_9 h_9 = 0.0 \quad (16)$$

Assuming that the HRSG is well insulated, one obtains the following relation from Eqs. (12, 13, 14 and 15, and rearranging, for the calculation of the mass flow rate of feed-water enters the HRSG:

$$\dot{m}_{11} = \dot{m}_4 \left(\frac{h_9 - h_4}{h_{11} - h_{17}}\right) + \beta \times (h_{12} - h_{13}) + \alpha - \left(\frac{h_{10} - h_{36}}{h_{16} - h_{36}}\right) + \beta \times \left(\alpha - \left(\frac{h_{10} - h_{36}}{h_{16} - h36}\right) \times (h_{14} - h_{18})\right) \quad (17)$$

where:

$$\beta = \left(\frac{\alpha}{1. - \alpha}\right) \quad (18)$$

$$\alpha = \frac{\dot{m}_{12}}{\dot{m}_{10}} = 0.364 \quad (19)$$

and:

$$\dot{m}_{12} = \frac{\alpha \times \dot{m}_{11}}{1. - \alpha} \quad (20)$$

Thus, the mass flow rate of each state point in Figure 1 can be now calculated using the above mass balance equation as following.

4.1.5. Splitter

$$\dot{m}_{13} - \dot{m}_{14} - \dot{m}_{15} = 0.0 \quad (21)$$

$$h_{13} = h_{14} = h_{15} = 0.0 \quad (22)$$

4.1.6. Expansion valve

$$\dot{m}_{15} - \dot{m}_{16} = 0.0 \quad (23)$$

$$h_{15} = h_{16} \quad (24)$$

4.1.7. Deaerator (DA)

$$-\dot{m}_{10} + \dot{m}_{16} + \dot{m}_{36} = 0.0 \quad (25)$$

$$-\dot{m}_{10} h_{10} + \dot{m}_{16} h_{16} + \dot{m}_{36} h_{36} = 0.0 \quad (26)$$

4.1.8. High Pressure Steam Turbine (HPST)

$$\dot{m}_{17} - \dot{m}_{19} = 0.0 \quad (27)$$

$$P_{22} = \dot{m}_{17} h_{17} - \dot{m}_{19} h_{19} \quad (28)$$

ISSN 2522-6967

4.1.9. Mixer

$$\dot{m}_{18} + \dot{m}_{19} - \dot{m}_{20} = 0.0 \quad (29)$$

$$\dot{m}_{18}h_{18} + \dot{m}_{19}h_{19} - Q_{21} = 0.0 \quad (30)$$

Mixing points need mass flow data to calculate thermodynamic properties. Thus, the energy feed stream ‘21’was introduced and the enthalpy behind the mixing state point ‘20’ is calculated from assumed feed stream as follows:

$$h_{20} = \frac{Q_{21}}{\dot{m}_{20}} \quad (31)$$

4.1.10. Low Pressure Steam Turbine (LPST)

$$\dot{m}_{20} - \dot{m}_{27} - \dot{m}_{30} = 0.0 \quad (32)$$

$$P_{23} = \dot{m}_{20}h_{20} + P_{22} - \dot{m}_{27}h_{27} - \dot{m}_{30}h_{30} \quad (33)$$

The net electrical power (P_{25}) output from steam turbines is

$$P_{25} = P_{24} - P_{26} \quad (34)$$

$$P_{24} = P_{23} \times \eta_G \quad (35)$$

$$P_{26} = P_{37} + P_{38} + P_{39} \quad (36)$$

4.1.11. Pumps

Cooling water pump (CWP)

$$\dot{m}_{32} - \dot{m}_{33} = 0.0 \quad (37)$$

$$P_{39} = \dot{m}_{33}h_{33} - \dot{m}_{32}h_{32} \quad (38)$$

$$h_{33} = \frac{(p_{33} - p_{32}) \times 100}{\rho_w \times \eta_p} + h_{32} \quad (39)$$

Condenser extraction pump (CEP)

$$\dot{m}_{35} - \dot{m}_{34} = 0.0 \quad (40)$$

$$P_{38} = \dot{m}_{35}h_{35} - \dot{m}_{34}h_{34} \quad (41)$$

$$h_{35} = \frac{(p_{35} - p_{34}) \times 100}{\rho_w \times \eta_p} + h_{34} \quad (42)$$

Boiler Feed-water pump (BFWP)

$$\dot{m}_{10} - \dot{m}_{11} - \dot{m}_{12} = 0.0 \quad (43)$$

$$h_{11} = \frac{(p_{11} - p_{10}) \times 100}{\rho_w \times \eta_p} + h_{10} \quad (44)$$

$$h_{12} = \frac{(p_{12} - p_{10}) \times 100}{\rho_w \times \eta_p} + h_{10} \quad (45)$$

$$P_{39} = \dot{m}_{11}h_{11} + \dot{m}_{12}h_{12} - \dot{m}_{10}h_{10} \quad (46)$$

4.1.12. Steam condenser (CND)

$$\dot{m}_{33} - \dot{m}_{31} = 0.0 \quad (47)$$

$$\dot{m}_{29} + \dot{m}_{30} - \dot{m}_{34} = 0.0 \quad (48)$$

$$\dot{m}_{29}h_{29} + \dot{m}_{30}h_{30} - \dot{m}_{34}h_{34} - \dot{m}_{31}h_{31} + \dot{m}_{33}h_{33} = 0.0 \quad (49)$$

4.1.13. Feed-water Heater (FWH)

$$\dot{m}_{35} - \dot{m}_{36} = 0.0 \quad (50)$$

$$\dot{m}_{27} - \dot{m}_{28} = 0.0 \quad (51)$$

$$\dot{m}_{27}h_{27} - \dot{m}_{28}h_{28} + \dot{m}_{35}h_{33} - \dot{m}_{36}h_{36} = 0.0 \quad (52)$$

4.1.14. Steam Trap (STRP)

$$\dot{m}_{28} - \dot{m}_{29} = 0.0 \quad (53)$$

$$h_{28} = h_{29} \quad (54)$$

4.2. Exergy Analysis

The value of physical exergy flow rate at various state points in the objective system can be calculated by the following equations [6]: For steam and water,

$$EX_i = \dot{m}_i\left(\left(h_i - h_0\right) - T_0\left(s_i - s_0\right)\right) \quad (55)$$

and for ideal gas,

$$EX_i = \dot{m}_i\left(\left(h_i - h_0\right) - T_0\left(\left(s_i - s_0\right) - R\ln\left(\frac{p_i}{p_0}\right)\right)\right) \quad (56)$$

Where h_i, s_i and p_i are the enthalpy, entropy and pressure of the substance i respectively, and h_0, s_0, T_0 and p_0 are those at standard ambient conditions.

With using these equations (55 and 56) for determined all points, the values of exergy flow rates are calculated. Also, having of input and output exergy flow rate amount of each power plant components, the exergy destruction rate in each component is calculated with using relations shown in Table 2.

Table 2: Exergy Destruction Rate Equations for Power Plant Components.

Component	*Exergy Destruction (EXD)*	*Energy loss (ENL)*
AC	$=EX_1+P_6-EX_2$	-
CC	$=EX_2-EX_3+EX_5$	-
GT	$=EX_3-EX_4-P_6-P_7$	-
GTG	$=EX_7-EX_8$	-
HRSG	$=EX_4-EX_9+EX_{11}+EX_{12}$ $-EX_{13}+EX_{14}-EX_{17}-EX_{18}$	$=ENL_9$
HP-ST	$=EX_{17}-EX_{19}-P_{22}$	-
LP-ST	$=EX_{20}+P_{22}-P_{23}-EX_{27}$ $-EX_{30}$	-
CND	$=EX_{29}+EX_{30}+EX_{33}$ $-EX_{31}-EX_{34}$	$=ENL_{31}$
FWH	$=EX_{27}-EX_{28}+EX_{35}-EX_{36}$	-
DA	$=-EX_{10}+EX_{16}+EX_{36}$	-
BFWP	$=EX_{10}-EX_{11}-EX_{12}+P_{37}$	-
CWP	$=EX_{32}-EX_{33}+P_{39}$	-
CEP	$=EX_{34}-EX_{35}+P_{38}$	-
Splitter	$=EX_{13}-EX_{14}-EX_{15}$	-
Valve	$=EX_{15}-EX_{16}$	-
Mixer	$=EX_{18}+EX_{19}-EX_{20}$	-
Steam Trap	$=EX_{28}-EX_{29}$	-
STG	$=P_{23}-P_{24}$	-

Total exergy destroyed in the power plant (EXD_{total}) is given as:

$$EXD_{total}=\sum EXD_i \tag{57}$$

Total exergy losses in the power plant (EXL_{total}) is given as

$$EXL_{total}=\sum EXL_i \tag{58}$$

The exergy destruction ratio (EXDR) and the exergy loss ratio (ENLR) can be compared to the rate of exergy flow of fuel in the plant and written as:

$$EXDR=\left(\frac{EXD_i}{EX_{fuel}}\right)*100\% \tag{59}$$

$$ENLR=\left(\frac{EXL_i}{EX_{fuel}}\right)*100\% \tag{60}$$

The overall exergy efficiency (η_{EX}) of the power plant is given as:

$$\eta_{EX}=\left(\frac{Exergy\ \ rate\ \ output}{Exergy\ \ rate\ \ input}=1-\frac{EXD_{total}+EXL_{total}}{EX_{fuel}}\right)*100\% \tag{61}$$

Where, EX_{fuel} is the exergy flow rate of the fuel and is given by [2,9]:

$$EX_{fuel}=1.064\times\dot{m}_f\times LHV_{fuel} \tag{62}$$

The overall energy efficiency (η_{EN}) of the power plant is given as:

$$\eta_{EN}=\left(\frac{Energy\ \ rate\ \ output}{Energy\ \ rate\ \ input}=\frac{P_8+P_{25}}{Q_{fuel}}\right)*100\% \tag{63}$$

Where:

$$Q_{fuel}=\dot{m}_f\times LHV_{fuel} \tag{64}$$

The heat rate (HR) is a measure used to determine how efficiently a generator uses heat energy. It can be expressed as:

$$HR=\frac{Heat\ \ Supplies}{Power\ \ Generated}=\frac{3600}{\eta_{EN,plant}} \tag{65}$$

The specific fuel consumption (SFC) is the ratio of fuel used by the power plant to a certain amount of power produced. It can be determined by the equation:

$$SFC=\frac{3600\times\dot{m}_5}{P_8+P_{25}} \tag{66}$$

5. Calculation Results and Discussions

A computer program was developed based on the thermodynamic models as discussed in previous sections. The computational procedure is outlined in the flow chart of the program shown in Figure 2.

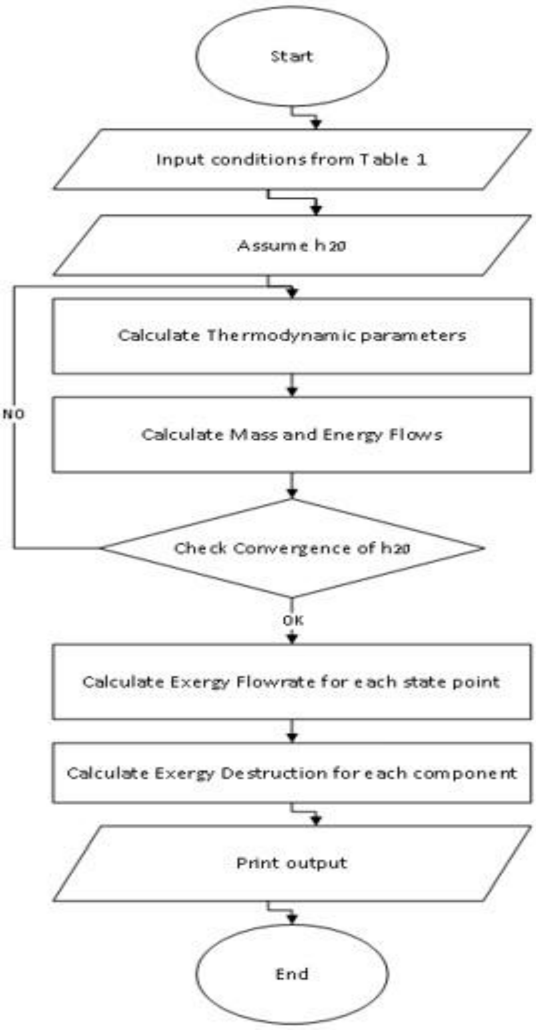

Fig. 2: Calculation Flow Chart.

ISSN 2522-6967

The energy and exergy analysis on the power plant are performed with assumptions made above and given parameters in Table 1. Firstly, different thermodynamic parameters at each state point (Fig. 1) in the power plant are calculated, secondly the results of mass, energy and exergy rates are obtained, and tabulated in Table 3.

Finally, the values in Table 3 are used to calculate the energy and exergy balance and exergy destruction and energy losses ratios for each component (Table 4). Moreover, energy and exergy efficiencies, heat rate and specific fuel consumptions of the power plant are calculated. The obtained results are tabulated in Table 5 and were validated with manufacture's published data for design operating condition. They showed high compatibility with the proposed model.

Table 3: Mass, energy and exergy rates and thermodynamic parameters at varies power plant state points in Fig. 1.

State	*Substance*	*p(bar)*	*T(°C)*	*h(kJ/kg)*	*s(kJ/kg.K)*	*ṁ(kg/s)*	*EN(MW)*	*EX(MW)*
1	Air	1.013	25.0	26.34	0.00	900.00	23.85	0.00
2	Air	12.50	359.2	380.9	0.073	900.00	342.81	299.3
3	Combustion gases	12.00	1141.9	1296.0	1.056	919.41	1191.56	877.83
4	Combustion gases	1.034	530.6	578.12	1.074	919.41	531.53	212.68
5	Natural gas	30.00	25.0	56.25	-1.762	19.41	863.94	919.23
6	Power to AC	-	-	-	-	-	318.96	318.96
7	Net power output GT	-	-	-	-	-	341.07	341.07
8	Electrical power GT	-	-	-	-	-	334.25	334.25
9	Combustion gases	1.012	125.8	131.0	0.304	919.41	120.44	12.87
10	Water	1.19	104.6	438.48	1.359	174.60	76.56	6.65
11	Water	115.0	106.5	454.81	1.37	111.05	50.51	5.66
12	Water	7.5	104.7	439.26	1.359	63.55	27.9	2.47
13	Water	5.90	158.4	682.72	1.926	63.55	43.40	7.18
14	Water	5.90	158.4	682.72	1.926	27.5	18.76	3.1
15	Water	5.90	158.4	682.72	1.926	36.10	24.63	4.08
16	Water	1.19	104.6	682.72	2.01	36.1	24.63	3.23
17	Superheat steam	80.60	515.0	3434.61	6.769	111.1	381.4	157.83
18	Superheat steam	5.50	287.6	3037.71	7.370	27.47	83.5	23.21
19	Superheat steam	4.930	164.1	2775.72	6.884	111.1	308.3	80.8
20	Superheat steam	4.910	187.2	2827.68	7.01	138.5	391.7	102.9
21	Energy flow	-	-	-	-	-	391.7	391.7
22	Power from HP-ST	-	-	-	-	-	73.2	73.2
23	Power from LP-ST	-	-	-	-	-	147.5	147.5
24	Gross elec. power ST	-	-	-	-	-	144.5	144.5
25	Net elec. power ST	-	-	-	-	-	142.0	142.0
26	Auxiliary Power	-	-	-	-	-	2.5	2.5
27	Steam	0.77	92.5	2547.2	7.13	14.1	35.8	6.00
28	Saturated water	0.77	92.5	387.5	1.221	14.1	5.5	0.40
29	Water	0.063	37.1	387.50	1.282	14.1	5.5	0.14
30	Wet steam	0.063	37.1	2262.50	7.33	124.5	281.6	10.33
31	Water	1.5	34.3	143.76	0.495	8713.0	1252.5	6.54
32	Water	1.013	27.0	113.2	0.395	8713.0	986.4	0.0
33	Water	1.57	27.01	113.3	0.396	8713.0	986.98	1.39
34	Saturated water	0.063	37.1	155.20	0.533	138.5	21.5	0.13
35	Water	5.00	37.1	155.80	0.533	138.5	21.6	0.21
36	Water	1.19	89.5	374.90	1.20	138.5	52.0	3.6
37	Power to BFWP	-	-	-	-	-	1.86	1.86
38	Power to CEP	-	-	-	-	-	0.08	0.08
39	Power to CWP	-	-	-	-	-	0.57	0.57

Table 4: Energy and Exergy balance of each component.

Component	EXD+EXL		ENL	
	MW	%	MW	%
2xAC	19.655	2.14	-	-
2xCC	340.70	37.06	-	-
2xGT	5.122	0.56	-	-
2xGTG	6.822	0.74	-	-
2xHRSG	35.688	3.88	120.4	14.0
HLP-ST	16.104	1.75	-	-
CND	11.735	1.28	266.2	31.0
FWH	2.245	0.25	-	-
DA	0.143	0.02	-	-
BFWP	0.389	0.04	-	-
Cont. Table 4				
CWP	0.363	0.04	-	-
CEP	0.0064	0.001	-	-
Splitter	0.000	0.00	-	-
Valve	0.846	0.10	-	-
Mixer	1.146	0.13	-	-
Steam Trap	0.252	0.03	-	-
STG	2.949	0.32	-	-
Total	444.20	48.3	386.6	45.0

ISSN 2522-6967

Table 5: Performance of the power plant.

Overall Energy efficiency	55.0 %
Overall Exergy efficiency	52.0 %
Heat Rate	6530.53 kJ/kWh
Specific Fuel Consumption	0.147 kg_f/kWh

In Figure 3, the exergy destruction rates for all Benghazi north power plant components at the design operating condition are shown. The greatest exergy destruction rate is shown at the combustion chamber, due to large temperature differences, mixing and chemical reactions as confirmed by [2,6,8]. The HRSG represents the second major source of exergy destruction rate in the plant, which may attribute to the temperature differences among the gases and steam streams. The third source of exergy destruction occurs in air compressor, as a result of compression and friction. The steam turbine represents the forth source, as a result of expansion and friction. The fifth source of exergy destruction occurs in steam condenser, feed-water heater and deaerator due to heat transfer and mixing in the deaerator. Finally, the exergy destructed in the electrical generators, steam mixer and expansion valve and steam trap, which attributed to the electrical heat rejected, friction and throttling processes respectively.

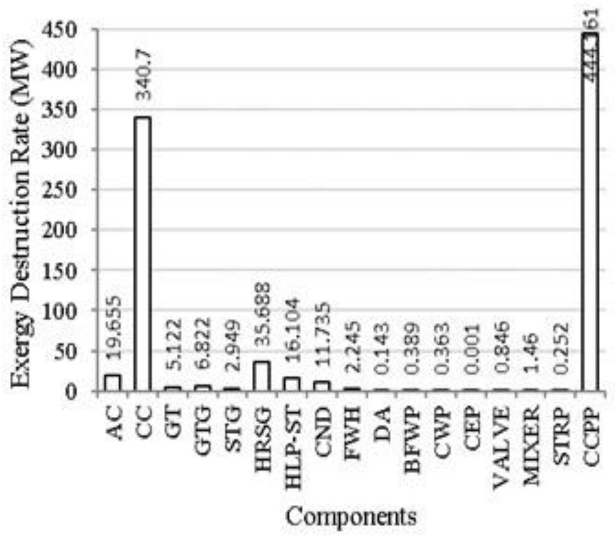

Fig. 3: Exergy destruction rate of the CCPP components.

Figure 4 and 5 shows the detailed energy and exergy balance of the power plant at the operating design condition. The only major components in the power plant are considered in this comparison. It shows that there are very significant differences between energy lost and exergy destruction for different process components. The energy balance showed that the primary source of energy loss is the condenser where 31% of the total loss occurs. In contrast, the exergy analysis showed that the loss from the condenser was only 1.28% of the total. According to the energy balance, the second largest source of energy loss is the HRSGs, which accounts for 14%. The exergy balance revealed that the loss of useful energy (exergy) is in the CCs, with losses of 37.06 %. It indicates that the waste heat in the condenser does not match potential to be utilized as a source of useful work and to improve the power plant efficiency. On other hand, farther investigation of exergy lost in the combustion chamber may show some opportunities for improvement. The results of exergy analysis are markedly different from the results of the energy balance, which shows most of the energy being lost in the condenser.

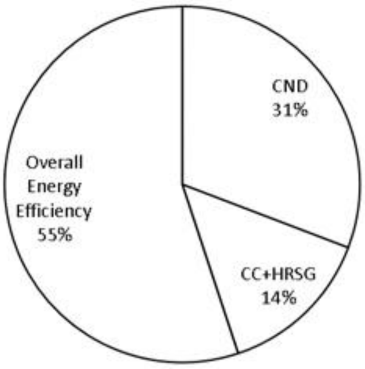

Fig. 4: Energy balance of the CCPP

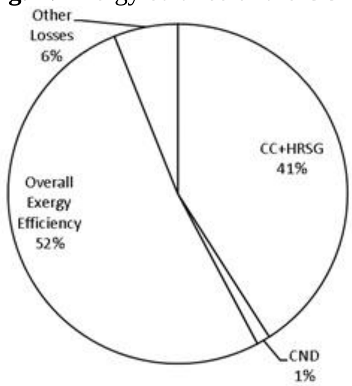

Fig. 5: Exergy balance of the CCPP.

6. Conclusions

This study reveals that, the exergy analysis approach provides a useful thermodynamic tool than energy analysis approach for the performance analysis of the power plant. The exergy analysis identifies areas where most of the useful energy is lost and discusses potential of the lost energy for improvement of the power plant efficiency, also enables all loss sources to be located and quantified. An energy and exergy balance of the complete plant was made. It has been observed that the energy losses are associated mainly with energy loss in condenser and stack whereas exergy losses are dominated by the losses in the combustion chamber and steam generator unit (HRSG). The results showed that maximum exergy destruction occurs in the CC (340.7 MW, 37.06% of fuel input exergy), followed by the HRSG (35.7 MW, 4. 0%), AC (19.7 MW, 2.14%) and turbines (16.1MW, 1.8%). The energy and exergy efficiencies of the power plant are calculated as 55. % and 52.%, respectively. Certain processes like throttling, heat transfers, expansion and friction involve no energy losses but they degrade the quality of energy and therefore involve exergy destruction. Exergy analysis is valuable not only for pinpointing useful energy (exergy) losses but also for direct application to the design of energy systems and for other engineering projects as maintenance and power plant modification to improve the thermodynamic performance.

ISSN 2522-6967

References

[1] Electricity Company in Libya.

[2] Ameri M., Ahmadi P., and Khanmohammadi S. H. (2008). Exergy analysis of a 420 MW combined cycle power plant. Int. J. Energy Res., Vol. 32, No. 2. pp. 175–183.

[3] El-Masri M. A. (1987). Exergy Analysis of Combined Cycles: Part 1—Air-Cooled Brayton-Cycle Gas Turbines. J. Eng. Gas Turbines Power. Vol. 109, No. 2. pp. 228–236.

[4] Dincer I. and Rosen M. A. (2012). Exergy: energy, environment and sustainable development. Newnes.

[5] Rahim M. A. (2011). Combined cycle power plant performance analyses based on the single-pressure and multi pressure heat recovery steam generator. J. Energy Eng. Vol. 138, No. 3. pp. 136–145.

[6] Szargut J., Morris D. R. and Steward F. R. (1988). Exergy Analysis of Thermal, Chemical, and Metallurgical Processes. Hemisphere Pub. Co USA.

[7] Bejan A., Tsatsaronis G. and Moran M. (1996). Thermal design and optimization. John Wiley & Sons.

[8] GaggioliR. A. and *et al.*(1975). Pinpointing the real inefficiencies in power plants and energy systems. Proc. Am. Power Conf.Vol. 37. USA.

[9] Kotas T. J.(2013). The exergy method of thermal plant analysis. Elsevier. New York.

[10] Moran M. J. and *et al.* (2010). Fundamentals of engineering thermodynamics. John Wiley & Sons. New York.

[11] Rahim M. A. (2013). Thermodynamic evaluation and parametric study of a combined cycle power plant: Application for Ankara city. J. Energy Eng. Vol. 140, No. 2, pp. 04013012.

[12] Ersayin and Ozgener L. (2015). Performance analysis of combined cycle power plants: A case study. Renew. Sustain. Energy Rev. Vol. 43. pp. 832–842.

[13] Balli O., Aras H. and Hepbasli A. (2007). Exergetic performance evaluation of a combined heat and power (CHP) system in Turkey. Int. J. Energy Res. Vol. 31, No. 9. pp. 849–866.

[14] Rosen M. A., Dincer I. and Kanoglu M. (2008). Role of exergy in increasing efficiency and sustainability and reducing environmental impact. Energy Policy. Vol. 36, No. 1. pp. 128–137.

Nomenclature

C_p - specific heat at constant pressure (kJ/kg.K)
EX - exergy flow rate (kW)
EN - energy flow rate (kW)
ENL - energy loss (kW)
EXD - exergy destruction rate (kW)
EXDR - exergy destruction ratio (%)
EXL - exergy loss rate (kW)
EXLR - exergy loss ratio (%)
h - specific enthalpy (kJ/kg)
HR - heat rate (kJ/kWh)
$\dot{m}$ - mass flow rate (kg/s)
LHV - lower heating value (kJ/kg)
p - pressure (bar)
P - power (kW)
Q - heat transfer rate (kW)
SFC - specific fuel consumption (kg/kWh)
s - specific entropy (kJ/kg.K)
r_C - compression ratio (-)
r_T - expansion ratio (-)
R - universal gas constant (kJ/kg.K)
T - temperature (°C or K)

Abbreviations

AC - air compressor
BFWP - boiler feedwater pump
CC - combustion chamber
CCPP - combined cycle power plant
CEP - condenser extraction pump
CND - steam condenser
CWP - cooling water pump
DA - deaerator
GT - gas turbine
GTG - gas turbine generator
HRSG - heat recovery steam generator
HP-ST - low pressure steam turbine
HPE - high pressure evaporator
HLP-ST - high and low pressure steam turbines
LP-ST - low pressure steam turbine
LPE - low pressure evaporator
STRP - steam trap
STG - steam turbine generator

Greek Letters

α - mass ratio (-)
γ - specific heat capacity ratio (-)
ρ - density, kg/ m^3
η - efficiency (%)

Subscripts

a - air
C - compressor
CC - combustion chamber
EN - energy
EX - exergy
f - fuel
g - gas products
G - electrical generator
o - ambient condition
P - pump
T - turbine
w - water
1 to 39 - cycle state points in Fig.1

ISSN 2522-6967

Using Artificial Neural Networks (ANN) to Control Chaos

Ibrahim Ighneiwa*, Salwa Hamidatou, and Fadia Ben Ismael

Department of Electrical and Electronics Engineering,Faculty of Engineering, University of Benghazi, Benghazi, Libya

**Corresponding author. Tel.: +218-92-4036057; e-mail: Ibrahim.ighneiwa@uob.edu.ly*

ABSTRACT

Controlling Chaos could be a big factor in getting great stable amounts of energy out of small amounts of not necessarily stable resources. By definition, Chaos is getting huge changes in the system's output due to unpredictable small changes in initial conditions, and that means we could take advantage of this fact and select the proper control system to manipulate system's initial conditions and inputs in general and get some desirable outputs out of undesirable Chaos. In this work,Artificial Neural Networks (ANN) techniques were used to get a desirable output out of otherwise a Chaotic system. Thatwasaccomplishedby first building some known chaotic circuit (Chua circuit) and then NI's MultiSim was used to simulate the ANN control system. It was shown that thistechnique can also be used to stabilize some hard to stabilize electronic systems.

Keywords: *ANN; Chaos; Chua Circuit; Control; Lorenz Oscillator*

1. Introduction

Chaotic systems control have received the interest of many researchers [1], due to the fact that chaotic systems, which are known for its Undesirable behavior, could be beneficial in many areas of science and technology. It has many potential applications [2], such as heat transfer, biological systems, laser physics, chemical reactor, biomedical, economics, weather, and secure communication.Many methods for controlling chaos have been developed, most of which using classic control techniques, such as linear feedback method, active control approach, adaptive technique, nonlinear controller[1,3].New methods in chaos control were developed by utilizing intelligent control, such as Artificial Neural Networks (ANN), Fuzzy Logic, Genetic Algorithm and Genetic Programming, to name a few[4].

In this workANN intelligent techniquewas used to controlchaos in electronic circuits. A well known chaos model, namely Chua circuit model, was used to implement such technique. After building the electronic circuit,the ANN control was applied to it and through changing ANN weights of the circuit control it was verified that some desirable outputs could be accomplished.

This paper is organized as follows.Section 2 is about Chaos and its mathematical aspects and how it could be shown both as a real output on an oscilloscope and as a simulated output of some known electronic circuits such as Chua circuit.Section 3 is a discussion of Artificial Neural Networks (ANN), which was used to control chaos. It also discuss the different parts of the network and its various mathematical functions.Section 4 is a discussion ofthe ANN techniques that was used to control chaos and show that this work leads to getting some desirable stable outputs out of a chaotic system.The final section containssome conclusions and some suggestions that couldlead to improving the efficiencyofthe controlled chaotic system.

2. Chaos

Chaos is defined as thepropertyofsomenon-lineardynamicsystemswhichexhibitsensitivedependenceoninitialc onditionsand it is happening when the smallest of changes in a system results in very large differences in system's behavior [5,14].The so-called butterfly effect has become one of the most popular images of chaos; the idea is that the flapping of a butterfly's wings in Argentina could cause a tornado in Texas [6].

Chaos does not mean that things happen at random, chaos is orderly disorder and not random at all, it is unpredictable in the sense that you cannot predict in what way the system's behavior will change for any change in the input [7].

2.1. Lorenz Oscillator

A good example of Chaos is the so called Lorenz Oscillator, wherethree ordinary differential equations (ODEs) define the chaotic behavior of such Oscillator. These equations are [8]:

$$dx/dt = \delta\,(y - x) \qquad (1)$$

$$dy/dt = x\,(\rho - z) - y \qquad (2)$$

$$dz/dt = x\,y - \beta\,z \qquad (3)$$

Where x, y and z define the state of the system, t is time, and δ, ρ and βaresystem parameters

Generally, the systemdoes not show any kind of chaotic behavior, But for certain values of its parameterslike: $\beta = 8/3$, $\delta = 10$, $\rho = 28$, the system may produce the following chaotic diagram (Fig. 1) [9].

Fig. 1:A plot of theLorenz attractorfor values$\rho = 28$,$\sigma = 10$,$b = 8/3$.

Another good example of Chaos occurs when increasing μ in the logistic map equation ($x_{n+1} = \mu x_n (1 + x_n)$) beyond 3.3.[9] For $\mu < 3.3$, the system oscillates between two values of x (period-2 cycle). Increasingμany further, makes the system oscillate between four values (bifurcation/period-4 cycle). And as proved in [9], if we keep increasing μ, period-doublings will happen at smaller intervals of parameter μ (see Fig. 2 below) [10].

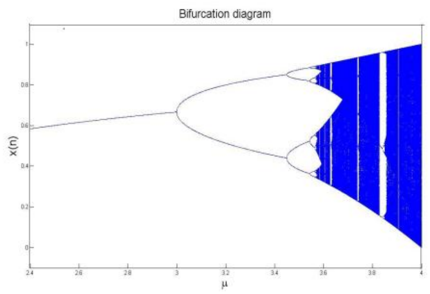

Fig. 2: Bifurcation diagram for logistic map.

2.2. Chua Circuit

Chua' Circuit is one of the simplest types of chaotic systems (see Fig. 3.a and Fig. 3.b).

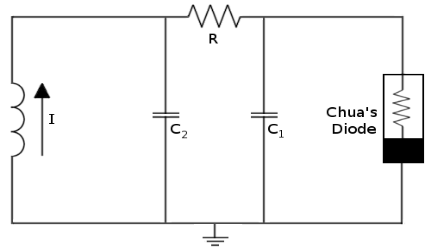

Fig. 3.a: Chua Circuit.

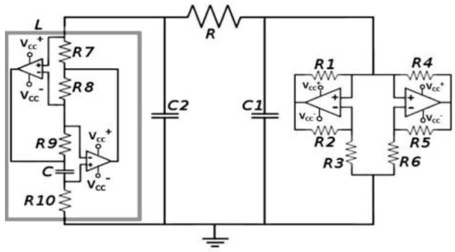

Fig. 3.b: Chua Circuit,

Notice that the inductor and Chua's diode (nonlinear resistance) are replaced by their equivalent Op Amp circuits

Using an oscilloscope one can watch a Chua circuit creating the chaotic double scroll (Fig. 4), which can be modeled by three equations[11], which are

$$C_1\, dv_1/dt = (v_2 - v_1) / R - g(v_1) \qquad (4)$$

$$C_2\, dv_2/dt = - (v_2 - v_1) / R + I \qquad (5)$$

$$L\, dI/dt = - r\, I - v_2 \qquad (6)$$

Where v_1 and v_2 are voltages across C_1 and C_2 respectively, g(v1) is the conductance of the nonlinear resistance (the equivalent of Chua's diode) and r is inductor's resistance[11].

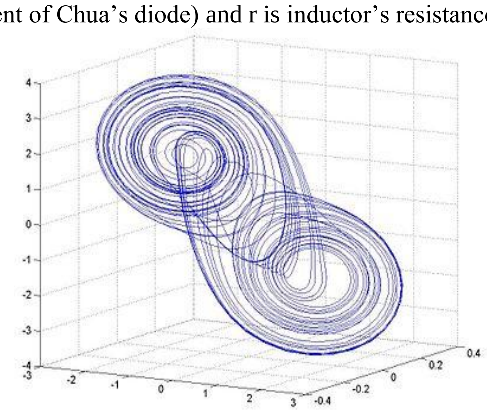
Fig. 4: Double-scroll chaos.

Since the goal is to control the chaotic behavior of the circuit above by using Artificial Neural Networks (ANN), the next section will be devoted to discussing various aspects of ANN.

3. Artificial Neural Network (ANN)

ANN is part of Artificial Intelligence (AI) which emphasizes the creation of intelligent machines that work and react like humans [12]. It isbased on the biological neural system. The Information that flows through the network affects the structure of the ANN because a neural network changes or learns, in a sense based on that input and its output's feedback. Fig. 5 shows an example of an Artificial Neuron and Fig. 6 shows an example of an Artificial Neural Network[12].

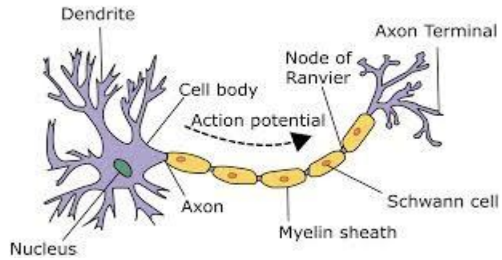

Fig. 5: An example of an Artificial Neuron.

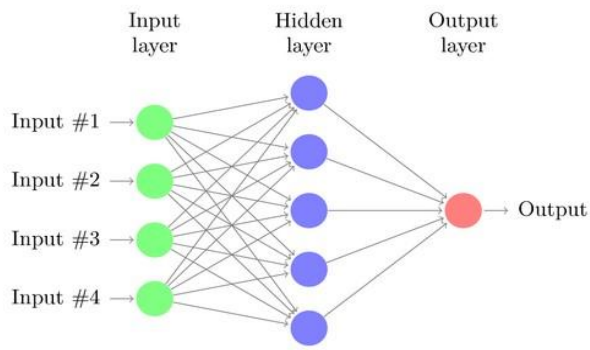

Fig. 6: An Artificial Neural Network (ANN)

AnArtificial Neuron could be represented as in Fig. 7, where its output is governed by the following equation:

$y = f\,(v)$, where f(v) is the activation function and

$v = w_1\, x_1 + w_1 x_1 + \ldots\ldots + w_m x_m + w_0\, b_0$

where

$w_0, w_1, w_2, \ldots\, w_m$ are the weights,

$x_1, x_2, \ldots\, x_m$ are the inputs, and b_0 is the bias.

To get some desired output y_d, we propagate the neurons' outputsback to the system and that will adjust the weights so as to get the desired output. Fig 7.1.a shows a simple neuron system andFig 7.1.b shows the backprobagation (feedback) system.

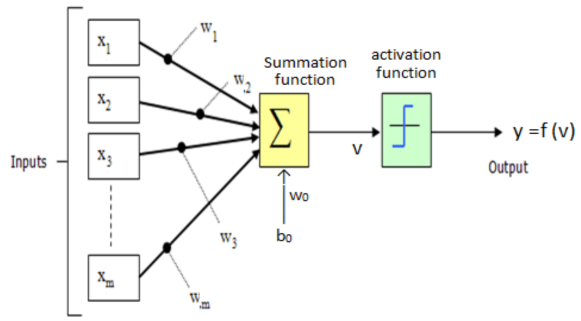

Fig. 7.a: An example of anArtificial Neuron showing its Inputs, weights, summing function and activation function

ISSN 2522-6967

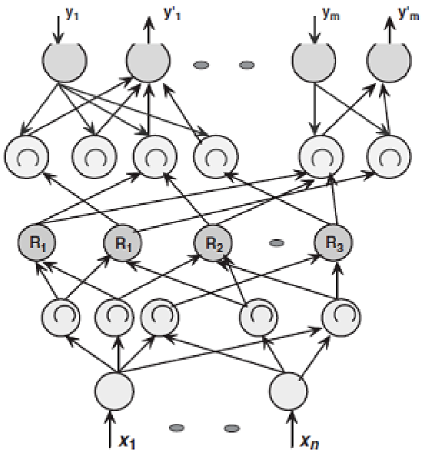

Fig. 7.b: An example of a backprobagation system.

There are many types of activation functions (see [8] for many examples). The activation function we use here is the sigmoid function (Fig. 8).

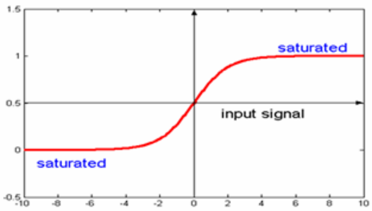

Fig. 8: Activation function;Sigmoid,$f(x) = 1 / (1 + e^{-x})$, $-\infty<x<\infty$

4. Using ANN to Control Chaos

To control the chaotic behavior exhibited by Chua circuit, we first built Chua circuit on a bread board (Fig. 9), tested it and got the output shown on an oscilloscope (Fig. 10).

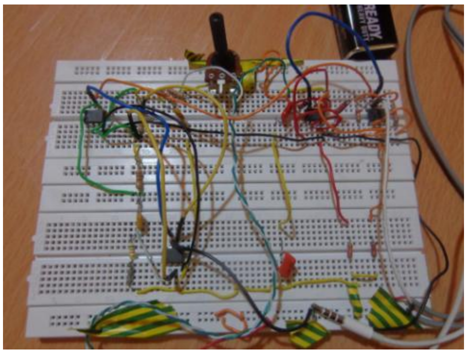

Fig. 9: Chua circuit we built on a breadboard.

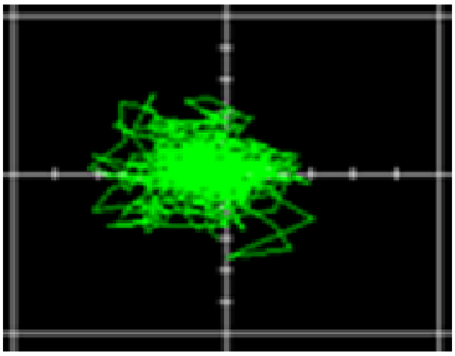

Fig. 10: The chaotic output of the circuit we built

By adjusting the values of the resistance R and C (see Fig. 3.b) it was possible to get rid of the chaotic behavior and forced the circuit to give some desired stable outputs (see Fig. 11.a thru Fig. 11.E for response to different choices of R and C).

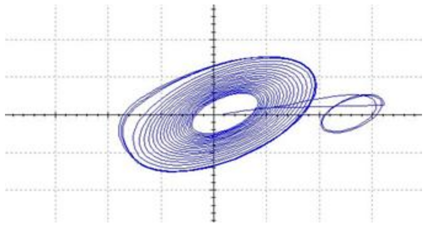

Fig. 11.a: The output response to the first choice of R and C

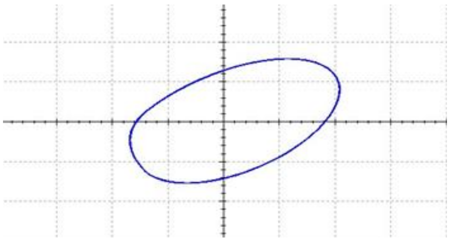

Fig. 11.b: The output response to the second choice of R and C

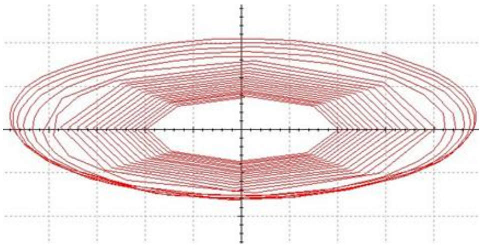

Fig. 11.c: The output response to the third choice of R and C.

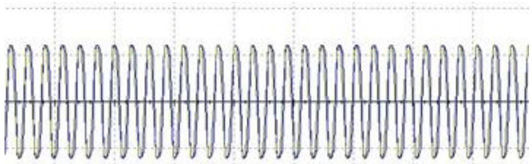

Fig. 11.d: The output response to the fourth choice of R and C.

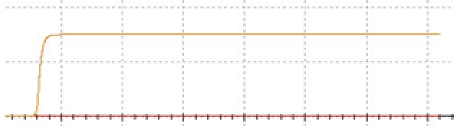

Fig. 11.e: The output response to the fifth choice of R and C.

Mat Lab was also used to simulate the circuit above, using the available Chua circuit's program [6] for its equations, and the expected chaotic behaviorhappened (Fig. 12.a). By adjusting the system's parameters we ended up with outputs showing no chaotic behavior.

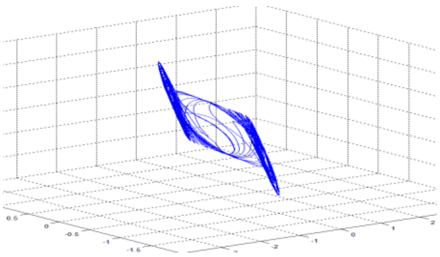

Fig. 12: The output of the MatLab simulation; chaotic behavior

ISSN 2522-6967

After getting the chaotic behavior by using our electronic circuit built on a breadboard and then by using MatLab available program, VI's Multisim program was used to redraw the electronic circuits for the individual parts of ANN (weights, summing functions, activation functions) (as in [13]) and then all circuits were connected together. Finally, the output of the ANN big circuitwas connected to Chua circuit, and part of Chua's circuit output was feedback to the ANN to adjust the weights accordingly.

Once all circuits were connected together (Fig.13), it was possible to use different initial values for the ANN weights and then let the ANN, through learning, adjust Chua circuit's parameters so it gives some desired output instead of the Chaotic behavior which it usually manifests. Samples of the output are shown on Fig. 14.a thru Fig.14.c.

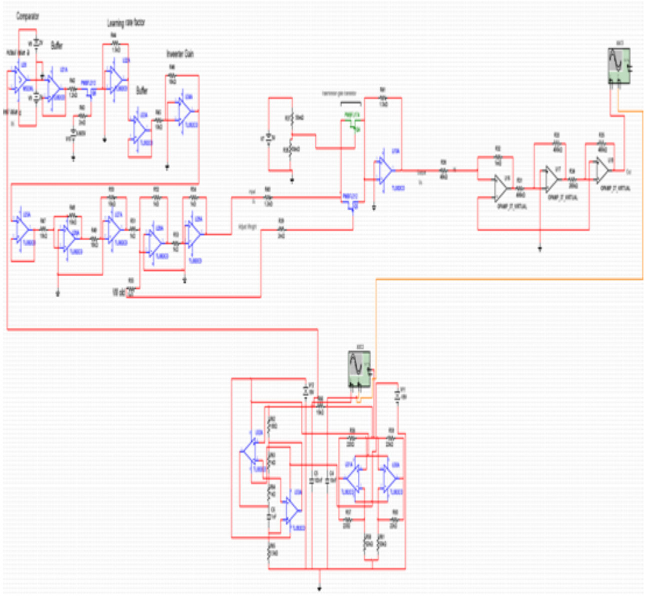

Fig.13: All ANN circuits connected togetherand their final output connected to Chua circuit

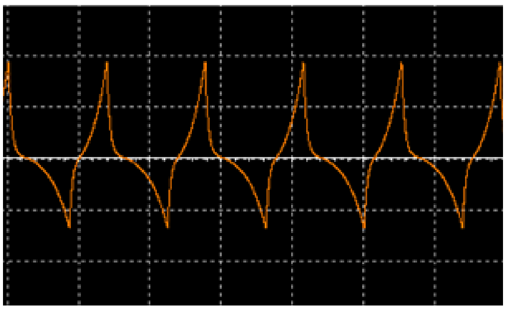

Fig.14.a: Sample (a) of the outputof the ANN controlled Chua circuit.

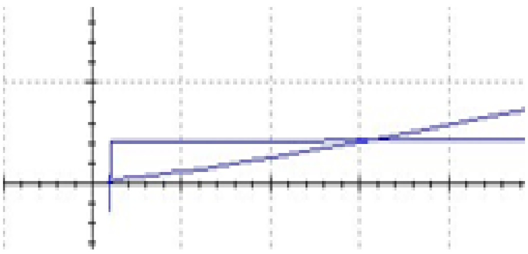

Fig.14.b: Sample (b) of the outputof the ANN controlled Chua circuit.

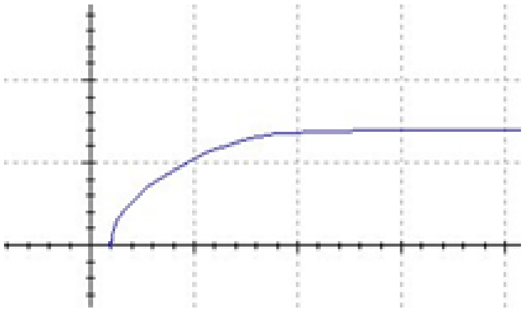

Fig.14.c: Sample (c) of the outputof the ANN controlled Chua circuit.

5. Conclusions

Using Artificial NeuralNetworks (ANN)proved to be very effective in controlling Chaos;that is getting some desired outputs out of chaotic systems. It was also shown that using ANN could lead to stabilizing chaotic systems.The main problem in accomplishing such desired results was the time taken to adjust the ANN weights, first manually one by one then through adjustingChua's output resistance, then automatically by the feedback control system. This work could be improved by combining ANN control techniques with some other intelligent control techniques such as Fuzzy Logicand GeneticAlgorithms, to get the benefit of all.

References

[1] Chen, Heng-Hui, et al. "Chaos synchronization between two different chaotic systems via nonlinear feedback control." *Nonlinear Analysis: Theory, Methods & Applications* 70.12 (2009): 4393-4401.

[2] Cai, Guoliang, and Zhenmei Tan. "Chaos synchronization of a new chaotic system via nonlinear control." *Journal of Uncertain Systems* 1.3 (2007): 235-240.

[3] Xu, Chang-Jin, and Yu-Sen Wu. "Chaos control and bifurcation behavior for a Sprott E system with distributed delay feedback." *International Journal of Automation and Computing* 12.2 (2015): 182-191.

[4] Yoo, Sung Jin, Jin Bae Park, and Yoon Ho Choi. "Stable predictive control of chaotic systems using self-recurrent wavelet neural network." *international journal of control, automation, and systems* 3.1 (2005): 43-55.

[5] Liu, Bo, et al. "Improved particle swarm optimization combined with chaos." *Chaos, Solitons & Fractals* 25.5 (2005): 1261-1271.

[6] Bishop, Robert C. "What could be worse than the butterfly effect?." *Canadian Journal of Philosophy* 38.4 (2008): 519-547.

[7] Heylighen, Francis, Paul Cilliers, and Carlos Gershenson. "Complexity and philosophy." *arXiv preprint cs/0604072* (2006).

[8] Sparrow, Colin. *The Lorenz equations: bifurcations, chaos, and strange attractors.* Vol. 41. Springer Science & Business Media, 2012.

[9] Liapunov Exponent, http://math.uhcl.edu/shiau/Course/MATH4136(2011)/LiapunovV2pdf. Accessed 11 Sept. 2016.

[10] Li, Damei, et al. "Estimating the bounds for the Lorenz family of chaotic systems." *Chaos, Solitons & Fractals* 23.2 (2005): 529-534.

[11] Elwakil, A. S., and M. P. Kennedy. "Chua's circuit decomposition: a systematic design approach for chaotic oscillators." *Journal of the Franklin Institute* 337.2 (2000): 251-265.

[12] Rashid, Tariq.*Make Your Own Neural Network*, 2016, Amazon Edition.

[13] Khuder, A. I., and Sh H. Husain. "Hardware Realization of Artificial Neural Networks Using Analogue Devices." *Al-Rafadain Engineering Journal* 21.1 (2013).

[14] The Stanford Encyclopedia of Philosophy, http://plato.stanford.edu/entries/chaos. Accessed 11 Sept. 2016.

ISSN 2522-6967

Power Factor Correction for ABO-TRABA Desalination Plant Case Study

Zakariya Rajab[a]*, Mohammed Buamud[b] and Mukhtar Elwalid[c]

[a, b, c]Electrical and Electronic Engineering Department Faculty of Engineering, University of Benghazi, Benghazi - Libya.
*E-mail: Zakreia.hassan@uob.edu.ly, and bargathy81@yahoo.com

ABSTRACT

Power factor is a way of measuring the percentage of reactive power in an electrical system. Reactive power represents the wasted energy electricity. Reactive power is used by inductive load (such as, motors, transformers, fluorescent light, arc welders and induction furnaces) to sustain their magnetic fields. Electric systems with many motors exhibit low power factors, increasedconductorandtransformerlosses,andlowervoltages.Utilities must supply both active and reactive power to compensate these losses. However, the influence of voltage and current harmonics on equipment connected to electrical system can cause serious problems in power factor correction; it can be improved by adding shunt capacitors. Capacitors act in opposition to inductive loads,therebyminimizingthereactivepowerrequiredtoservethem.Unfortunately,powerfactorcorrectioncapacitorsmayproduceharmonicresonance and magnify utility capacitor-switching transients. Therefore, it is often desirable to implement one or more capacitor banks in a facility as a harmonic filter [1].
The main objective of this paper is to raise the power factor for ABO TRABA desalination plant to the economic and optimum value. The scope of the paper includes studying the phenomena's that can cause significant damage and distortion to a given power system such as harmonics and resonance.
The study includes billing data monthly collected, which is a plant survey. From the study, some calculations have been done such as power factor penalty savings, Loss savings, payback period, losses reductions and increase system capacity.

Keywords:*Power factor correction, increased System capacity, and harmonics*

1. Introduction

Alternating current (ac) system supply two forms of energy: Active energy, which is converted into mechanical work, heat, light, etc. Reactive energy, which again takes two forms: reactive energy required by inductive circuits (transformers, motors, etc) and reactive energy required by capacitive circuits (Cable capacitance, power capacitors, etc) [2].

All inductive (i.e. electromagnetic) machines and devices that operate on ac. system convert electrical energy from the power system generators into mechanical work and heat. This energy is measured by KWhr meters, and is referred to be active, in order to perform this conversion, magnetic fields have to be established in the machines, and these fields are associated with another form of energy to be supplied from the power system, known as reactive energy. This energy is measured by Kvarhr meters. All ac plants and appliances that include electromagnetic devices, or depend on magnetic coupled windings, required some degree of reactive current to create magnetic flux. Power factor is a ratio of useful power to perform real work (active power) to the power supplied by a utility (apparent power), in the sinusoidal case there is only one phase angle between the voltage and the current since only the fundamental frequency is present; the power factor can be computed as the cosine of the phase angle and is commonly referred as the displacement power factor [2, 3].

In the non-sinusoidal case, the power factor cannot be defined as the cosine of the phase angle. The power factor that takes into account the contribution from all active power, including both fundamental and harmonic frequencies, is known as true power factor. The true power factor is simply the ratio of total active power for all frequencies to the apparent power delivered by the utility. Poor PF due to an inductive load can be improved by the addition power factor correction, but poor power factor due to a distorted current waveform requires a change in equipment design or expensive harmonic filters to gain an appreciable improvement. Many inverters are quoted as having a PF of better than 0.95 while in reality, the true power factor is between 0.5 and 0.75. The figure of 0.95 is based on the Cosine of the angle between the voltage and current but does not take into account that the current waveform is discontinuous and therefore contributes to increase losses on the supply. Many devices such as switch mode power supplies and PWM adjustable-speed drives have a near unity displacement power factor, but the true power factor may be 0.5 to 0.6 [4].

2. Specific Case ABO-TRABA desalination plant

Case study involves ABO-TRABA desalination plant fed at 66/11KV from the utility. The plant consists of motors as main load. Nine of the main motor connected at 11KV and the other at 400V. Thus, the overall KW level tends to be relatively varying for extended periods. The typical peak demand at present is 6 MW. Figure .1 shows a simplified one-line diagram of the facility.

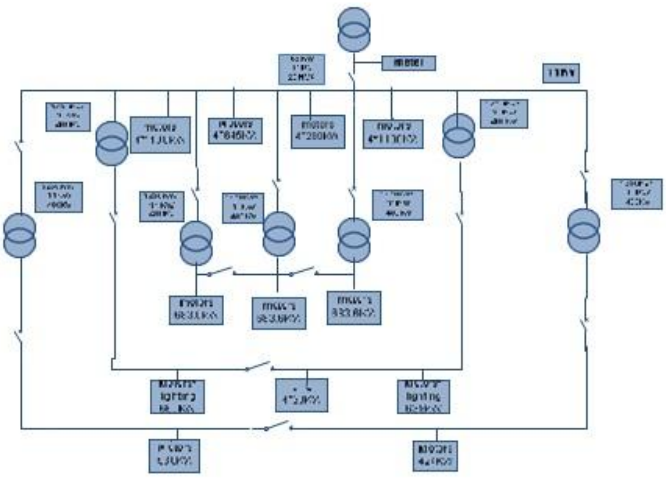

Fig. 1: ABO-TRABA plant single line diagram.

3. Plant survey

Site survey for ABO TRABA desalination plant has been done in order to study the power factor correction:

- Monthly bills consumption.
- Measurements of active and reactive power and instantaneous power factor.

- Load type.
- The existing electrical installation and equipment.
- Harmonic level (Total harmonic distortion).
- Size of the main cables.
- The motors in the plant were identified and monitored

4. Preliminary Evaluation

During the study, the history of the plant consumption has been checked. Table 1 shows the monthly bills consumption of KWh, Kvarh, and average power factor of ABO TRABA desalination plant for the previous one year that obtained from the plant.

Table 1: Monthly consumption of the plant

month	MWh	Mvar	Pmax	PF
2/2014	41241.2	18956.8	4.4	0.9
3/2014	44429	20972.3	4.49	0.9
4/2014	47617.8	22950.5	5.35	0.9
5/2014	49823.6	24336.9	3.9	0.9
6/2014	52018	25706.2	3.61	0.89
7/2014	54722.2	27374.9	4.45	0.89
8/2014	57642.1	29210.8	4.4	0.89
9/2014	60776.8	31166.3	4.45	0.89
10/2014	63268.4	32703.1	5.81	0.88
11/2014	59902.7	34330.8	4.4	0.89
12/2014	67462.1	35303.1	5.16	0.89

The saving of electricity cost per month under two power factor improvements levels

Table 2: The electricity saving under two values of power factor correction.

Power factor	Penalty saving LD	Losses saving LD	Total saving LD
0.93	3861.98	33.03	3895.01
0.95	5406.77	87.25	5494.08

5. Measurements

There are two energy digital meters installed in the plant's main feeders. Both are capable of reading in KWh and KVarh, the names of these meters are:

1. VIP MK3 energy and harmonic analyzer.
2. EMH-COMBI.

Using these meters, different measurements were performed to study the power factor of the plant. Namely, these measurements are active power measurement. Reactive power measurement. Power factor measurement. Harmonic distortion measurement. The plant was monitored and measurements were made during a period of one week, in steps of 30 minutes. These measurements are shown in figures for one day.

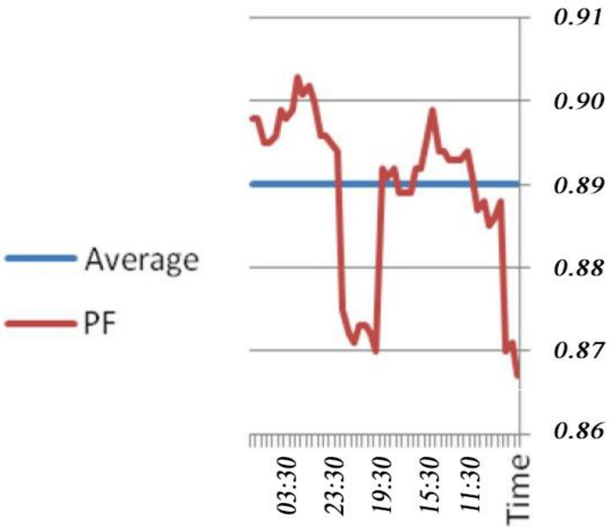

Fig. 2: Power factor for one day.

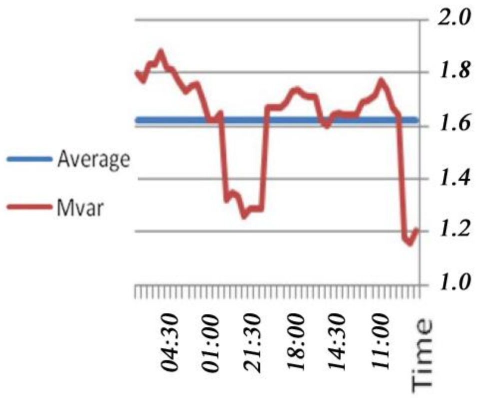

Fig. 3: Power factor for one day.

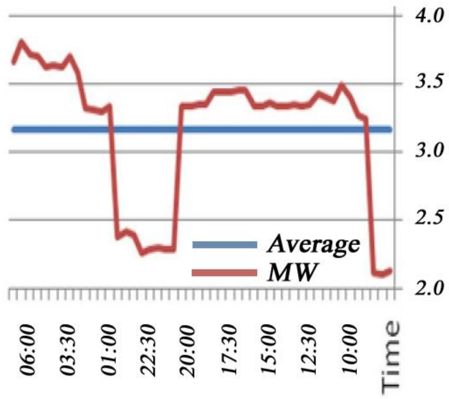

Fig. 4: Power factor for one day.

It is noticed that the instantaneous power factor level vary from 0.867 to 0.903 and is to be low. In addition, the percentage harmonic distortion has been measured and vary from 0.02 to 0.81.

6. Calculations

It is found from the measurement that the maximum percentage harmonic distortion is 0.81. This value is within the acceptable limits according to IEEE 518-1992 recommendation. 5% [8].

The required KVAr for improving the power factor from 0.88 to 0.93 is 900KVar. From the load curve, the minimum load is 2.1MW. The average correction step can be calculated as follows:

$$KW\ (\tan\theta 1 - \tan\theta 2) + C \quad (1)$$

Where θ1and θ2 are the phase angle of initial and final power factor. Moreover, C is the capacitor ratings connected to transformers for magnetizing current compensation [8]. Since the transformer is not connected directly to the load, therefore the value of C is ignored. The value of C in the equation above equal 20 KVar [8].

The average step = 2.1MW *(0.540-0.395) =304.5 KVar.

The available standard= 300 Kvar. The required KVar capacitive load under the two standard cases of target power factor are shown in the table 3 below.

Table 3. Required KVar for two cases of target power factor

Initial PF	Target PF	KVAr	Number of stages
0.88	0.93	900	3*300
	0.95	1300	4*325

7. Results

The total power factor correction cost can be calculated with respect to required KVAr using capacitor fixed cost and capacitor running cost under the two case of power factor improvement monitoring above as shown in the table below. Study cost equal 10% of capacitor cost and installation cost equal 20% of capacitor cost [6].

Table 4: Total power factor cost under two cases of improvement.

Initial PF	Target PF	Capacitor fixed cost LD	Capacitor running cost LD
0.88	0.93	109675.38	5221
0.88	0.95	158420.00	7542
Study cost	Installation Cost	Total cost in LD	
10967.538	21935.076	147799	
15842	31684	213488	

8. Payback period

The simple payback indicates approximately how many years it will take to recover the investment in the capacitors. Typically, industrial facilities prefer to see this number no higher than 2-3 years for simple capacitor installations and 3-5 years for more complex installations with automatic controllers and filters. [1, 7].

Table 5: Show the benefits that achieved by correcting power factor.

Target PF	Penalty Saving LD	Losses Saving LD	Increased system capacity %	Losses Reduction%
0.93	3861.98	33.03	5.4	10.5
0.95	5406.77	87.25	7.4	14.2

It is clear from tables 5 that as PF increases the total saving increases, System capacity increases and losses saving increase. Then the optimum power factor is 0.95 from both technical and economical side of view.

Table 6:payback period corresponding to target power factor.

Initial PF	Target PF	Total saving LD	Total saving LD*12	Total capacitor cost LD	Payback period Year
0.88	0.93	3895.01	46740.12	147799	3.16
	0.95	5494.08	65928.96	213488	3.24

It is found from the measurement in table 6 that the maximum percentage harmonic distortion is 0.81. This value is within the acceptable limits according to IEEE 518-1992 recommendation. 5% [10, 11].

9. Conclusions

Power factor correction provides several technical and economic advantages for customer and utilities and it has been presented in the paper, which has offered the following achievements: Penalty saving, Losses saving, and released system capacity. Power factor cost analysis study for ABO- TRABA desalination plant was conducted in order to determine the economic and optimum power factor. Power factor rates have been tested and it has been noticed that, the tested power factor values were slightly low even. As a result of that, an increase in both electrical energy cost and power losses is highly expected, in addition to system overloading and voltage decreasing. During the study of this research, the following are recommended for future research. The plant has two transformers rated 20MVA 66/11K. One of these transformers is stand by. Therefore, in future study the measurements of all the transformers supply the plant should be taking into account. The devices of the measurements are not capable to measure individual harmonics. Therefore, in the future the measurements should be conducted using more accurate devices denoting all electrical measurements of KW, KVAr, KVA, PF, THD and the individual harmonics.

1. References

[1] Industrial Power Factor Analysis Guidebook Bonneville power administration (March1995).

[2] Full technical support thru hotline 1977 Schneider electric

[3] Schneider Electric. (2002). Electrical Installation Guide according to IEC International Standards, which is compiled and printed in English, facilitates utilization of the IEC 60364 series of international standards.

[4] Ming-Yin Chan**,** Ken KF Lee and Michael WK Fung**.** (2007**)** a Case Study Survey of Harmonic Currents Generated from a Computer Centre in an Office Building.

[5] Schneider electric. (2005). Power factor correction and harmonic filtering.

[6] ABB. July (2008). Power factor correction and harmonic filtering in electrical plants.

[7] Roger C. Dugan / Mark F. Mc Granaghan, Surya santoso / H. Wayne Beaty. (2003). Electrical power systems quality; Second Edition.

[8] Faraj omish and taufik omesh. (2002).Study and Improvement of Power Factor problems For Libyan Distribution Net-Works. Spring.

[9] Eng. Mohamed H. Helal. (2009). Egypt Effects of harmonicon power factor. Egypt. 25May.

[10] Faraj ameish and taufik omesh.(2003).Effect of low power factor in Libyan electrical distribution system**.** . 15may.

[11] J. Gilleskie San Diego Gas & Electric San Diego, California 92123. (1993). Harmonics and how they relate to power factor Robert. November.

[12] Alan Gobi. (2009). Understanding power factor and input current harmonic sin switched mode power supplies. Feb.

[13] Hussein A. Attia1, M. El-Metwally and Osama M. Fahmy. (2010) Journal of American Science Harmonic distortion effects and mitigation in distribution systems**.** March.

Analysis of Human Resource Management System Using Data Flow Diagram

Elham .F. Bograin

Higher Institute of Engineering Professions, Benghazi - Libya
Tel.: +218-92-578-6821; e-mail: elhammail25@yahoo.co.in , author@university.edu

ABSTRACT

يقترح هذهالورقة منهجية لتحليل لنظام إدارة الموارد البشرية (HRM) باستخدام مخططات تدفق البيانات (DFDS) .إن مخطط تدفق البيانات هو رسم بياني لتدفق البيانات بين مختلف العمليات في الأعمال التجارية، وهو أيضاً تقنية رسم بياني تصوّر تدفق المعلوماتالتي تطبق في نقل البيانات من المدخلات إلى المخرجات. ويصف مخطط تدفق البيانات بأنه الرسم الذي يوضح حركة البيانات بين الكيانات الخارجية والعمليات ومخازن البيانات داخل النظام.

لتحقيق مخطط لتدفق البيانات لنظام إدارة الموارد البشرية نحتاج للعديد من الخطوات، حيث تتضمن الخطوة الأولى تحديد حدود النظام، والعمليات، والكيانات الخارجية ، الخطوة الثانية مصادر النظام الاساسي (HRM) والكيانات أو الانظمة الخارجية (Entities) وهذا الذي يمثل المستوى الاعلى للنظام (High Level) وهو ما يسمى ب (Context Level)، تم تقديم وصلات البيانات والعمليات الفرعية على مخططات تدفق البيانات من المستوى 0 و المستوى 1 والمستوى 2 على التوالي, توثيق نموذج منطقي كامل يمثل تحليل نظام (HRM) باستخدام(DFD)إدارة عمليات الأعمال الناجحة تعتمد على نماذج فعالة لتدفق العمل، مع التركيز بشكل أساسي على مراقبة وتنسيق المهام مثل تقنية مخطط تدفق البيانات ، يستخدم (DFD)كمخطط يمثل التدفق من خلال نظام المعلوماتية لتمثيل العمليات في إدارة الصيانة من وجهة نظر البيانات.

This paper search a system analysis methodology for Human Resource Management System (HRMS) using Data Flow Diagrams (DFDs). Several steps will be required to accomplish this work. The first step includes the determination of system boundaries, processes, and data entities. In the second steps, system sources and destinations will be presented on context diagram (level 0). Then data links, processes, and sub-processes will also be presented on data flow diagrams of level 1 and level 2 respectively. Finally, a complete logical model representing a system analysis of HRMS will be documented using DFDs. The use of DFDs lead directly into physical design, with processes suggesting programs and procedures, data flows suggesting composites, and data stores suggesting data entities; files; and database.

Keywords: *Data Flow Diagrams, Human Resource Management*

1. Introduction

In global knowledge economy, information is power for efficient management of Human Assets, HR Professionals requires accurate and timely data on recruitment, selection, training, development, career planning, compensation, productivity, skills inventory, attrition rate etc. [8]. Performance Management consists of three steps – planning, coaching and feedback which is ongoing and not an isolated event, and evaluation. The diagram shows,Figure 1, how the components and steps integrate to form a cohesive process[11].

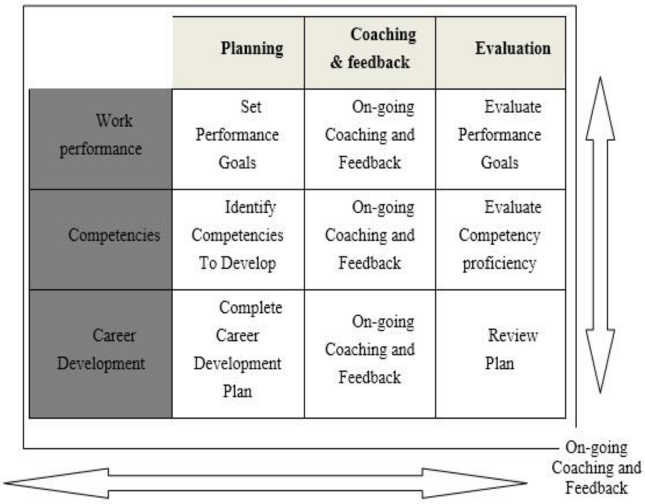

Fig. 1: The diagram of the components and steps integrate to form a cohesive process [11].

Analyze data input or data flow systematically, processing or transforming data, data storage and information output within the context of a particular business. Analyze, design and implement improvement in the functioning of business that can be accomplished thru the use of computerized information system. The SystemAnalysis isthe scientific study of the systems process, including investigation of inputs and outputs, in order to find better, more economical and more efficient means of processing. To improve the productivity of the system. Tools of Structured Analysis Modeling System Functions – ex. Data Flow Diagram, Modeling Stored Data – ex. Entity Relation Diagram, Modeling Program Structure – ex. Program Flowchart, Modeling Time – ex. Gantt chart [1].

Data Flow Diagram (DFD): a modeling tools use to describe the transformation of inputs into outputs. DFD is a graphic illustration that shows the flow of data and logic within the system [7].

2. Research Objectives

Workflow technology has become a standard solution to managing increasingly complex business processes [1]. Successful business process management depends on effective workflow modeling techniques. Recently, researchers have developed a variety of workflow models, focusing mainly on the control and coordination of tasks such as DFD, i.e. the control flow perspective. However, most of these workflow models found it have paid little attention to the data flow perspective. In this paper work, we investigate the data flow issues and propose a data flow modeling approach for HRM in the context of business process management.

A data flow diagram help managers to understand and facilitate the process of decision-making activities. DFD is graphically represent the flow of data through a system without any indication of time. Use DFD in business process model as a graphical representation of the flow of data through an information system, it enables the represent the processes in

ISSN 2522-6967

Human ResourceManagement information system from the viewpoint of data. The DFD can be visualize how the system operates, what the system accomplishes and how it will be implemented, when it is refined with further specification. Data flow diagrams are used by systems analysts to design information-processing systems but also as a way to model whole organizations. The building of DFD at the very beginning of the business process modeling enables the functions of the system to be entered, carry out the interaction between those functions together, and will focuses on data exchanged between processes. It associates data with conceptual, logical, and physical data models and object-oriented models.

3. Human Resource Management

3.1. Introduction of Human Resource Management

The policies and practices involved in carrying out the "people" or human resource aspects of a management position, including recruiting, screening, training, rewarding, and appraising[4]. The term 'human resource management' (HRM) "That part of the management process that specializes in the management of people in work organizations. HRM emphasizes that employees are critical to achieving sustainable competitive advantage, that human resources practices need to be integrated with the corporate strategy, and that human resource specialists help organizational controllers to meet both efficiency and equity objectives." Naturally, the definition of human resource management would be incomplete without further explaining what the terms 'human resources' and 'management' are.First, people in work organizations, endowed with a range of abilities, talents and attitudes, influence productivity, quality and profitability. People set overall strategies, goals, design work systems, produce goods, and services, monitor quality, allocate financial resources, and market the products and services. Individuals, therefore, become 'human resources' by virtue of the roles they assume in the work organization. Employment roles are defined and described in a manner designed to maximize particular employees' contributions to achieving organizational objectives.In theory, the management of people is no different from the management of other resources of organizations. In practice, what makes it different is the nature of the resource, people. One set of perspective views the human being as potentially a creative and complex resource whole behavior is influenced by many diverse factors originating from either the individual or the surrounding environment. Organizational behavior theorists, for example, suggest that the behavior and performance of the 'human resource' is a function of at least four variables: ability, motivation role perception and situational contingencies. Another set of perspectives emphasizes the problematic nature of employment relations: The human resources differ from other resources the employer uses, partly because individuals are endowed with varying levels of ability (including aptitudes, skills and knowledge), with personality traits, gender, role perception and differences in experience, and partly as a result of differences in motivation and commitment. The main process of HR as shown in Figure (2). In other words, employees differ from other resources because of their ability to evaluate and to question management's actions and their commitment and co-operation always has to be won. In addition, employees have the capacity to form groups and trade unions to defend or further their economic interest. Human resource is often referred to as personnel, staff or workers [2].

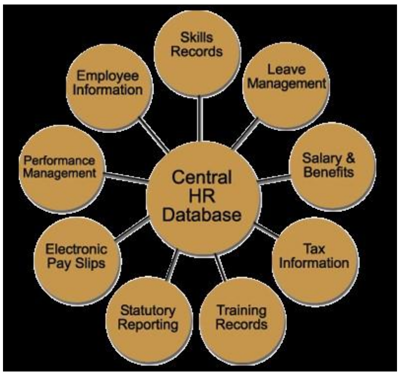

Fig. 2: Main Process of HR [2].

3.1.1. What isHRM and HRD?

HRM is best understood as the "process of managing human talents to achieve organization's objective". The process of managing human talents is said to include the process of recruitment and selection, compensation and benefits, labor and industrial relations and the management of employees' safety and health in organizations. On the other end, researchers and writers have proposed numerous definitions for HRD. These definitions varied from the perspectives of an individual researcher or theorists to definitions of HRD by country. In addition, theorists have even tried to define HRD from a global and international perspective. Indeed, many definitions have been suggested; even before the emergence of HRD in 1970s through today. A definition by Nadler and Nadler in 1970s described HRD as "a series of organized activities conducted within a specified time and designed to produce behavioral change" through training activities. The latest definition by DeSimone, Werner & Harris (2002) for HRD was defined as "a set of systematic and planned activities designed by an organization to provide its members with the opportunities to learn necessary skills to meet current and future job demands". These systematic and planned activities are said to include training and development, career planning and development, performance appraisals and management and change management for organizational development. In the context of professionals, this activity is termed as continuing professional education and development. To all intents and purposes, the continuing professional education and development activities are the same as in training and development but it is labeled differently directed to professionals' education and development [6].

3.1.2. The relationship of HRM and HRD

Traditionally, some writers suggested that HRD is a component of HRM in which HRD supports the HRM function in employees' training and development and the notion of training and development fitting in or integrated with HRM as in the 'HRM's wheel' . All the four components of HRD, namely; training and development, performance appraisals and management, career planning and development as well as change management [5]. At Table (1) comparison of HRM and HRD

Components was advocated as positioned under the 'umbrella' or function of HRM along with other components such as recruitment and selection, compensation and benefits, employee and industrial relations as well as safety & health [2].

Table 1: Comparison of HRM and HRD

HRM	HRD
Definition: HRM is process of managing human talents to achieve organization's objective	Definition: HRD is a series of organized activities conducted within a specified time and designed to produce behavioral change
Process: 1. Recruitment and selection 2. Compensation and benefits 3. Labor and industrial relations 4. Safety and health management	Activities: 1. Training and development 2. Performance and appraisals 3. Career planning and development 4. Change management

3.1.3. HRM and productivity

HRM effects on productivity as:

- Increase in productivity from individual and group pay schemes
- True across many sectors/firms
- Large selection effect but also incentive effect
- More effective when introduced as a package of
- complementary" practices – Teams
- Human Capital – ICT
- Non-pay HRM practices have (i) had less high quality studies, (ii) positive correlations tend to disappear when fixed effects included [5].

3.2. Strategic Human Resource Management

Today, HRM has become more important to strategic management, mainly because of its role in providing competitive advantage and the rush to competitiveness. [14]. Human resources management in the context of finding, attracting and selecting employees has a significant effect on improving the effectiveness of staff, it effective in the evaluation of their performance, effectiveness of employees` performance in designing and implementing training programs of development [12.]

The nature of management skills are culturally specific, a management technique or philosophy that is appropriate in one country is not necessarily appropriate in another, In addition, cultural dimensions namely, Individualism/Collectivism; Power Distance; Masculinity/ Femininity; there are impact of national culture on human resource management practices [13]. theory in strategic human resource management must continue to increase if the field of strategic is to move forward. Strategic in reality is not usually a formal, well –articulated and linear process which floes logically from the business strategy. However, there is a growing literature on the impact of HRM practice on organizational performance [14].

4. Data Flow Diagrams

4.1. Introduction of Data Flow Diagrams

A picture of the movement of data between external entities, the processes, and data stores within a system. DFDs depict logical data flow independent of technology. May be used as a discovery technique for processes and data, or as a technique for verification of a Functional Decomposition and Entity Relationship Diagram that have already been completed. Most users find these diagrams quite easy to understand generally considered a useful analysis deliverable to developers in a structured programming environment [9].

4.2. Data flow diagram symbols

There are four primary symbols used to create a data flow diagram shown in figure (3).

- A source or destination (sink) is represented by a (shaded) square. Sources and destinations define the system's boundaries; each one represents a person, organization, or other system that supplies data to the system, gets data from the system, or both.
- A process, or transform (a round-cornered rectangle) identifies an activity that changes, moves, or otherwise transforms data.
- A data store (an open-ended, horizontal rectangle) represents data at rest and implies that the data are held (for some logical reason) between processes.
- A data flow (an arrow) represents data in motion. Additionally, Gane and Sarson use thick arrows to show physical or material flows.

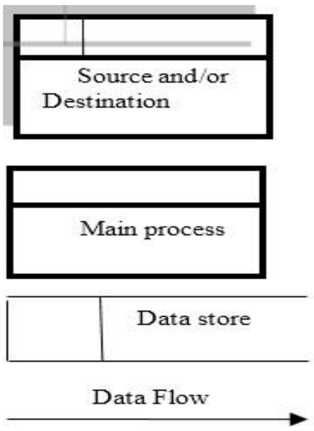

Fig. 3: Symbols of data flow diagram [4].

4.3. Logical and physical data flow diagrams

A logical data flow diagram's symbols are used to describe logical not physical entities. A process might eventually be implemented as a computer program, a subroutine, or a manual procedure. A data store might represent a database, a file, and a book, a folder in a filing cabinet, or even notes on a sheet of paper. Data flows show how the data move between the system's components, but they do not show the flow of control. The idea is to create a logical model that focuses on what the system does while disregarding the physical details of how it works.

A physical data flow diagram uses data flow diagram symbols

ISSN 2522-6967

to represent the system's physical processes (programs, manual procedures) and physical data stores (files, databases, reports, screens, etc.) and shows how the system works. Some analysts like to start the analysis process by preparing a physical data flow diagram of the present system. Following the analysis stage, physical data flow diagrams can be used to document alternative solutions [10].

4.4. Why use DFD for analysis of HRMS

The data for the HR system project could be termed in the operational, technical and economic feasibility. A project needs two types of information to compute the feasibility that are primary and secondary data [1]. The data is transmitted after analyzing and checking the effectiveness and the usefulness of the information for the project. It is also essential for that the information, which is gathered, should be dependable and suitable. The information or data collecting procedure should be efficient to examine the system. For it, a new and efficient data move policy should be adopted. To investigate the effectual data transfer. The data flow diagram could be used to determine the validity of the fact of data [2].

5. Discussion and Results

The overall methodology of the proposed research work can be summarized into phases

- Understanding the business requirements of the HRMS.
- Identifying the business processes of the HRMS.
- Preparing a high-level business design. Present and review the completed high level business process design.
- Determining the processes, external entities, data stores and data flows of every identified process [4].
- Drawing the data flow diagrams corresponding to these identified elements.
- Presenting numerous a DFD by decomposition, Child diagrams and Balancing.

Decomposition: is the process of representing the system in a hierarchy of DFD diagrams. **Child diagrams:** show a portion of the parent diagram in detail. **Balancing:** involves insuring that information presented at one level of a DFD is accurately represented in the next level DFD.

The steps involved in Building DFDs are summarized as follows:

- Build the context diagram
- Create DFD fragments for each use case
- Organize DFD fragments into level 0 diagram
- Decompose level 0 processes into level 1 diagrams as needed; decompose level 1 processes into level 2 diagrams as needed; etc.
- Validate DFDs with user to ensure completeness and correctness. [9]

Benefits of data flow diagrams: The data flow diagrams are the basis of structured systems analysis. A data flow diagram acts as a bridge between users and systems developers. Thus, a data flow diagram is a:

- Graphical representation that eliminates thousands of words;
- Logical representations that represents WHAT a system does, rather than physical models showing HOW it does it;
- Hierarchical representation illustrating systems at any level of detail and
- Jargon less representation that allow user to clearly understand and review the system.

The advantages of data flow diagram include:

1. It helps technical and non-technical users to easily understand systems design.

a. It helps in validating the correctness of the system. It is therefore easy to determine whether requirements are correct. The probability of a better system is increased.

2. It allows the analyst to abstract to whatever level of detail is required so that it is possible to examine a system in overview and at a more detailed level.
3. It specifies the system at a logical level rather than a physical level i.e. it shows what the system will do rather than how it will be done.
4. It helps to understand the inter-relatedness of systems and subsystems of the system.
5. It provides a means of analysis of a proposed system to determine if the necessary data and processes have been defined [1].

6. Conclusion

The general objective of this research work is to develop a Data Flow Diagram for Human Resource Management System. In order to achieve this objective the following specific objectives have to be accomplished:

- Investigation some of the existing HRMS to understand how the systems boundaries, processes and data entities are logically related.
- Developing the context diagram (level o) which documents the systems boundaries by highlighting its sources and destinations.
- Developing the level 1 data flow diagram, which shows the system reviewing, processes, data stores, sources and destinations linked by data flows.
- Developing level 2 data flow diagrams which consists of several sub process that are listed on the process description.
- Reporting a final logical model, which consists of a complete set of data flow diagrams for HRMS.

References

[1] Tech, B. (1999) "System Analysis & Design", KSOU, [Available at: http://www.sharadavikas.com/courcemeterials/btc33.doc].

[2] Out D.O.A.B.U. Zaria, (2000)"Human Resource Management in Education Course Development ,EDA 721", [available at: http://www.nou.edu.ng]

[3] Dessler,G. (2004) "Human Resource Management",10 edition, [available at: https://evergreenvmw.files.wordpress.com]

[4] Sui Generis Team. (2006) "Data Flow Diagram Process", CMPE202-5-Sui2, [Available at: www.engr.sjsu.edu]

[5] Bloom,N. Reenen,J (2009) "Human Resource Management (HRM) and Productivity", [available

ISSN 2522-6967

at:www.iza.org/en/webcontent/personnel/vitae/2577_cv.pdf]

[6] Haslinda, A. (2009) "Evolving Terms of Human Resource Management and Development (PMENT)", The Journal of International Social Research Volume, [available at: www.sosyalarastirmalar.com].

[7] Thomas, B. and Taquiqui, M. (2010) "System Analysis and Design for Business",COMP13D, [Available at: www.doc-txt.com/sales-IPO-and-flowchart]

[11] Guide,Lead@uva, (2013)"Managing Performance for success" , [available at: www.hr.virginia.edu]

[12] Alami, R. Sohaei, R. Berneti, A. Younesi, A. Farnia, M. And Mirzajani,H (2015) "The Effectiveness of Human Resource Management on Improving the Performance of Education Staff" , International Journal of Business and Social Science, [available at: //ijbssnet.com/journals/Vol_6_No_5_May_2015/28.pdf]

[13] Sarayrah, S. Tarhini,A. Obeidat ,B. Al-Salti,Z. and Kattoua, T., (2015) Practices: A Theoretical Perspective" , International Journal of Business

[8] Bhavsar, A. (2011) "A Conceptual Paper on Human Resource Information System (HRIS)", M.S.G College, Malegaon Camp Dist. Nashik. Pin 423 105, [available at: http://documents.mx/documents/research-paper-on-hris-2.html].

[9] Lecture, (2011)"Introduction to data flow modeling", BCIS 4610, University of North Texas [available at: www.studysoup.com]

[10] Sybase. Co, (2012) "Data Flow Diagram", [Available at: Management and Economic Research(IJBMER), available at: www.ijbmer.com/docs/volumes/vol7issue4/ijbmer2016070402.pdf "The Effect of Culture on Strategic Human Resource Management

[14] Sajeevanie, T. (2015) "Strategic Human Resource Management and Theoretical Background: A Critical Review Perspective", Third Asia-Pacific Conference on Global Business, Economics, Finance and Banking, available at:

http://globalbizresearch.org/Singapore_Conference2015

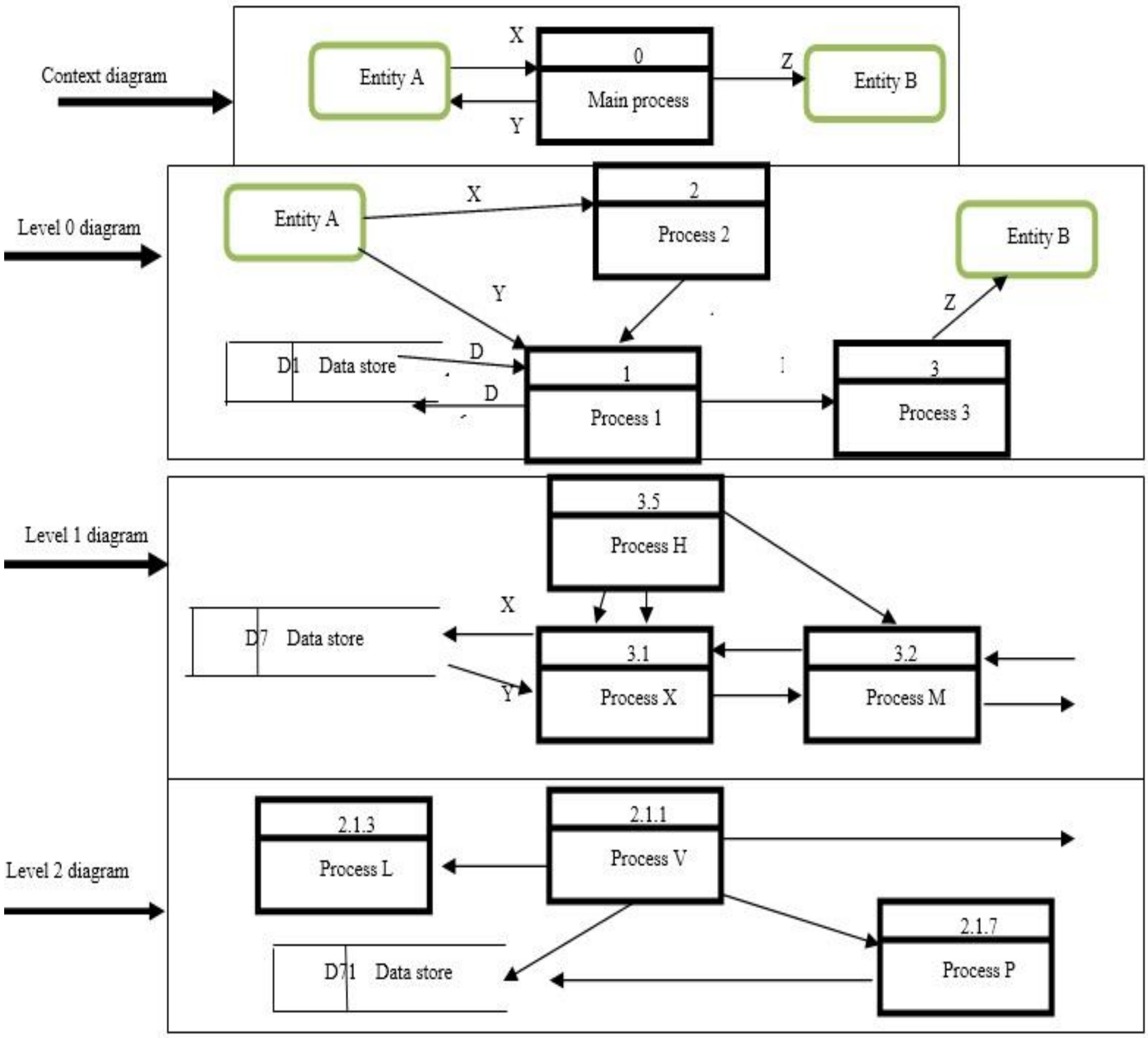

Fig. 3: Relationship among levels of DFDs [1].

ISSN 2522-6967

Building Integrated Photovoltaics for Energy Load Reduction and Supply

Mohamed Milad Hawiwo

Architecture and Urban Planning Department, University of Benghazi, Benghazi, Libya
Tel.: +218-924418549; e-mail: Mohamed.hawiwo@uob.edu.ly

ABSTRACT

Photovoltaics as an environmentally friendly source of energy are still considered as an economically expensive method of electricity production. However, replacing the conventional elements of the building envelope (façade, shading devices, skylights, etc.) with PV modules, the total cost of a built construction is remarkably reduced. The main aims of this study to use building integrated photovoltaic (BIPV) system beside its functions that has mentioned above, to reduce the energy consumption from the cooling load of buildings in warm climate regions. The paper investigated the optimum integration of the photovoltaic system into the building envelope that could produce a reasonable power output and minimizes the heat gains in warm climate regions. The simulation software Autodesk Ecotect Analysis was used to simulate three main PV integrations, window sunshade, roof screen and double skin façade into an assumed office-building model located in the city of Benghazi, Libya. The simulations provided good information for analyzing the potential contribution of the BIPV system on the energy saving according to the PV thermal performance and the power supply generated from the sun, and the final discussion results in choosing the sunshade PV integration as the optimum integration that could produce a reasonable power output and minimizes the heat gains in warm climate regions.

Keywords: *building integrated photovoltaic, energyconsumption, coolingload, poweroutput.*

1. Introduction

There is plenty of information around about the suitability and characteristics of timber, masonry, glass, steel and concrete construction, and other building industry materials, but what do we know about "photovoltaic construction"? What kind of material is this, which has become available to architects in square meters of building envelope surface?

Architects as a consultant for customers, they must carefully design the function, the aesthetic and the technical of the building. Therefore, in the case of building integrated photovoltaic, the consideration at the primary design of the project will result in a useful integration. For some integration systems such as facade and atrium, it is significant to know the thermal properties of PV materials. Thus, architects should have the knowledge and the techniques to promote PV integration in the building's envelope.

2. Solar and Energy in Libya

At any location, the information on solar energy properties and the meteorology parameters play an important role for studying, planning and designing solar energy applications. Libya is located in the heart of North Africa with 6 million occupants distributed over an area of 1,750,000 Km^2, 88% of its area is desert areas, the high inherent of solar in the Sahara desert in the south could be used to produce electricity by both thermal and solar energy conversions Photovoltaic. The daily average of solar radiation on a horizontal plane is 7.1kwh/m^2/day in the coastal region and 8.1kwh/m^2/day in the southern region, with sun period of more than 3500 h /annum [10].

The high potential of solar energy in Libya could be considered as a future source of electricity, in hot climatic conditions, a substantial share of electricity goes to theair-conditioning of buildings [6].

3. Building and Energy Consumption

Buildings generate significant impacts on the environment during their life cycle; these impacts come from the energy consumed during the occupation of the building and from the materials used for the construction. However, the fossil fuels from are not inexhaustible, and burning them discharges carbon dioxide (CO_2), one of the main greenhouse gases, which are believed to be responsible for global warming. Buildings consume 42% of the world's total energy, responsible for all atmosphere emissions with about 40%, and 30% of all building materials used; all these can be substantially influenced by architects and engineers [13].

To design a building, environmentally friendly and perfect energy conversion system, it could be hard to create something more effective than the PV cell. In the Photovoltaic cell, a gadget exploits an energy source that is the most plentiful of those available on the planet [2].

4. Building and PV Interaction (BIPV)

The first installation of building-integrated Photovoltaics (BIPV) was realized in 1991 in Aachen, Germany [1]; the photovoltaic elements were integrated into a curtain wall facade with isolating glass. After finishing the first BIPV installation, the demand for modules constructed for building-integration grew rapidly.

For general energy supply, it will be necessary to integrate a large photovoltaic system. The architectural treatment of large areas of photovoltaic and selecting from vireos types of modules will be the key design considerations, vireos shapes, vireos colors or vireos textures of modules to be applied to face off the building. For buildings with energy independent, the accurate size of the photovoltaic system will be depended on the system efficiency and the yearly output that could be generated. The designer will have to carefully design the building around the integrated system to accommodate a specific number of modules [9].

To qualify a project as 'well-integrated', building quality and the technical performance of the photovoltaic system have to be done in a professional way, and of course, the architectural quality has to be of a high standard. A poorly integrated PV system on a good designed building might be disturbing, but a poorly integrated PV system on a poorly designed building is clearly worse. Similarly, an elegant PV system will not necessarily improve the overall design.

The building envelope provides a number of possibilities for the integration of PV. According to Stark, 2009, the main options are [12]:

- Roofs integration.
- Facades integration.
- Solar Control (Sunshade elements) integration.

If designers have to decide a single PV integration into the building envelop to save costs, in this case, what is the optimum integration of the photovoltaic system into the building envelope that could produce a

ISSN 2522-6967

reasonable power output and minimizes the heat gains in warm climate regions?

5. Methodology withData Collection and Analysis.

The answer for the main study question that been asked, will be discussed by using computer simulation of three main different PV integrations into an assumed office building in Benghazi city, Thus the first step of this discussion should be outlining the features of the software program that will be used to simulate the building module and then analyzing the weather data of the location of the office building will be situated by using this program.

5.1. The Software Program

'Autodesk Ecotect Analysis', integrates an interactive design and 3D modeler with an expanded range of environmental analysis tools, which enables designers to simulate their building performance from the primary stages, a time when simple decisions can have long-term effects on almost every performance feature of the final project.

5.2. Location Data

The city of Benghazi, Libya Latitude: (32°07'12"N), Longitude: (20°04'12"E), Altitude: 131 m. The assumed office building will be situated in the heart of Libya's second largest city, Benghazi, on the Mediterranean Sea.

5.3. Weather Analysis

Summer's season in Benghazi is warm and dry; winter is mild with infrequent rain, spring and autumn are the finest times' year round. The following table (1) show the years average weather condition readings for Benghazi. As it can be seen, a notable high average temperature during June, July, August and September, thus the highest energy using for air conditioning system will be in these months.

Table 1. Solar surface meteorologyof Benghazi [7].

Variable	J	F	M	A	M	J	J	A	S	O	N	D
Insolation, kWh/m²/day	2.71	3.64	4.90	6.36	7.14	7.93	7.97	7.26	5.92	4.40	3.06	2.47
Clearness, 0 - 1	0.49	0.53	0.57	0.63	0.65	0.70	0.71	0.70	0.65	0.59	0.52	0.48
Temperature, °C	14.76	14.62	15.90	18.73	21.83	24.63	25.96	26.90	25.91	23.34	19.85	16.31
Wind speed, m/s	6.41	6.79	6.65	6.31	6.05	5.61	5.75	5.65	5.64	5.23	5.86	6.45
Precipitation, mm	69	36	24	7	4	0	0	0	3	21	28	60

5.4. The Assumed Office Building Parameters

The shape of the building is a simple rectangular with dimensions of 35m long, 14m wide and 14m high. Four-story building with total living space area equal 1960m^2, exterior wall area (excluding glazing area) is 1485m^2; the area is 376 m^2, and the roof area is 490m^2, with a whole volume amount to 6860 m^3, Figure (1).

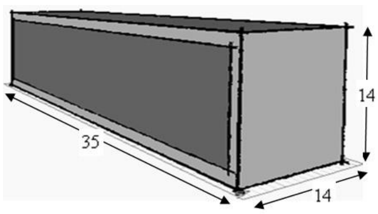

Fig. 1: The assumed office building parameters.

The building materials and properties were extracted from the wide choice of materials standard data available in the Ecotect program.

The maximum number of staff could use this office is 210 member (9.3m^2/person), the comfort temperature is 22°C, fresh air rate is 20 CFM/person, the office equipment is 22W/m^2, the lighting levels are fluorescent lights, 20 W/m^2, with a full air conditioning system (Ecotect).

The common type of material for external wall in Libya is (Concrete Block Render), 20mm externally rendered, 150mm concrete block with 20mm plaster inside, with an overall U-value 1.830 W/m^2.k (Ecotect), Figure (2).

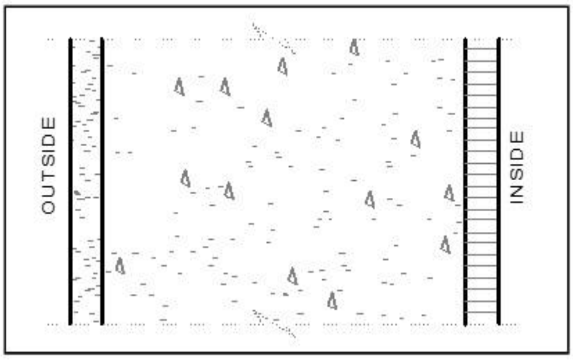

Fig. 2: The external wall (Concrete Block Render).

The common type of material for roof in Libya is (Concrete Roof Asphalt), 6mm asphalt cover, 200mm concrete Light weight, 600mm air gap and gypsum, with an overall U-value 0.720 W/m2.k (Ecotect), Figure (3).

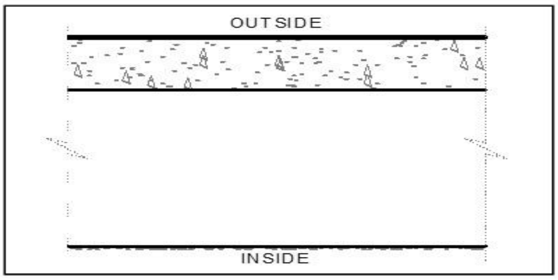

Fig. 3: The roof (Concrete Roof Asphalt).

The window is double-glazed with aluminum frame, 6mm glass standard, 30mm air gap, 6mm glass standard, and theU-value is 2.70 W/m^2.k (Ecotect), Figure (4).

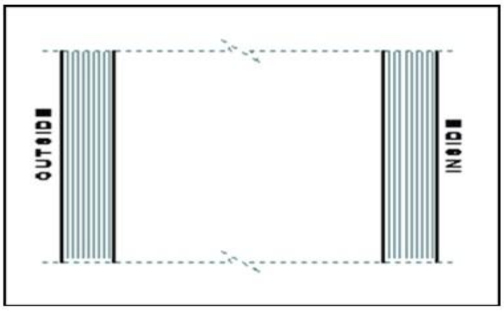

Fig. 4: The window double-glazed with aluminum frame.

5.5. Simulate The Building Model

Once the building parameters and the envelope data are defined and uploaded into the program, and the location weather data as well, the window side of the building will be faced the south, the simulation of the model is performed using the Ecotect program to calculate the energy loads for cooling demands during the peak period of the warmest months in the year, June, July, August and September.

Figure (5) shows the first simulation for the base model without any PV integration, this reference model will be used as a foundation to compare and level the result of each of the next integrations of the PV into the building envelope.

ISSN 2522-6967

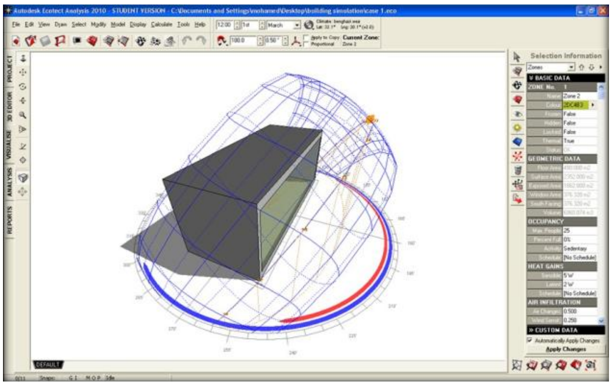

Fig. 5: The reference model simulation (Ecotect).

Figure (6) illustrates the energy calculations for cooling and heating along the year. To focus on the peak energy demand for cooling periods; it is obvious that the most demand usually during July and August months, Figure (7).

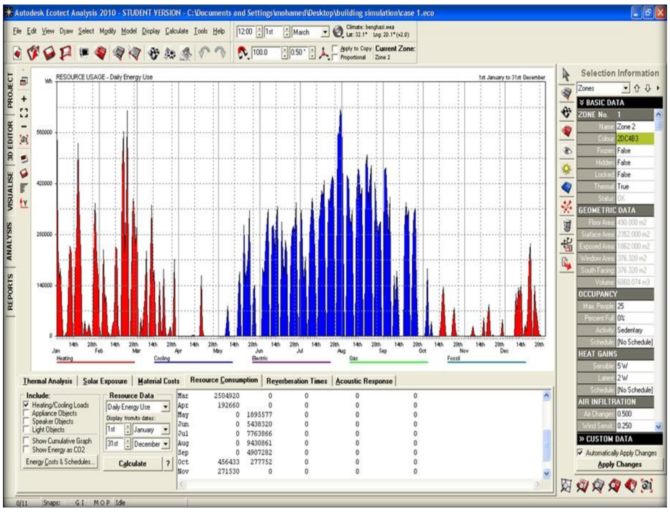

Fig. 6: The energy calculation for cooling and heating periods (Ecotect).

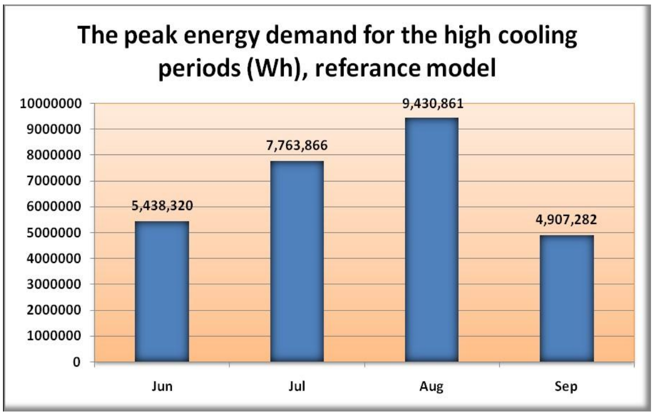

Fig. 7: The peak energy demands for cooling periods (Ecotect).

5.6. Simulate the Building Model in Different PV Integrations

Using the same reference model parameters to integrate the PV into the building envelope in three main different ways to compare their results with the base model result and Figuring out the optimum integration that will be answering the study question.

To start the simulation, the type of the PV module needs to be chosen, thus, among a hundreds of the good quality PV module producers, the decision is been made to choose Schottsolar company, and The reason for this choice is the company's attention to the issue of thermal and the high temperature of the PV modules.

5.6.1. Simulate the Building Model with the PV WindowSunshades Integration

The PV module that has chosen to be integrated into the building as window sunshades from Schott Company will be SCHOTT POLY™180, with nominal power ≥ 180W, the cell type is polycrystalline, and the module dimensions are 1.62m×82m [11].

The total area of the PV modules is 110.692 m^2, that means 84 modules distributed in four floors as illustrated in Figure (8), and these modules should produce a total power equal 15,120W, the approximately total cost of these modules will be amounted to $13,144 [8].

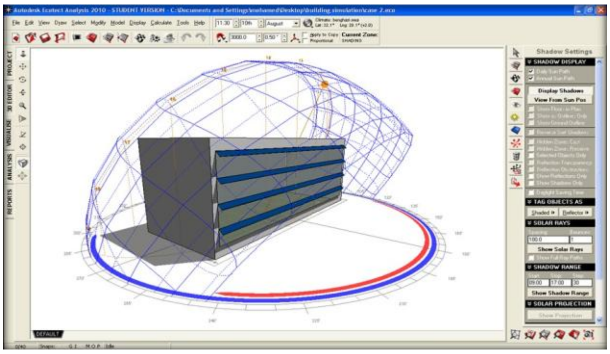

Fig. 8: The PV integrated into the building as windowsunshades (Ecotect).

The photovoltaic cell's ideal tilt is derived from the degree of latitude of the location, therefore, the optimum tilt of the shading PV modules to receive the maximum solar radiation calculated with this simple formula: tilt = 0.9 × latitude, thus, the optimum tilt will be equaled to 29◦ (the city latitude 32.1 × 0.9), [4].

Figure (9) illustrates the energy calculations for cooling and heating along the year for this integration. The peak energy demand for cooling periods that illustrated showed a good reduction in this integration, especially in July and August months when it is compared with the reference model results.

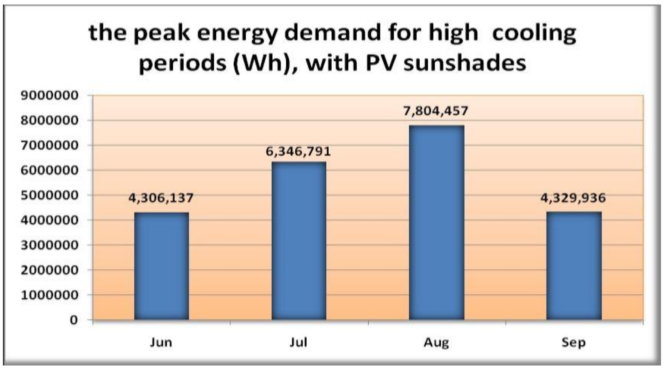

Fig.9: The peak energy demands for cooling periods with the sunshades integration(Ecotect).

The PV modules energy output in this integration was calculated by using Ecotect program and the total energy output will be equaled 6,590,813Wh per annum. Figure (10) illustrates the daily solar collector calculations according to this integration (Ecotect).

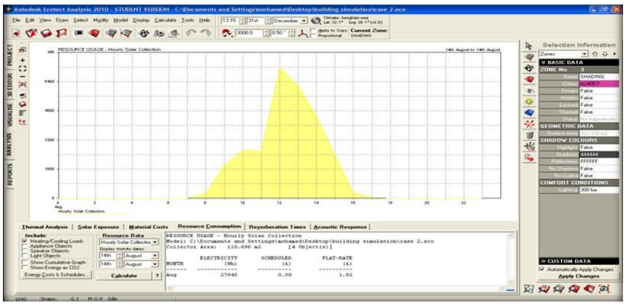

Fig.10: the daily solar collector calculations with sunshade integration (Ecotect).

5.6.2. Simulate the building model with the PV integrated as a screen over the roof

The same PV module that used in the previous integration will be used in this one as well; the total area of the PV modules is 416 m^2, which means 317 modules integrated into the building as a screen over the roof, with 3m high to get a useful space underneath it as illustrated in Figure (11). These modules should produce a total power equal 57,060W; the approximately total cost of these modules will be amounted to $49,620[8].

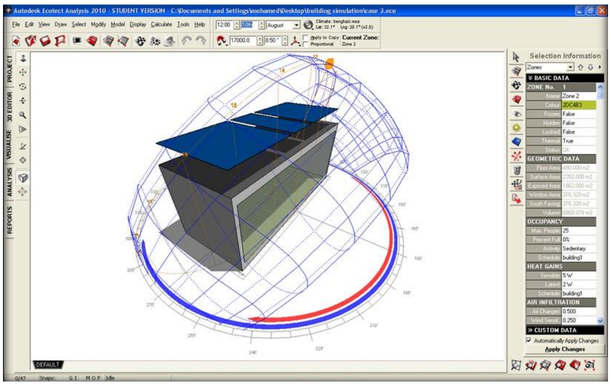

Fig. 11:the PV integrated into the building as a screenover the roof (Ecotect)

Figure (12) illustrates the energy calculations for cooling and heating along the year for this integration. The peak energy demand for cooling periods that illustrated showed just a slightly reduction in this integration when it is compared with the reference model results.

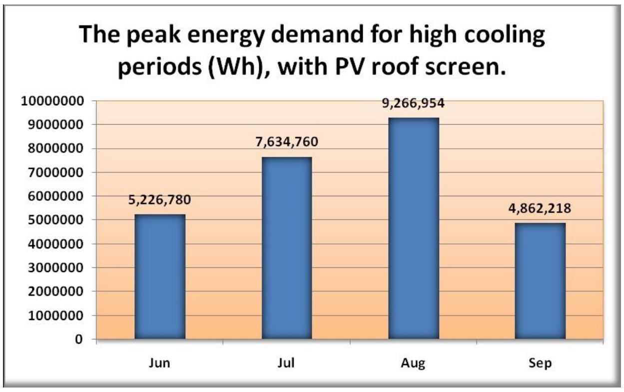

Fig. 12: the peak energy demands for cooling periods with the PV roof screen integration (Ecotect).

The PV modules energy output in this integration was calculated and the total energy output will be equaled 35,542,735Wh per annum. Figure (13) illustrates the daily solar collector calculations according to this integration (Ecotect).

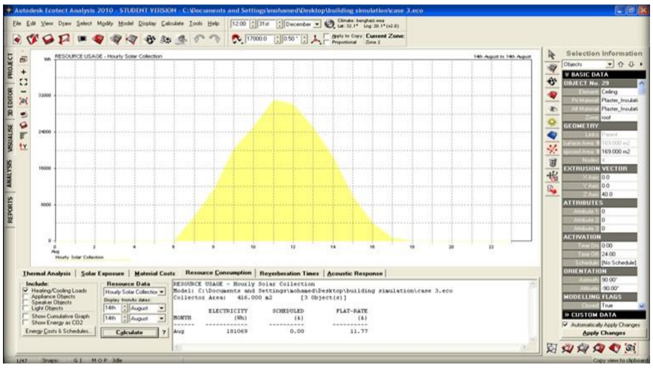

Fig. 13: The daily solar collector calculations with the PV roof screen integration (Ecotect).

5.6.3. Simulate the building model with the PV as double skin facade integration

As the position of The PV module needs transparency and thermal resistance, therefore, the PV module type that has chosen to be integrated into the building as double skin facade with air gap equals to 20cm, will be from Schott Company as well with a see- through effect, semi-transparent thin film with a-Si cells SCHOTT ASI™100, with nominal power ≥ 100W, and the module dimensions are 1.108m ×1.308m, the U-value will be 1.4 W/m^2.k [11].

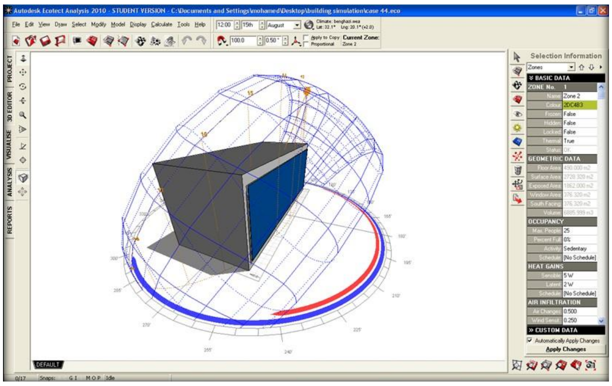

Fig. 14: The PV integrated into the building as a double skin façade (Ecotect).

The total area of the PV modules is 376 m^2, which means 260 modules integrated into the building as a screen over the roof, as illustrated in Figure (14) above. These modules should produce a total power equal 26,000W; the approximately total cost of these modules will be amounted to $22,610 [8].

Figure (15) illustrates the energy calculations for cooling and heating along the year for this integration. The peak energy demand for cooling periods that illustrated showed a little reduction in this integration when it is compared with the reference model results.

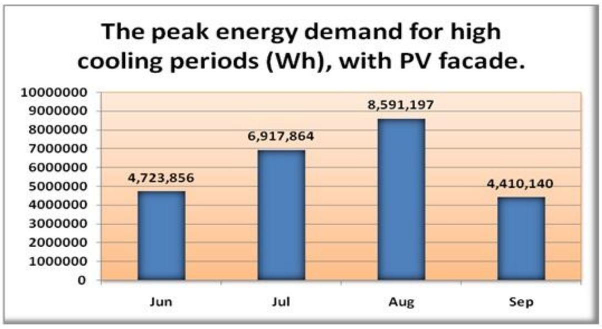

Fig. 15: The peak energy demands for cooling periods with the PV as double skin facade integration (Ecotect).

ISSN 2522-6967

The PV modules energy output in this integration was calculated and the total energy output will be equaled 1,901,537Wh per annum. Figure (`16) illustrates the daily solar collector calculations according to this integration (Ecotect).

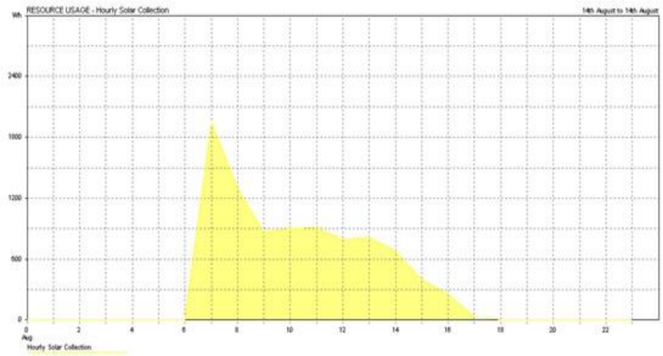

Fig. 16: The daily solar collector calculations with the PV as double skin facade integration(Ecotect).

6. Results discussion

The simulations provide good information to analyze the potential contribution of the BIPV system on the energy saving according to the PV thermal performance and the power supply generated from the sun.

6.1. The PV thermal effect:

Reducing the cooling demands during the peak load of the summer months was the first issue of these different types of integrations. Therefore, the effect of each type of PV integration will be discussed. Figures (17,18 and 19) show the energy saving after integrate three different types of PV modules compared with the reference model.

It can be seen that the window sunshade integration resulted in significant reductions in the amount of the summer months solar radiation entering into the building spaces, this reflected to a good saving in the energy with overall 17.26% reduction when it is compared with the reference model. The other integrations (roof screen and double skin façade) are not good saving as much as the sunshade integration with 4.83% and 10.52% respectively.

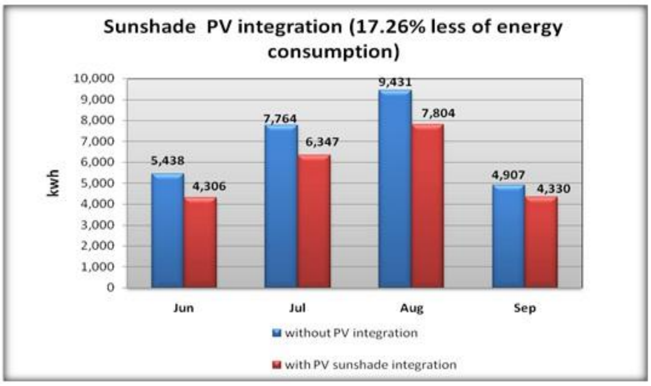

Fig. 17: The energy saving during the peak cooling load with sunshade PV integration.

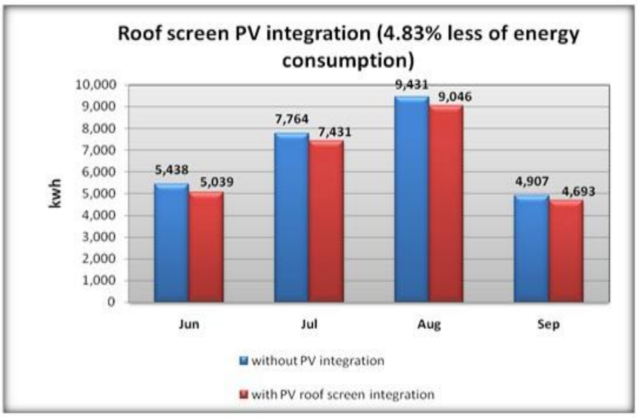

Fig. 18: the energy saving during the peak cooling load with roof screen PV integration.

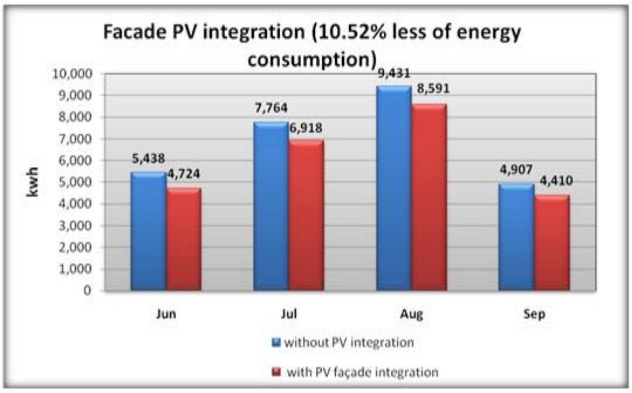

Fig. 19: The energy saving during the peak cooling load with double skin façade integration.

6.2. The PV Solar Power Generation

The second performance that should be discussed after the thermal effect is the solar power generation from the three types of integrations. Figure (20) shows the output energy that could be used as renewable clean energy from each type of the three integrations.

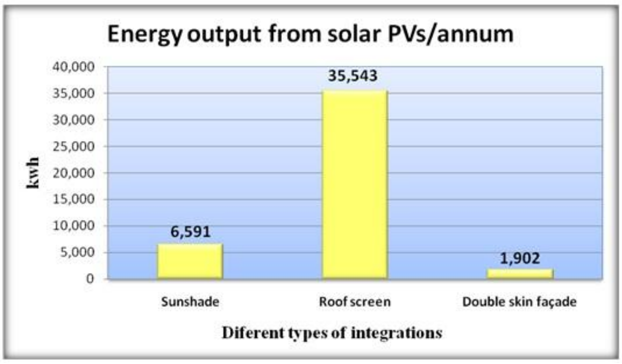

Fig.20: The annually energy output from the different types of the PV integrations

It is obvious that the roof screen PV integration has the higher output of energy with 35,543kwh, which could cover the peak load of cooling demand and more, while the other types of integrations are very low. If the PV area of each type is taken into account in the three integrations, as showed in Figure (21), it can be seen that the double skin façade has the lowest efficiency, and the reason behind that is the tilt of the PV modules 90◦.

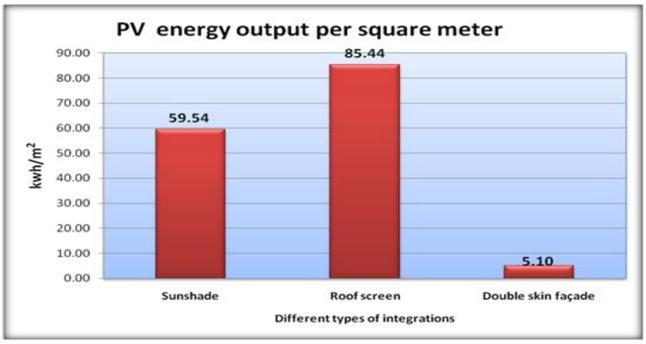

Fig. 20: The annually energy output from the different types of the PV integrations / m^2

Most of the solar radiation can be generated from the summer solar where the useful tilt can be figured according to the altitude of the building location, and according to Benghazi city altitude, the maximum output will be in the tilt between 0◦ to 35◦. The output energy from the sunshade PV is still reasonable compared with its area.

6.3. The cost of the PV Modules and the Power output

According to the power output and area of the PV module, the cost of the total modules in each of integrations was calculated according to Gupta, 2010, that mentioned before and which resulted in Figure (21) below [8].

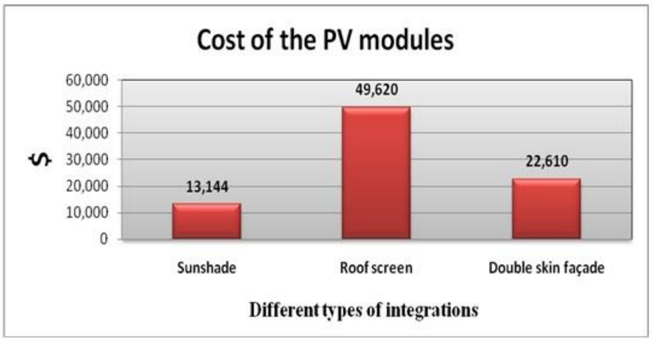

Fig. 21: The PV modules cost of the different types of integrations

On one hand, it can be seen from the above Figure that the cost of the roof screen PV integration is very high compared with the other integrations because of the PV modules area, on the other hand, the cost of the energy output from this integration will be the minimum as showed in the Figure below, this output cost can be figured out according to the lifetime of the PV modules (±25 years) and the total power output during this period with the total cost of the PV models ($/kwh) in the different types of integrations, Figure (22).

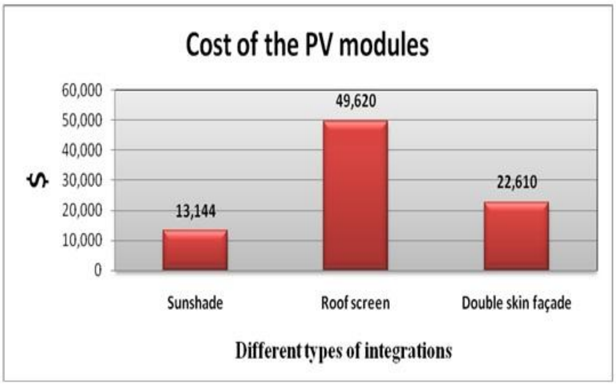

Fig. 22: The output cost of the different PV types

6.4. The different PV integrations and the CO_2 emissions reduction

The CO_2 emissions that could be saved from the reduction of the energy which converted according to Defra, 2015; it is obvious that the roof screen is the higher saving, Table (2) [3].

Table 2: The annually PV modules CO_2 reduction of the different types of integrations (kg/year).

CO_2 emissions reduction (kg/year)	Sunshade	Roof screen	Double skin façade
From the PV thermal effect	2,595	727	1,582
From the PVsolar output	3,599	19,406	1,048
Both thermal & solar	**6,194**	**20,133**	**2,630**

6.5. The Different PV Integrations and the Comfort:

Concerning the day lighting, in an office building, artificial light accounts for a high percentage of energy use, lighting levels are set to improve the performance in an office environment. In warm and sunny climate like the assumed office building location, it is not practical to install big area of windows especially south facing, as the heat gains could be high from the direct solar radiation and the building cooling throughout the day. Another issue might be occurred from the direct solar radiation that is the glare and the visual comfort. However, the direct solar radiation can be controlled by using an optimum size and tilt of the PV sunshade device, and this integration can protect the area of windows from the solar radiation during the summer months and its glare, while the winter direct solar radiation can still pass through the windows area and maintain a good passive solar for heating and good level of visual comfort, furthermore, will offer a uniform distribution of light and good thermal performance, especially the office spaces that close to the windows. According to the previous results, Sunshade PV has succeeded in these issues with good performance while the double skin façade PV could be quite good at the building thermal performance, but not efficient with the visual comfort. Roof screen PV integration has no effecting on the building comfort.

7. Conclusion and recommendations

The simulations provided good information for analyzing the potential contribution of the BIPV system on the energy saving according to the PV thermal performance and the power supply generated from the sun, and the final discussion results summarized in the table (3) below, to evaluate the different PV integrations and choose the optimum one.

It can be seen that the double skin façade has the lowest performance, and the reason behind that is the tilt of the PV modules 90◦, and most of the solar radiation can be generated from the summer solar and the useful tilt during this period. According to Benghazi sun path and altitude, the useful tilt in the overall should be in between 0◦ to 35◦. Thus, this type will not be succeeded.

Table 3: The performance of the different types of PV integrations (summary)

ISSN 2522-6967

Costs & Benefits	Sunshade PV	Roof screen PV	Double skin façade PV
	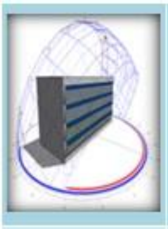	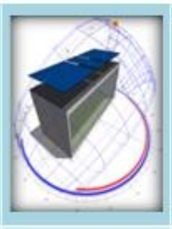	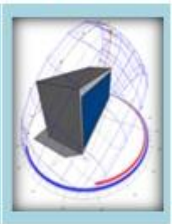
Energy reduction by thermal effect during the peak cooling load	17.26%	4.83%	10.52%
PV energy total output (kwh/year)	6,591 kWh/year	35,543 kWh/year	1,902 kWh/year
PV modules total budget ($)	$13,144	$49,620	$22,610
PV energy output (kwh/m2)	59.54 kWh/m^2	85.44 kWh/m^2	5.10 kWh/m^2
Cost of the PV power output ($/kwh) for 25 years lifetime	$0.08/kWh	$0.06/kWh	$0.47/kWh
CO2 emissions reduction (kg/year)	6,194 kg/year	20,133 kg/year	2,630 kg/year
Their effect on the building Comfort	Very good effect	No effect	Quite good effect

It is obvious from the summary table above that the Sunshade PV integration has a good performance in thermal effect, PV energy output per square meter and cost of the PV power output per kWh. Furthermore, it has a very good effect on the building comfort with low system budget, if it is compared with the roof screen integration.

The roof screen PV integration has a significant advance in the total PV energy annually output and CO_2 emissions' reduction, this advance has happened because of the medium storey building of the assumed office model that has used in the simulation, where the façade is similar to the roof area, and the space for the sunshade PV integration is limited. This advance can be completely opposite in the case of tall office buildings, which nowadays are more common due to the lake of the land space. Therefore, in this case, the roof space will be limited and the roof screen PV productivity as well, whereas the sunshade integration will have plenty of space, and its productivity will be multiple. For these reasons, the sunshade PV integration is the optimum one that could produce a reasonable power output and minimizes the heat gains in warm climate regions, and this choice is the answer of the study question.

Finally, a significant recommendation for further future research in this subject area is to use the Ecotect simulation program in focusing on the different types of sunshade PV integrations such as simple fixed, moveable or the louver one, in order to maximize their total power output and CO_2 emissions' reduction.

References

[1] Benemann, J., Chehab, O., & Schaar-Gabriel, E. (2001). Building-integrated PV modules. Solar Energy Materials & Solar Cells 67, 345-354.

[2] Boyle, G.(2004). Rennewable Energy, Section 3.

[3] Defra.(2015). Retrieved 8 14, 2015, from Defra web site: http://www.defra.gov.uk/environment/business/reporting/pdf/guidelines-ghg-conversion-factors.pdf

[4] Duffie JA and Beckman WA (1974), Solar Energy Thermal Processes. New York: Wiley; John Wiley & Sons, Inc.

[5] Ecotect. Retrieved 8 03, 2015, from Autodesk web site:http://usa.autodesk.com/adsk/servlet/pc/index?siteID=123112&id=12602821

[6] Ekhlat, M., Salah, I. M., & Kreama, N. M. (2007). Energy Efficiency and Renewable Energy,Libya - National study. Monaco: Plan Bleu.

[7] Gaisma.(2015). Retrieved 8 03, 2015, from Gaisma web site: http://www.gaisma.com/en/location/bangazi.html

[8] Gupta, S.(2010). How Low Will Price Fall? in Photvoltaic Technology Show Europe. April 27, 2010. Stuttgart,Germany.

[9] Prasad, D., & Snow, M. (2005). Designing With Solar Power. London & Victoria: the images publishing group pty ltd and Earthscan.

[10] Saleh, I. M. (2006). Prospects Of Renewable Eenergy In Libya. International Symposium on Solar Physics and Solar Eclipses

[11] Schottsolar. (2015). Retrieved 8 13, 2015, from SchottSolarWeb site:http://www.schottsolar.com/global/products/photovoltaics/schott-poly-175/

[12] Stark, T. (2009). Energy. In C. Luling, Energizing Architecture (pp. 103-117). Berlin: Jovis Verlag Gmbh.

[13] Szokolay, s. v. (2008).*Introduction to architectural science*. Oxford: Elsevier ltd.

ISSN 2522-6967

A New Approach to Cell Formation in Group Technology with Alternative Solutions

Mohammad Raafat A. Abou-zeid[a]*, Amer A. Boushaala[b], Haneya J. Madi[c]

[a, b, c] I &MSE Dept, University of Benghazi, Benghazi, Libya.
*Corresponding author: Tel.: +218-770-4902; e-mail: mrabouzeid@uob.edu.ly.

ABSTRACT

The concept of group technology (GT) in design of manufacturing systems is explained. Achieving the highly appreciated benefits of applying GT mainly depends on proper design of manufacturing cells within a manufacturing system. As the ideal design of manufacturing cells is practically unattainable, research work aims at optimizing this process within a number of objectives. This paper categorizes and briefly introduces some of the previously published research work. Then, a proposed approach for design of manufacturing cells is introduced with the objective of minimizing the number of exceptional elements, needing processing in more than one cell, thus reducing the material handling needs between cells which reduces efficiency and increases costs. The mathematical model for this approach, based on the 0-1 incidence matrix of parts/machines, is explained. Five performance measures for the approaches of design of cells are applied to the proposed approach. Twelve previously published bench mark problems with eighty eight different solutions, based upon different approaches from literature, were used in the comparison and evaluation of the performance of the proposed approach/ model. The result of comparison indicated that the proposed approach gave better solutions in forty nine percent of the cases, with equal performance in the remaining cases. Thus, the proposed approach is a highly valued addition to the available approaches.

Keywords: *Group technology, Formation of manufacturing cells, Mathematical programming, Exceptional elements.*

1. Introduction

The group technology (GT) concept evolved to face growing competition in industry and the need to successfully and economically meet the current trend towards low volume production of a variety of products. This is achieved through following the principle that similar things should be done similarly. Therefore, GT is a tool for organizing and using information about component similarities to improve the production efficiency of a manufacturing firm. Component similarities form the basis for creating families of components to be produced by all machines needed, in a manufacturing cell. This leads to form a number of cells for to manufacture all components / parts.

The ideal, mostly, un attainable, configuration for a manufacturing firm is where components and machines are grouped in a diagonal form as depicted in Figure1 for three cells. However, in practice, some parts may need processing in more than one cell. These are called "exceptional parts" and machines processing them are "bottleneck machines". The intercellular moves of parts can be eliminated by duplicating sufficient number of bottleneck machines. However, this involves additional costs and should be kept at a minimum such as not to offset the advantages of GT.

Implementation of GT resulted in significant benefits for all the functional areas of manufacturing, e.g., design manufacturing, manufacturing engineering, production control quality [8,10].

	1	2	3	4	5	6	7	8	9	10	11	12
A	1	1	1	1								
B	1		1	1	1	1						
C			1	1	1	1						
D							1	1	1	1		
E							1	1	1	1		
F							1	1		1		
G											1	1
H											1	1

Figure 1: The ideal solution for components and machines.

2. Strategies for manufacturing cells formation

Strategies for manufacturing cells formation depend on where to start from, either from machines, parts, or concurrently considering machine cells and part families.

3. Performance measures for methods of forming manufacturing cells

The performance measures consider, for purpose of evaluation of methods, the number of ones and zeros in the diagonal blocks and in the off diagonal blocks, as well as voids in the diagonal blocks. The mostly used measures are grouping efficiency η_3 [31], grouping efficacy η [8], weighted grouping efficacy ω [31], modified grouping efficacy τ_2 [30], grouping index GI [29], grouping capability index GCI [31], and number of exceptional elements e_0. For example, weighted grouping efficacy ω is calculated by placing a weight q on each entry inside the diagonal blocks and a weight 1-q on the exceptional elements.

4. Approaches for formation manufacturing cells, an overview

Relevant literature may be classified into four categories. These are similarity coefficients based methods [13, 32, 38, 41], mathematical programming techniques [2, 4, 6, 12, 21, 33, 36, 42], heuristic methods [14, 18, 24, 28, 37, 40], and genetic algorithms based methods [10, 43].

Kusiak [22], considered basically the matrix approach for forming cells of a specified number. Then, Visvanathan [38], developed on Kusiak's model to relieve its limit and to find the optimal number of cells.

The objectives of the mathematical programming formulations varied among a number of researchers. Examples of such objectives are minimizing number of exceptional elements [5], minimizing intercellular part movements [23], minimizing dissimilarity between parts in each cell [4], finding optimal labor assignment and groupings [36], and increasing productivity while maximizing cell independency [42].

ISSN 2522-6967

In heuristic methods, considerations were given, for example, to operations sequence [34], operation sequence and number of cells [24], sequence based material flow [37], balanced workload [40], and increasing total profits of the system [14].

The genetic algorithm's based approaches considered reducing setup times and work-in- process [10], parts volume and processing time [43], operations times [26], layout design to minimize material handling costs [20], among other objectives.

5. A proposed approach for formation of manufacturing cell

The proposed approach [25], is based on Won and Lee's approach [42], with a modification to give the designer the ability to control cell sizes while beingable to use the basic commercial integer linear programming software available. Moreover, number of alternatives are produced for the same number of cells. This gives flexibility to the system's designer.

The objective function and constraints are as follow:

$$Z=\sum_{i=1}^{m}\sum_{j=1}^{n} a_{ij}\left(\sum_{k=1}^{p}\left|X_{ik}-Y_{jk}\right|\right)/2 \quad (1)$$

The objective function Z can be linearized in the following manner as treated by Boctor [5], by introducing two sets of non-negative variables u_{ikj} and v_{ikj}, where

$$X_{ik}-Y_{jk}+u_{ikj}-v_{ikj}=0,\ \forall(i,j)\in R,\ k=1\ldots p \quad (2)$$

Then minimizing Z becomes equivalent to:

$$\text{Minimize: } \sum_{k=1}^{p}\sum_{(i,j)\in R}(u_{ikj}+v_{ikj})/2$$

The modification entails the use of just one variable u_{ikj} instead of using two variables u_{ikj} and v_{ikj}.

The objective function:

$\sum_{k=1}^{p}\sum_{(i,j)\in R}(u_{ikj}+v_{ikj})/2$ is replaced by

$\sum_{k=1}^{p}\sum_{(i,j)\in R}(u_{ikj})$ to reduce the repetition.

Thus, objective function and necessary constraints can then be formulated as follows:

$$\text{Minimize } \sum_{k=1}^{p}\sum_{(i,j)\in R}(u_{ikj}) \quad (3)$$

Subject to (3) and:

$$\sum_{k=1}^{p}X_{ik}=1 \quad i=1,\ldots,m \quad (4)$$

$$L_c\le\sum_{i=1}^{m}X_{ik}\le U_c,\quad k=1,\ldots,p \quad (5)$$

$$\sum_{k=1}^{p}Y_{jk}=1,\quad j=1,..,n \quad (6)$$

$$L_f\le\sum_{j=1}^{n}Y_{jk}\le U_f,\quad k=1,\ldots,p \quad (7)$$

$$X_{ik}\ge 0,\ i=1,..,m;\ k=1,\ldots,p \quad (8)$$

$$y_{jk}\ge 0,\ j=1,..,n;\ k=1,\ldots,p \quad (9)$$

$$u_{ikj},\ v_{ikj}\ge 0,\ k=1,\ldots,p;\ (i,j)\in E \quad (10)$$

Where:

n: number of parts, m: number of machines, ***p***: number of cells, ***i***: index of machine type, i=1,……m, ***j***: index of part type, j= 1,….n, ***k***: index of cells (families), k = 1,….p, L_c= lower limit on machine cell size, U_c=upper limit on machine cell size, L_f = lower limit on part family size, U_f = upper limit on part family size, ***A*** = $[a_{ij}]$, binary PMIM, n_j: Total number of operations required for part j, ***r*** : index of operation sequence number r = 1….n_j,

Decision variables:

Y_{jk}: binary variable indicating if part j is assigned to cell k, X_{ik}: binary variable indicating if machine i is assigned to cell k. The objective function (3), is accompanied by the constraints (2) and (4) to (10). Constraint (4) ensures that each machine is assigned to exactly one machine cell. Constraint (5) means that at least L_c machines must be assigned to each cell and at most U_c machines are assigned to each cell. Constraint (6) requires that each part belongs to exactly one part family. Constraint (7) ensures that at least L_f parts must be assigned to each family and at most U_f parts are assigned to each family. Constraints (8) and (9) guarantee the binary solution for machine assignment and part assignment, respectively. Constraint (10) ensures the binary property of continuous variables u_{ikj} and v_{ikj}

6. Computation results and evaluation of the quality of the performance measures of the problems considered

The final block diagonal matrix can be checked to evaluate the quality of the solution relative to the chosen performance measures. For the purpose of comparing the performance of our proposed approach with previously published approaches, thirteen problems with eighty nine solutions resulting from different procedures, were prepared, Table1. The size of the problems ranges from five machines and seven parts to sixteen machines and forty three parts, thus, the ranges represent small problems to comparatively large ones.

The problems were solved by different methods. the solutions of some problems are taken from published papers while other problems are solved for the current work by applying a MATLAB program

to calculate the similarity coefficients and the IMROVE algorithm [11], to obtain final solutions. The performance measures are: grouping index GI, weighted grouping efficacy ω, grouping capability index GCI, modified grouping efficacy τ_2 and grouping efficacy η and number of exceptional elements e_0.

7. Results and Discussion

Table2 presents a summary of computational results regarding comparative performance of the earlier solution procedures and the proposed approach.

It should be noticed that a solution is better when:

ISSN 2522-6967

a. It has a higher value of the following measures: grouping index, weighted grouping efficacy, grouping capability index, modified grouping efficacy and grouping efficacy, and

Because of their dependence on the number of clusters, values of grouping index (GI), weighted grouping efficacy (ω), grouping capability index (GCI), modified grouping efficacy (τ_2) and grouping efficacy (η) were not compared for cases with unequal number of clusters. The comparison of the performance measures resulted in the following:

a. The ω measure has low discriminating capability and weakness sensitivity.

b. The η measure gives the best result for the worst solution, so η has the worst discriminating characteristic, since this method does not consider the weight factor.

c. GCI has high the discrimination compared with other performance measures.

d. GI and τ_2 have the same values for all solutions in all problems because they have the same equation for all problems, since A=0 for all problems. GI and τ_2 show no preference for any solution for all problems even

b. It is with minimum number of exceptional elements (e_0).

with changing the method or with different number of clusters.

It is worthy to point out that results presented in Table 2 demonstrate that the proposed approach results in solutions of better or equal quality when its solutions are compared with the solutions obtained by conventional algorithms for the test problems.

Due to space limitation, two example problems are given to demonstrate the superiority of the proposed approach.

Example 1[25]

Solution of problem 4/6, Table 1 for three cells, the solution of Kusiak's approach as an input to IMPROVE algorithm, applying ROC approach, and using the proposed approach are given in Figures 3, 4, 5. The proposed approach approach's solution is better in terms of the performance measures, as given in Table2.

	1	2	3	4	5	6	7	8	9	1	1	1
1				1	1	1	1	1			1	1
2						1	1		1			
3				1		1						
4	1	1	1	1								
5	1	1										
6				1		1		1		1	1	
7					1	1	1	1				
8				1			1	1	1	1	1	1
9		1										
1		1		1	1			1		1		1

Figure 2. Machine – part incidence matrix for problem 4 [38].

	1	2	3	6	7	9	4	5	8	1	1	1
4	1	1	1				1					
5	1	1										
9		1										
2				1	1	1						
3				1			1					
7				1	1			1	1			
1				1	1		1	1	1		1	1
6				1			1		1	1	1	
8					1	1	1		1	1	1	1
1		1					1	1	1	1		1

Figure 3. Solution for problem 4/6 of IMPROVE algorithm by using solution of (Kusiak's approach with p=3 as input) [11].

ISSN 2522-6967

	1	2	3	4	5	8	1	1	1	6	7	9
4	1	1	1	1								
5	1	1										
9		1										
1		1		1	1	1	1		1			
1				1	1	1		1	1	1	1	
6				1		1	1	1		1		
8				1		1	1	1	1		1	1
2										1	1	1
3				1						1		
7					1	1				1	1	

Figure 4. Solution for problem 4/7 by applying ROC approach [11].

	4	5	6	7	8	1	1	1	1	9	2	3
1	1	1	1	1	1		1	1				
3	1		1									
6	1		1		1	1	1					
7		1	1	1	1							
8	1			1	1	1	1	1		1		
1	1	1			1	1		1			1	
2			1	1						1		
5									1		1	
4	1								1		1	1
9											1	

Figure 5. Solution of the proposed approach [25].

Example 2 [25]

The machine – part incidence matrix for a 16x43 problem [19],is utilized to demonstrate the effectiveness of the proposed approach. The data for problem 6 are given in Figure 6 [19]. In the following section a solution for 3 cells, and applying ROC2 algorithm [3], the solution is given in Figure 7, resulting in 31 exceptional elements and performance measures GI, ω, and GCI as 0.64, 0.25 and 0.76 respectively.

ISSN 2522-6967

Table 1: Selected problems, sources, solutions approaches and characteristics of solutions [25].

Problem No./ Solution No.	Source	Approach	m	n	p
1/1, 1/2, 1/3, 1/4, 1/5, 1/6, and 1/7	Waghodekar and Sahu(1984,) Fig. 2(a) [39]	ROC, MACE algorithm, *Kusaik's model, *Viswanathan model, *Islam and Sarker model, *MP1 model, and *MP2 model	5	7	2
2/1	Chandrasekharan and Rajagopalan, (1986) [7]	HGGA algorithm	8	20	2
3/1, 3/2, 3/3, 3/4, 3/5, 3/6, 3/7, 3/8, 3/9, 3/10, 3/11, 3/12, 3/13, and 3/14	James et al.. (2007) [17]	Ideal seed Nonhierarchical, HPH algorithm, ROC2, *Kusiak model, *Viswanthan model, CAN, GRAFICS, *Islam and Sarker model, *MP1 model, *MP2 model, ROC, IMPROVE, HGGA, and ACO-TS	8	20	3
4/1, 4/4, and 4/5	Viswanathan (1996) [38]	Kusiak model, Ben-Arieh and Chang approach, and IMPROVE	10	12	2
4/2, 4/3, 4/6, and 4/7	Viswanathan (1996) [38]	Kusiak model, and Viswanthan model, IMPROVE, and ROC	10	12	3
5/1, 5/2, 5/3, 5/4, 5/5, 5/6, 5/7, 5/8, and 5/9	Chattopadhyay et al. (2011), Fig. 4 (a) [8]	ROC, MACE, *Kusaik's model, *Viswanathan model, *Islam and Sarker model, *MP1 model, *MP2 model, HGGA, and SOM.	5	7	2
6/1, and 6/2	King (1980) [19]	ROC2, and CFP	16	43	3
6/3, 6/4, 6/5, 6/6	King (1980) [19]	ROC2, ROC, IMPROVE ROC, and CFP	16	43	4
6/7, 6/8, and 6/9	King (1980) [19]	ALC, HPH, and CFP	16	43	5
7/1, 7/2, 7/3, 7/4, 7/5, 7/6, 7/7, 7/8, 7/9, 7/10, 7/11	Chattopadhyay et al.(2011) [8]	*Kusiak model, SLINK, ALC, *Viswanthan model, *Islam and Sarker model, *MP1 model, *MP2 model, ROC, IMPROVE, HGGA, and SOM	5	18	2
8/1, 8/2, 8/2, and 8/4	Won (2000) [41]	Kusiak model, *Viswanthan model, *Islam and Sarker model, and *MP2 model	6	10	2
9/1, 9/2, 9/3, 9/4 and 9/5	Agrawal et al. (2011) [1]	ALC, *MP1 model, *Kusiak model, *Viswanthan model, and *Islam and Sarker model	8	12	3
9/6, 9/7, and 9/8	Agrawal et al. (2011) [1]	SAM, HGGA, and ACO-TS,	8	12	4
10/1, 10/2, 10/3, 10/4, 10/5, 10/6, and 10/7	Waghodekar and Sahu(1984), Fig.5(a) [39]	ROC, MACE, *Kusiak model, *Viswanathan model, *MP1 model, *MP2 model, and IMPROVE	5	7	2
11/1, and 11/2	Askine et al.(1991) [3]	ROC2, and HPH	12	19	3
12/1	Chen and Cheng (1995) [9]	ART1	15	15	4
13/1	Sule (1994) [35]	-	11	21	3

ISSN 2522-6967

Table 2: Summary of computational results

Pro. /sol.	Approach	Problem information			p	Earlier models results									Proposed model results									comp-arison
		m	n	e		e_1	e_o	e_v	B	GI	w	GCI	τ_2	η	e_1	e_o	e_v	B	GI	w	GCI	τ_2	η	
1/1	ROC Fig(2) a	5	7	16	2	14	2	3	17	0.77	0.56	0.88	0.77	0.74	14	2	3	17	0.77	0.56	0.88	0.77	0.74	Equal
1/2	MACE Fig(2) a	5	7	16	2	14	2	3	17	0.77	0.56	0.88	0.77	0.74	14	2	3	17	0.77	0.56	0.88	0.77	0.74	Equal
1/3	*Kusaik's model Fig(2) a	5	7	16	2	14	2	3	17	0.77	0.56	0.88	0.77	0.74	14	2	3	17	0.77	0.56	0.88	0.77	0.74	Equal
1/4	*Viswanathan model Fig(2) a	5	7	16	2	14	2	3	17	0.77	0.56	0.88	0.77	0.74	14	2	3	17	0.77	0.56	0.88	0.77	0.74	Equal
1/5	*Islam and SarkermodelFig(2) a	5	7	16	2	14	2	3	17	0.77	0.56	0.88	0.77	0.74	14	2	3	17	0.77	0.56	0.88	0.77	0.74	Equal
1/6	*MP1 model Fig(2) a	5	7	16	2	14	2	3	17	0.77	0.56	0.88	0.77	0.74	14	2	3	17	0.77	0.56	0.88	0.77	0.74	Equal
1/7	*MP2 model Fig(2) a	5	7	16	2	14	2	3	17	0.77	0.56	0.88	0.77	0.74	14	2	3	17	0.77	0.56	0.88	0.77	0.74	Equal
2/1	HGGA	8	20	91	2	64	27	18	82	0.53	0.34	0.7	0.53	0.59	67	24	29	96	0.59	0.35	0.74	0.59	0.56	Best
3/1	Ideal seed Nonhierarchical	8	20	61	3	52	9	0	52	0.76	0.59	0.85	0.76	0.85	52	9	0	52	0.76	0.59	0.85	0.76	0.85	Equal
3/2	HPH	8	20	61	3	52	9	0	52	0.76	0.59	0.85	0.76	0.85	52	9	0	52	0.76	0.59	0.85	0.76	0.85	Equal
3/3	ROC2	8	20	61	3	46	15	9	55	0.6	0.4	0.75	0.6	0.66	52	9	0	52	0.76	0.59	0.85	0.76	0.85	Best
3/4	*Kusiak model	8	20	61	3	52	9	0	52	0.76	0.59	0.85	0.76	0.85	52	9	0	52	0.76	0.59	0.85	0.76	0.85	Equal
3/5	*Viswanthan model	8	20	61	3	52	9	0	52	0.76	0.59	0.85	0.76	0.85	52	9	0	52	0.76	0.59	0.85	0.76	0.85	Equal
3/6	CAN	8	20	61	3	52	9	0	52	0.76	0.59	0.85	0.76	0.85	52	9	0	52	0.76	0.59	0.85	0.76	0.85	Equal
3/7	GRAFICS	8	20	61	3	52	9	0	52	0.76	0.59	0.85	0.76	0.85	52	9	0	52	0.76	0.59	0.85	0.76	0.85	Equal
3/8	*Islam and Sarker model	8	20	61	3	52	9	0	52	0.76	0.59	0.85	0.76	0.85	52	9	0	52	0.76	0.59	0.85	0.76	0.85	Equal
3/9	*MP1 model	8	20	61	3	47	14	4	51	0.62	0.44	0.77	0.62	0.72	52	9	0	52	0.76	0.59	0.85	0.76	0.85	Best
3/10	*MP2 model	8	20	61	3	52	9	0	52	0.76	0.59	0.85	0.76	0.85	52	9	0	52	0.76	0.59	0.85	0.76	0.85	Equal
3/11	ROC	8	20	61	3	46	15	6	52	0.6	0.41	0.75	0.6	0.69	52	9	0	52	0.76	0.59	0.85	0.76	0.85	Best
3/12	IMPROVE	8	20	61	3	52	9	0	52	0.76	0.59	0.85	0.76	0.85	52	9	0	52	0.76	0.59	0.85	0.76	0.85	Equal
3/13	HGGA	8	20	61	3	52	9	0	52	0.76	0.59	0.85	0.76	0.85	52	9	0	52	0.76	0.59	0.85	0.76	0.85	Equal
3/14	ACO-TS	8	20	61	3	52	9	0	52	0.76	0.59	0.85	0.76	0.85	52	9	0	52	0.76	0.59	0.85	0.76	0.85	Equal

Pro. /sol.	Approach	Problem information			p	Earlier models results									Proposed model results									comp-arison
		m	n	e		e_1	e_o	e_v	B	GI	w	GCI	τ_2	η	e_1	e_o	e_v	B	GI	w	GCI	τ_2	η	
4/1	Kusiak model	10	12	41	2^a	34	7	26	60	0.7	0.39	0.83	0.7	0.51	39	2	33	72	0.8	0.49	0.95	0.8	0.53	Best
4/2	Kusiak model	10	12	41	3	29	12	12	41	0.55	0.33	0.71	0.55	0.55	34	7	22	56	0.7	0.4	0.83	0.7	0.54	Best
4/3	Viswanthan model	10	12	41	3	33	8	15	48	0.67	0.41	0.8	0.67	0.59	34	7	22	56	0.7	0.4	0.83	0.7	0.54	Best
4/4	Ben-Arieh and Chang approach	10	12	41	2^a	29	12	23	52	0.57	0.29	0.71	0.57	0.45	39	2	33	72	0.8	0.49	0.95	0.8	0.53	Best
4/5	IMPROVE	10	12	41	2	39	2	33	72	0.8	0.49	0.95	0.8	0.53	39	2	33	72	0.8	0.49	0.95	0.8	0.53	Equal
4/6	IMPROVE	10	12	41	3	31	10	11	42	0.61	0.38	0.76	0.61	0.6	34	7	22	56	0.7	0.4	0.83	0.7	0.54	Best
4/7	ROC	10	12	41	3	26	15	14	40	0.46	0.26	0.63	0.46	0.47	34	7	22	56	0.7	0.4	0.83	0.7	0.54	Best
5/1	ROC Fig. 4 (a)	5	7	20	2^b	16	4	9	25	0.67	0.39	0.8	0.67	0.55	17	3	5	22	0.73	0.5	0.85	0.73	0.68	Best
5/2	MACE Fig. 4 (a)	5	7	20	2	17	3	5	22	0.73	0.5	0.85	0.73	0.68	17	3	5	22	0.73	0.5	0.85	0.73	0.68	Equal
5/3	*Kusaik model Fig. 4 (a)	5	7	20	2	17	3	5	22	0.73	0.5	0.85	0.73	0.68	17	3	5	22	0.73	0.5	0.85	0.73	0.68	Equal
5/4	*Viswanathan model Fig. 4 (a)	5	7	20	2	Single cell									17	3	5	22	0.73	0.5	0.85	0.73	0.68	Best
5/5	*Islam and Sarker model Fig. 4 (a)	5	7	20	2	17	3	5	22	0.73	0.5	0.85	0.73	0.68	17	3	5	22	0.73	0.5	0.85	0.73	0.68	Equal
5/6	*MP1 model Fig. 4 (a)	5	7	20	2	14	6	3	17	0.52	0.34	0.7	0.52	0.61	17	3	5	22	0.73	0.5	0.85	0.73	0.68	Best
5/7	*MP2 model Fig. 4 (a)	5	7	20	2	14	6	3	17	0.52	0.34	0.7	0.52	0.61	17	3	5	22	0.73	0.5	0.85	0.73	0.68	Best
5/8	HGGA Fig. 4 (a)	5	7	20	2	16	4	3	19	0.67	0.46	0.8	0.67	0.7	17	3	5	22	0.73	0.5	0.85	0.73	0.68	Best
5/9	SOM Fig. 4 (a)	5	7	20	2	17	3	5	22	0.73	0.5	0.85	0.73	0.68	17	3	5	22	0.73	0.5	0.85	0.73	0.68	Equal
6/1	ROC2	16	43	126	3	96	31	161	260	0.64	0.25	0.76	0.64	0.33										
6/2	CFP	16	43	126	3^a	96	30	116	212	0.64	0.29	0.76	0.64	0.4	109	(a)17	181	290	0.71	0.3	0.87	0.71	0.36	Best
				126											109	(b)17	186	295	0.71	0.3	0.87	0.71	0.35	Best
				126											109	(c)17	202	311	0.7	0.29	0.87	0.7	0.33	Best
				126											108	(d)18	176	284	0.7	0.3	0.86	0.7	0.36	Best
				126											107	(e)19	150	257	0.7	0.32	0.85	0.7	0.39	Best
				126											106	(f)20	139	245	0.7	0.33	0.84	0.7	0.4	Best
				126											104	(g)22	131	235	0.69	0.32	0.83	0.69	0.4	Best

Pro. /sol.	Approach	Problem information			p	Earlier models results									Proposed model results									comp-arison
		m	n	e		e_1	e_o	e_v	B	GI	w	GCI	τ_2	η	e_1	e_o	e_v	B	GI	w	GCI	τ_2	η	
6/3	ROC2	16	43	126	4	90	36	83	173	0.58	0.28	0.71	0.58	0.43										
6/4	ROC	16	43	126	4[a]	60	66	116	176	0.4	0.14	0.48	0.4	0.25										
6/5	IMPROVE	16	43	126	4	100	26	77	177	0.66	0.36	0.79	0.66	0.49										
6/6	CFP	16	43	126	4[a]	97	29	76	173	0.64	0.34	0.77	0.64	0.48	105	(a)21	118	223	0.69	0.34	0.83	0.69	0.43	Best
				126											105	(b)21	126	231	0.69	0.33	0.83	0.69	0.42	Best
				126											102	(c)24	97	199	0.68	0.35	0.81	0.68	0.46	Best
				126											102	(d)24	100	202	0.68	0.34	0.81	0.68	0.45	Best
				126											102	(e)24	100	202	0.68	0.34	0.81	0.68	0.45	Best
				126											102	(f)24	106	208	0.67	0.34	0.81	0.67	0.44	Best
6/7	ALC	16	43	126	5	99	27	77	176	0.65	0.35	0.79	0.65	0.49	99									
6/8	HPH	16	43	126	5	95	31	51	146	0.61	0.35	0.75	0.61	0.54	99									
6/9	CFP	16	43	126	5[a]	97	29	54	151	0.63	0.36	0.77	0.63	0.54	99	(a)27	58	157	0.65	0.37	0.79	0.65	0.54	Best
																(b)27	59	158	0.65	0.37	0.79	0.65	0.54	Best
																(c)27	77	176	0.65	0.35	0.79	0.65	0.49	Best
7/1	*Kusiak model	5	18	46	2	39	7	3	42	0.74	0.56	0.85	0.74	0.8	41	5	7	48	0.8	0.6	0.89	0.8	0.77	Best
7/2	SLINK	5	18	46	2	39	7	3	42	0.74	0.56	0.85	0.74	0.8	41	5	7	48	0.8	0.6	0.89	0.8	0.77	Best
7/3	ALC	5	18	46	2	41	5	7	48	0.8	0.6	0.89	0.8	0.77	41	5	7	48	0.8	0.6	0.89	0.8	0.77	Equal
7/4	*Viswanthan model	5	18	46	2	41	5	7	48	0.8	0.6	0.89	0.8	0.77	41	5	7	48	0.8	0.6	0.89	0.8	0.77	Equal
7/5	*Islam and Sarker model	5	18	46	2	41	5	7	48	0.8	0.6	0.89	0.8	0.77	41	5	7	48	0.8	0.6	0.89	0.8	0.77	Equal
7/6	*MP1 model	5	18	46	2	41	5	7	48	0.8	0.6	0.89	0.8	0.77	41	5	7	48	0.8	0.6	0.89	0.8	0.77	Equal
7/7	*MP2model	5	18	46	2	41	5	7	48	0.8	0.6	0.89	0.8	0.77	41	5	7	48	0.8	0.6	0.89	0.8	0.77	Equal
7/8	ROC	5	18	46	2	41	5	7	48	0.8	0.6	0.89	0.8	0.77	41	5	7	48	0.8	0.6	0.89	0.8	0.77	Equal
7/9	IMPROVE	5	18	46	2	41	5	7	48	0.8	0.6	0.89	0.8	0.77	41	5	7	48	0.8	0.6	0.89	0.8	0.77	Equal
7/10	HGGA	5	18	46	2	39	7	3	42	0.74	0.56	0.85	0.74	0.8	41	5	7	48	0.8	0.6	0.89	0.8	0.77	Best
7/11	SOM	5	18	46	2	41	5	7	48	0.8	0.6	0.89	0.8	0.77	41	5	7	48	0.8	0.6	0.89	0.8	0.77	Equal
8/1	Kusiak model	6	10	27	2	23	4	9	32	0.73	0.48	0.85	0.73	0.64	23	4	9	32	0.73	0.48	0.85	0.73	0.64	Equal
8/2	*Viswanthan model	6	10	27	2[a]	23	4	13	36	0.72	0.44	0.85	0.72	0.58	23	4	9	32	0.73	0.48	0.85	0.73	0.64	Best
8/3	*Islam and Sarker model	6	10	27	2	23	4	9	32	0.73	0.48	0.85	0.73	0.64	23	4	9	32	0.73	0.48	0.85	0.73	0.64	Equal

ISSN 2522-6967

Pro. /sol.	Approach	Problem information			p	Earlier models results									Proposed model results									comp-arison
		m	n	e		e_1	e_o	e_v	B	GI	w	GCI	τ_2	η	e_1	e_o	e_v	B	GI	w	GCI	τ_2	η	
8/4	*MP2 model	6	10	27	2^a	22	5	8	30	0.69	0.44	0.81	0.69	0.63	23	4	9	32	0.73	0.48	0.85	0.73	0.64	Best
9/1	ALC	8	12	35	3	28	7	6	34	0.67	0.45	0.8	0.67	0.67	28	7	6	34	0.67	0.45	0.8	0.67	0.67	Equal
9/2	*MP1 model	8	12	35	3	28	7	6	34	0.67	0.45	0.8	0.67	0.67	28	7	6	34	0.67	0.45	0.8	0.67	0.67	Equal
9/3	*Kusiak model	8	12	35	3	28	7	6	34	0.67	0.45	0.8	0.67	0.67	28	7	6	34	0.67	0.45	0.8	0.67	0.67	Equal
9/4	*Viswanathan model	8	12	35	3	28	7	6	34	0.67	0.45	0.8	0.67	0.67	28	7	6	34	0.67	0.45	0.8	0.67	0.67	Equal
9/5	*Islam and Sarker model	8	12	35	3	28	7	6	34	0.67	0.45	0.8	0.67	0.67	28	7	6	34	0.67	0.45	0.8	0.67	0.67	Equal
9/6	SAM	8	12	35	4	25	10	1	26	0.52	0.38	0.71	0.52	0.69	25	10	1	26	0.52	0.38	0.71	0.52	0.69	Equal
9/7	HGGA	8	12	35	4	25	10	1	26	0.52	0.38	0.71	0.52	0.69	25	10	1	26	0.52	0.38	0.71	0.52	0.69	Equal
9/8	ACO-TS	8	12	35	4	25	10	1	26	0.52	0.38	0.71	0.52	0.69	25	10	1	26	0.52	0.38	0.71	0.52	0.69	Equal
10/1	ROC Fig. (5)a	5	7	20	2^b	15	5	7	22	0.61	0.36	0.75	0.61	0.56	17	3	5	22	0.73	0.5	0.85	0.73	0.68	Best
10/2	MACE Fig. (5)a	5	7	20	2	17	3	5	22	0.73	0.5	0.85	0.73	0.68	17	3	5	22	0.73	0.5	0.85	0.73	0.68	Equal
10/3	*Kusiak model Fig. (5)a	5	7	20	2	17	3	5	22	0.73	0.5	0.85	0.73	0.68	17	3	5	22	0.73	0.5	0.85	0.73	0.68	Equal
10/4	*Viswanathan model Fig. (5)a	5	7	20	2	Single cell									17	3	5	22	0.73	0.5	0.85	0.73	0.68	Best
10/5	*MP1 model Fig. (5)a	5	7	20	2	14	6	3	17	0.52	0.34	0.7	0.52	0.61	17	3	5	22	0.73	0.5	0.85	0.73	0.68	Best
10/6	*MP2 model Fig. (5)a	5	7	20	2	14	6	3	17	0.52	0.34	0.7	0.52	0.61	17	3	5	22	0.73	0.5	0.85	0.73	0.68	Best
10/7	IMPROVE Fig. (5)a	5	7	20	2	17	3	5	22	0.73	0.5	0.85	0.73	0.68	17	3	5	22	0.73	0.5	0.85	0.73	0.68	Equal
11/1	ROC2	12	19	75	3^a	41	34	35	76	0.38	0.19	0.55	0.38	0.37	56	19	24	80	0.6	0.36	0.75	0.6	0.57	Best
11/2	HPH	12	19	75	3	52	23	24	76	0.53	0.31	0.69	0.53	0.53	56	19	24	80	0.6	0.36	0.75	0.6	0.57	Best
12/1	ART1	15	15	50	4	43	7	13	56	0.74	0.51	0.86	0.74	0.68	43	7	13	56	0.74	0.51	0.86	0.74	0.68	Equal
13/1	-	11	21	73	3	-	-	-	-	-	-	-	-	-	62	11	30	92	0.72	0.46	0.85	0.72	0.6	-

ISSN 2522-6967

Because of their dependence on the number of clusters, values of grouping index (GI), weighted grouping efficacy (ω), grouping capability index (GCI), modified grouping efficacy (τ_2) and grouping efficacy (η) were not compared for cases with unequal number of clusters. The comparison of the performance measures resulted in the following:

a) The ωmeasure has low discriminating capability and weakness sensitivity
b) The ηmeasure gives the best result for the worst solution, so η has the worst discriminating characteristic, since this method does not consider the weight factor.
c) GCIhas high the discrimination compared with other performance measures.
d) GIand $\tau_2$have the same values for all solutions in all problems because they have the same equation for all problems, since A=0 for all problems. GIand $\tau_2$show no preference for any solution for all problems even with changing the method or with different number of clusters.

It is worthy to point out that results presented in Table 2 demonstrate that the proposed approach results in solutions of better or equal quality when its solutions are compared with the solutions obtained by conventional algorithms for the test problems.

Due to space limitation, two example problems are given to demonstrate the superiority of the proposed approach.

Example 1[25]

Solution of problem 4/6, Table 1 for three cells, the solution of Kusiak's approach as an input to IMPROVE algorithm, applying ROC approach, and using the proposed approach are given in Figures 3, 4, and 5. The proposed approach approach's solution is better in terms of the performance measures, as given in Table2.

	1	2	3	4	5	6	7	8	9	10	11	12
1				1	1	1	1	1			1	1
2						1	1		1			
3				1		1						
4	1	1	1	1								
5	1	1										
6				1		1		1		1	1	
7					1	1	1	1				
8				1			1	1	1	1	1	1
9		1										
10		1		1	1			1		1		1

Figure 2: Machine – part incidence matrix for problem 4, [38].

	1	2	3	6	7	9	4	5	8	10	11	12
4	1	1	1				1					
5	1	1										
9		1										
2				1	1	1						
3				1			1					
7				1	1			1	1			
1				1	1		1	1	1		1	1
6				1			1		1	1	1	
8					1	1	1		1	1	1	1
10		1					1	1	1	1		1

Figure 3: Solution for problem 4/6 of IMPROVE algorithm by using solution of (Kusiak's approach with p=3 as input) [11].

	1	2	3	4	5	8	10	11	12	6	7	9
4	1	1	1	1								
5	1	1										
9		1										
10		1		1	1	1	1		1			
1				1	1	1		1	1	1	1	
6				1		1	1	1		1		
8				1		1	1	1	1		1	1
2										1	1	1
3				1						1		
7					1	1				1	1	

Figure 4: Solution for problem 4/7 by applying ROC approach [11].

	4	5	6	7	8	10	11	12	1	9	2	3
1	1	1	1	1	1		1	1				
3	1		1									
6	1		1		1	1	1					
7		1	1	1	1							
8	1			1	1	1	1	1		1		
10	1	1			1	1		1			1	
2			1	1						1		
5									1		1	
4	1								1		1	1
9											1	

Figure 5: Solution of the proposed approach [25].

Example 2 [25]

The machine – part incidence matrix for a 16x43 problem [19],is utilized to demonstrate the effectiveness of the proposed approach. The data for problem 6 are given in Figure 6 [19]. In the following section a solution for 3 cells, and applying ROC2 algorithm [3], the solution is given in Figure 7, resulting in 31 exceptional elements and performance measures GI, ω, and GCI as 0.64, 0.25 and 0.76 respectively.

	1	2	3	4	5	6	7	8	9	10	11	12	13	14	15	16	17	18	19	20	21	22	23	24	25	26	27	28	29	30	31	32	33	34	35	36	37	38	39	40	41	42	43
1																																					1					1	
2		1								1																		1				1					1	1		1		1	
3							1										1																	1	1	1							
4					1				1					1					1		1		1						1														
5					1			1	1					1	1	1			1		1		1						1				1								1		1
6	1	1				1	1	1				1	1	1			1		1				1									1	1	1			1		1	1		1	1
7	1												1												1																		
8	1	1	1					1	1		1	1			1				1	1	1		1	1			1	1			1						1	1			1		1
9		1		1						1								1										1				1					1	1		1		1	
10	1											1	1												1	1					1								1				
11			1						1											1				1			1			1													
12											1											1		1			1			1													
13			1																					1																			
14		1				1											1																		1								
15					1									1					1		1												1								1		1
16		1					1			1								1														1					1	1				1	

Figure 6: Machine – part incidence matrix for problem 6 [19].

	2	4	7	8	10	12	18	28	32	37	38	40	42	1	5	6	9	13	14	15	16	17	19	21	23	25	26	29	31	33	34	35	36	39	41	43	3	11	20	22	24	27	30
1										1			1																														
2	1				1			1	1	1	1	1	1																														
6	1		1	1		1			1	1		1	1	1		1		1	1			1	1		1					1	1			1		1							
8	1			1		1		1		1	1			1			1			1			1	1	1				1						1	1	1	1	1		1	1	
9	1	1			1		1	1	1	1	1	1	1																														
16	1		1		1		1		1	1	1		1																														
3			1																			1									1	1	1										
4															1		1		1				1	1	1			1															
5				1											1		1		1	1	1		1	1	1			1		1					1	1							
7														1				1								1																	
10						1								1				1								1	1		1					1									
14	1															1						1										1											
15															1				1				1	1						1					1	1							
11																	1																				1		1		1	1	1
12																																						1		1	1	1	1
13																																					1				1		

Figure 7: Solution for problem 6/1 by applying ROC2 algorithm [3].

Figure 8 depicts the solution obtained by the proposed approach where the performance measures increased to 0.71, 0.3 and0.87. Moreover, the proposed approach produces seven alternative solutions with the same number of cells [25] that outperform the previously published solutions.

ISSN 2522-6967

	2	4	5	7	8	9	10	12	14	15	16	18	19	21	23	28	29	32	33	37	38	40	41	42	43	1	6	13	17	25	26	31	34	35	36	39	3	11	20	22	24	27	30
1																				1				1																			
2	1						1									1		1		1	1	1		1																			
4			1			1			1				1	1	1		1																										
5			1		1	1			1	1	1		1	1	1		1		1				1		1																		
6	1			1	1			1	1				1		1			1	1	1		1		1	1	1	1	1	1				1			1							
8	1				1	1		1		1			1	1	1	1				1	1		1		1	1						1					1	1	1		1	1	
9	1	1					1					1				1		1		1	1	1		1																			
15			1						1				1	1					1				1		1																		
16	1			1			1					1						1		1	1			1																			
3				1																									1				1	1	1								
7																										1		1		1													
10								1																		1		1		1	1	1				1							
14	1																										1		1					1									
11						1																															1		1		1	1	1
12																																						1		1	1	1	1
13																																					1				1		

Figure 8: Solution by applying the proposed approach with e_o=17, Lc=3, Uc=9 and Lf=7, Uf=25 [25].

8. Conclusions

The proposed approach seeks to minimize the number of exceptional elements through an integer programming formulation. Machine cells and part families are created simultaneously. The numerical solutions obtained by this approach, to benchmark problems, were superior to solutions obtained by other approaches in forty nine percent of the cases. None of the solutions were of inferior quality.

8.1. Conclusions related to the capability of the approach

These can be summarized as follows

a) The proposed approach permits the designer to set the number of cells.

b) The proposed approach can easily improve, develop, add constraints, change number of cells, puts upper and lower limits on number of machines or parts in each cell, or to cluster machines and parts based on other objectives such as maximization of the actual processing time within each cell.

8.2. Main advantages of the approach

The advantages can be set as follows

a) The proposed approach can be applied for both small and large problems.

b) The proposed approach was prepared to overcome the deficiencies in other approaches with significant advantage where it generates more than one optimal solution with the same objective function values by changing the upper and lower limits for machines and parts allowable in each cell. As a result, this can present more than one choice for the decision maker.

References

[1] Agrawal A. K., Bhardwaj P. and Srivastava V., (2011), "Ant colony optimization for group technology applications", Int. J. Adv. Manuf. Techno., Vol. 55, pp783-795.

[2] Akturk M. S. and Balkose H. O., (1996), "Part-machine grouping using a multi-objective cluster analysis", Int. J. Prod. Res., Vol. 34, Issue:8, pp 2299-2315.

[3] Askin, R. G. Cresswell, S. H. Goldberg, J. B. and Vakharia, A. J., (1991), "A Hamiltonian path approach to reordering the part-machine matrix for cellular manufacturing", Int. J. Prod. Res., Vol. 29, Issue 6, pp 1081-1100.

[4] Baykasoglu, A. and Gindy, N. N. Z., (2000), "MOCACEF1.0:multiple objective capability based approach to form part-machine groups for cellular manufacturing application", Int. J. Prod. Res., Vol. 38, Issue 5, pp 1133-1161.

[5] Boctor, F. F., (1991), "A linear formation of the machine part-cell formation problem", Int. J. Prod. Res., Vol. 29, Issue 2, pp 343-356.

[6] Boctor, F. F., (1996), "The minimum-cost, machine-part cell formation problem", Int. J. Prod. Res., Vol. 34, Issue 4, pp1045-1603.

[7] Chandrasekharan, M. p. and Rajagopalan, R., (1986), "MODROC: an extension of rank order clustering for group technology", Int. J. Prod. Res., Vol. 24.Issue 5, pp 1221-1233.

[8] Chattopadhyay, M. Chattopadhyay, S. and Dan, P. K., (2011), "Machine- part cell formation through visual decipherable clustering of self- organization map", Int. J. Adv. Manuf. Technol. Vol.5, pp 1019-1030.

[9] Chen, S. J. and Cheng, C. S., (1995), "A neural network-based cell formation algorithm in cellular manufacturing", Int. J. Prod. Res. Vol. 33, Issue 2, pp 293-318.

[10] Dimopoulos, C. and Mort, N., (2001), "A hierarchical clustering methodology based on genetic programming for the solution of simple cell- formation problem", Int. J. Prod. Res. Vol. 39, Issue 1, pp1-19.

[11] Elmogassabi, H.A. Spring 2006/2007A cost-based heuristic approach for machine cell formation in-group technology. M.Sc. Thesis, I & MSE Dept, University of Garyounis Benghazi, Libya.

[12] Feyzioglu, O. and Pierreval, H., (2009), "Hybrid organization of functional departments and manufacturing cells in the presence of imprecise data", Int. J. Prod. Res., Vol. 47. Issue 2, pp 343-368.

[13] Foulds, L. R. and Wilson, J. M., (2003), "The General Cell formation Problem: manufacturing cell creation with machine modification costs", Southborough University, Business School, Research Series,paperIssue:5.

[14] Gravel, M. Price, W. and Gagne, C., (2000), "An interactive tool for designing manufacturing cells for an assembly job-shop", Int. J. Prod. Res., Vol.38, Issue 2, pp 309-322.

[15] Ho, Y. C. and Moodie, C. L., (1996), "Solving cell formation problems in a manufacturing environment with flexible processing and routing capabilities", Int. J. Prod. Res., Vol. 34, Issue 10, pp 2901-2923.

[16] Islam, K. M. S. and Sarker, B. R., (2000), "A similarity coefficient measure and machine- parts grouping in cellular manufacturing systems", Int. J. Prod. Res., Vol. 38, Issue 3, pp 699-720.

[17] James,T. L. Brown, E. C. and Keeling, K. B., (2007), "A hybrid grouping genetic for the cell formation problem", Computers and Operations Research, Vol. 34, pp 2059-2079.

[18] Kamal, S. and Burke, L. I., (1996), "FACT: a new neural network-based clustering algorithm for group technology", Int. J. Prod. Res., Vol. 34, Issue 4, pp .919-946.

[19] King, J. R., (1980), "Machine-component grouping in production flow analysis: an approach using a rank order clustering algorithm", Int. J. Prod. Res., Vol.18, Issue 2, pp 213-232.

[20] Krishnan, K. K. Mirzaei, S. Venkatasamy, V. and Pillai, V. M., (2011), "A comprehensive approach to facility layout design and cell formation", Int. J. Adv. Manuf. Technol, Published online: 02August.1-17.

[21] Kumar, L.and Jain, K. P., (2008), "Part- machine group formation with operation sequence, time and production volume", .Int. J. Simulation Model, Vol. 7, Issue 4, pp 198-209.

[22] Kusiak A., (1987), "The generalized group technology concept", Int. J. Prod. Res., Vol. 25, Issue 4, pp 561-569.

[23] Lee, H. and Garcia-diaz, A., (1996), "Network flow procedures for the analysis of cellular manufacturing systems", IIE Transaction Vol. 28, Issue 4, pp 333-345.

[24] Loggenran, R., (1991), "Impact of sequence of operation and layoutof cells in cellular manufacturing", Int. J. Prod. Res., Vol. 29, Issue 2, pp 375-390.

[25] Madi, H. J., (2014), "A proposed clustering methodology based on mathematical formulation for operationssequenceand time dependent cell formation", M.Sc. Thesis, I&MSE Dept, University of Benghazi, Libya.

[26] Mahapatra, S. S. Pandian, R.S., (2008), "Genetic cell formation using ratio leveldata in cellular manufacturing systems", Int. J. Adv. Manuf. Technol., Vol. 38, pp 630-640.

[27] Malakooti, B. Malakooti, N. R. and Yang, Z., (2004), "Integrated group technology, cell formation, process planning, and production planning with application on the emergency room", Int. J. Prod. Res., Vol. 42, Issue 9, pp 1769-1786.

[28] Mukhopadhyay, S. K. Babu, K. R. and Sai, K. V. V., (2000), "Modified Hamiltonian chain: a graph theoretic approach to group technology", Int. J. Prod. Res., Vol. 38, Issue 11, pp 2459-2470.

[29] Nair, G. J. K. and Narendran, T. T., (1996), "Grouping index: a new quantitative criterion for goodness of block-diagonal forms ingroup technology", Int. J. Prod. Res., Vol. 34, Issue 10, pp 2767-2782.

[30] Sarker, B. R. and Khan, M., (2001), "A comparison of existing grouping efficiency measures and a new weighted grouping efficiency measure", IIE Transactions, Vol. 33, pp 11-27.

[31] Sarker, B. R. and Mondal, S., (1999), "Grouping efficiency measures in cellular manufacturing: a survey and critical review", Int. J. Prod. Res., Vol. 37, Issue 2, pp 285-314.

[32] Seifoddini, H. and Wolfe, P. (1986), "Application of the similarity coefficient method in group technology", IIE Transaction, Vol. 18, Issue 3.

[33] Seifoddini, H. (1989), "A note on the similarity coefficient method and the problem of improper machine assignment in group technology application**",** Int. J. Prod. Res., Vol. 27, Issue 7, pp 1161-1165.

[34] Selvam, R. P. and Balasubramanian, K. N., (1985), "Algorithmic grouping of operation sequences", Eng. Costs and Production Economics, Vol. 9, Issue 1-3, pp 125-134.

[35] Sule, D. R., (1994), Manufacturing facilities location, planning and design, PWS publishing company, Boston, Second edition.

[36] Sureh, N. C. and Slomp, J., (2001), "A multi objective procedure for labour assignments and grouping incapacitated cell formation problems", Int. J. Prod. Res., Vol. 39, Issue 18, pp 4103- 4131.

[37] Verma, P. and Ding, F. Y., (1995), "A sequence based materials flow procedure for designing manufacturing cells", Int. J. Prod. Res., Vol. 33, Issue 12, pp 3267-3281.

[38] Viswanathan, S., (1996), "A new approach for solving the p-median problem in group technology", .Int. J. Prod. Res., Vol. 34, Issue 10, pp 2691-2700.

[39] Waghodekar, p. H. and Sahu, S., (1984), "Machine-component cell formation in group technology: MACE", Int. J. Prod. Res., Vol. 22, Issue 6, pp 937-948.

[40] Wen, H. Smith, H. and Minor, E., (1996), "Formation and dynamic routing of part families among flexible manufacturing cells", Int. J. Prod. Res., Vol. 34, Issue 8, pp 2229-2245.

[41] Won, Y., (2000), "New p-median approach to cell formation with alternative process plans", Int. J. Prod. Res. Vol. 38, Issue 1, pp 229-240.

[42] Won, Y. and Lee, K. C., (2001), "Group technology cell formation considering operation sequences and production volumes", Int. J. Prod. Res., Vol. 39, Issue 13, pp 2755-2768.

[43] Yasuda, K. Hu, L. and Yin, Y., (2005), "A grouping genetic algorithm for the multi- objective cell formation problem", Int. J. Prod. Res., Vol. 43, Issue 4, pp 829-853.

ISSN 2522-6967

Designand Implementation of Networked Control SystemviaEthernetforSelf Excited Induction Generator Using OPC Server

Abdalla El-Manife[a]* and Salwa Almoshity[b]

[a& b]College of Electrical & Electronic Technology, Benghazi, Libya
*E-mail: Abdalla_ayad2004@yahoo.co.uk

ABSTRACT

Induction generators are increasingly being used in nonconventional energy systems such as wind, micro/mini hydro, etc. The advantages of using an induction generator instead of a synchronous generator are well known. Some of them are reduced unit cost and size, ruggedness, brushless (in squirrel cage construction), absence of separate dc source, ease of maintenance, self-protection against severe overloads and short circuits, etc. In isolated systems, squirrel cage induction generators with capacitor excitation, known as self-excited induction generators (SEIGs), are very popular. Remotely control applications over a wide area had been commonly used in the industries today. One of the common applications requires remote control and monitoring is output voltage control of SEIGs supplied insensitive frequency loads. Drive system has various types of controller, in order to perform some actions such as control the speed to control the output voltage of SEIGs, switching On or Off loads supplied by the generator. This control system can be done by Programmable Logic Controller (PLC), and with the rise of the technology, Ethernet module will be used in order to achieve the remotecontrol system. Plus the PLC today can be controlled not only using its original software, but 3rd party software as well, such as LabVIEW). LabVIEW is a human machine interfaces design software that is user friendly. It can be easily communicate with different hardware using OLE for Process Control (OPC) server.

Keywords:*Ethernet, LabVIEW,Networked Control System, PID controller, PLC, OPC Servers, Self Excited Induction Generator*.

1. Introduction

Industrial control has been moving more and more towards distributed implementations of control systems. Networks are used to communicate the data instead of using traditional point-to-point communication. Networks require less wiring and less maintenance compared to a point-to-point architecture. Such networks carry a large number of small control signals between many nodes and these signals have to meet the delay constraints of real-time control systems. The main difference between such control networks and conventional data networks is that control networks must be able to support time-critical applications [1].

Networked Control Systems (NCSs) consist of sensors, controllers and actuators that communicate together over a network. Sensors send packets to the controllers which calculate the control action that should be delivered to the actuators, and these transmissions must meet the control system's deadline. There are four factors that affect the utilization of the network bandwidth: the sampling rate, the number of nodes requiring synchronous operation, the size of the information sent and the protocol used. Traditionally, for proper control, there are different protocols used which have a deterministic behavior such as DeviceNET and ControlNET [2, 3]. Also, many real-time applications were studied using protocols such as Controller Area Network (CAN), PROFIBUS and EtherNet/IP which is a merger between Ethernet and ControlNET [3, 4, 5, 6, 7].

Recently, Ethernet has been used in Networked Control Systems. Although Ethernet is a nondeterministic protocol, in many studies, that it can be used in NCSs. Ethernet is widespread nowadays in communication systems because it has been proven to be a very successful protocol. By using such a protocol, installation and maintenance costs can be reduced in industrial applications. In [8], real-time as well as non-real time traffic were integrated without any changes to the IEEE 802.3 protocol. A system consisting of 16 sensors, one controller and 4 actuators was able to meet the required time constraints.

The system was running on-top-of Gigabit Ethernet. On the other hand, in [9].The architecture with an integrated control design was also a possible solution where each actuator would have its own controller integrated in the same node instead of one controller for the entire system. This same concept is implemented in Sensor Actuator Networks (SANETs) where group(a) of sensors and actuators are distributed geographically and communicate together through wired or wireless networks.

Previously, engineers and scientists had been designing the engineering systems that require a lot of hardware. It is merely impossible to design distance control of the system as more hardware and wiring were needed. In addition, with the rise of the technology, programmable logic controller (PLC) have eased the engineering design and reduce materials required, it is because the entire design is implemented in software programming Pattern. PLC had been commonly used in the industry, including controlling both digital and analog signals. Design distance control machinery is now possible, even by using Ethernet as the communication device between the computer and the PLC [10].

Apart of design the program structure by its own proprietary software, the convenience part of PLC is the accessibility and controllability by other software. Such software must have driver utility of the particular PLC. Therefore engineers can use LabVIEW [11], which has various types of industrial applications which are in virtual instrument (VI) instead of the real and heavy instrument, to control the PLC.

ISSN 2522-6967

2.Project Design Configuration & Preparation

2.1. OPC Server

OLE for Process Control (OPC), which stands for Object Linking and Embedding (OLE) for Process Control, is the original name for a standard specification developed in 1996. The standard specifies the communication of real-time plant data between control devices from different manufacturers. OPC is a software interface standard that allows Windows programs to communicate with industrial hardware devices as illustrated in Figure 1.

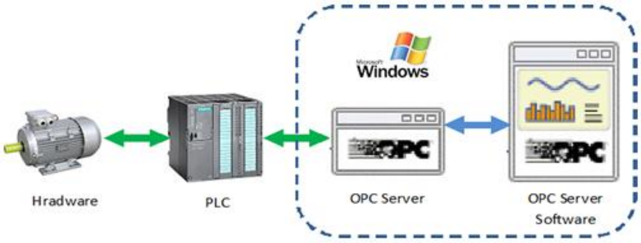

Figure 1. OPC server.

The basic concept in OPC is that we have an OPC Server and one or more OPC Clients that communicate with the server in order to write or read data. An OPC server has implemented a set of services, and the clients are using these services.

OPC is implemented in server/client pairs. The OPC server is a software program that converts the hardware communication protocol used by a PLC into the OPC protocol. The OPC client software is any program that needs to connect to the hardware, such as an HMI. The OPC client uses the OPC server to get data from or send commands to the hardware.

Although OPC is primarily designed for accessing data from a networked server, OPC interfaces can be used in many places within an application. At the lowest level they can get raw data from the physical devices into a SCADA or DCS, or from the SCADA or DCS system into the application. The architecture and design makes it possible to construct an OPC Server which allows a client application to access data from many OPC Servers provided by many different OPC vendors running on different nodes via a single objectFigure 2 shows the OPC sever structure.

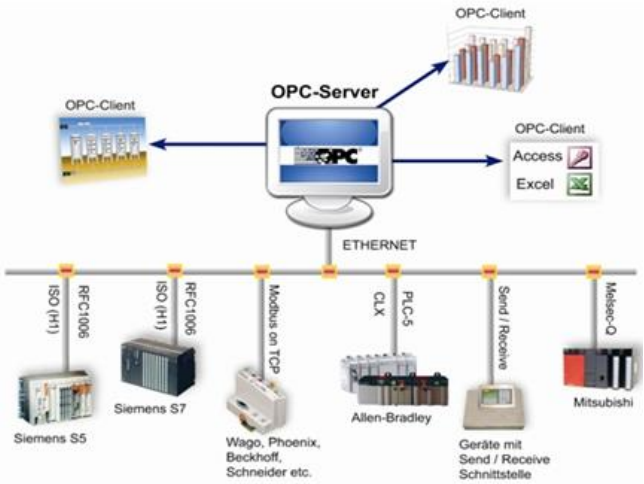

Figure 2: OPC server, OPC clients and different OPC vendor's hardware devices.

The value of OPC is that it is an open standard, which means lower costs for manufacturers and more options for users. Hardware manufacturers need only provide a single OPC server for their devices to communicate with any OPC client. Software vendors simply include OPC client capabilities in their products and they become instantly compatible with thousands of hardware devices. Users can choose any OPC client software they need.

Tags are used a lot in the process industry and are normally assigned to a piece of information. A tag consists of a name describing a single point of information so a process system can consists of hundreds and even thousands of tags. The OPC server has one tag for each measurement points and controller points in the plant and it is the responsibility of the OPC server to get the information from the controllers. This is one of the reasons for the complexity of the servers, they need to have drivers for a lot of controllers and measurement systems.

2.2. NI OPC Server

The NI OPC Servers Bridge converts proprietary industrial protocols to the open OPC Classic and OPC Unified Architecture (UA) protocols. This conversion to OPC then enables NI LabVIEW software to communicate to many different programmable logic controllers (PLCs) and third-party devices through the OPC Client that is included with the Lab VIEW Data logging and Supervisory Control (DSC) Module. The combination of NI OPC Servers and LabVIEW provides a single platform for delivering high-performance measurements and control to industrial systems.

The OPC Client I/O servers for communicating with any server implementing the OPC Foundation OPC server interface. This allows LabVIEW to communicate with any PLC that is interacting with an OPC Server. An OPC Client I/O server will list all available OPC servers that are installed and running on a local or network computer. Figure 3 shows the relationship of the components involved in communication between LabVIEW and a PLC.

PLCs publish data to the network. An OPC Server program uses the PLC's proprietary driver to create OPC tags for each physical I/O on the PLC. NI OPC Servers contains a list of drivers for many of the industry's PLCs. The OPC Client I/O servers provided with the DSC Module can connect to each OPC tag using the OPC DA standard. The configuration of the multiple OPC Client I/O servers in the SVE with different update rates, dead band percentages, and reconnect poll rates can be done easily. The SVE provides a PSP(PublishSubscribe Protocol)URL for each OPC tag that other Shared Variables can bind to by enabling aliasing. Once you deploy the Shared Variables in the SVE and the Shared Variables receive values, LabVIEW can easily read and write to the Shared Variables using a VI.

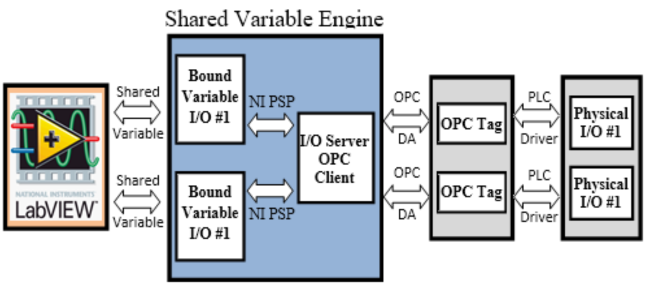

Figure 3: LabVIEW and the SVE Can Communicate with PLCs through OPC.

ISSN 2522-6967

NI OPC Server has Siemens TCP/IP Ethernet driver that allow the communication between SIMATIC S7-300 CPU315F-2 PN/DP PLC with LabVIEW. Siemens supplies their customers with Profinet gateway, interfacing software that communicates with the PLC and its proprietary software, SIMATIC MANAGER over the Ethernet network.

With the Siemens Ethernet driver in NI OPC, users can setup the server by just a few simple setups and create variable tags that can be linked directly to the PLC's registers. These tags are named as OPC tags. The NI OPC Servers also have NI OPC Quick Client that enable users to monitor the status of the PLC in real-time.

As long as the OPC tags had been created, the communication between the LabVIEW and PLC had been simplified as the driver can automatically apply the relevant Profinet commands provided the tags are correctly configured [3]. Meanwhile in LabVIEW, the program can be design by using Shared Variables which is link to the OPC tags.

LabVIEW is a graphical development environment for generating flexible and scalable design, control, and test applications rapidly at minimal cost. With LabVIEW, engineers and scientists are able to interface with real-time signals, analyses data for meaningful information, and share results through intuitive displays, reports, and the Web. Regardless of programming experience, LabVIEW makes development fast and easy for all users.

The programming language used in LabVIEW, also referred to as G, is a dataflow programming language. Execution is determined by the structure of a graphical block diagram on which the programmer connects different function nodes by drawing wires.

These wires propagate variables and any node can execute as soon as all its input data become available. Since this might be the case for multiple nodes simultaneously, G is inherently capable of parallel execution. Multi processing and multi-threading hardware is automatically exploited by the built-in scheduler, which multiplexes multiple OS threads over the nodes ready for execution. Similar to other conventional programming, LabVIEW has standard features such as looping structures, data structures, event-handling, object-oriented programming. LabVIEW also has an extensive library of math functions similar to MATLAB libraries and also formula nodes that allow text-based programming for certain sections of the code that require complex logical structures. Besides that, LabVIEW also has networking library functions that can easily allow users to reference.

Compared to other software like Microsoft Visual Basic, LabVIEW is a better option as it comes together with a library of functions included Shared Variables Project Library, which is bound to the OPC tags that allow server and client communication by connecting relevant icons with the Shared Variables. If Microsoft Visual Basic (VB) is used, the Siemens Ethernet driver must be developed using the MS Comm. function and this would require more time to develop the code [12].

In general LabVIEW has two main elements: the front panel and the block diagram. The front panel allows the user to build the controls and indicators. The controls are including knobs, push buttons, dials, and other input mechanism. Indicators are graphs, LEDs, and other output displays. Meanwhile, the block diagram let user to add code using VIs and structures to control the front panel objects. The elements are illustrated in Figure 4.

LabVIEW has front-end interface applications that allow user to design and then use for controlling systems. Shared variable is a library function variable that allows sharing of data between applications or different data sources across a network. There are many existing data sharing method in LabVIEW, such as UDP/TCP, LabVIEW queues, and Real-Time FIFO [12, 13].

2.3. Programmable Logic Controller

The PLC used for this implementation is SIEMENS SIMATIC S7-300 series. There are 4 modules in addition Power Supply Unit PS307 used in the PLC controller:

Module1: CPU Unit with Ethernet function (6ES7-315-2FH13-0AB0) the Benefits of the CPU is reduction of stock-keeping by saving components, One controller for standard and safety automation, Coexistence of standard and safety programs on one controller is possible,one PROFIBUS or PROFINET transmitting medium for standard and safety communication to SIL 3/Category 4 ,one distributed I/O configuration with standard and safety I/O modules, high speed scan rate (CPU processing time for bit operation is 0.1 μ sec.)and automatic detection of transmission rate 10/100 Mbit/s

Module2: An accurate resolution analog input (AI8 12 BIT -331-7KF00-0AB0)

Module3: High speed digital input and output module (6ES7-322-1BH01-0AB0), is used for digital operation like On/Off the whole system, switch On/Off load different loads supplied by the generator.

Module4: AO4 12bit -332-5HD01-0AB0) basic digital output Unit (6ES7-321-1BH01-0AB0).

All these modules can be connected by assembled and connected them together via backplane plugged in the back of the modules In order to let the PLC to operate through the Ethernet, the PLC must be given an IP address with a Destination node number that is not a duplicate of other IP addresses in the network. The destination node number is also known as the last octet of an IP address.

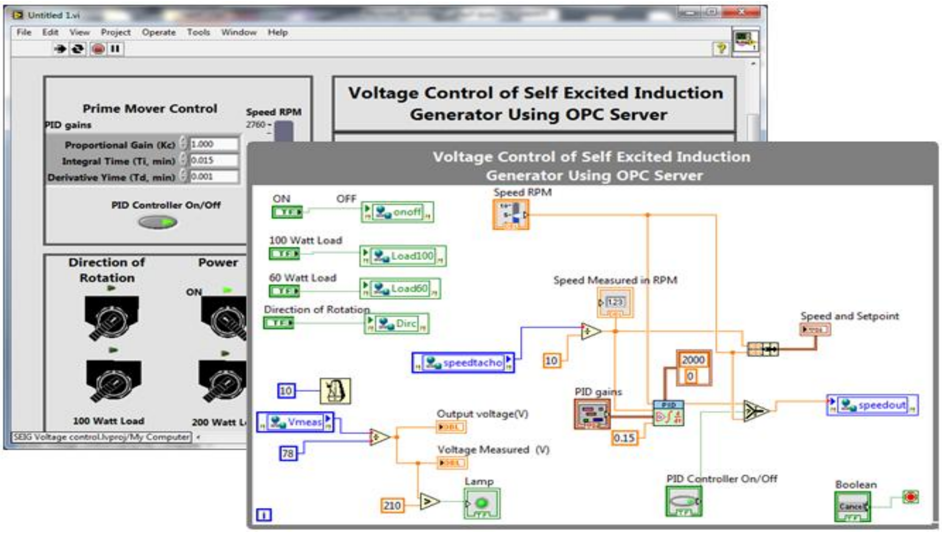

Figure 4: Two main elements of LabVIEW software.

2.4. Self Excited Induction Generator

Induction machines acts as a generator when the slip of machine is negative i.e. the rotor rotates with speed above synchronous speed. When slip is negative, the rotor e.m.f., rotor current and power becomes negative. Under such condition, the electric torque developed is negative (opposite to prime mover) and the machine delivers power to supply mains or loads. The induction generators are two types depending upon the source of magnetizing current:

1. Self-excited induction generator
2. Separately-excited induction generator

Self-excited induction generator (SEIG) means cage rotor induction machines with shunt capacitors connected at their terminals for self-excitation. The shunt capacitors may be constant or may be varied through power electronics. A capacitor bank supply the reactive power to the induction generator for self excitement process and as well as to the load.

2.4.1 Advantages of Induction Generator over Synchronous Generator

- IGs are capable of generating power from variable speed as well as constant speed prime movers.
- Rugged in construction, low cost and easily available.
- Parallel operation is possible without hunting.
- The induction generator has self-protection feature. In the case of the short circuit or overloads, if a fault occurs on its terminals, the excitation fails, and the machine stops the generation itself.
- It needs less auxiliary equipment, do not need a separate DC exciter and other equipment such as field breaker and synchronization circuit.
- Require very less maintenance.
- It does not have to be synchronized to the supply line as that of the synchronous generator.

2.4.2 Single-Phase Power Generation

In remote and rural areas, the population is sparsely distributed and most of the electrical loads are of single-phase type. Single-phase supply is suitable up to the load of 20 kW due to cost effectiveness of the distribution system. Also, load balancing becomes difficult in three-phase SEIG for small-scale power generation. Single-phase induction motors can be operated as single-phase SEIG, but these are limited to small power outputs, i.e., up to 5 kW. Above this load, three-phase machines are cheaper, more readily available and have higher efficiency than equivalent sized single-phase machine. For these reasons, three-phase machines may be used for single-phase power generation, the main schemes for single phase power generation using three-phase machine are as follows:

1. C – 2C scheme for delta connected machine as shown in Figure 5.
2. Csh – Cse configuration
3. Cp – Cs scheme

The power system as a whole runs on a single frequency and in order to maintain stability as well as efficiency the frequency of the system must remain constant at every point of time. The transients can occur at any stage of power system but when talk about frequency, load is one of the biggest driving factor which needs to be monitored.

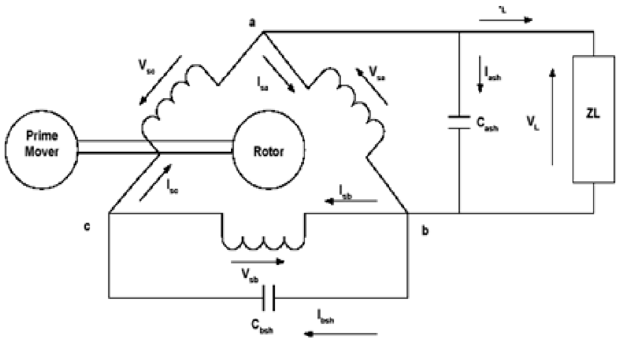

Figure 5: Connection of Self Exited Induction Generator of C–2C Scheme.

When we talk of total change in electrical power of the system we consider both frequency independent sources and non-frequency sources. For resistive loads, such as lighting and heating loads, the electrical power is independent of frequency. But for motor loads and other variable loads, such as fans and pumps, electrical power change with frequency due to change in motor speeds. Thus the concept of non sensitive and sensitive frequency loads arise.

2.4.3 Classification of Induction Generators:

Depending upon the prime movers used and their locations, generating schemes can be broadly classified as under

ISSN 2522-6967

- *Constant speed constant frequency [CSCF] :*

In Constant speed constant frequency scheme, by continuously adjusting the blade pitch and/or generator characteristics the prime mover speed is made constant. At a slip of 1% to 5% above the synchronous speed, an induction generator can operate on an infinite bus bar. Induction generators have many advantages like they are easier to operate, control, maintain, and do not have any synchronization problems.

- *Variable speed constant frequency [VSCF]:*

The variable-speed operation of wind electric system yields higher output for both low and high wind speeds. This results in higher annual energy yields per rated installed capacity. Both horizontal and vertical axis wind turbines exhibit this gain under variable-speed operation.

- *Variable-Speed Variable Frequency [VSVF]:*

The performance of synchronous generators can be affected with variable prime mover speed. For variable speed corresponding to the changing derived speed, SEIG can be conveniently used for resistive heating loads, which are essentially frequency insensitive. This scheme is gaining importance for stand-alone wind power applications.

3. Implementation

3.1. Implementation Process

The Ethernet control systems presented in this paper is to control output voltage of Self Excited Induction generator (SEIG). In order to achieve the objectives, the establishment of the communication between PLC and LabVIEW is crucial as LabVIEW is 3rd party software using OPC server. Thus, the implementation used LabVIEW to perform the start and stop operation of the prime mover, either in forward or reverse direction, and varying the speed by changing the frequency of the motor using **Micromaster 420**inverterand connect or disconnect anelectrical load to output terminal of Induction generator. However, this system is also a supervisory control and data acquisition (SCADA) since there is practical data measurement acquire from the actual output of the system , this feedback is the output voltage of the SEIG and the actual speed that can be read from the tachogenerator install at the same shaft.

3.2 PID controller

One of the control system strategies to dominate like this close loop system is PID "Proportional-Integral-Derivative" controller to achieve the objectives parameters, to tune the controller parameters K_p, T_i, and T_d. The PID control algorithm is a robust and simple algorithm that is widely used in the industry. The algorithm has sufficient flexibility to yield excellent results in a wide variety of applications and has been one of the main reasons for the continued use over the years [23, 24].

However, it is difficult to design when the accurate model of plant is complicated or the environment of the load on the plant is variable. So there is no PID hardware were designed and implemented, in this paper,the PID controller of control design and simulation toolbox of LabVIEW is used, abasic PID loop controller structure is shown in Figure 6.

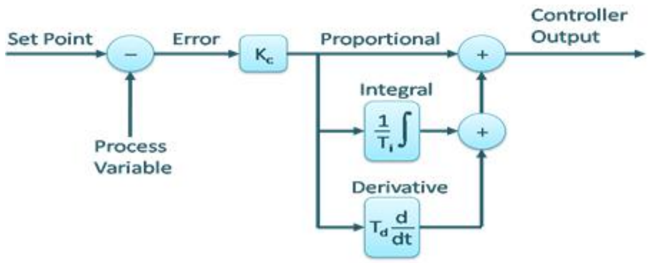

Figure 6:Basic PID loop controller structure.

Proportional action is the controller gain times the error, the PID VIs express the proportional component in terms of controller gain. In integral action (Trapezoidal Integration) there are several options for discreteizing integral action, such as forward difference, backward difference, and trapezoidal approximation, which is also known as Tustin or Bilinear transformation. The PID VIs use trapezoidal integration to avoid sharp changes in integral action when there is a sudden change in PV or SP. Abrupt changes in SP can generate bumps to the output of the controller as a result of applying derivative action to the error e. These bumps are referred to as derivative kick. To avoid derivative kick, you can apply derivative action to the PV only, and not to the error e . Controller output is the summation of the proportional, integral, and derivative action, as shown inFigure 6.

The loop-cycle time, or interval in seconds, at which this VI is called this VI calculates the time since it was last called using an internal timer with 1 ms resolution.

The system has three-layer network architecture illustrated in Figure 7. As illustrated in Figure 8, user gets the authority to control through the host computer, which is a laptop.

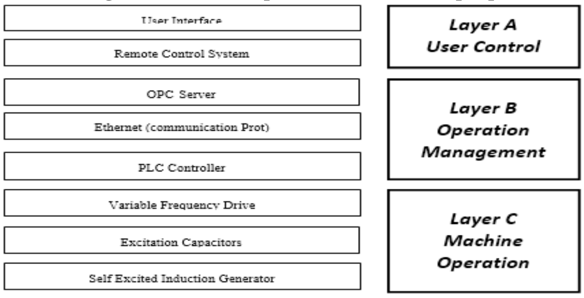

Figure 7: Three layer network architecture.

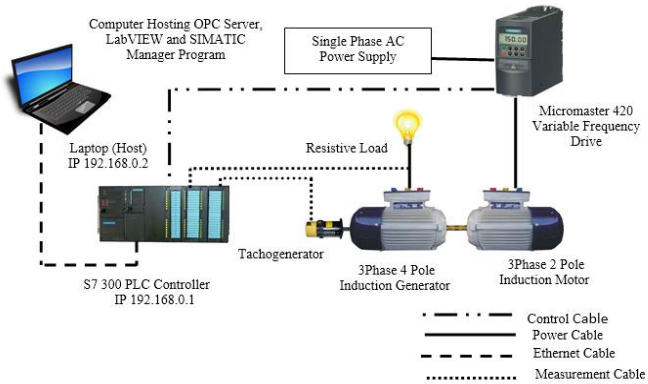

Figure 8:Actualnetworkconfiguration.

3.3. Implementation of VI Design

The objective of the VI program is to allow user to make the decision of the start and stop operation of the prime mover, either in forward or reverse direction, and varying the speed by changing the frequency of the motor, by perform two simple step. Firstly select the turning direction by press the push button in the VI Front Panel, which is either forward or reverse. Secondly, vary the speed by turning the Frequency slider to the value of the frequency that the user desire. Figure9 illustrates the V I Front Panel of the LabVIEW project.

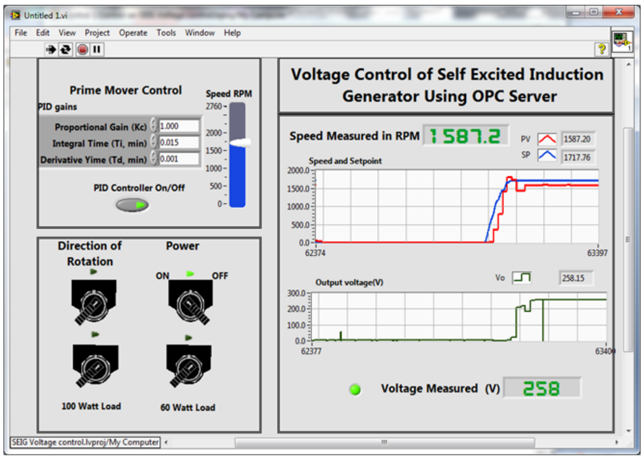

Figure 9. VI front panel of the project.

Before running the VI, make sure all the hardware have been switched on and configured correctly, and launch the NI OPC Quick Client so that the OPC tags can be browsed by the shared variables in this VI. There are 7 OPC tags was created and used in the implementation, and the details of the tags have been tabulated in Table 1.

Table 1. The details of OPC tags and its PLC Addresses.

OPC Tags	PLC Addresses	Data type	Description
Dirc	M60.0	Bool	To Change the Direction
load100	M60.1	Bool	To Switch Load 100 Watt
Load60	M60.2	Bool	To Switch Load 100 Watt
On/Off	DB1.DBX8.2	Bool	To Switch On/Off Prime Mover
speed tacho	MD18	Double word	Measure the Actual Speed
Vmeas	IW290	word	Measure the Actual Output Voltage
vout	DB1.DBW0	word	Control Voltage of the Inverter

By referring to Figure 9, the Power switch is to switch the prime mover on and off and the direction of rotation switch is turning in forward direction and backward direction. The sliderlabeled as “Speed RPM” is the key program to control the frequency as well as the speed of the motor. The PID gains can be adjusted by tuning the proportional gain$K_p$integral time $T_i$and derivative time. The upper waveform chart for data logging of set point speed and the actual speed of the generator via Tachogenerator and the output voltage of the generator is plotted in the lower waveform chart.

Figure 10 and Figure 11 illustrate the Time response of the speed and the output voltage when the PID controller gains are K_p =1.0, T_i =0.0015 min., T_d=0.001 min. after applied a resistive load of 60 watts and 100 watts respectively.

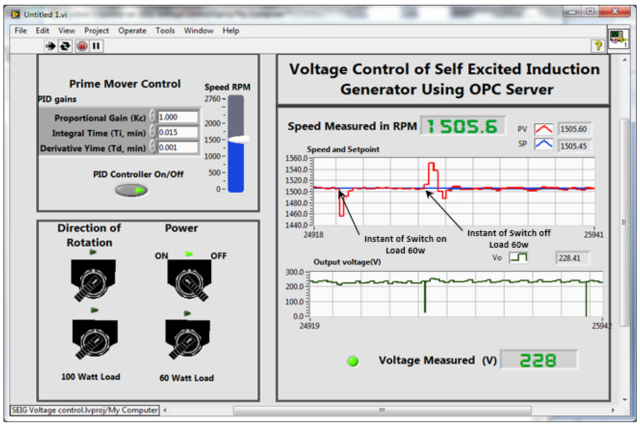

Figure 10: Time response of the speed and the output voltage when the PID controller gains are K_p=1.0,T_i=0.0015 min., T_d=0.001 min. after a resistive load of 60 watt is applied.

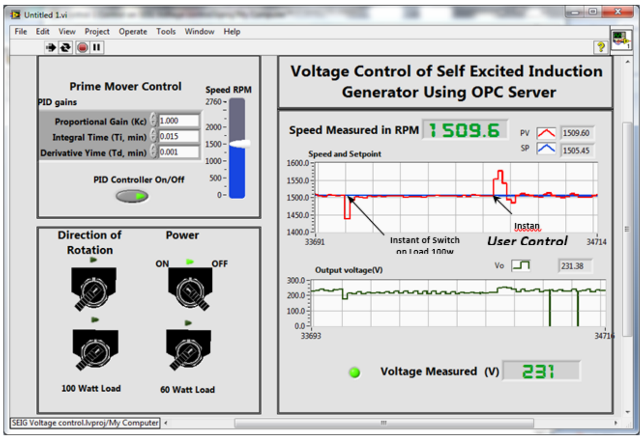

Figure 11: Time response of the speed and the output voltage when the PID controller gains are K_p=1.0,T_i=0.0015 min., T_d=0.001 min. after a resistive load of 100 watt is applied.

The time response of the speed and the output voltage when the generator is regulated the PID controller gains are K_p =1.0, T_i =0.0015 min., T_d=0.001 min. for deactivate and Activate the PID controller while startup are shown in Figure 12 and Figure 13 respectively.

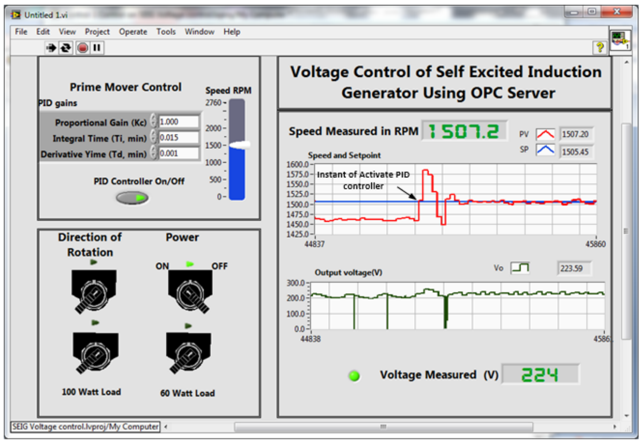

Figure 12: Effect of PID Controller When Activated.

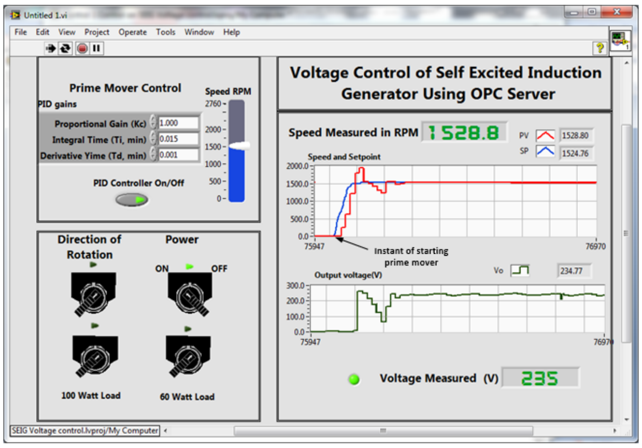

Figure13: Effect of PID Controller When Starting up.

4. Testing and Verification

After the implementation, test is performed in order to verify that the system is working smoothly. Figure 14 shows the front view of the system. Figure 15 shows the PLC Ethernet Module light indicators that light up when the project VI is executing.

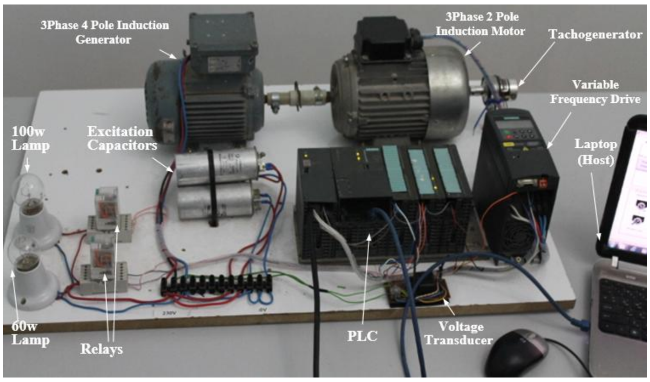

Figure 14. Shows the Front View of the System.

Figure 15. PLC Ethernet module light indicator status.

5. Conclusions

The objective, scope and fundamental requirements of the project had been achieved. A major system design requirement for Networked Control Systems (NCSs) is to meet real-time delay requirementfor sensors, controllers and actuators. Different protocols were purposed to maintain requirements of speedand correctness such as Controller Area Network (CAN) and PROFlBUS. ETHERNET in NCS is now one of themost widespread and low cost protocols available. the time response of the controller used Ethernet protocol was encouraging, there is no considerable end-to-end time delay during the execution, the scan rate of OPC server and the loop-cycle time, in VI is 10 ms, when the project VI is executing by Laptop (Intel(R) Core(TM) i7-2670QM-CPU@2.20 GHz and 8Gb RAM and integration time of the PID controller was 0.15 second.

From the operation of an induction machine under standalone generating mode and a generating scheme for constant voltage and variable frequency by a proportional gain control technique. A laboratory test is performed where the induction machine is controlled as a self excited induction generator. The effect of rotor speed is observed. From the experimentation, it is confirmed that as the rotor speed is increased at a particular speed, voltage builds up faster and the magnitude of voltage increases due to availability of more VAR. But frequency remains constant. As the speed increases at a fixed capacitance, both magnitude and frequency of generated voltage increases, self excited induction generator C-2C scheme used with the alternative energy sources, such as windmills or with energy recovery systems in the industrial processes. They are also used to supply additional power to a load in a remote area that is being supplied by a weak transmission line.

In overall, choosing LabVIEW as the human machine interface (HMI) for the implementation is a proper decision as it has various types of applications and functions that are easy to understand and use. Additionally, this approach is more economical as the objectives of the system implementation have been achieved with only basic functionality of the LabVIEW toolkits used, which are shared variables and NI OPC Servers.

The CPU processing time ofSiemens S7 300 series PLC was able to meet the required time constraints, and the control unit is easy to install and setup. Both hardware and software configuration can be easily done. It can carry out additional functions by simply add more units with various functions, like the digital/analog modules or Ethernet units.

References

[1] Lian, F.L., Moyne, J.R. and Tilbury, D.M. Performance Evaluation of Control Networks: Ethernet, ControlNet, and DeviceNet. *IEEE Control* Systems Magazine, 21, 66-83 2001.

[2] Daoud, R., Elsayed, H., Amer, H. and Eid, S. (2003) Performance of Fast and Gigabit Ethernet in Networked ControlSystems. Proceedings of the 46th IEEE Midwest Symposium on Circuits and Systems MWSCAS, Cairo, December 2003.

[3] Wittenmark, B., Bastian, B. and Nilsson, J. (1998) Analysis of Time Delays in Synchronous and Asynchronous Control Loops. Proceedings of the 37th IEEE Conference on Decision and Control, Tampa, December 1998, 283-288.

[4] Official Site for PROFIBUS and PROFINET.http://www.profibus.com

[5] Moss, B. (2000) Real-time Control on Ethernet. Dedicated Systems, No. 00q2, 53-60.

[6] EtherNet/IP Performance and Application Guide, Allen-Bradley, Rockwell Automation, Application Solution.

[7] Official Site for Control Net. http://odva.org/default.aspx?tabid=244

[8] Nilsson, J. Real-Time Control Systems with Delays, Ph.D. Thesis, Department of Automatic Control, Lund Institute of Technology, Lund 1998.

[9] Lian, F.L., Moyne, J.R. and Tilbury, D.M. Networked Control Systems Toolkit: A Simulation Package for Analysis and Design of Control Systems with Network Communication. Technical Rep., UM-ME-01-04, July 2001.

ISSN 2522-6967

[10] W.-F. Chang, Y.-C. Wu and C.-W. Chiu, "Design and Implementation of a Web-Based Distance PLC Laboratory," Proceedings of the 35th Southeastern Symposium on System Theory, Morgantown, 16-18 March 2003

[11] M. Rodrigues, J. Mendes and J. Fonseca, "Application of a Web-Based Monitoring and Control System in Plastic Rotational Moulding Machine," IEEE International Conference on Industrial Technology, Hammamet, 8-10 pp. 819-823 December 2004,

[12] N. N. Barsoum and J. A. Roland, "Ethernet LabVIEW Control," Undergraduate Thesis, Curtin University Sarawak Campus, Sarawak, , 2010.

[13] National Instruments, "Using the LabVIEW Shared Variable," 2010.

[14] [M. Aoulkadi, A. Binder, "Evaluation of different measurement methods to determine stray load losses in induction machines," in Proc. of International Symposium on Power Electronics, Electrical Drives, Automation and Motion (SPEEDAM 2006), Taormina, Italy, May 23-26, S1, pages 13 – 18, 2006.

[15] [IEEE Standard Test Procedure for Polyphase Induction Motors and Generator, IEEE Std 112-2004, 2004.

[16] A. Ghorashi, S. Murthy, B. B. Singh, B. Singh, "Analysis of wind driven grid connected induction generators under unbalanced grid connections," IEEE Trans on Energy Conversion, vol. 9, no. 2, pp. 217-223, 1994.

[17] [18] F. Jiang, Z. Q. Bo, L. Roumei, "Performance of induction generator in parallel with an unbalanced three phase system," in Proc. of International Conference on Power System Technology (POWERCON), Beijing, China, Aug. 18-21, vol. 2, pp.1193 – 1197, 1998.

[18] W Deprez, A Dexters, J Driesen, "Energy efficiency of small induction machine. Comparison between motor and generating mode" - ICEM 2006, 2006

[19] [20] Yogesh K Chauhan, Satnam Mahley, "Steady state analysis of three phase self excited induction generator" Thapar University, June 2008

[20] S. Raghavan, "Digital Control for Speed and Position of a DC Motor," MS Thesis, Texas A & M University Kings-ville, 2005.

[21] Z. Xiu, and G. Ren, "Optimization Design of TS-PID Fuzzy Controllers Based on Genetic Algorithms," 5th World Congress on Intelligent Control and Automation, Hangzhou, pp. 2476-2480, 2004.

[22] S. Z. He, S. Tan and F. L. Xu, "Fuzzy Self-Tuning of PID controllers," Fuzzy Sets and Systems, Vol. 56, No. 1, pp. 37-46, 1993.

APPENDIX-A

3 ϕ induction motor(Prime mover) parameters:

Connection	Rated Voltage	Rated power	Full load current	Motor speed
YY	400V	0.6kW	1.6A	2760 rpm
Δ	400V	0.45kW	1.5A	1320 rpm

3 ϕ induction generator parameters:

Connection	Rated Voltage	Rated power	Full load current	Motor speed
Y	220V	0.37kW	1.85A	1395 rpm
Δ	380V	0.37kW	1.1A	1395 rpm

ISSN 2522-6967

Artificial Neural Network Modelling of Total Dissolved Solid (Elzawia city – Libya, as a case study)

Lubna S. Ben Taher

Assistant Lecturer, Civil Engineering Department, University of Benghazi, Libya.
Corresponding author; e-mail: lina7981@yahoo.com

ABSTRACT

In this study Mathematical, and statistical methods to simulate an aquifer water quality parameters have been considered. It is necessary to measured water quality for groundwater zonation maps. Therefore, more accurate maps produced more essential role in the discussionmanagement. Water samples were collected from thirty wells at Elzawi city located around 45km west of Tripoli and analysed for water quality parameters including: EC(Electrical Conductivity), TDS(Total Dissolved Solids), Ca (Calcium), Mg (Magnesium), and pH using standard methods. The wells location andwater level at wells observed by Global positioning system (GPS) type Garmin GPS 12XL. An artificial neural network (ANN) models were investigated to predict the TDS in water of Elzawi city wells. The input variables were the wells longitude, latitude, EC, Ca, Mg, and pH while the TDS in water was the output. The Levenberg–Marquardt (LM) algorithm and Back propagation used for training of the feed forward ANN. The ANN models performance were compared using the coefficient of determination(E), mean absolute percentage error (MAPE %), and 95% confidence interval(CI95%).It has been a good agreement between actual data and the ANN outputs for training, validation and testing data sets at the forth model (ANN4) while based on all inputs . ANN4 model performed superior to the other models in predicting TDS with high E=0.94 and lowest MAPE= 5.6% and the result average within the range of observed 95CI%. Also the ANN models could be successfully applied and provide high accuracy and reliability for water quality parameters forecasting.

Keywords:*Artificial Neural Networks, Total Dissolved Solid, Zawia city, Water Quality*.

1. Introduction

Water is the source and continuity of life. Water supply in developing countries has a major role in agriculture and industries. Elzawia city located at the sea costa –Libya as Figure.1. Libya is located greatly in the dry or semi-dry climatic conditions and shortage of water, the extraction and use of groundwater has been the main of water supply in the country. Vast increase in the utilization of underground water resources has led to an annual decline of groundwater table, which has been growing in the past two decades. Excessive extraction of groundwater resources in dropped down changes its quality. So it is necessary to measure it to manage the decision making entails a comprehensive project that should be provided based on the data and the maps from the surface of groundwater as well as zonation maps of the groundwater quality. Therefore, the more accurate maps result produced more essential role in the management because it is the basis for correct management and operation of groundwater extraction, assessment of the groundwater quality and quantity of zoning map changes [1, 3]. Much research has been done for underground water quality parameters, here are some studies in this field to be mentioned:

Nemati et al. [2] they studied of Total Dissolved Solid (TDS) time series reported in their paper using local water quality parameters of Calcium (Ca), Chloride (Cl), Magnesium (Mg), Sodium (Na), Bicarbonate (HCO3), Sulfate (SO4), and water discharge (Q) for a set of recorded data in Simineh River at Dashband gauging station during 1993-2011. Also employed the Garson equation to assess the relative importance of the variables to determine appropriate input combinations. The ANNs with different numbers of neurons in the hidden layer were constructed, and model performance estimated by means of several indicators, including data sequence, scatter diagrams, and quantitative measures of RMSE, MAE, and R^2. The modeling results indicated that reasonable prediction accuracy was achieved for the ANNs model.

Moasheri et al. [1], in their study, spatial distribution of the parameter TDS with two models of Kriging and Kriging-ANN model was examined. The correlation coefficient for the model Kriging = 0.684 and for model Kriging-ANN was obtained = 0.96 the results showed a significant superiority of the combined model Kriging-ANN. Besides the advantage prediction, it makes possible spatial to predict TDS distribution with access to parameters such as PH and EC.

Moasheri et al. [3], they obtained results from their research showed that estimated parameters of quality spatial distribution of sodium, calcium and magnesium with the optimized combination method with genetic algorithm provided more accurate results than the geo-statistical method in kriging. Water quality parameters that could be used to estimate the unknown values it could be used in the estimation of spatial and temporal distribution of quality parameters of groundwater of Kashan plain.

Sattari et al. [4], their research was motivated by determine an accurate and affordable method to predict EC and TDS; the research had demonstrated that TDS could be accurately predicted using only five parameters. Another motivation for the research was to evaluate suitability of data-mining algorithms to model relationships between parameters of the river water. The research had shown that the best scenario to estimate the TDS in water and EC involved a combination of the following parameters: Sodium, Mg, and Ca, Chloride, and Bicarbonate ion. The computational results showed no need to use the costly process of sampling hydro chemical parameters that affect river water quality. Rather, using fewer hydro chemical parameters had led to acceptable accuracy in estimating TDS and EC values.

Kheradpisheha et al. [5], their study's results, using artificial neural network with the back-propagation algorithms for modeling qualitative parameters of groundwater, such as Cl, EC, SO4, was accurate according to the chosen input parameters. They used back-propagation algorithm and obtained good results because they used a different water source or experienced the impact of other parameters. According to the highly expensive and time-consuming tests, these parameters could be modeled to

ISSN 2522-6967

estimate their range, a quick and cost-effective method for management practices, especially in emergency situations.

Salem and Alshergawi [6], studied the quality of groundwater of fifty one wells for drinking water from Alshati district and assessed for its suitability for drinking. Water samples were collected and analyzed for various physico-chemical parameters such as pH, Temperature (C°), Electrical Conductivity (EC), Total Hardness (TH), Total Dissolved Solids (TDS), Alkalinity (Alk), Chloride (Cl^-), Iron (Fe^{++}), Manganese (Mn^{++}), Calcium (Ca^{++}), Magnesium (Mg^{++}), Nitrate (NO_3^-), Sodium (Na^+), Potassium (K^+), Sulphate (SO_4^{--}) and Phosphate ($PO4^{--}$). The results revealed that some parameters of water samples were out of limit according to the WHO standards and Libyan standards for drinking water. The results shows rising of Fe^{++} and Mn^{++} in most of the wells studied, rising of Ca^{++} in water samples of wells of Al-Mansura and Abu-gadgud, rising of SO_4^{--}, TDS and EC in water samples of wells rising of Cl^- in water samples of Idri, Waanzarik, Taamasan, Al-Mansura and Al-kadra. NO_3^- was also rising in water samples of wells of Mahruga and Bergen.

Maedeh et al. [7], the results from their structures of different models of neural networks, was observed. The fifth model with least amount of data and, hence least number of tests to find out the different parameters, turns out to be the most cost-effective and involves lowest error, as regards TDS parameter prediction of Tehran groundwater, which in view of the inputs and the neural networks in models, the estimate thus obtained was remarkably and favorably high. In light of the model developed, a better future estimate and a more reliable forecast to enhance the quality and application of groundwater can be made via controlling the sulphide, chloride and sodium parameters in forecasting the TDS parameter.

Alshakel (2015), in his study some chemical analyses were carried out for about 30 samples of the Zawia city wells, to evaluation the concentration of total dissolved solids (TDS), Ca^+, Mg^+ Ions and the total hardness. The results of these analyses indicated to high concentration of (TDS), Ca^+, Mg^+ Ions and the total hardness in several samples .The source of these elements might from sea water intrusion because this area located beside the sea coast, or another source as sewage disposal.

Electrical conductivity and total dissolved solids are considered as important parameters in determining quality of drinking and agricultural water because they directly represent total salt concentration in the water. Increases in these parameter values indicate a reduction in water quality. In this study, estimation of the TDS in about thirty pumping well located at Elzawi city- Libya, was studied using the ANNs. The input variables were the well longitude, latitude, EC, Ca, Mg, and pH while the TDS in water was the output. The Levenberg–Marquardt (LM) algorithm was used to train ANN and back propagation used for the training of the feed forward ANN. The ANNs models performance were compared using the coefficient of determination (E), mean absolute percentage error (MAPE %), and 95% confidence interval.

2. Materials And Methodology

2-1 Study Area:

Elzawi city is located in around 45km west of Tripoli between North latitude 3244'53.160''N and East longitude 1243'23.160 see Figure. 1, and the population of it is about 186132. The average annual temperature in the region with 24.4 ºC, and the Annual rainfall 255 mm.

2-2 Data Analysis

A total of 30 water samples were collected from underground wells localities in El Zawia city the geographical location as longitude1243'41 to1244'74, latitude3246'25 to 3247'3. After collection, water samples were protected from direct sunlight and transported in a cooling box containing ice packs to the laboratory for analyses. Water samples were examined for physicochemical parameters (pH, Ec, Ca^{2+}, Mg^{2+} and TDS).Different maxima, minima, averages and deviations of standard have been calculated, the correlation between them and well latitude - longitude also see Table-1. Finally, the models designed by neural networks to predict the TDS parameter with different input combination. Figures 2 to 5 present the histogram and map distribution of the (pH, Ec, Ca^{2+}, $Mg2^+$, TDS) for the wells. The values presented in Table-2 indicate that the TDS is highly correlated with EC, Mg and Ca. noted that also there is a good correlated between the TDS, Mg, Ca, PH and Ec with the location of wells presented as the latitude and longitude presented as the latitude and longitude.

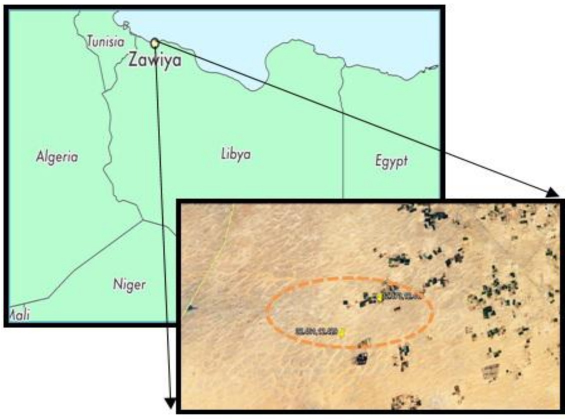

Fig. 1: Map showing El Zawia city and the places where the wells collected.

Table-1. Statistical Analysis of Field Measurement, El Zawia City Wells.

Variable	Mean	StDev	Minimum	Maximum
latitude	32.46	0.00312	32.461	32.473
longitude	12.43	0.00513	12.429	12.447
Mg^{2+} ppm	443.70	262.4	70.8	1318
Ca^{2+} ppm	504.3	207.4	140	1050
Ec Mc/cm	3040	1201	685	5905
PH	7.05	0.1874	6.68	7.44
TDs ppm	2049	1000	446	4900

Table-2.The correlation coefficient of Field Measurement, El Zawia City Wells

	latitude	longitude	Ec	PH	Mg^{2+}	Ca^{2+}
longitude	0.598					
Ec	0.528	0.313				
PH	-0.141	-0.249	-0.506			
Mg2+	0.612	0.277	0.906	-0.356		
Ca2+	0.324	0.045	0.873	-0.369	0.836	
TDs	0.524	0.228	0.932	-0.475	0.878	0.84

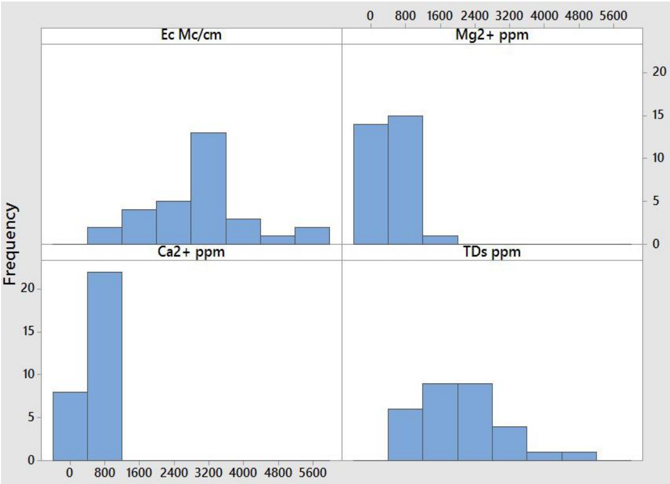

Fig.2: Histogram of Ec Mc/cm, Ca ppm, Mg ppm, and TDS ppm, El Zawia City Wells.

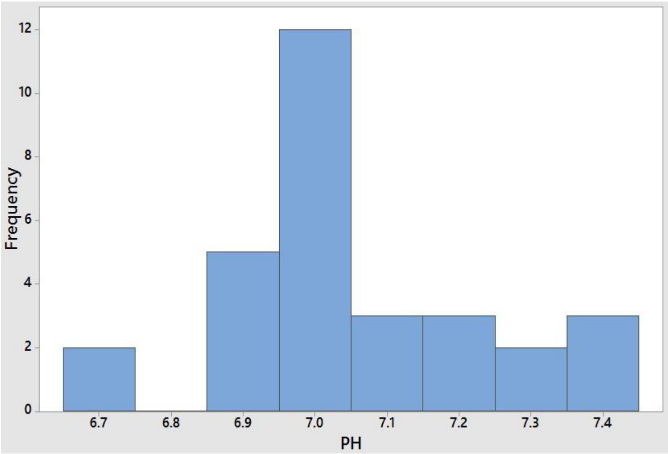

Fig.3: Histogram of the (PH)El Zawia City Wells.

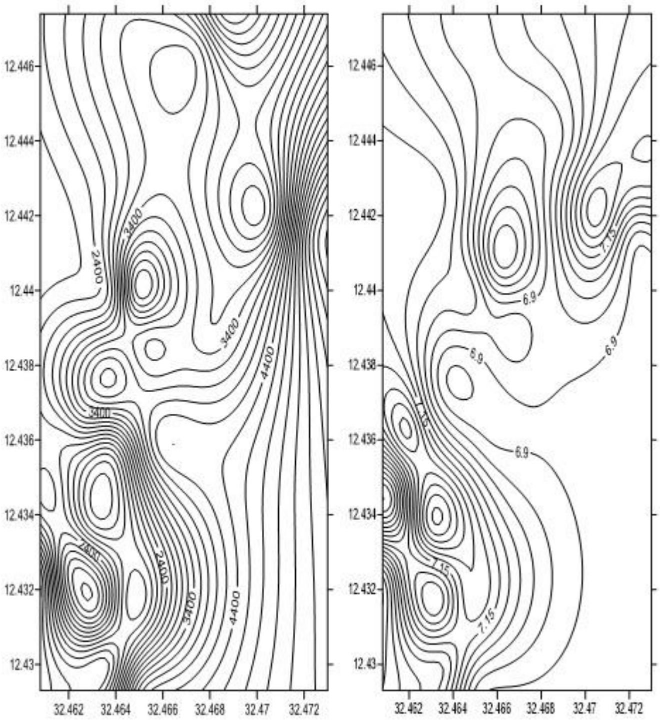

Fig.4: Map distribution of Ec Mc/cm and PH El Zawia City Wells.

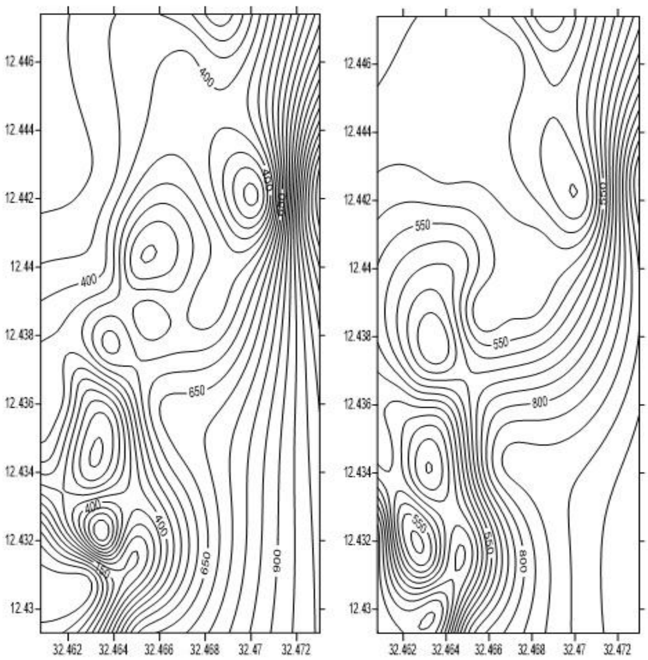

Fig.5. Map distribution of Mg^{+2} ppm and Ca^{+2}ppm, El Zawia City Wells.

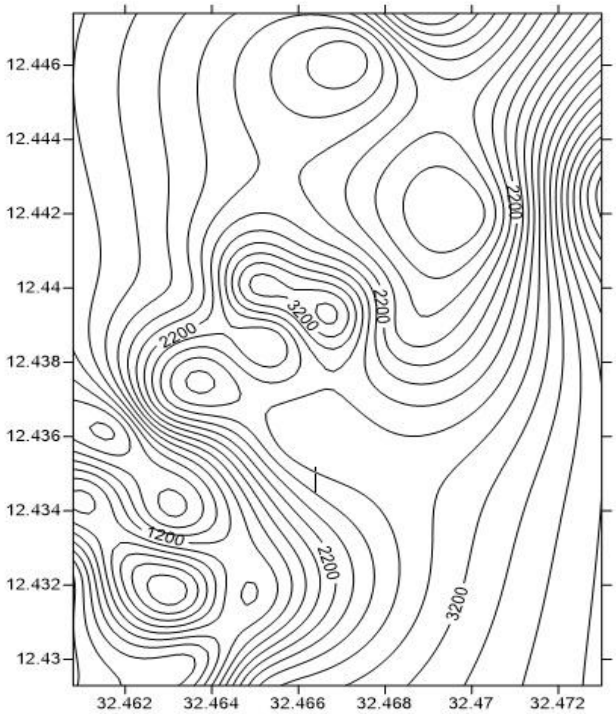

Fig.6: Map distribution ofTDS ppm, El Zawia City Wells.

3. Study Methodology

Artificial Neural Networks (ANN), are a form of computing inspired by the functioning of the brain and nervous system. Neural networks consist of a set of neurons or nodes arranged in layers, and in the case weighted inputs are used, these nodes provide suitable inputs by conversion functions. Each neuron in a layer is connected to all the neurons of the next layer but without any interconnection among the neurons in the same layer. The weight learned for each neuron in ANNs model remains internal,

ISSN 2522-6967

and therefore, their associations with physical systems are often overlooked (Nemati, 2014).

The feed forward ANN has been adopted in many environmental modeling studies because of its applicability to a variety of different problems. Noted that more than one hidden layer may require in feed forward networks because a three-layer network can generate arbitrarily complex decision regions. Also, the appropriate input vector to the ANN model can be identified according to the procedure of the modeler. Back propagation is the most popular algorithm used for the training of the feed forward ANN. An objective function that considers both the ANN's structure and error, minimizes a linear combination of the resulting ANN's squared errors, weights, and biases in order to develop a less complex model at the end of training the resulting network has good generalization qualities.

The Levenberg–Marquardt (LM) training algorithm is a trust region based method with a hyper-spherical trust region. This algorithm was implemented in this study using the Neural Network Toolbox of MATLAB, an example of developed structure of ANN with 6 inputs see in Figure 7.

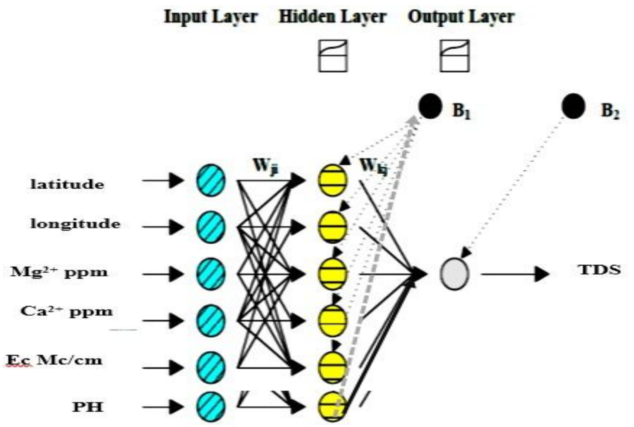

Fig.7: Developed Structure of ANN with 6 inputs.

In this study, several statistical parameters were used to evaluate the performance of predicted models, which were given by the following relations:

1- Mean absolute percentage error (MAPE %)

$$MAPE\% = \frac{100}{n}\sum_{t=1}^{n}\left|\frac{TDS obs. - TDS pre.}{TDS obs.}\right| \quad ------1$$

2- 95% confidence limit (95CI%):Standard error of the mean is given as; $1.\ S_{\bar{X}} = \frac{s}{\sqrt{n}}$

The quantity (TDS. - μ) / Sx has a t-distribution with n-1 degrees of freedom, And for 95% confidence limit

$$1.\ \overline{TDS.} - 1.95\left(\frac{s}{\sqrt{n}}\right) < \mu < \overline{TDS.} + 1.95\left(\frac{s}{\sqrt{n}}\right) \quad 2$$

The value on the left side of the inequality yields the lower limit, and on the right side yields the upper limit for the mean

3- *E*, Coefficient of Determination

$$E = 1 - \left(\frac{\sum_{i=1}^{n}\left(TDS.obs._i - TDS.pre._i\right)^2}{\sum_{i=1}^{n}\left(TDS.obs._i - \overline{TDS.obs.}\right)^2}\right) \quad -------3$$

Where:

n= number of data,

TDS.obs.= observed value,

TDS.pre.= predicted value,

S = standard deviation, and

$1.\ \overline{TDS.obs}$ = the average of the observed da

A better fit, with zero indicating MAPE% and high value of E. Coefficient of determination(E = 0 to 1) is calculated on the basis of the relationship between the predicted and observed mean deviations and it can show the correlation between the predicted and observed data. E is better suited to evaluate model than the square root of the correlation coefficient between the predicted and observed value (R^2).The probability of procedure produces an interval that contains the actual true parameter value is known as the Confidence Level and is generally chosen to be 95CI%. So the model if have a good performance well produce a results within the range of 95CI% of the mean observed data. The models are used to generate data which conserve the main statistical characteristics of the historical data. This is verified through comparing values of mean, of generated data with those of historical data.

4. Estimate the spatial distribution TDS by artificial neural networks

In this study, the water quality data of 30 wells located at El Zawia city were used. Concentrations of the parameters have been measured, and record consists of 5 parameters including: (Ca), (Mg), PH, (EC), and (TDS). In order to develop ANN models for prediction TDS, the data were divided into two groups randomly: training data, accounting for 70 percent and testing and validation data, making up 30 percent of the total data. The ANN models were trained using Bayesian Regularization (BR) and Levenberg–Marquardt (LM) algorithms. In ANN models the number of neurons in the hidden layer were found by a trial and error procedure. The activation functions used for the hidden and output layers were the 'logsig' and 'purelin' functions, respectively. Table- 3 showing the structure of ANN models according to the input combinations, moreover the models were improved by the accuracy with respect to MAPE%, E, and CI 95%. ANN (6, 20, 1) model indicates model having 6, 20 and 1 for the input, hidden and output layer, respectively and the data divided in to (20 values for model training, 5 values for model validation, and 5 values for model testing). Over all ANN models showing best prediction for all input combination in both test and validation periods. Figure 8 presented the comparison between the predicted and observed TDS data. The best architecture was obtained for ANN TDS models (ANN-4) had been selected based on minimum value of MAPE% and maximum value of E. The output from the best selected architecture for the ANN-4 model was validated using the testing data set. The objective of the validation process is to investigate the ability of the model to work with an independent data series that have not been used in training of the evaporation model.

Looking into the models, it is found out that, forecasting the TDS parameter in the first and second models have a greater magnitude of error, as they have fewer input parameters. Therefore, this indicated the inefficiency of the simulating and training algorithms. In the third and the fourth models the error declines as the simulating and training algorithms were kept constant. It was also revealed that error dwindles to its minimum as the number of input neurons decreased and an extra layer was built into the fourth model. By contrast, the third and fourth model, consisting of 4 and 6 parameters, respectively result in

ISSN 2522-6967

acceptable error. Figurer 8 the distribution of the observed data (the vertical axis) and the predicted data (the horizontal axis) in the testing and training stage of the all models. It should be noted that the closer the data get to a one –to-one diagram, the more reliably the model evaluates the TDS proportion.

An examination of figure 8 shows that the sensitivity of different parameters in predicting the neural network of the four models was observed for (Ca), (Mg), (EC) parameters, and the latitude, longitude respectively. It goes through the Ec, latitude, and longitude of the wells, played a good pronounced role in predictions for TDS.

The spatial distribution of the parameter TDS with the ANN model was examined. The results show a significant superiority of the combined model ANN to the well latitude, longitude. The advantage prediction, it makes possible to predict spatially TDS distribution with access to other parameters such as EC.

Table-3. Error statistics for input combinations using ANN models in test and validation stage.

Input combinations	ANN Model architecture	MPE%	E	The average Predicted TDS. ppm	95% CI **Observed TDS. ppm**
Mg^{2+} ppm Ca^{2+} ppm	ANN1 (2,20,1)	17.6	0.88	1989.95	1675.6 –2422.5
PH Mg^{2+} ppm Ca^{2+} ppm	ANN 2 (3,20,1)	19.5	0.83	2080.44	
Ec Mc/cm PH Mg^{2+} ppm Ca^{2}+ ppm	ANN3 (4,20,1)	7.7	0.94	2098.10	
Latitude Longitude EcMc/cm PH Mg^{2+}ppm Ca^{2+}ppm	ANN 4 (7,20,1)	5.6	0.94	2028.97	

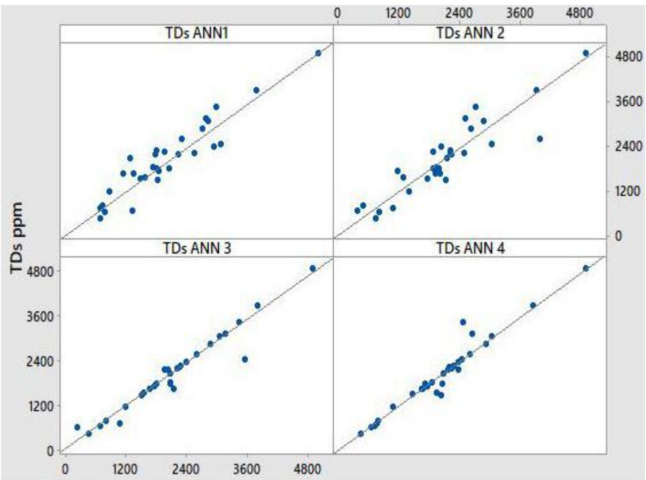

Fig.8: The observed and estimated TDS using ANN at El Zawia City Wells.

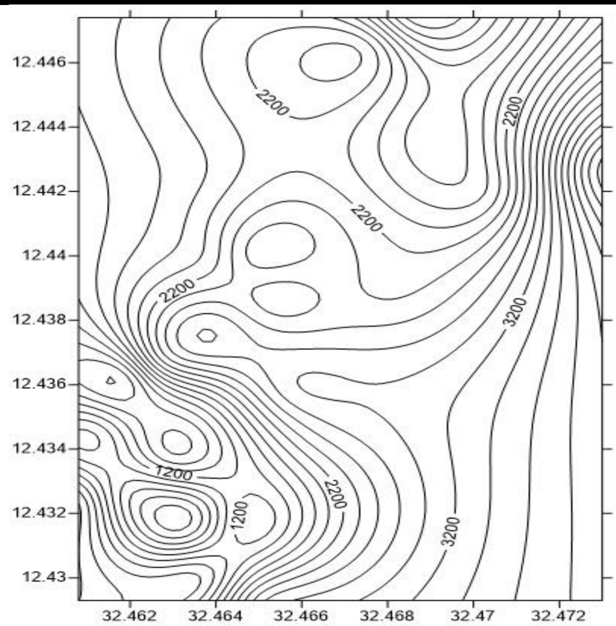

Fig.9: Map distribution ofpredicted TDS ANN4 El Zawia City Wells.

5. Conclusion

In this study, estimation of the TDS in thirty pumping well located at Elzawi city- Libya, was studied using the ANN models. The input variables were the well longitude, latitude, EC, Ca, Mg, and pH while the TDS the output. The Levenberg–Marquardt (LM) algorithm was used to train ANN and back propagation used for the training of the feed forward ANN. The ANN models performance were compared using the coefficient of determination (E), mean absolute percentage error (MAPE %), and 95% confidence interval.

The sensitivity of different parameters in predicting the neural network of the four models was observed for Ca, Mg, EC parameters, and the latitude, longitude respectively. It goes

ISSN 2522-6967

through the Ec, latitude, longitude of the wells, played a good pronounced role in predictions for TDS.

The models designed by neural networks to predict the TDS parameter with different input combination. There is a good correlation between the TDS, Mg, Ca, PH and Ec with the location of wells presented as the latitude and longitude.

ANN4 model performed superior to the other models in predicting TDS with high E=0.94 and lowest MAPE= 5.6% and have predicted mean within the range of observed 95CI%.

The results show a significant superiority of the combined model ANN of the well latitude, longitude. Besides the advantage prediction, it makes possible spatially prediction of TDS distribution with access to other parameters such as EC. This is a quick and cost-effective method for management practices, especially in emergency situations and makes.

References

[1] Moasheri S. A, KhammarG.A,Poornoori.Z,Beyranvand. Z,Soleimani M., 2013,Estimate the spatial distribution TDS the fusion method Geostatistics and artificial neural networks, International Journal of Agriculture and Crop Sciences., 7,410-420.

[2] Nemati S., Naghipour L, and Fazeli Fard MH. 2014,. Artificial Neural Network Modeling of Total Dissolved Solid in the Simineh River, Iran., J. Civil Eng. Urban., 4, 08-14.

[3] Moasheri S.A, RezapourO. M, Beyranvand .Z, Poornoori .Z ,2013, Estimating the spatial distribution ofgroundwater qualityparameters of Kashan plain with integration method of Geostatistics - Artificial Neural Network Optimized by Genetic-Algorithm ,International Journal of Agriculture and Crop Sciences.,20, 2434-2442.

[4] Sattari M. T, Joudi A. R, Kusiak.A,2016,Estimation of Water Quality Parameters With Data-Driven Model, http://dx.doi.org/10.5942/jawwa.2016.108.0012 Peer-Reviewed.

[5] Kheradpisheh. Z, Talebi .A, Rafati. L, Ghaneeian M.T, Ehrampoush M.H,Groundwater quality assessment using artificial neural network: A case study of Bahabad plain, Yazd, Iran, Desert Online at http://desert.ut.ac.ir, 20, 65-71.

[6] SalemM. A., AlshergawiM .I, 2013, Physico-chemical Evaluation of Drinking Water Quality in Alshati District of Libya,Journal Of Environmental Science, Toxicology And Food Technology (IOSR-JESTFT), 4, 46-51.

[7] MaedehP. A, Mehrdadi. N, Nabi Bidhendi1 G.R , Zare H. ,2013, Application of Artificial Neural Network to Predict Total Dissolved Solids Variations in Groundwater of Tehran Plain, Iran,International Journal of Environment and Sustainability, 2,45-51.